Monte Carlo simulations for the neutron guide shielding of the ODIN instrument at ESS

Florian Grünauer

10.1.2019

short report

preliminary results

Monte Carlo code: MCNP6

Content

1 General considerations 5
1.1 Fictive neutron source 5
1.2 Influence of the amount of steel and ordinary concrete in the shielding 6
1.2.1 Monte Carlo model 6
1.2.2 Neutron spectra outside the guide shielding in dependency of the steel and concrete amount 7
1.2.3 Dose rates outside the guide shielding in dependency of the steel and concrete amount 8
1.3 Influence of the arrangement of the steel and concrete layers 10
2 Preliminary common guide shielding version 1 (10cm Fe; 60cm conc.) 12
2.1 Version without gaps for the pillars 12
2.1.1 Monte Carlo model 12
2.1.2 Horizontal neutron dose rate distribution 13
2.1.3 Horizontal generated gamma dose rate distribution 16
2.1.4 Vertical dose rate distribution 18
2.2 Version with gaps for the pillars 19
2.2.1 Monte Carlo model 19
2.2.2 Vertical neutron dose rate distribution 20
2.2.3 Vertical generated gamma dose rate distribution 23
2.3 Influence of a 2cm boron carbide layer between the steel layer and the concrete layer on the neutron dose rate (version without gaps for the pillars) 26
3 Preliminary common guide shielding version 2 (10cm Fe; 50cm conc.) 28
3.1 New fictive neutron source 28
3.2 Monte Carlo model 30
3.3 Results for the original version 2 (10cm steel, 50cm ordinary concrete) 34
3.3.1 Horizontal neutron dose rate distribution 34
3.3.2 Horizontal generated gamma dose rate distribution 38
3.3.3 Vertical dose rate distributions 40
3.3.4 Conclusions 41
3.4 Variation of the steel/concrete thickness 41
3.4.1 Conclusions 42
3.5 Influence of the vertical length of the steel layer 43
3.5.1 10cm steel and 80cm ordinary concrete shielding 43
3.5.2 20cm steel and 70cm ordinary concrete shielding 46
3.5.3 Conclusions 49
4 Preliminary common guide shielding version 3 (20cm Fe; 70cm conc.) 50
4.1 New fictive neutron source 50
4.2 Monte Carlo model 51
4.3 Dose rate distributions for the opened chopper FOC5 54
4.3.1 Horizontal neutron dose rate distribution 54
4.3.2 Horizontal generated gamma dose rate distribution 55
4.3.3 Vertical neutron dose rate distribution along the beam axis 56
4.3.4 Vertical generated gamma dose rate distribution along the beam axis 57
4.3.5 Vertical neutron dose rate distribution through the guide shielding perpendicular to the beam axis 58

4.3.6 Vertical generated gamma dose rate distribution through the guide shielding perpendicular to the beam axis....58
4.3.7 Vertical neutron dose rate distribution through the chopper pit perpendicular to the beam axis....59
4.3.8 Vertical neutron dose rate distribution through the chopper pit perpendicular to the beam axis....59
4.3.9 Conclusions....60
4.4 Dose rate distributions for the closed chopper FOC5....61
4.4.1 Horizontal neutron dose rate distribution....62
4.4.2 Horizontal generated gamma dose rate distribution....63
4.4.3 Vertical neutron dose rate distribution through the chopper pit perpendicular to the beam axis....64
4.4.4 Vertical generated gamma dose rate distribution through the chopper pit perpendicular to the beam axis....64
4.5 Conclusions....66
5 Variation of the thickness of the steel and concrete layers in version 3....67
5.1 Shielding version 3 consisting of 25cm steel and 70cm concrete....68
5.2 Shielding version 3 consisting of 30cm steel and 70cm concrete....71
5.3 Shielding version 3 consisting of 35cm steel and 70cm concrete....74
5.4 Shielding version 3 consisting of 40cm steel and 70cm concrete....77
5.5 Shielding version 3 consisting of 45cm steel and 70cm concrete....80
5.6 Shielding version 3 consisting of 30cm steel and 80cm concrete....83
5.7 Shielding version 3 consisting of 30cm steel and 90cm concrete....84
5.8 Shielding version 3 consisting of 30cm steel and 100cm concrete....85
6 Radiography of the moderator and its surrounding....88
7 New fictive neutron source....92
7.1 Shielding version 3 consisting of 25cm steel and 70cm concrete....92
7.1.1 Conclusion....96
7.2 The influence of the ordinary concrete composition....96
7.2.1 Conclusion....98
7.3 Shielding version 3B consisting of 20cm steel and 70cm ESS ordinary concrete....99
7.3.1 Conclusion....104
7.4 The influence of polyethylene....105
7.4.1 Conclusion....106
7.5 Shielding version 3C consisting of 20cm steel and 80cm ESS ordinary concrete (chopper pit: 20cm steel and 70cm ordinary concrete)....107
7.5.1 Closed chopper FOC5....113
7.5.2 Conclusion....114
7.6 Shielding version 3D consisting of 20cm steel and 80cm ESS ordinary concrete and a 10cm steel layer below the neutron guide (chopper pit: 20cm steel and 70cm ordinary concrete)....115
7.6.1 Closed chopper FOC5....122
7.6.2 Conclusion....123
7.7 Shielding version 3E consisting of 20cm steel and 80cm ESS ordinary concrete and a 5cm steel layer below the neutron guide (chopper pit: 20cm steel and 70cm ordinary concrete)....124
7.7.1 Closed chopper FOC5....130
7.8 Conclusion....131

7.9 Shielding version 3F with collimators and interface between bunker wall and guide shielding 132
7.9.1 Closed chopper FOC5.....139
7.9.2 Conclusion 139
8 Appendix 140
8.1 Flux to dose rate conversion factors.....140

1 General considerations

1.1 Fictive neutron source

For the fictive neutron source in the ODIN channel data for the CSPEC channel, simulated by Douglas di Julio, was used, since the own data for the ODIN channel is lower and the simulation results for the guide shielding should be conservative. A fictive source was placed at the entrance of the ODIN guide causing the same neutron flux at 5.5m from the focal point as in the CPSEC channel (simulated by Douglas di Julio). This fictive neutron source causes a neutron flux of 1.5e8 cm^{-2} sec^{-1} at a distance of 28m from the focal point. In a second step a new fictive neutron source at 24m from the focal point was defined causing the same neutron flux at 28m from the focal point as the fictive source at the guide entrance. This second fictive neutron source was applied in the simulations presented in the following chapters.

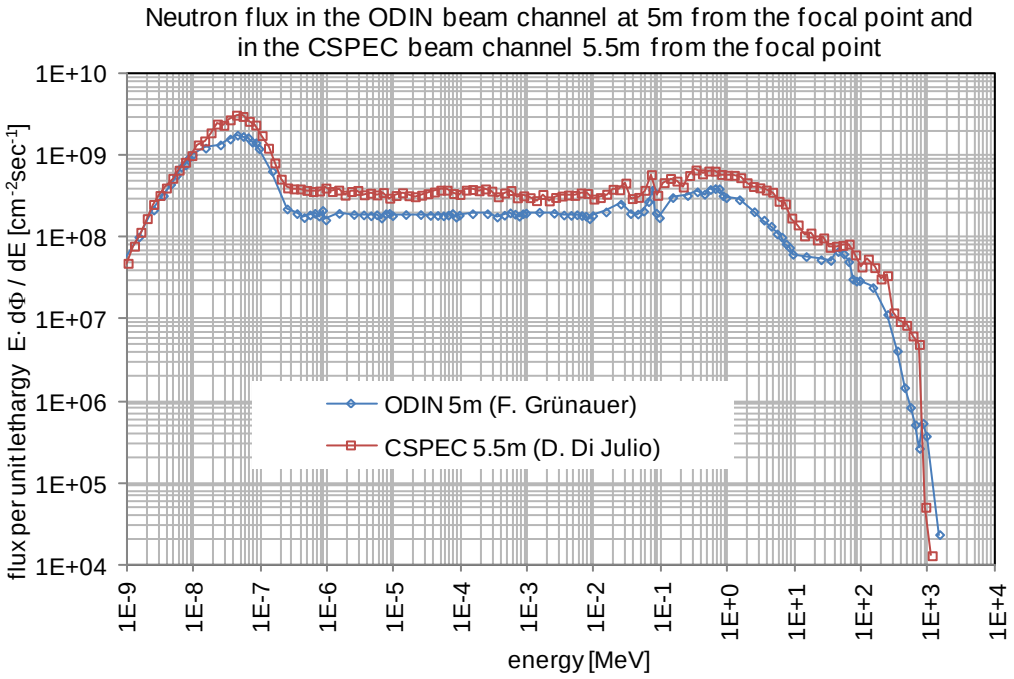

Fig. 1: Neutron flux in the ODIN beam channel at 5m from the focal point and in the CSPEC beam channel 5.5m from the focal point

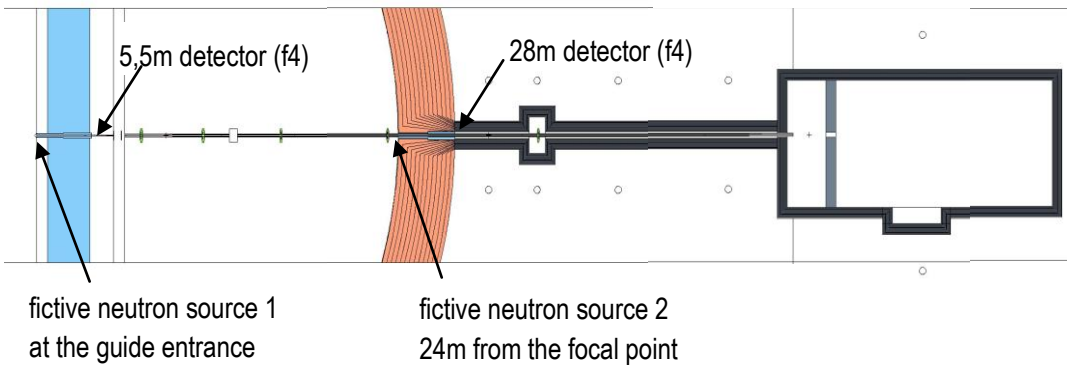

Fig. 2: Horizontal cut through the ODIN MCNP model with the locations of the fictive sources

1.2 Influence of the amount of steel and ordinary concrete in the shielding

1.2.1 Monte Carlo model

The shielding consists of one inner layer of steel (thickness t(steel)) and one outer layer of ordinary concrete (thickness t(concrete)). The total thickness of the shielding is 70cm. The thickness of the steel layer t(steel) is varied and the thickness of the concrete layer is adjusted: t(concrete) = 70cm – t(steel). The inner horizontal width of the shielding is 27cm.

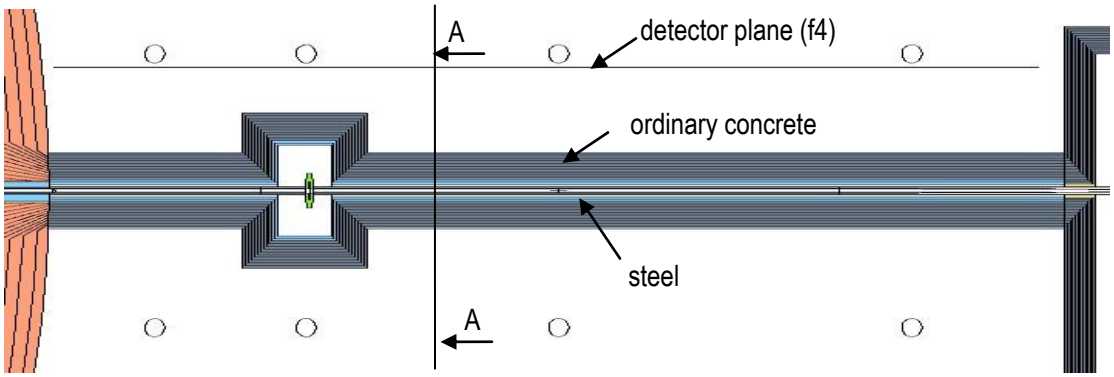

Fig. 3: Horizontal cut through the Monte Carlo model of the ODIN neutron guide shielding

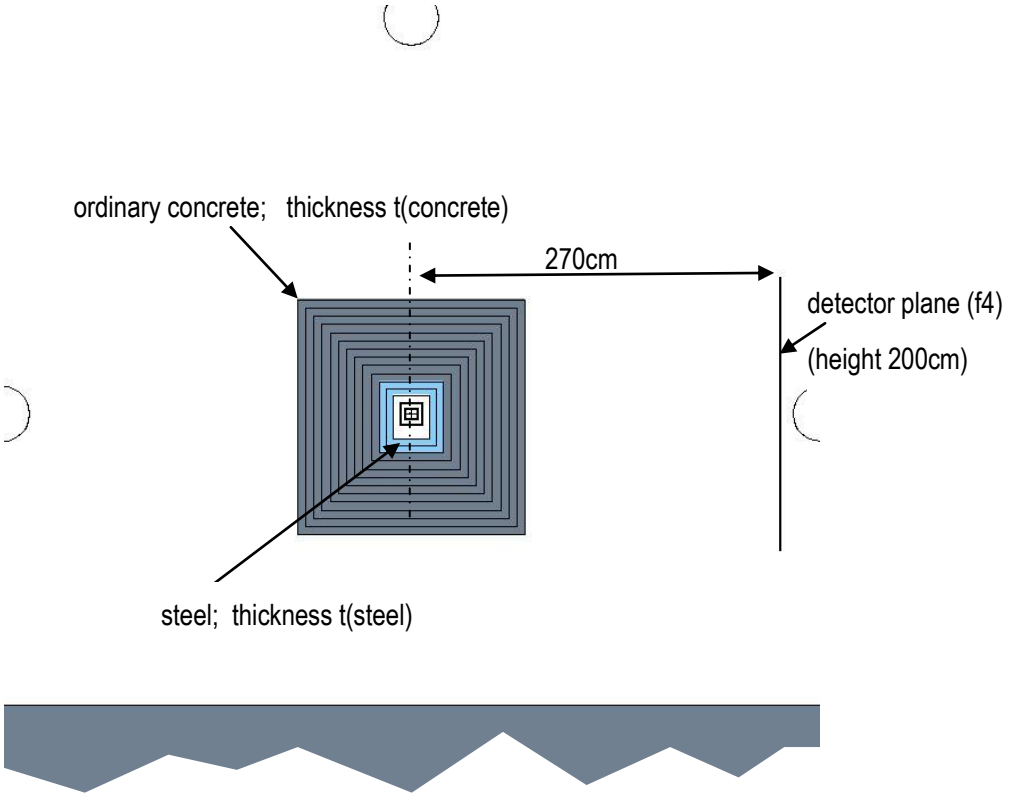

Fig. 4: Vertical cut A-A through the Monte Carlo model of the ODIN neutron guide shielding

1.2.2 Neutron spectra outside the guide shielding in dependency of the steel and concrete amount

The neutron spectra obtained in the detector plane beside the neutron guide shielding with the different steel and concrete amounts are shown in the diagram below.

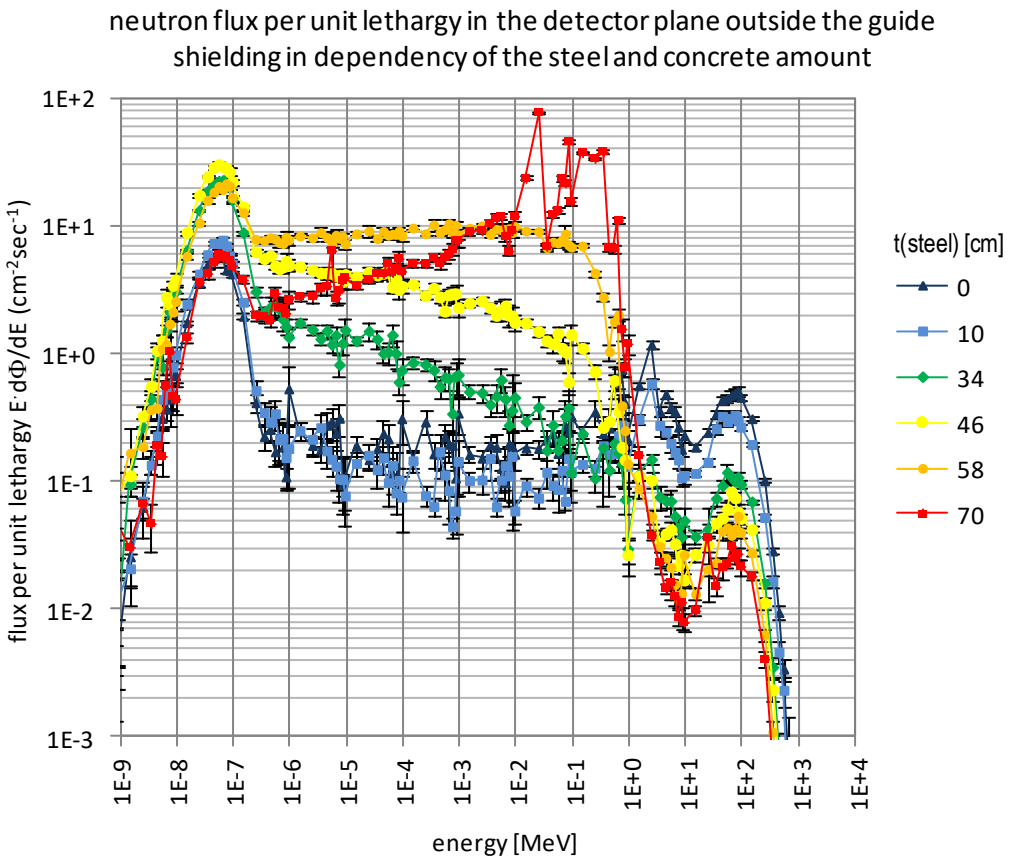

Fig. 5: Neutron flux per unit lethargy in the detector plane outside the guide shielding in dependency of the steel and concrete amount

With a pure steel shielding the transmission in the energy region 10keV to 1MeV becomes high due to the minima between the resonance peaks. With a pure concrete shielding transmission above 1MeV becomes high.

1.2.3 Dose rates outside the guide shielding in dependency of the steel and concrete amount

The dose rates obtained in the detector plane beside the neutron guide shielding with the different steel and concrete amounts are shown in the diagrams below.

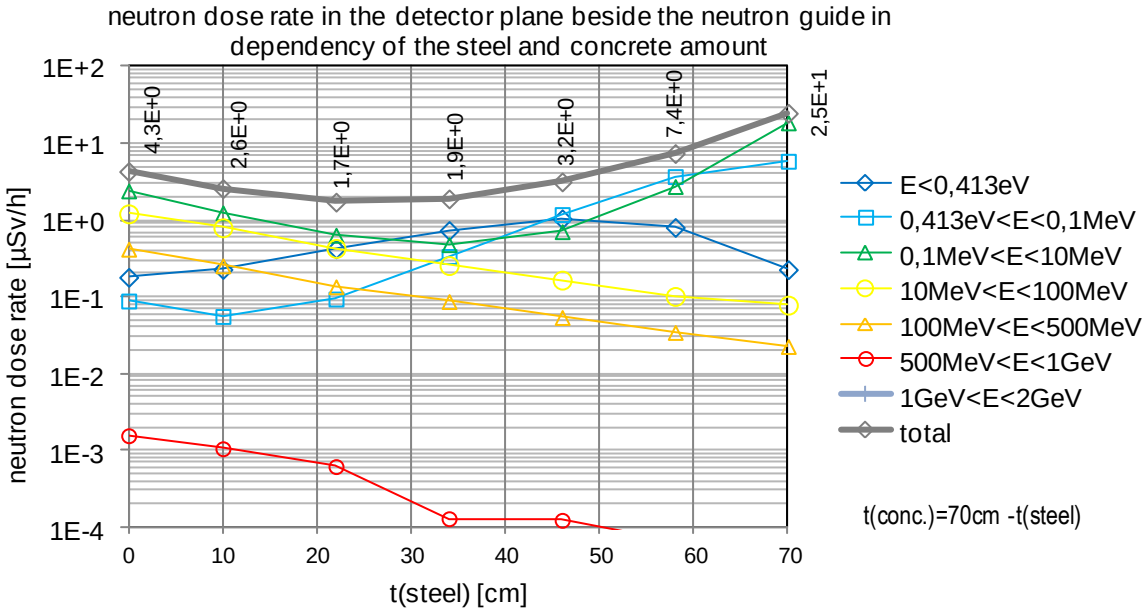

Fig. 6: Neutron dose rate in the detector plane beside the neutron guide in dependency of the steel and concrete amount

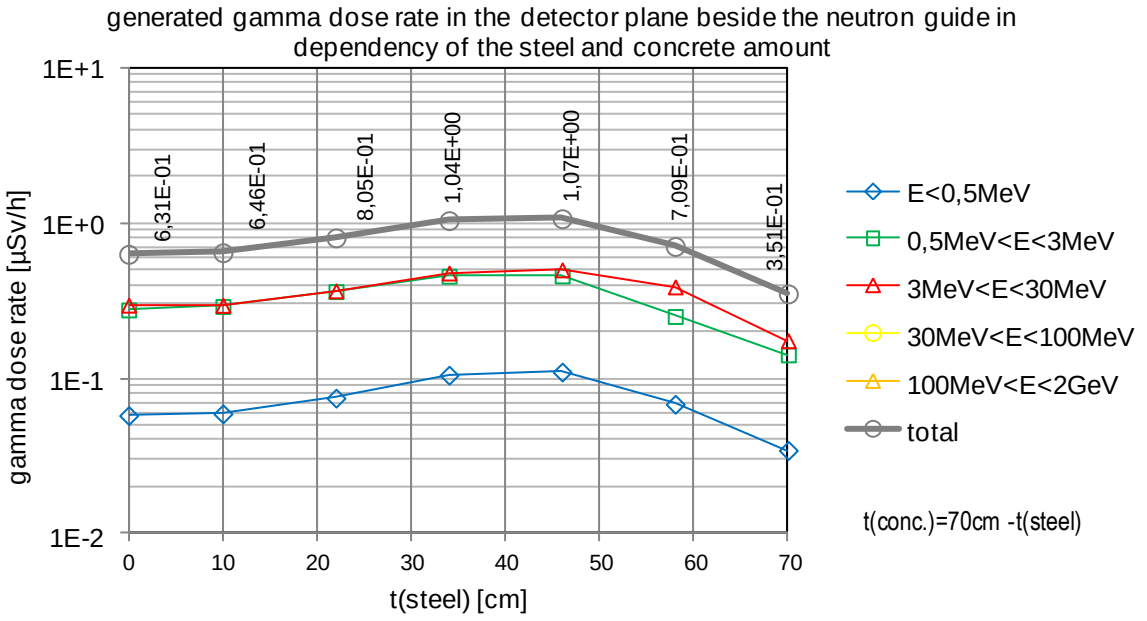

Fig. 7: Generated gamma dose rate in the detector plane beside the neutron guide in dependency of the steel and concrete amount

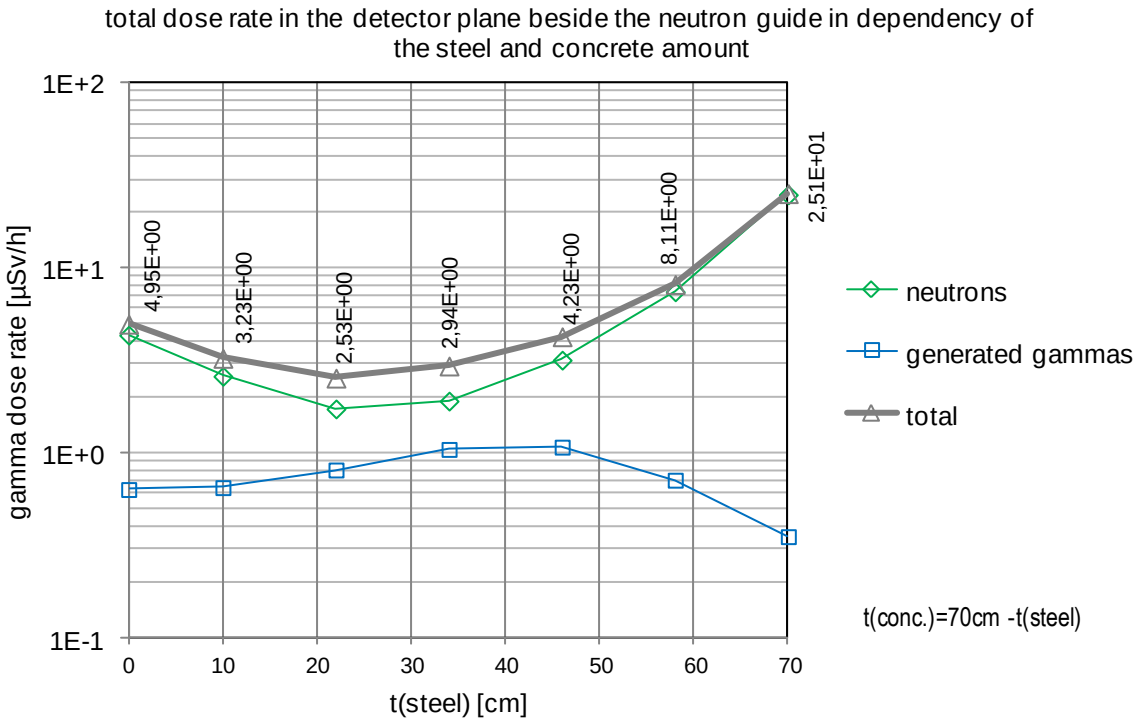

Fig. 8: Total dose rate in the detector plane beside the neutron guide in dependency of the steel and concrete amount

For neutrons the dose rate minimum is reached at ca. 20cm steel and 50cm concrete.

For the generated gamma radiation the dose rate is increasing with increasing steel thickness up to a steel thickness of ca. 45cm. For a higher steel thickness the generated gamma dose rate decreases with increasing steel thickness. This shows that the dose rate is dominated by gamma production inside the shielding and not from the neutron guide. For the component from the neutron guide the dose rate should decrease monotonically with increasing steel thickness.

The minimum of total dose rate is reached for ca. 20cm steel. It is dominated by neutron radiation.

1.3 Influence of the arrangement of the steel and concrete layers

Is it beneficial to have only one layer of each material or is it better to have several layers of each material? In order to answer this question the following two guide shielding versions were simulated:

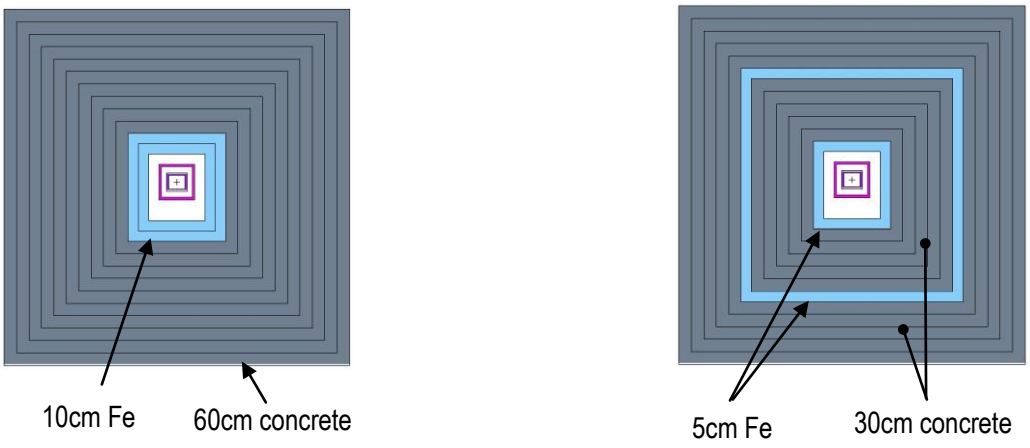

Fig. 9: Vertical cuts through the guide shielding with only one steel and one concrete layer (left hand side) and through the guide shielding consisting of two layers steel and two layers concrete (right hand side)

The dose rates in the detector plane beside the guide shielding are compared in the following diagrams.

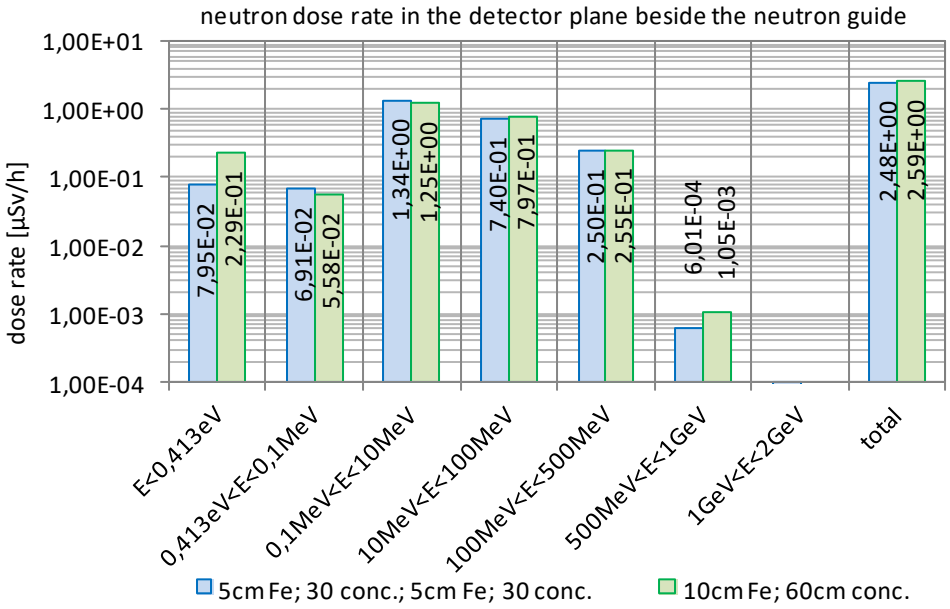

Fig. 10: Neutron dose rate in the detector plane beside the neutron guide

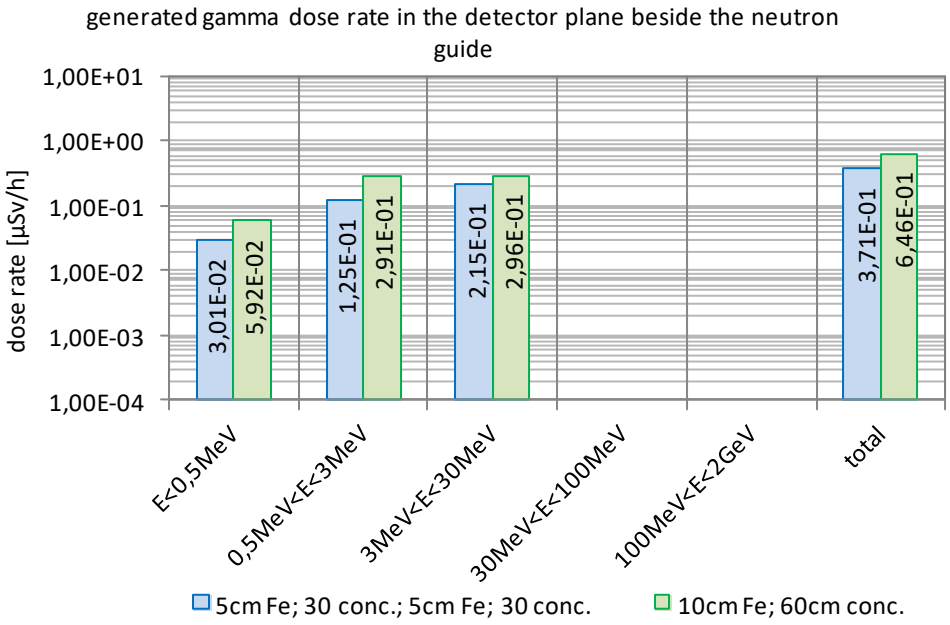

Fig. 11: Generated gamma dose rate in the detector plane beside the neutron guide

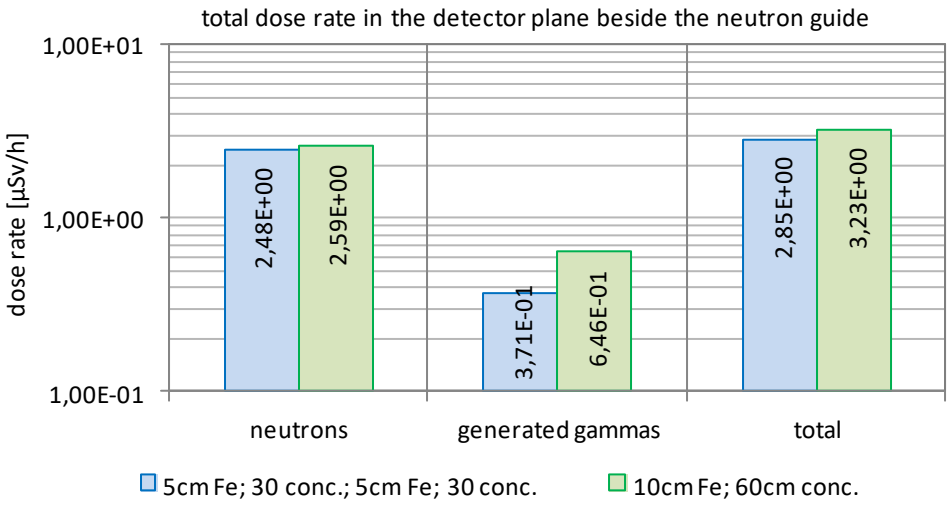

Fig. 12: Total dose rate in the detector plane beside the neutron guide

There is no major difference in the neutron dose rate for both versions of the guide shielding. The generated gamma dose rate is smaller for the case of the two separated layers of steel. However, since the neutron dose rate dominates total dose rate, there is no major difference in total dose rate.

2 Preliminary common guide shielding version 1 (10cm Fe; 60cm conc.)

2.1 Version without gaps for the pillars

2.1.1 Monte Carlo model

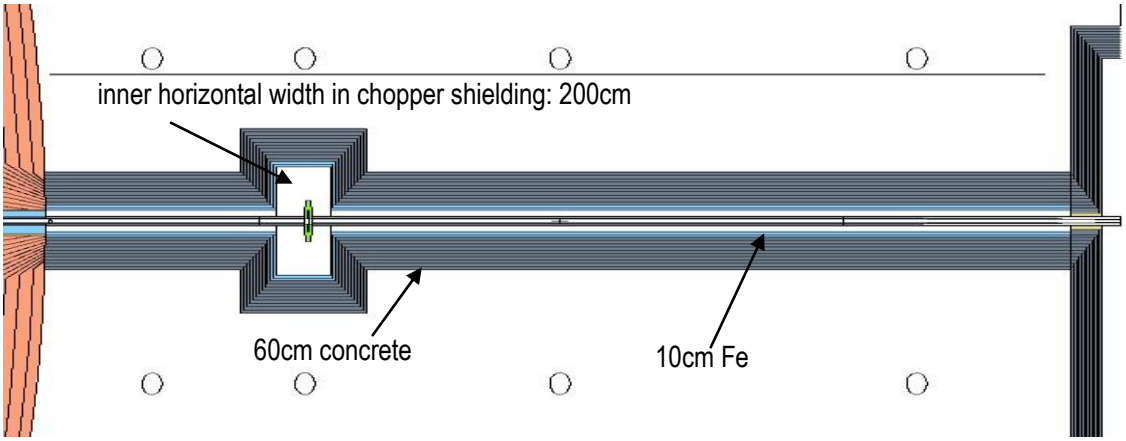

Fig. 13: Horizontal cut through the Monte Carlo model of the common guide shielding applied to the ODIN instrument

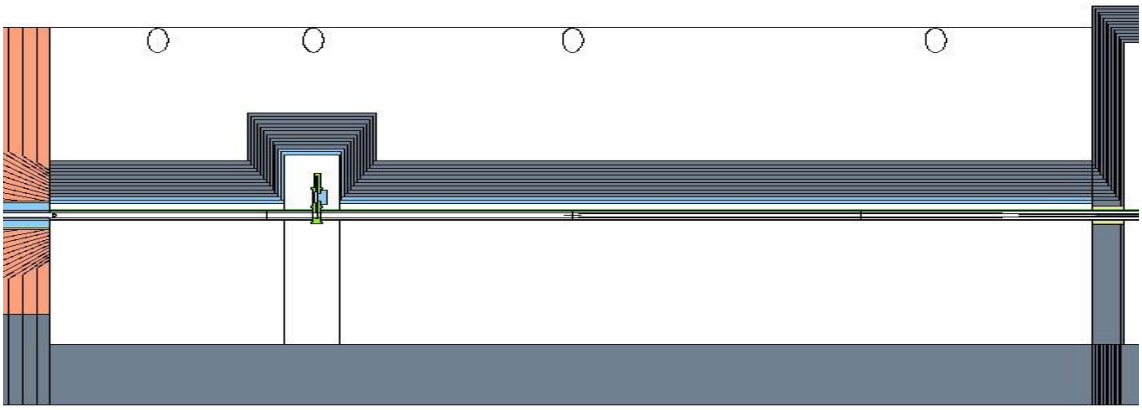

Fig. 14: Vertical cut along the beam axis through the Monte Carlo model of the common guide shielding applied to the ODIN instrument

Fig. 15 : Vertical cut perpendicular to the beam axis through the Monte Carlo model of the common guide shielding applied to the ODIN instrument

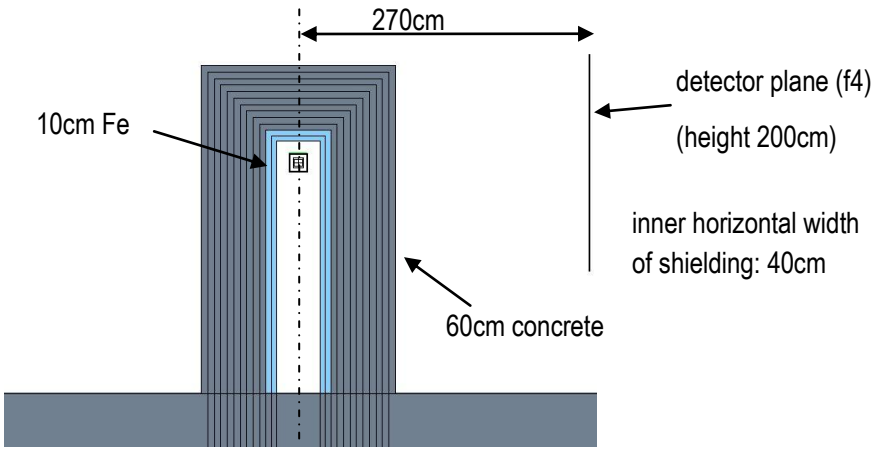

2.1.2 Horizontal neutron dose rate distribution

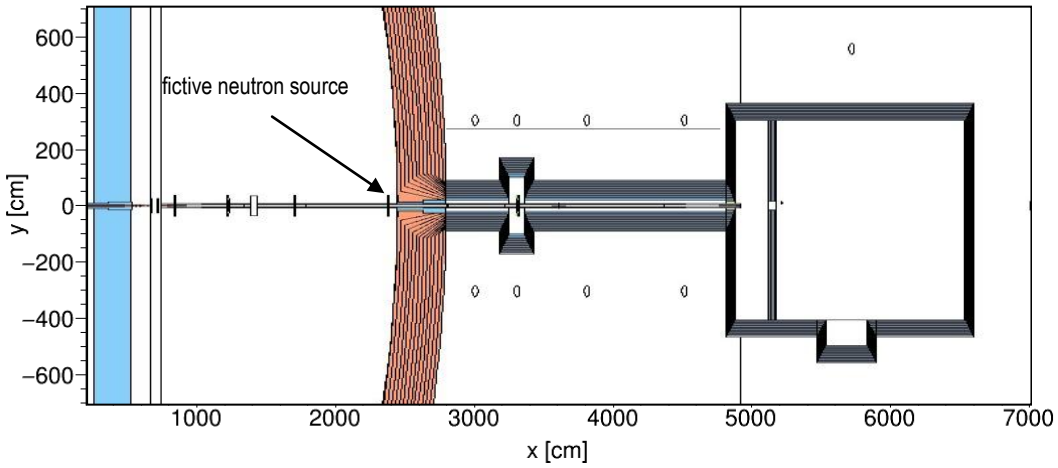

Fig. 16: Horizontal area through the Monte Carlo model of the ODIN instrument for which the radiation distributions are shown in the following images

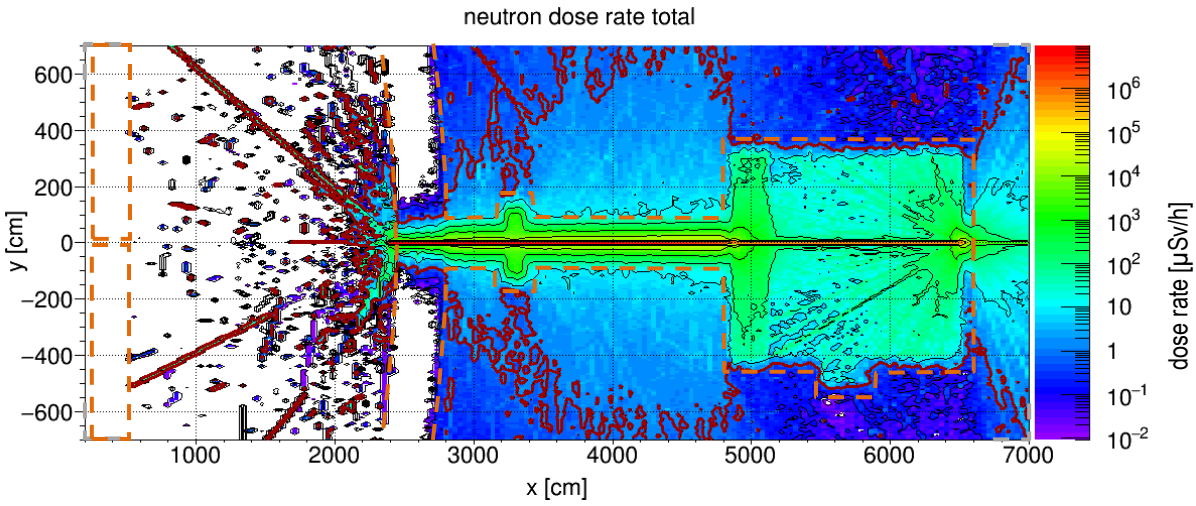

Fig. 17: Total neutron dose rate distribution in the horizontal area. The red line is the 1µSv/h border.

A neutron dose rate of ca. 10µSv/h is reached on the outer surface of the guide shielding.

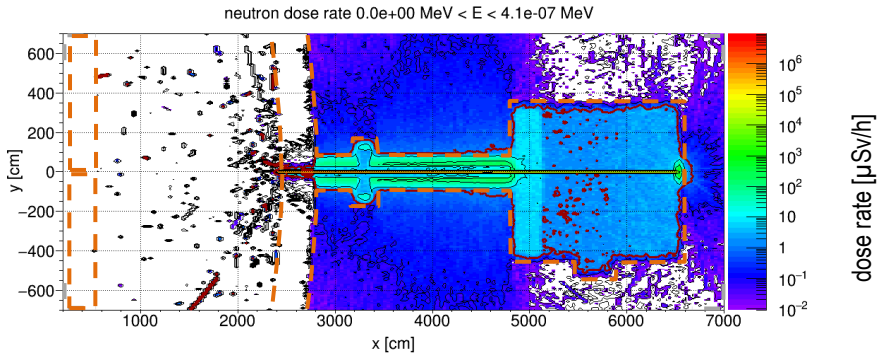

Fig. 18: Neutron dose rate distribution in the energy range below 0.41eV in the horizontal area. The red line is the 1µSv/h border.

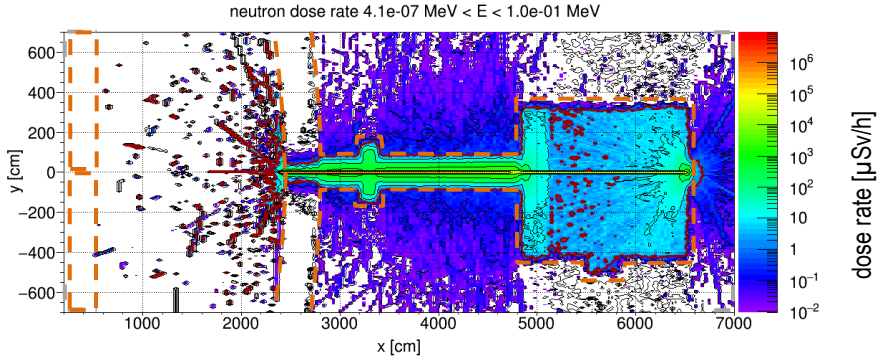

Fig. 19: Neutron dose rate distribution in the energy range between 0.41eV and 0.1MeV in the horizontal area. The red line is the 1µSv/h border.

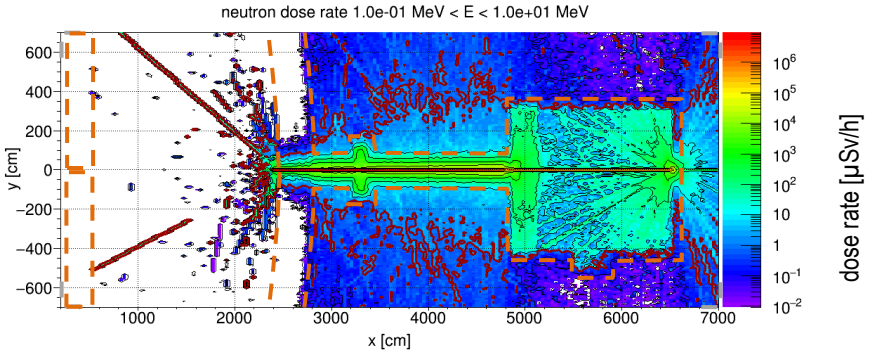

Fig. 20: Neutron dose rate distribution in the energy range between 0.1MeV and 10MeV in the horizontal area. The red line is the 1µSv/h border.

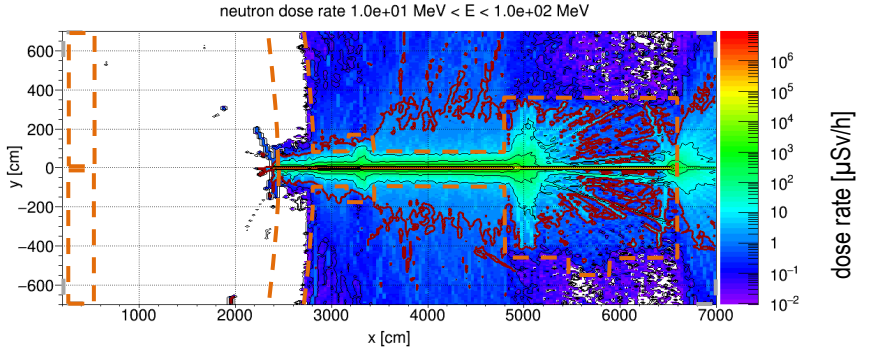

Fig. 21: Neutron dose rate distribution in the energy range between 10MeV and 100MeV in the horizontal area. The red line is the 1µSv/h border.

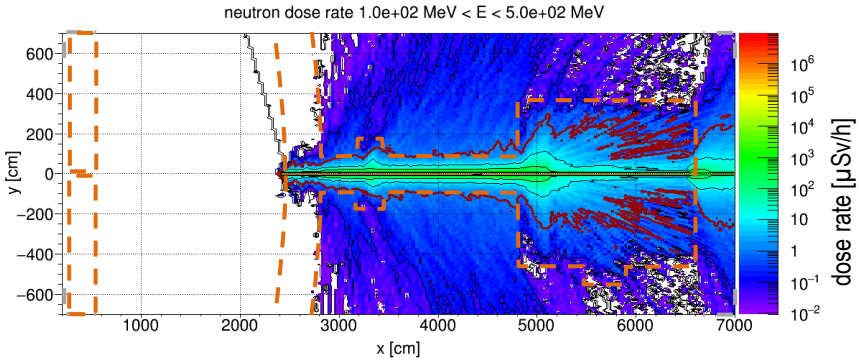

Fig. 22: Neutron dose rate distribution in the energy range between 100MeV and 500MeV in the horizontal area. The red line is the 1µSv/h border.

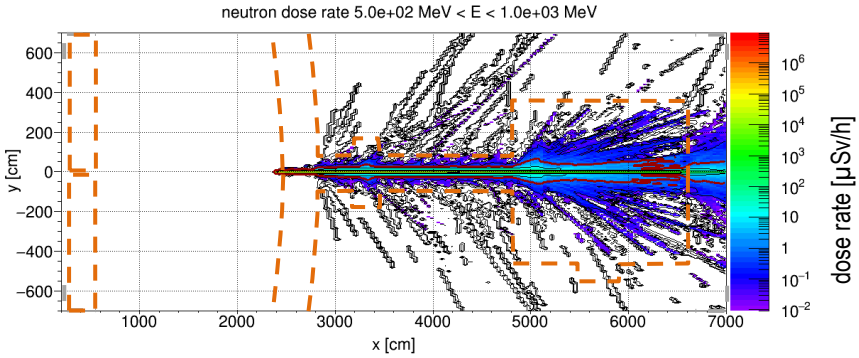

Fig. 23: Neutron dose rate distribution in the energy range between 500MeV and 1GeV in the horizontal area. The red line is the 1µSv/h border.

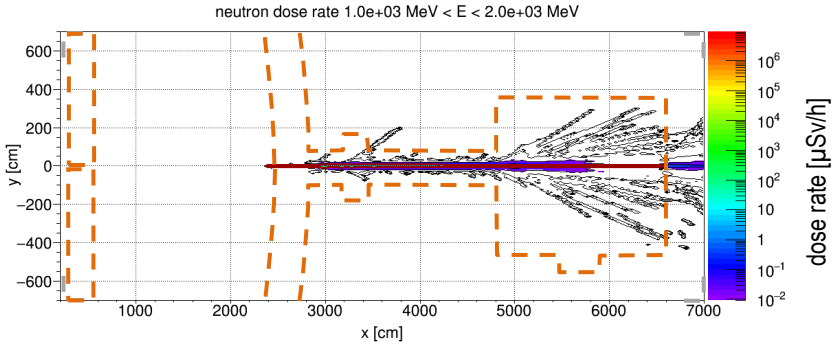

Fig. 24: Neutron dose rate distribution in the energy range between 1GeV and 2GeV in the horizontal area. The red line is the 1µSv/h border.

2.1.3 Horizontal generated gamma dose rate distribution

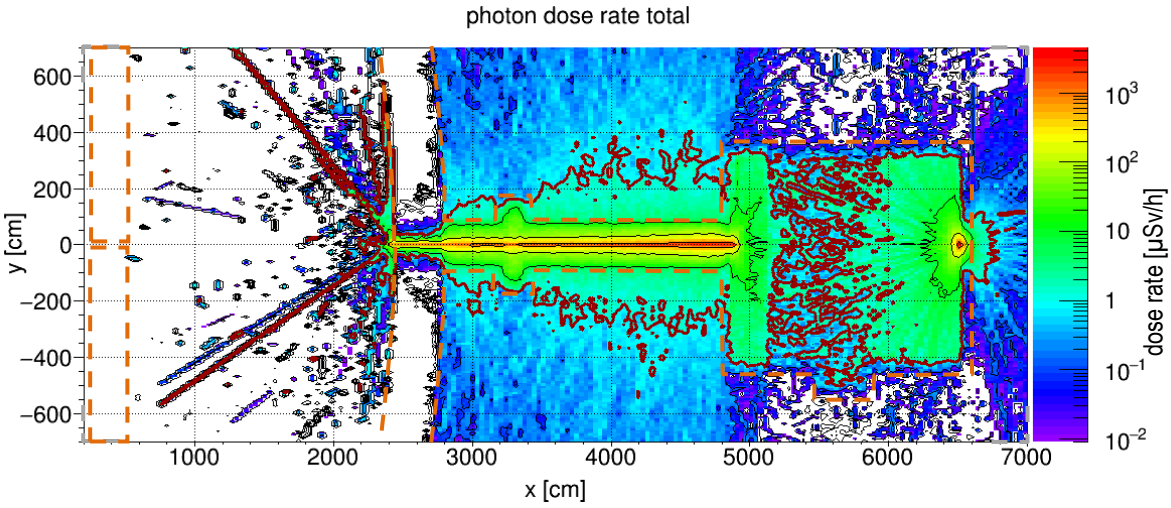

Fig. 25: Total generated gamma dose rate distribution in the horizontal area. The red line is the 1µSv/h border.

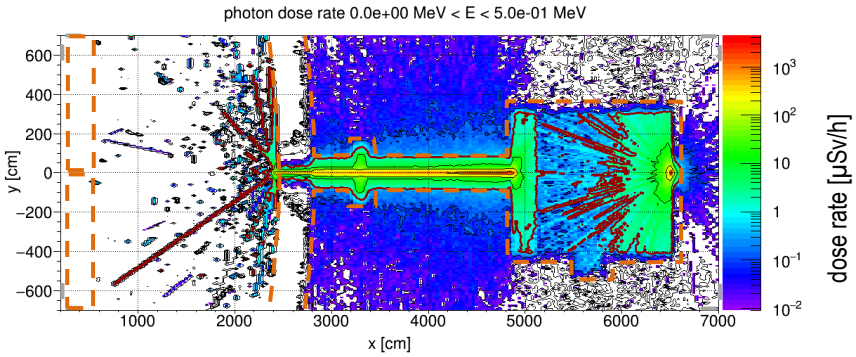

Fig. 26: Generated gamma dose rate distribution in the energy range below 0.5MeV in the horizontal area. The red line is the 1µSv/h border.

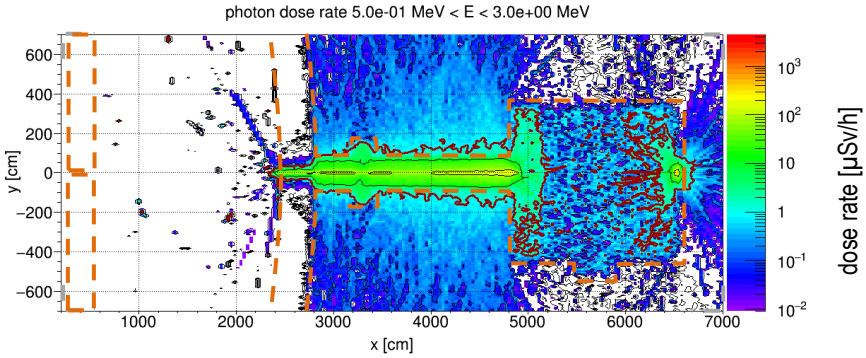

Fig. 27: Generated gamma dose rate distribution in the energy range between 0.5MeV and 3MeV in the horizontal area. The red line is the 1µSv/h border.

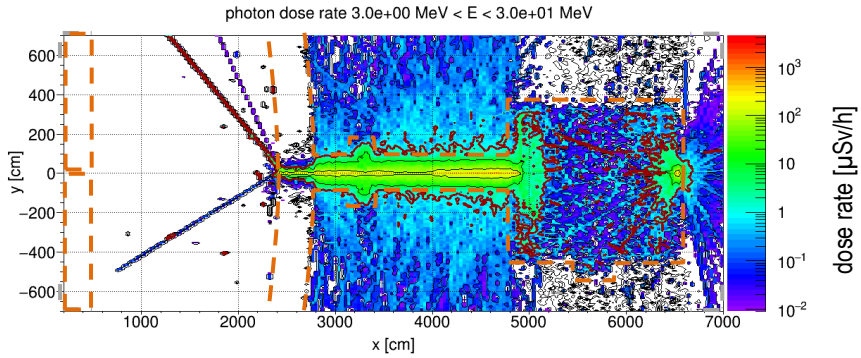

Fig. 28: Generated gamma dose rate distribution in the energy range between 3MeV and 30MeV in the horizontal area. The red line is the 1µSv/h border.

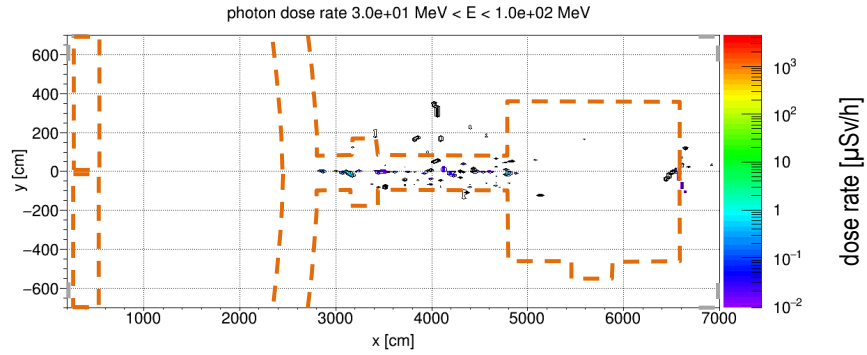

Fig. 29: Generated gamma dose rate distribution in the energy range between 30MeV and 100MeV in the horizontal area. The red line is the 1µSv/h border.

2.1.4 Vertical dose rate distribution

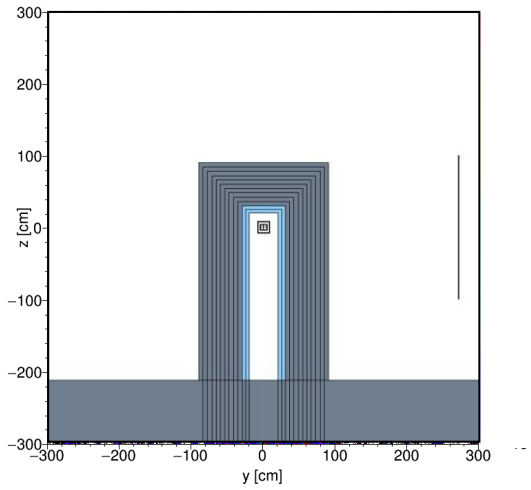

Fig. 30: Vertical area perpendicular to the beam axis through the Monte Carlo model of the ODIN guide shielding (40m from the focal point) for which the radiation distributions are shown in the following images

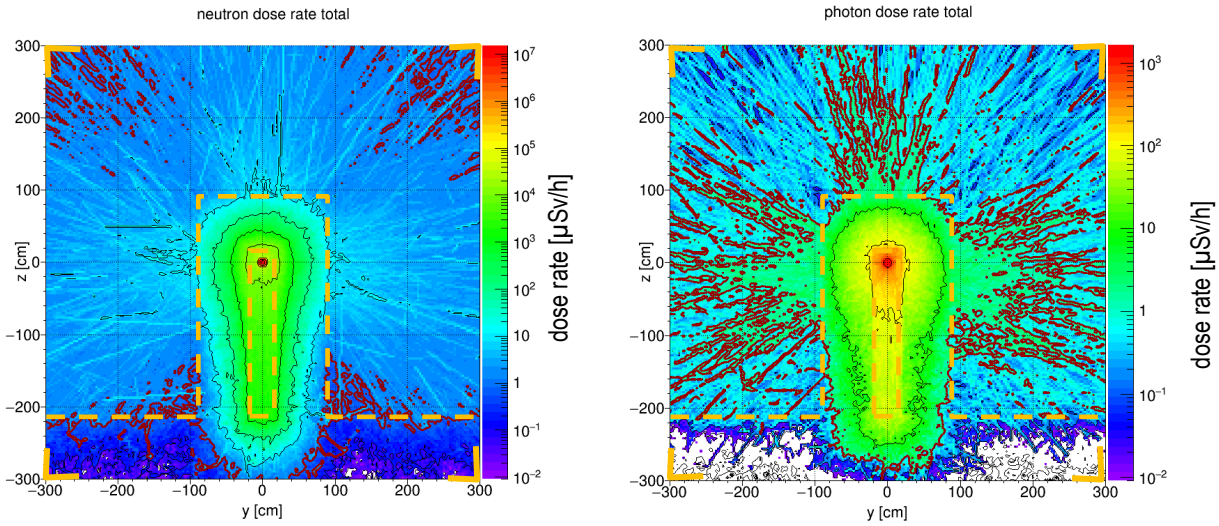

Fig. 31: Neutron dose rate (left hand side) and generated gamma dose rate (right hand side) in the vertical plane. The red line is the 1µSv/h border.

2.2 Version with gaps for the pillars

2.2.1 Monte Carlo model

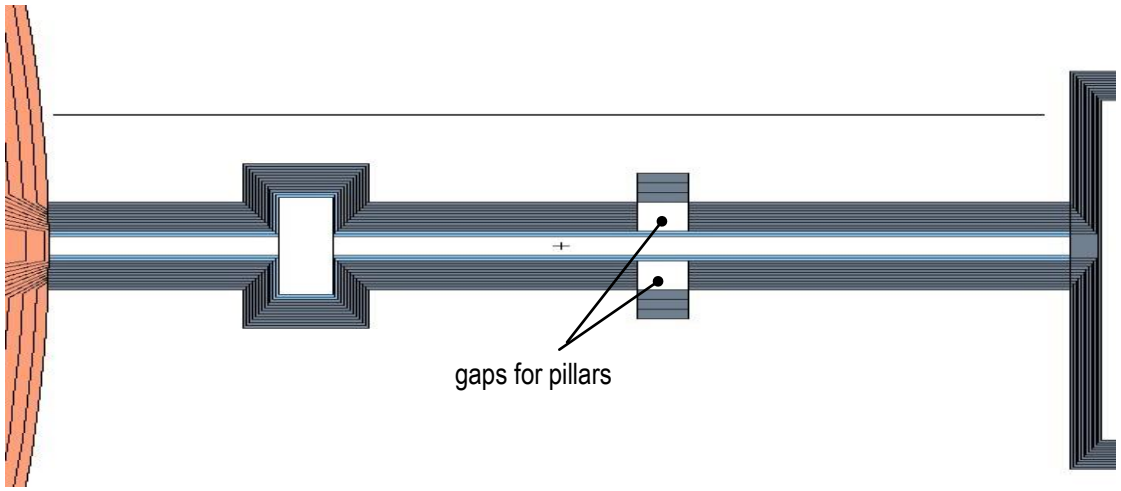

Fig. 32: Horizontal cut through the Monte Carlo model 30cm below the beam axis

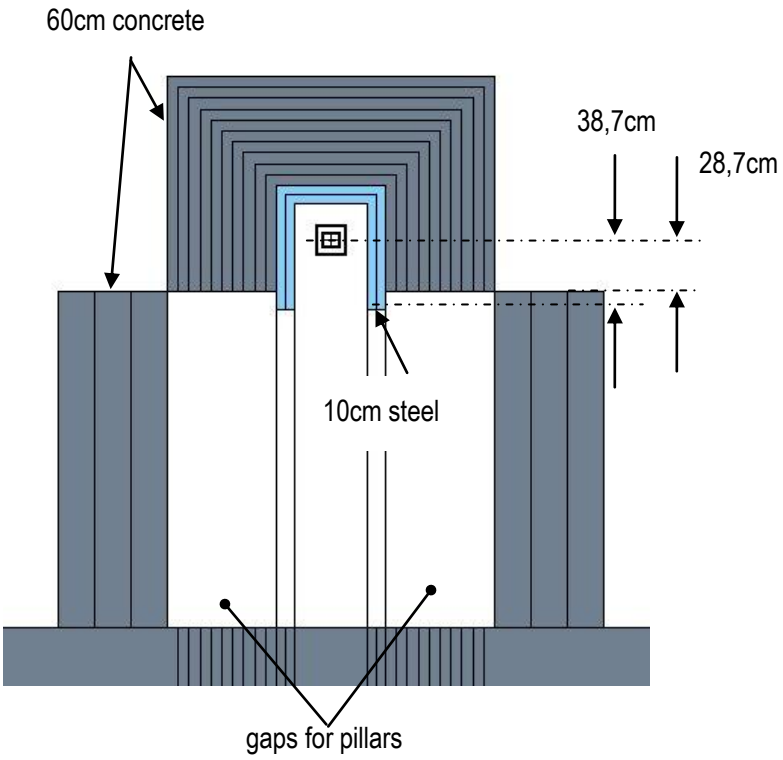

Fig. 33: Vertical cut through the Monte Carlo model 40m from the focal point

2.2.2 Vertical neutron dose rate distribution

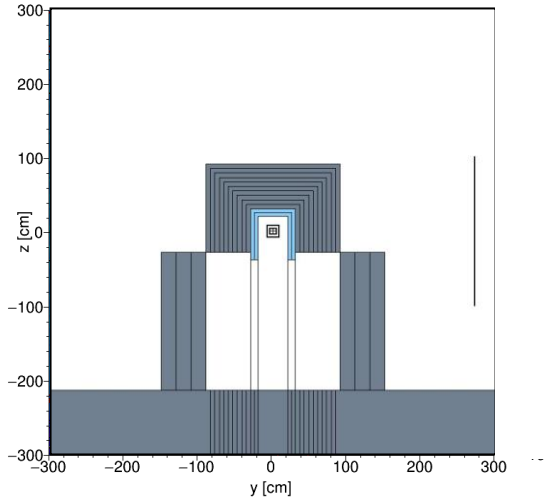

Fig. 34: Vertical area through the Monte Carlo model 40m from the focal point for which the radiation distributions are shown in the following images

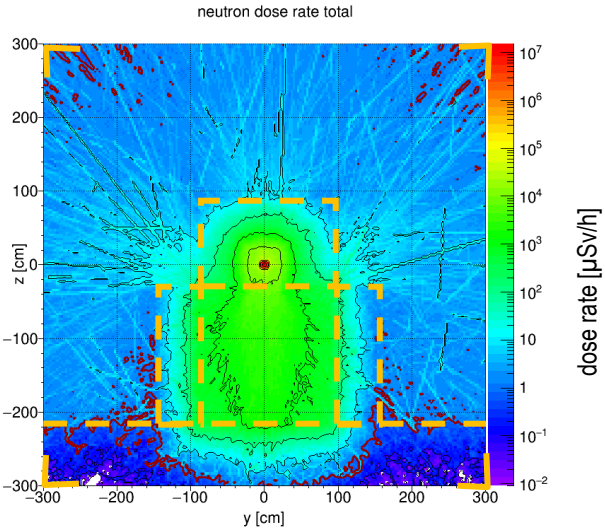

Fig. 35: Total neutron dose rate distribution in the vertical area. The red line is the 1µSv/h border.

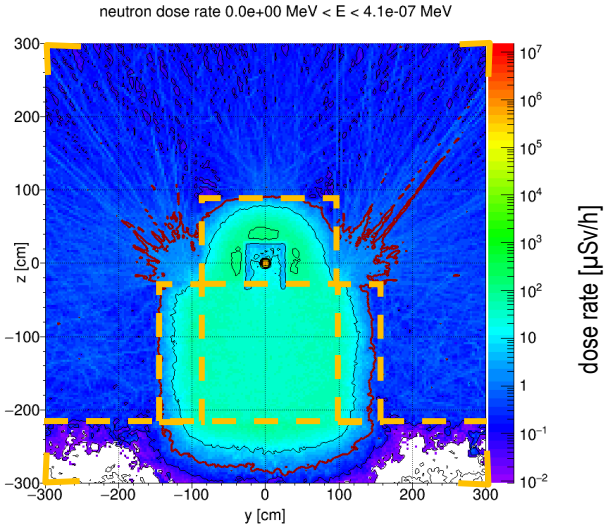

Fig. 36: Neutron dose rate distribution in the energy range below 0.41eV in the vertical area. The red line is the 1µSv/h border.

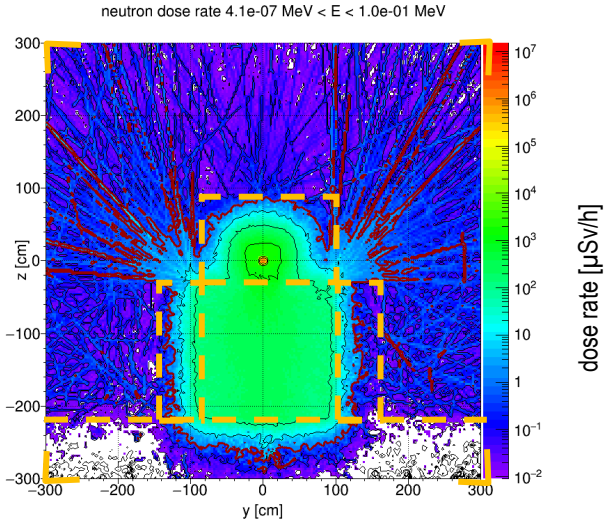

Fig. 37: Neutron dose rate distribution in the energy range between 0.41eV and 0.1MeV in the vertical area. The red line is the 1µSv/h border.

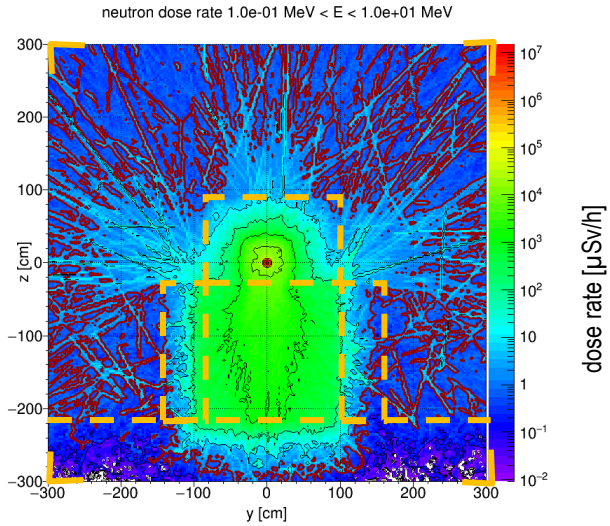

Fig. 38: Neutron dose rate distribution in the energy range between 0.1MeV and 10MeV in the vertical area. The red line is the 1µSv/h border.

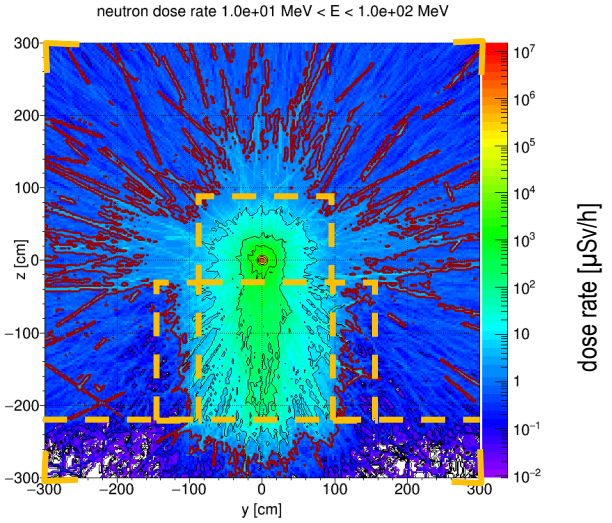

Fig. 39: Neutron dose rate distribution in the energy range between 10MeV and 100MeV in the vertical area. The red line is the 1µSv/h border.

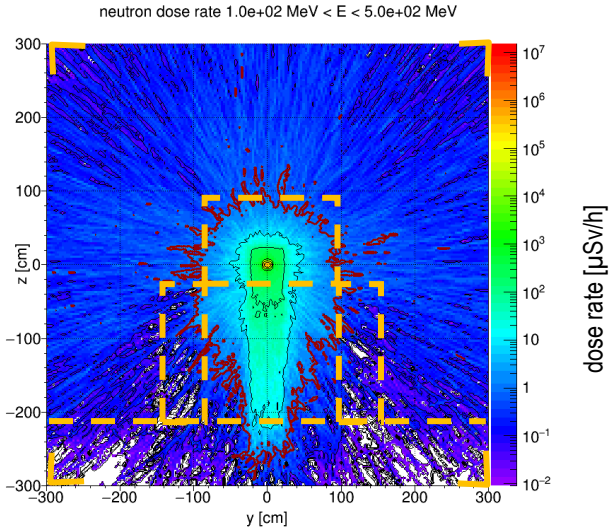

Fig. 40: Neutron dose rate distribution in the energy range between 100MeV and 500MeV in the vertical area. The red line is the 1µSv/h border.

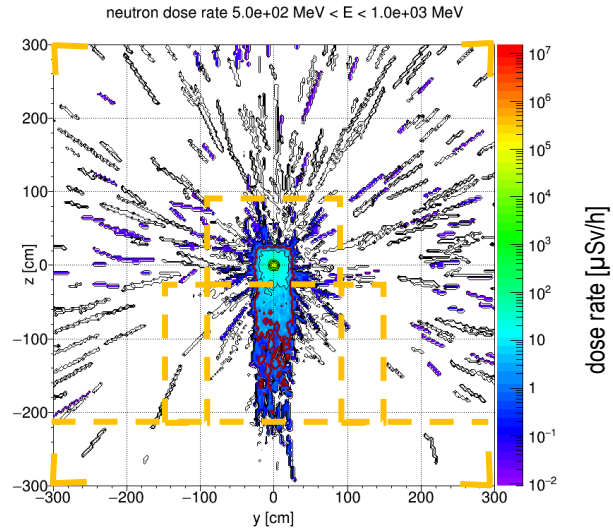

Fig. 41: Neutron dose rate distribution in the energy range between 500MeV and 1GeV in the vertical area. The red line is the 1µSv/h border.

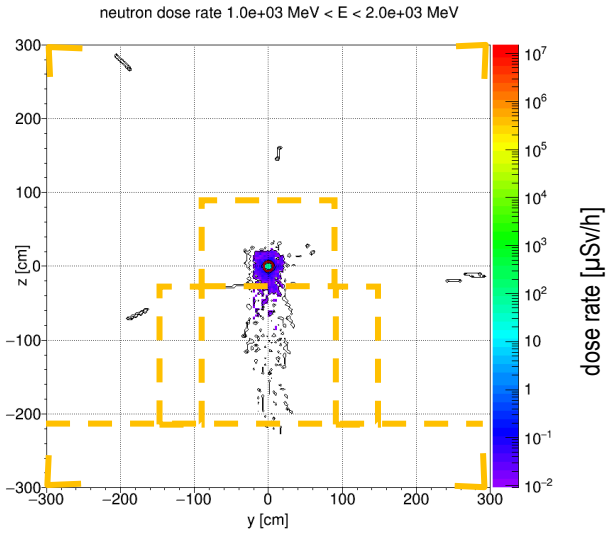

Fig. 42: Neutron dose rate distribution in the energy range between 1GeV and 2GeV in the vertical area. The red line is the 1µSv/h border.

2.2.3 Vertical generated gamma dose rate distribution

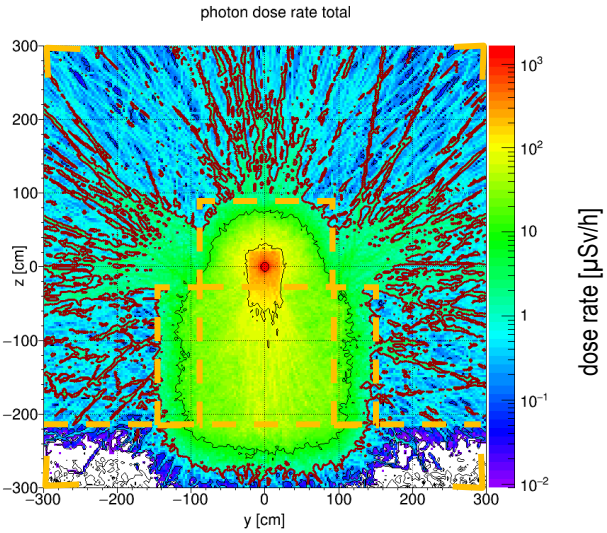

Fig. 43: Total generated gamma dose rate distribution in the vertical area. The red line is the 1µSv/h border.

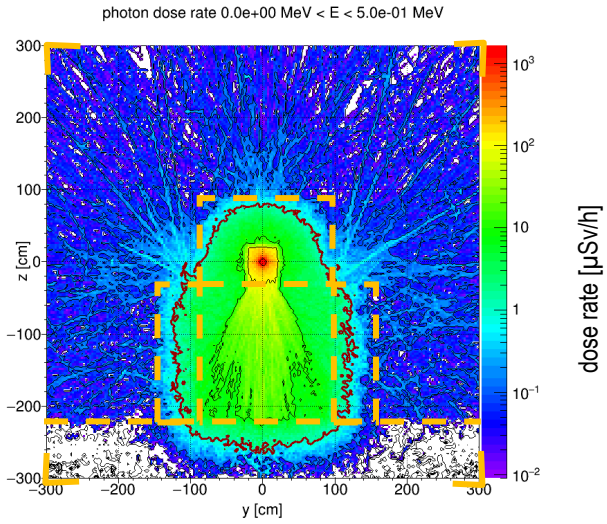

Fig. 44: Generated gamma dose rate distribution in the energy range below 0.5MeV in the vertical area. The red line is the 1µSv/h border.

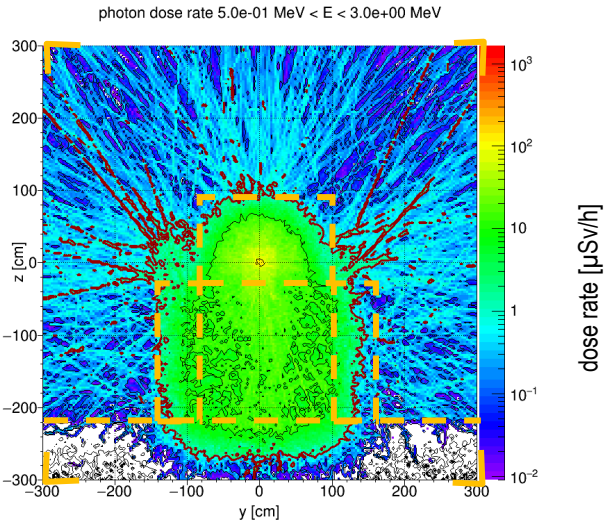

Fig. 45: Generated gamma dose rate distribution in the energy range between 0.5MeV and 3MeV in the vertical area. The red line is the 1µSv/h border.

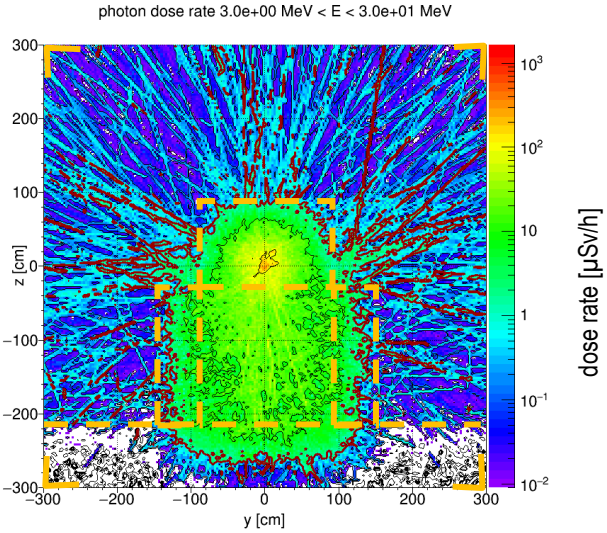

Fig. 46: Generated gamma dose rate distribution in the energy range between 3MeV and 30MeV in the vertical area. The red line is the 1µSv/h border.

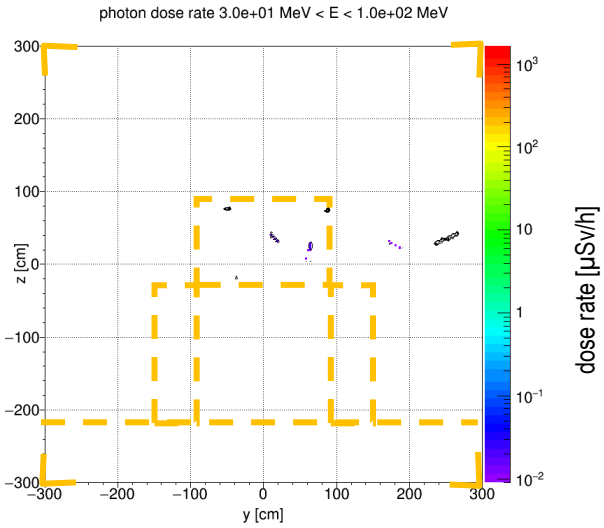

Fig. 47: Generated gamma dose rate distribution in the energy range between 30MeV and 100MeV in the vertical area. The red line is the 1µSv/h border.

2.3 Influence of a 2cm boron carbide layer between the steel layer and the concrete layer on the neutron dose rate (version without gaps for the pillars)

In the common guide shielding video conference on 25.10.2018 a 2cm B_4C layer between the steel and the concrete layer was proposed in order to decrease the neutron transmission in the energy region around 1MeV. The effect was tested by including this layer in the Monte Carlo model of the ODIN guide shielding described in the last section (without gaps for the pillars). The concrete layer thickness was adjusted to 58cm to get the same total shielding thickness as in the last section. Everything else is identical to the model described in the last section (e.g. same fictive neutron source). The density of the B_4C layer is assumed to be 1.8 g/cm^3.

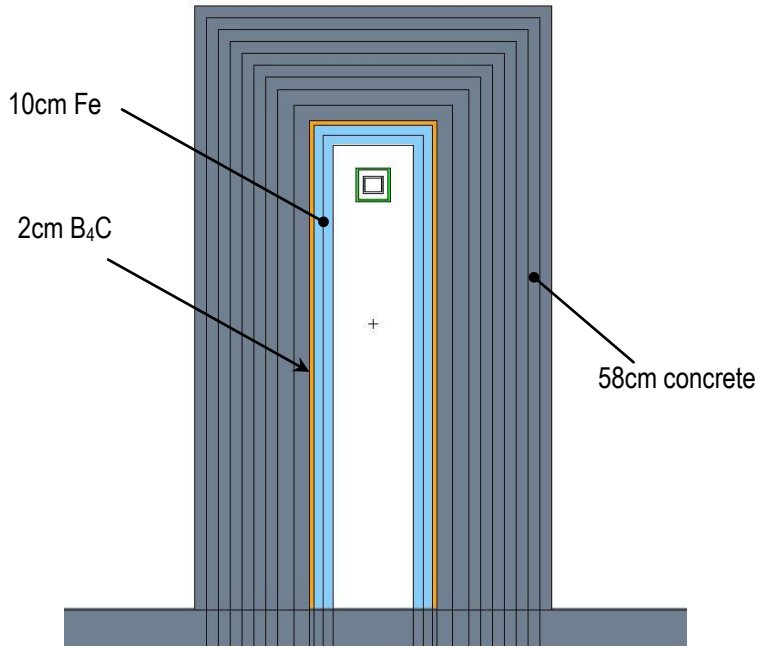

Fig. 48: Vertical cut through the guide shielding with boroncarbide layer

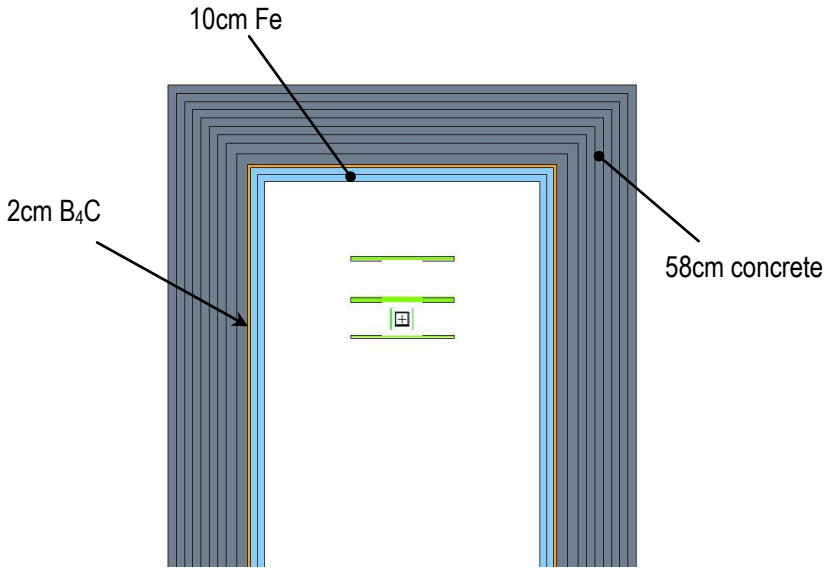

Fig. 49: Vertical cut through the chopper pit with boroncarbide layer

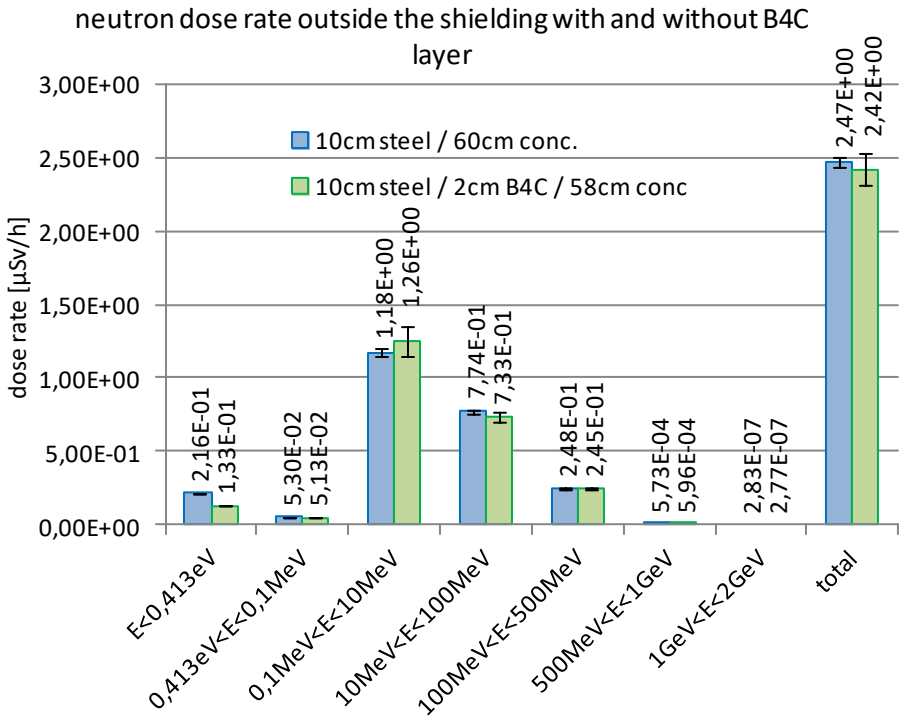

Fig. 50: Neutron dose rates outside the shielding (2.7m from the beam axis) with and without B_4C layer

Conclusion: No significant difference in the neutron dose rate above the thermal energy region can be observed.

3 Preliminary common guide shielding version 2 (10cm Fe; 50cm conc.)

Shielding version 2 consists of a 10cm layer of borated concrete, a 10cm layer of steel and a 50cm layer of ordinary concrete (from inside to outside). The inner layer of borated concrete is only used to minimize the activation of the shielding material. The shielding must reach the desired dose rate level without borated concrete (because the borated concrete layer is an option that will not be used by every instrument at ESS). Hence the borated concrete layer is considered as vacuum in the simulations presented in this chapter. The inner width of the shielding with borated concrete would be 40cm. Without borated concrete the inner width of the shielding is 60cm (which is the case for the simulations presented in this chapter).

The thicknesses of the steel and ordinary concrete layers are varied in further simulations.

3.1 New fictive neutron source

For the simulations in the last chapter a fictive neutron source at a distance of 24m from the focal point (fictive source at the bunkerwall) was used. However, there is an uncertainty in the beam divergency caused by this source. In the simulations presented in previous chapters/reports a fictive neutron source at the beginning of the neutron guide was applied (2m from the focal point). Even with this neutron source a problem occurs: The source yield of the fictive source is chosen in a way that the neutron flux at 5.5m from the focal point reaches the same value as with the simulations with the target model. However, the fictive neutron source at 2m causes at 5.5m a higher beam divergency compared to a fictive neutron source at 0m (at the focal point). Due to the higher beam divergency less neutrons will reach positions at large distances downstream the neutron guide. Test simulations with fictive neutron sources at the focal point (0m) and at the beginning of the neutron guide (2m), which both causes the same neutron flux at 5.5m from the focal point, showed that the neutron flux at 28m (beginning of the guide shielding) differs by ca. a factor of two. The diagram below shows an approximation with point sources which show the same effect.

For the simulations presented in this chapter a fictive neutron source at location of the focal point is applied (source area: 6cm (w) x 3cm (h)).

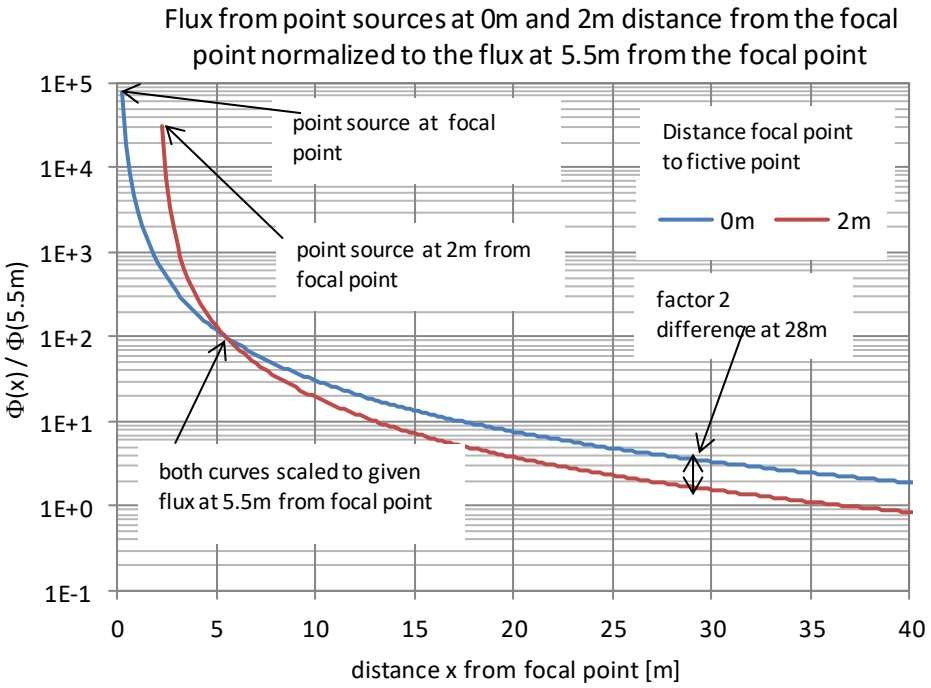

Fig. 51: Flux from point sources at 0m and 2m distance from the focal point normalized to the flux at 5.5m from the focal point

Similar to the last chapter the CSPEC source data (D. di Julio) is used as it is higher than the simulated ODIN source data (F. Grünauer) in order to obtain conservative results. However, in the last chapter CSPEC flux data at 5.5m from the focal point for the tilted CPEC channel was applied. In this chapter corresponding data for a direct channel is applied (neutron flux at 5.5m increases from $1.42 \cdot 10^{10}$ $cm^{-2}sec^{-1}$ to $1.82 \cdot 10^{10}$ $cm^{-2}sec^{-1}$)

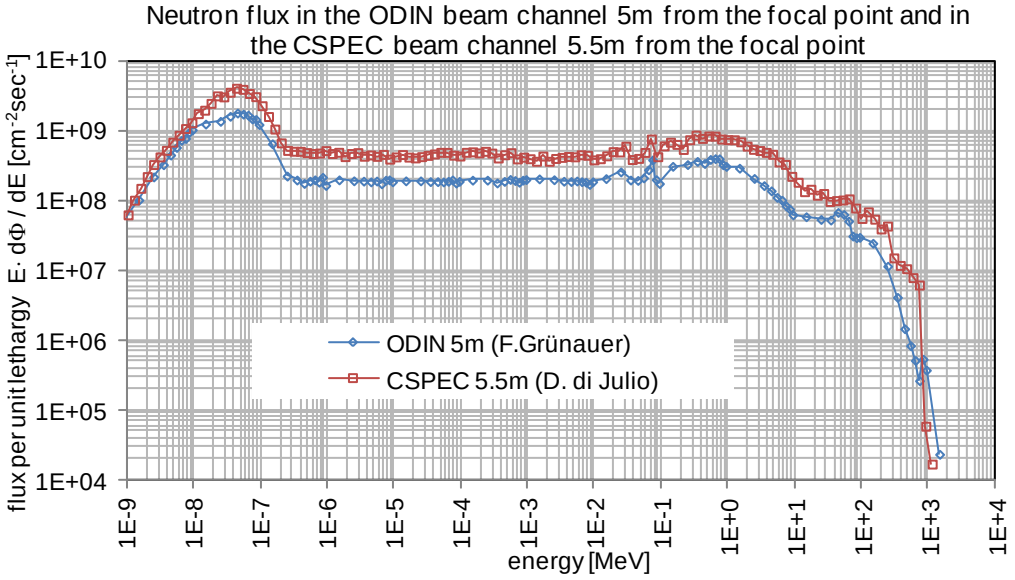

Fig. 52: Neutron flux in the ODIN beam channel 5m from the focal point and in the CSPEC beam channel 5.5m from the focal point

3.2 Monte Carlo model

Technical drawings of the common guide shielding version 2 and plots of the Monte Carlo model are shown in the following images.

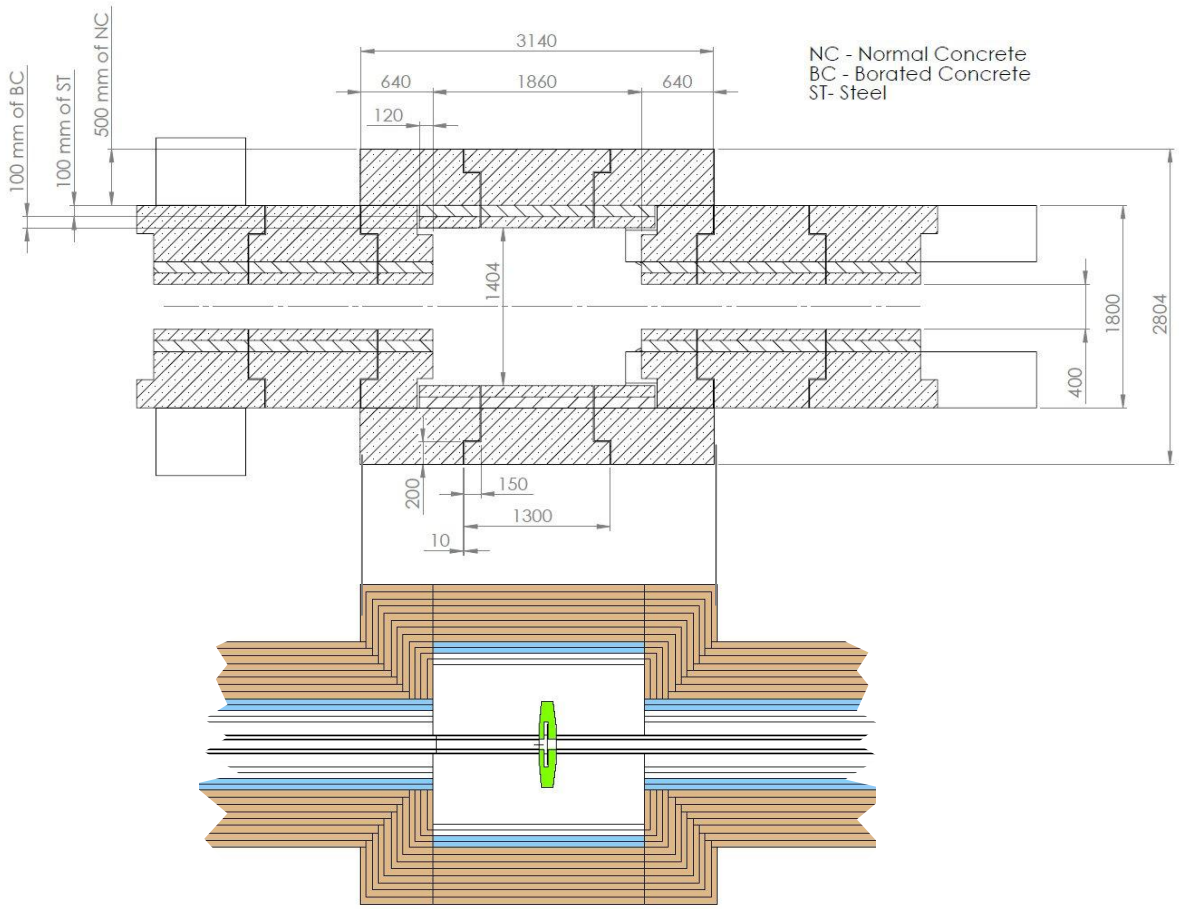

Fig. 53: Horizontal cut through the chopper pit. Top: Drawing; bottom: Monte Carlo model

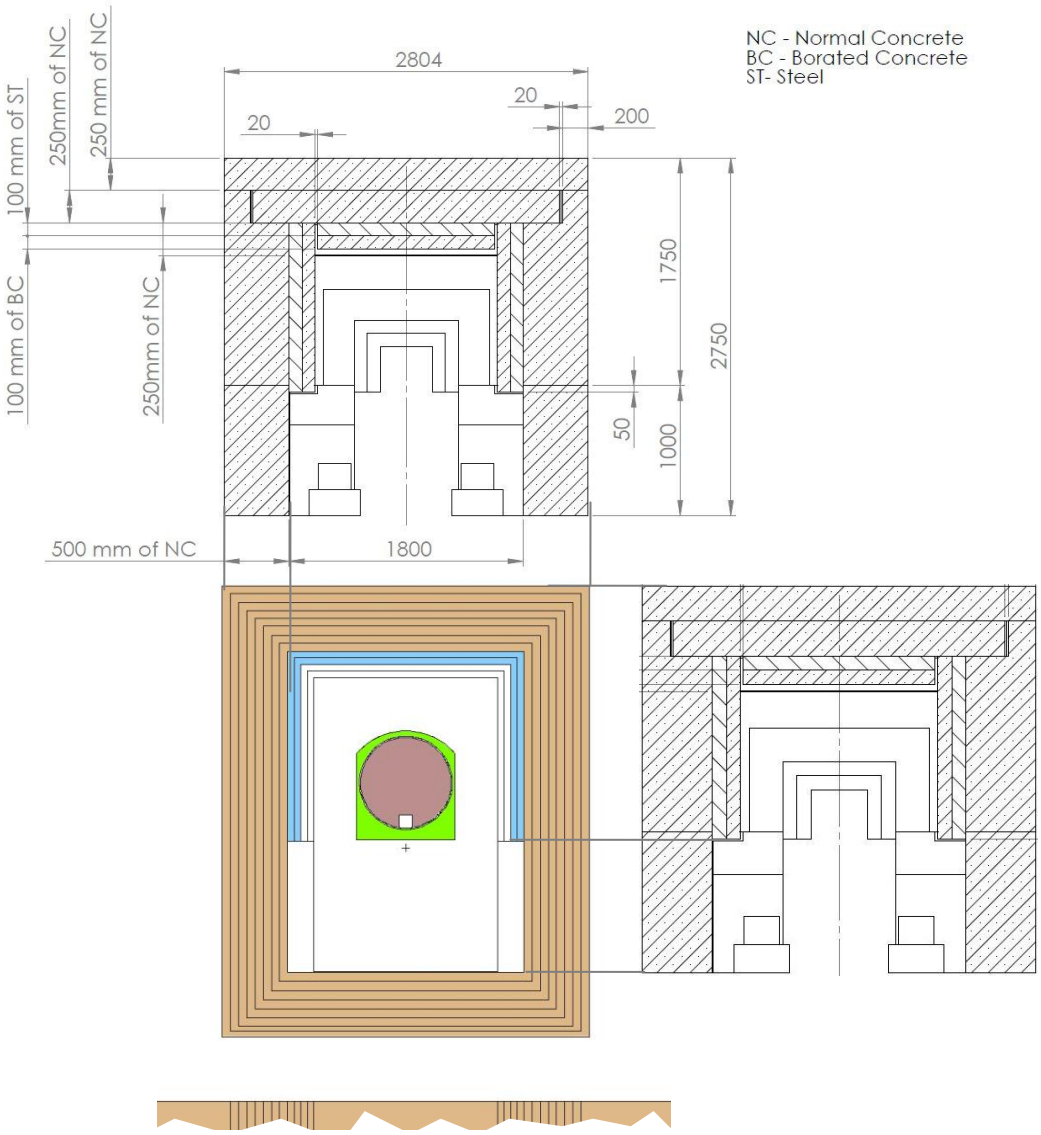

Fig. 54: Vertical cut through the chopper pit. Top: Drawing; bottom: Monte Carlo model

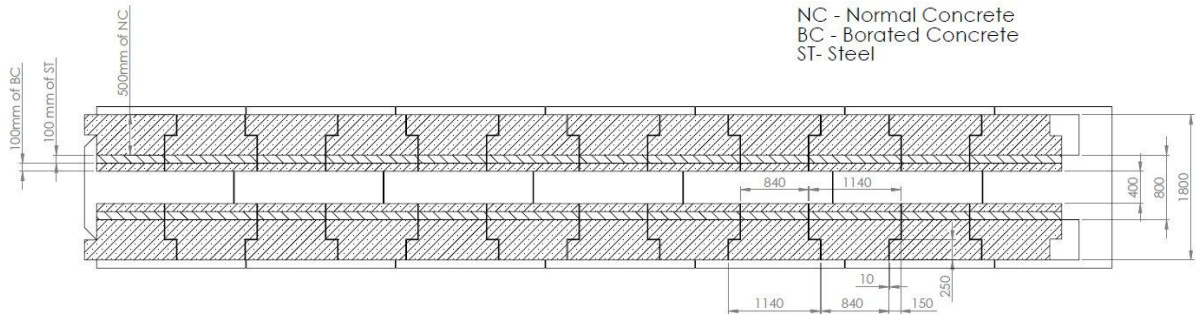

Fig. 55: Horizontal cut through the guide shielding (drawing).

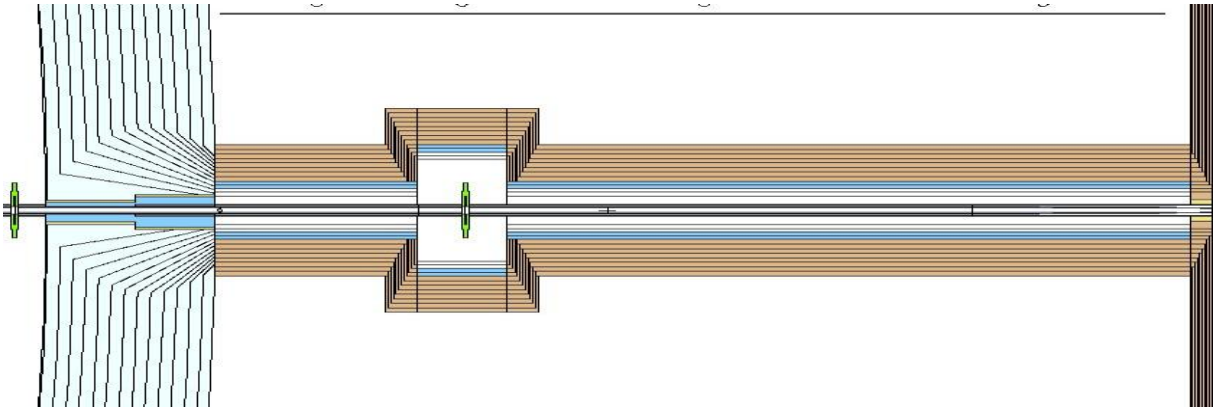

Fig. 56: Horizontal cut through the guide shielding (Monte Carlo model).

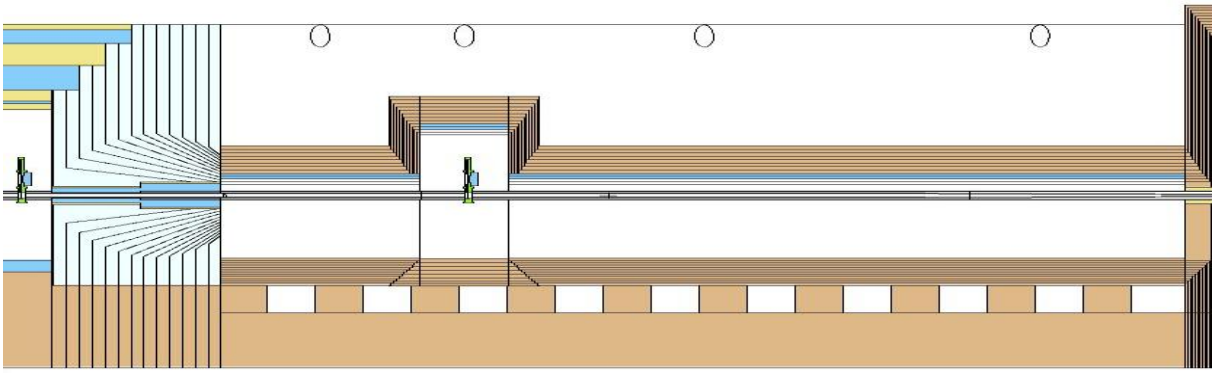

Fig. 57: Vertical cut through the guide shielding (Monte Carlo model).

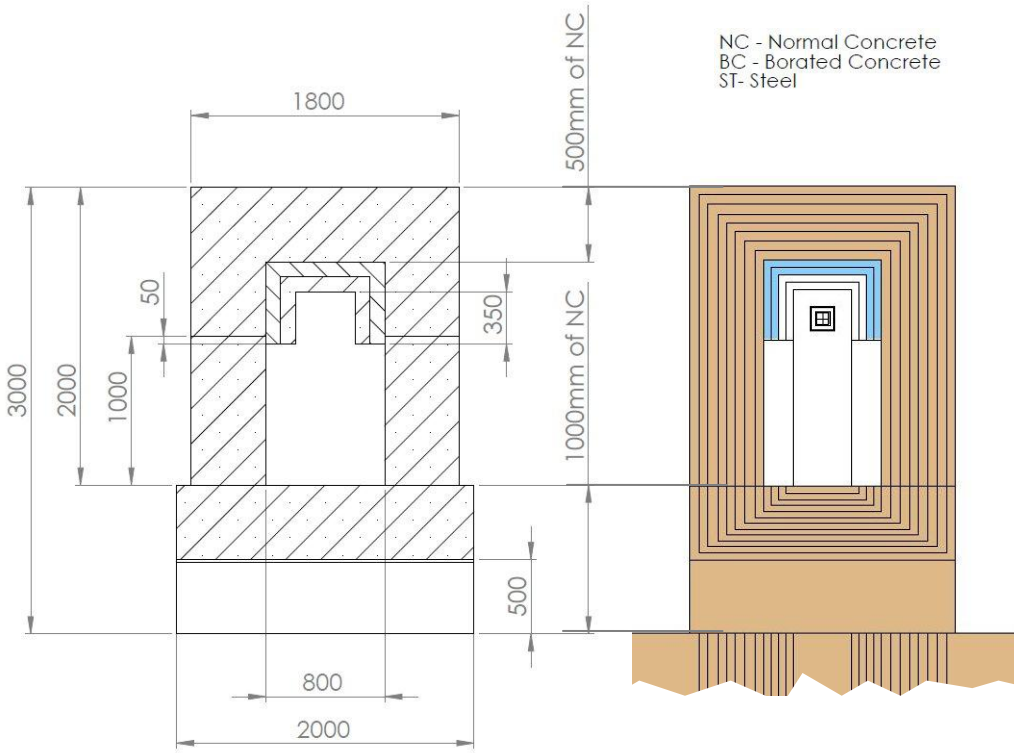

Fig. 58: Vertical cut through the guide shielding perpendicular to the beam axis (Monte Carlo model).

3.3 Results for the original version 2 (10cm steel, 50cm ordinary concrete)

The original version 2 of the guide shielding consists of 10cm steel and 50cm ordinary concrete. The dose rate distributions for this version are shown in this section. In following sections the results for increased shielding thicknesses are presented.

3.3.1 Horizontal neutron dose rate distribution

The image below shows an horizontal area through the Monte Carlo model of the ODIN instrument for which the neutron dose rate distributions are presented in the following images.

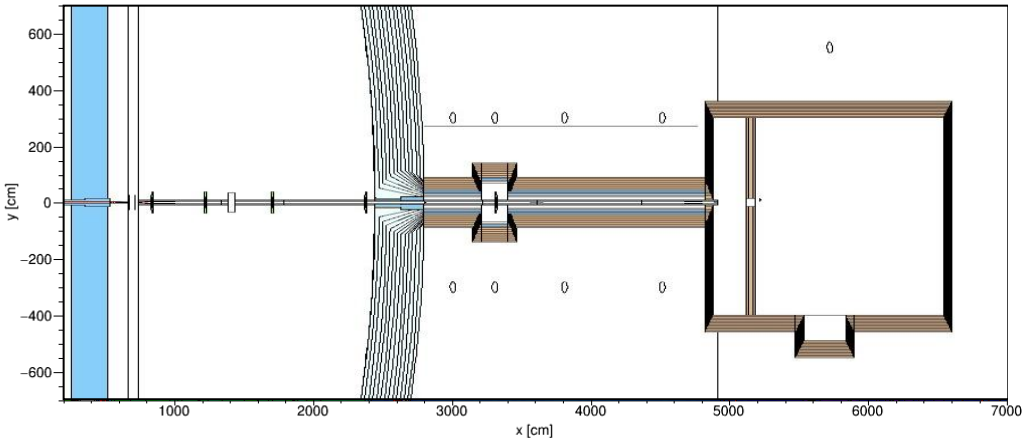

Fig. 59: Horizontal area through the Monte Carlo model of the ODIN instrument for which the radiation distributions are shown in the following images

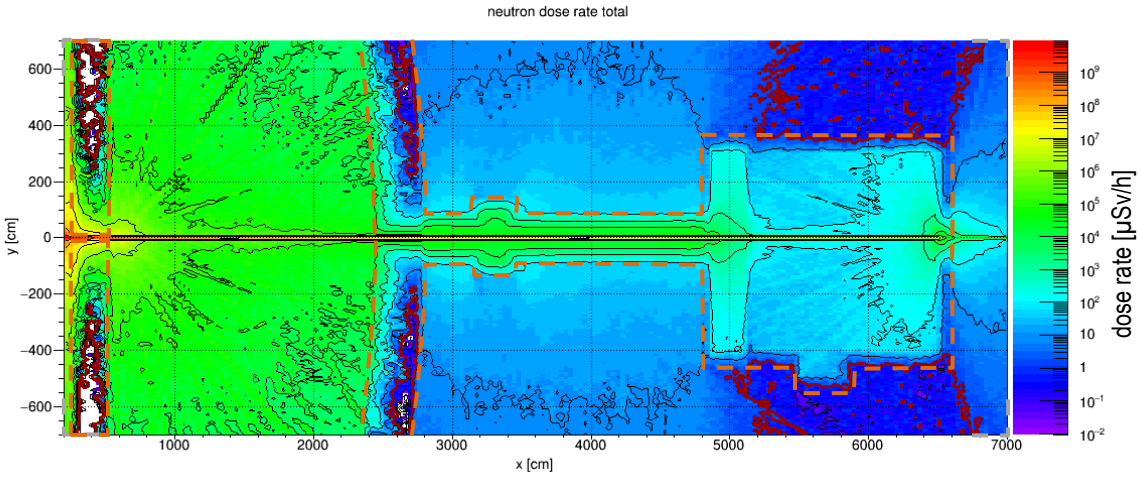

Fig. 60: Total neutron dose rate distribution in the horizontal area. The red line is the 1µSv/h border.

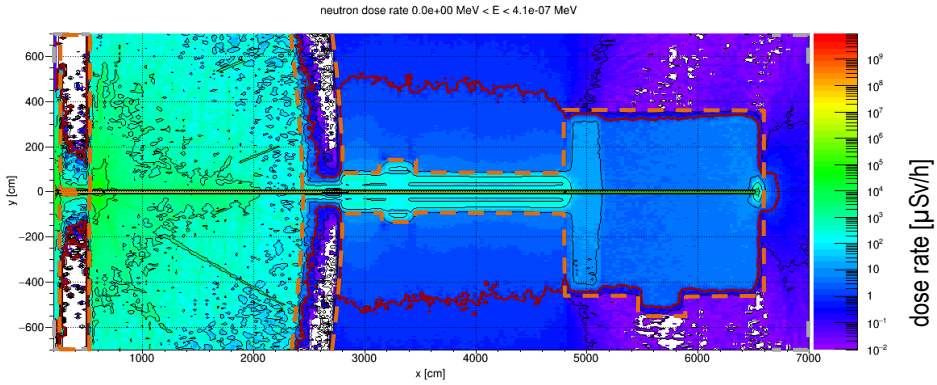

Fig. 61: Neutron dose rate distribution in the energy range below 0.41eV in the horizontal area. The red line is the 1µSv/h border.

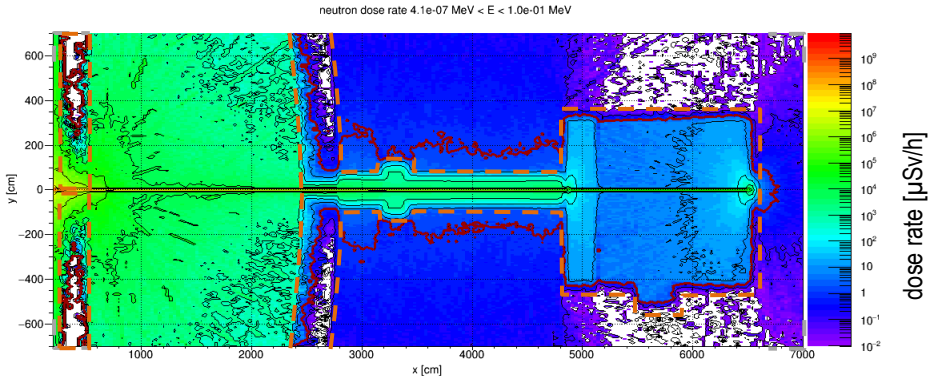

Fig. 62: Neutron dose rate distribution in the energy range between 0.41eV and 0.1MeV in the horizontal area. The red line is the 1µSv/h border.

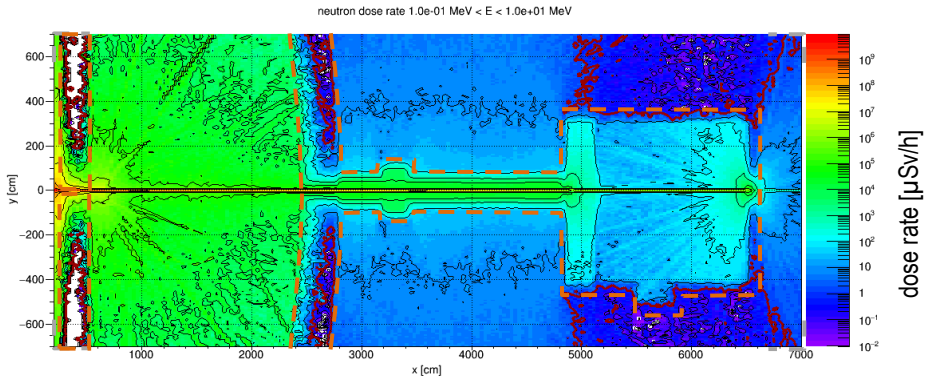

Fig. 63: Neutron dose rate distribution in the energy range between 0.1MeV and 10MeV in the horizontal area. The red line is the 1µSv/h border.

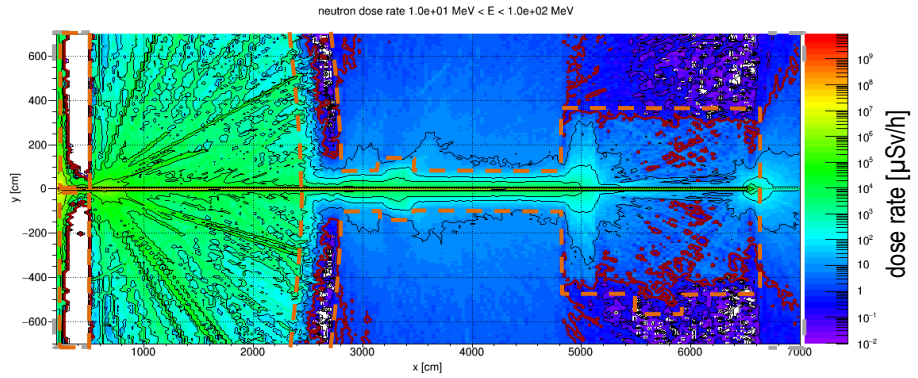

Fig. 64: Neutron dose rate distribution in the energy range between 10MeV and 100MeV in the horizontal area. The red line is the 1µSv/h border.

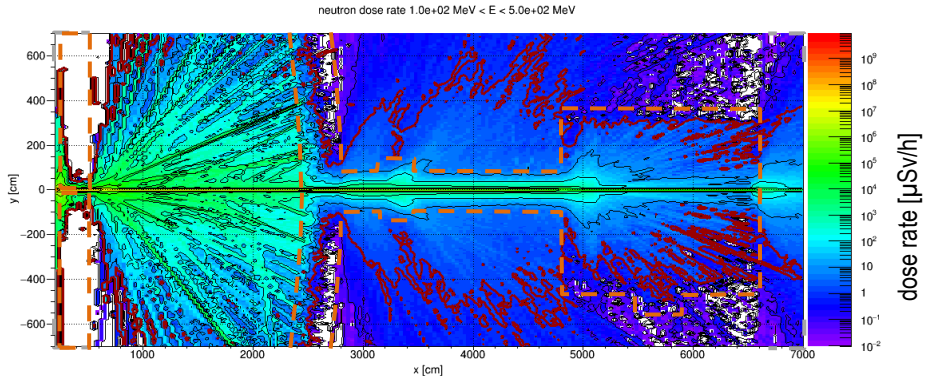

Fig. 65: Neutron dose rate distribution in the energy range between 100MeV and 500MeV in the horizontal area. The red line is the 1µSv/h border.

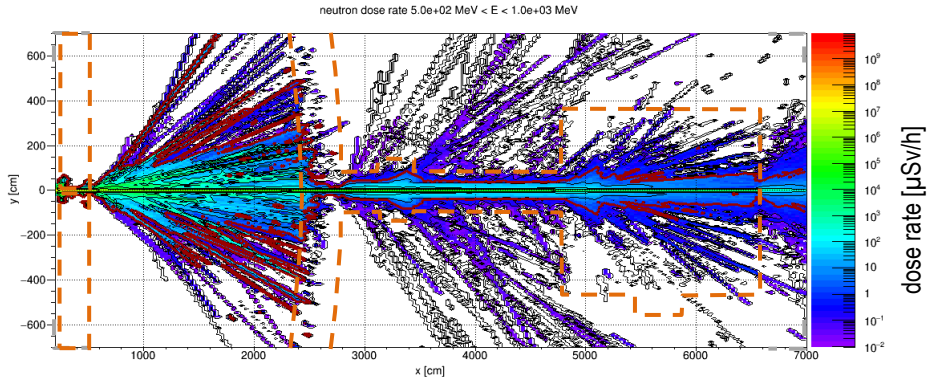

Fig. 66: Neutron dose rate distribution in the energy range between 500MeV and 1GeV in the horizontal area. The red line is the 1µSv/h border.

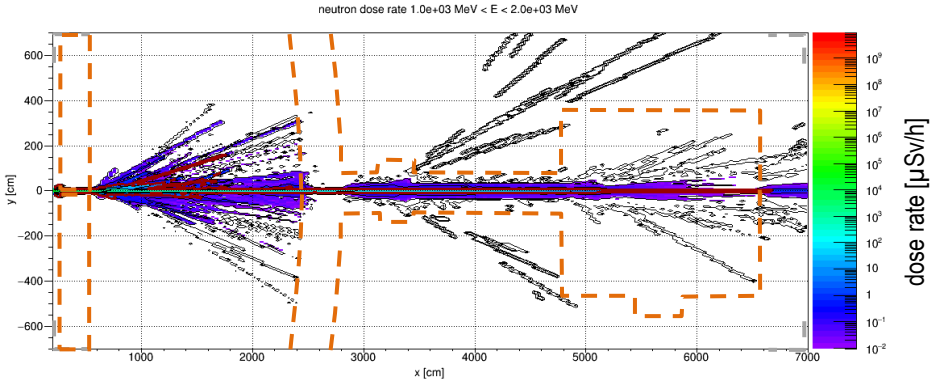

Fig. 67: Neutron dose rate distribution in the energy range between 1GeV and 2GeV in the horizontal area. The red line is the 1µSv/h border.

3.3.2 Horizontal generated gamma dose rate distribution

The image below shows an horizontal area through the Monte Carlo model of the ODIN instrument for which the generated gamma dose rate distributions are presented in the following images.

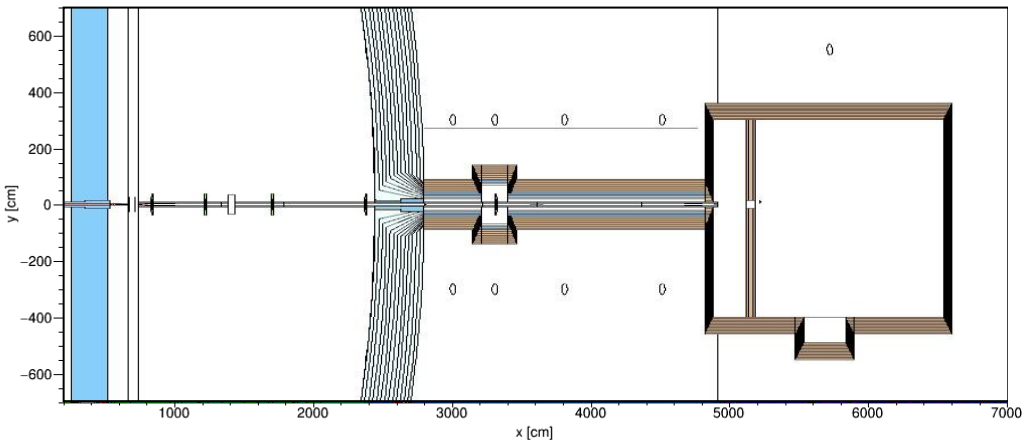

Fig. 68: Horizontal area through the Monte Carlo model of the ODIN instrument for which the radiation distributions are shown in the following images

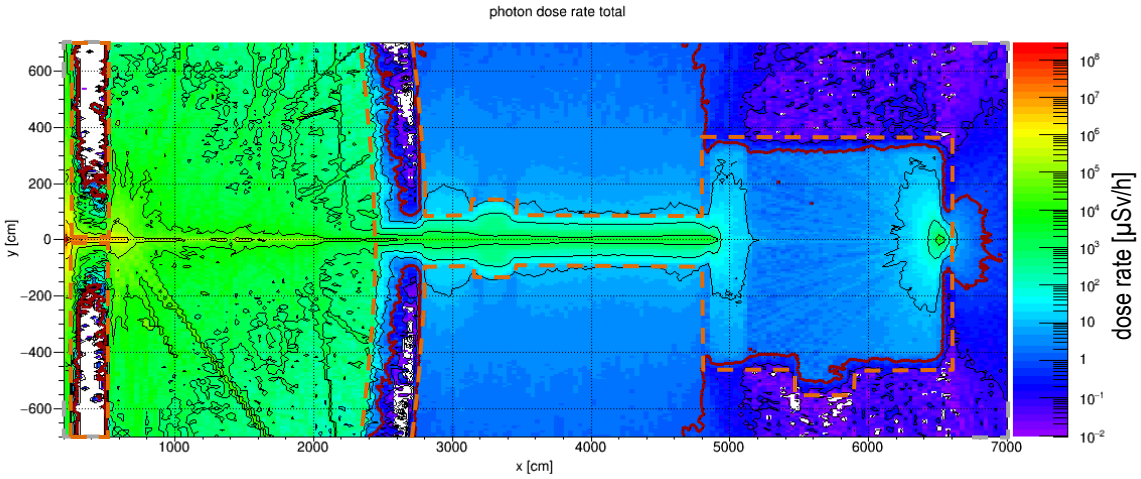

Fig. 69: Total generated gamma dose rate distribution in the horizontal area. The red line is the 1µSv/h border.

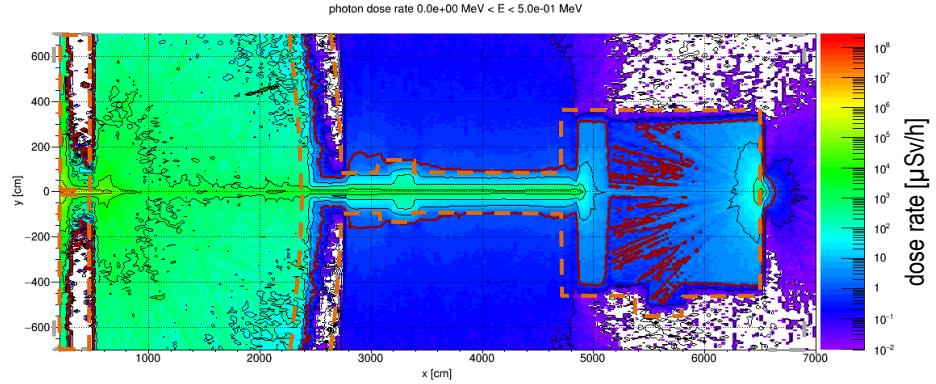

Fig. 70: Generated gamma dose rate distribution in the energy range below 0.5MeV in the horizontal area. The red line is the 1µSv/h border.

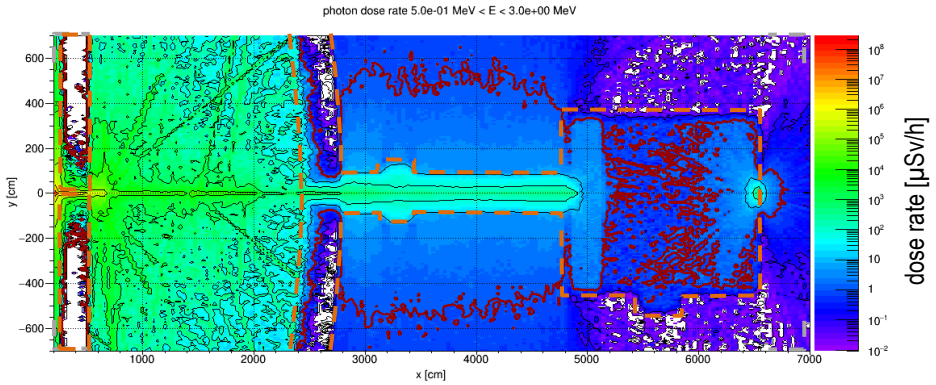

Fig. 71: Generated gamma dose rate distribution in the energy range between 0.5MeV and 3MeV in the horizontal area. The red line is the 1µSv/h border.

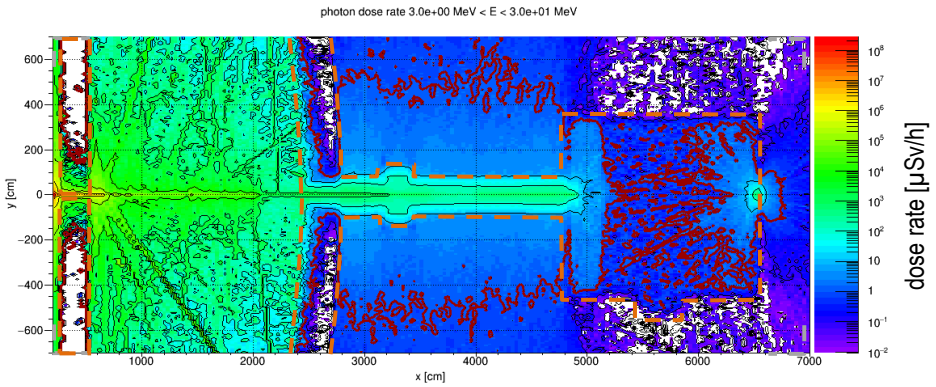

Fig. 72: Generated gamma dose rate distribution in the energy range between 3MeV and 30MeV in the horizontal area. The red line is the 1µSv/h border.

3.3.3 Vertical dose rate distributions

The image below shows a vertical area through the Monte Carlo model of the ODIN instrument (along the beam axis) for which the total neutron dose rate distribution and the total generated gamma dose rate distribution are presented in the following images.

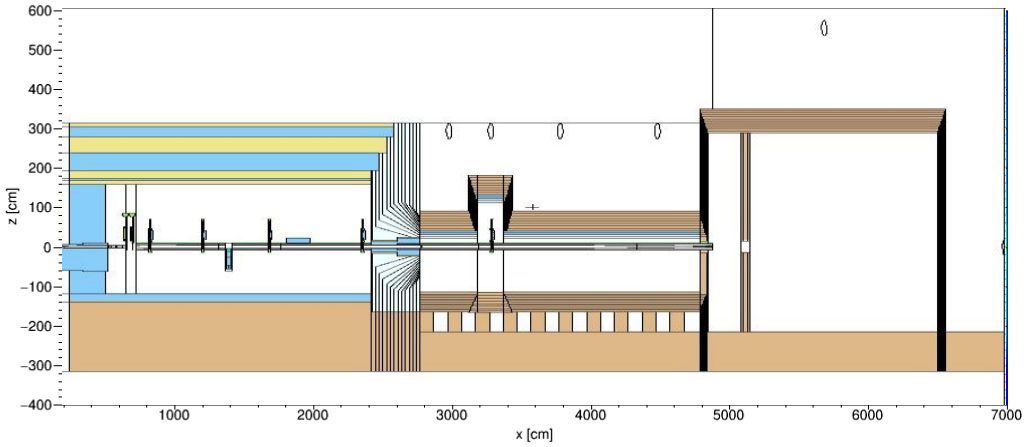

Fig. 73: Vertical area through the Monte Carlo model of the ODIN instrument for which the radiation distributions are shown in the following images

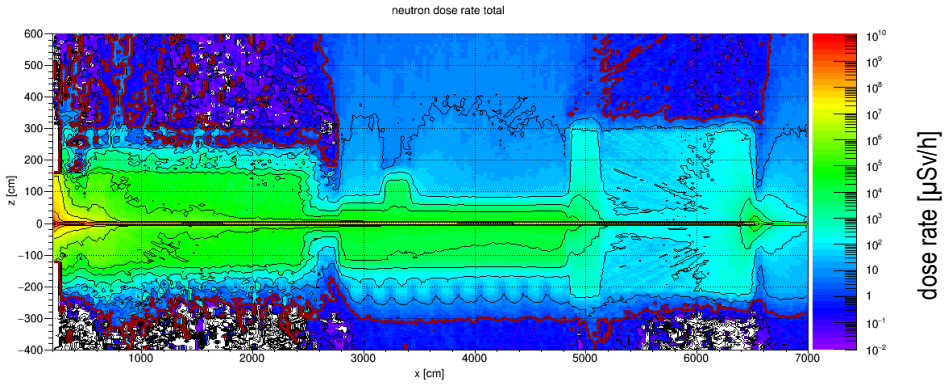

Fig. 74: Total neutron dose rate distribution in the vertical area. The red line is the 1µSv/h border.

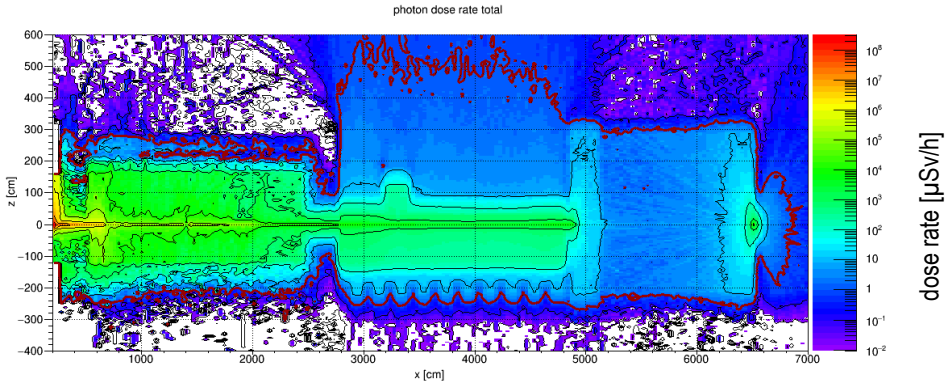

Fig. 75: Total generated gamma dose rate distribution in the vertical area. The red line is the 1µSv/h border.

3.3.4 Conclusions

With version 2 of the guide shielding consisting of a steel layer of 10cm thickness and an ordinary concrete layer of 50cm thickness a neutron dose rate of ca. 100µSv/h and a generated gamma dose rate of ca. 10µSv/h is reached on the outer surface of the shielding.

3.4 Variation of the steel/concrete thickness

In this section the steel thickness t(steel) is varied and the concrete thickness t(conc) is adjusted: t(conc)=90cm-t(steel). The neutron dose rate distributions in a vertical plane perpendicular to the beam axis at a distance of 40m from the focal point are presented.

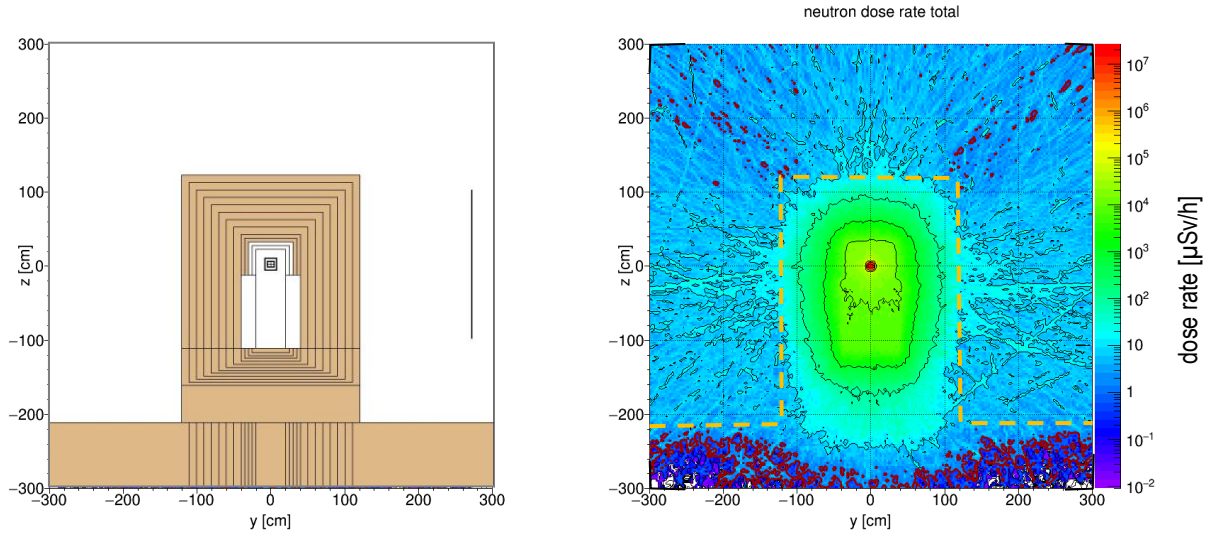

Fig. 76: Vertical plane through the Monte Carlo model of the guide shielding consisting of 90cm ordinary concrete (40m from the focal point, left hand side) and neutron dose rate distribution in the plane (right hand side)

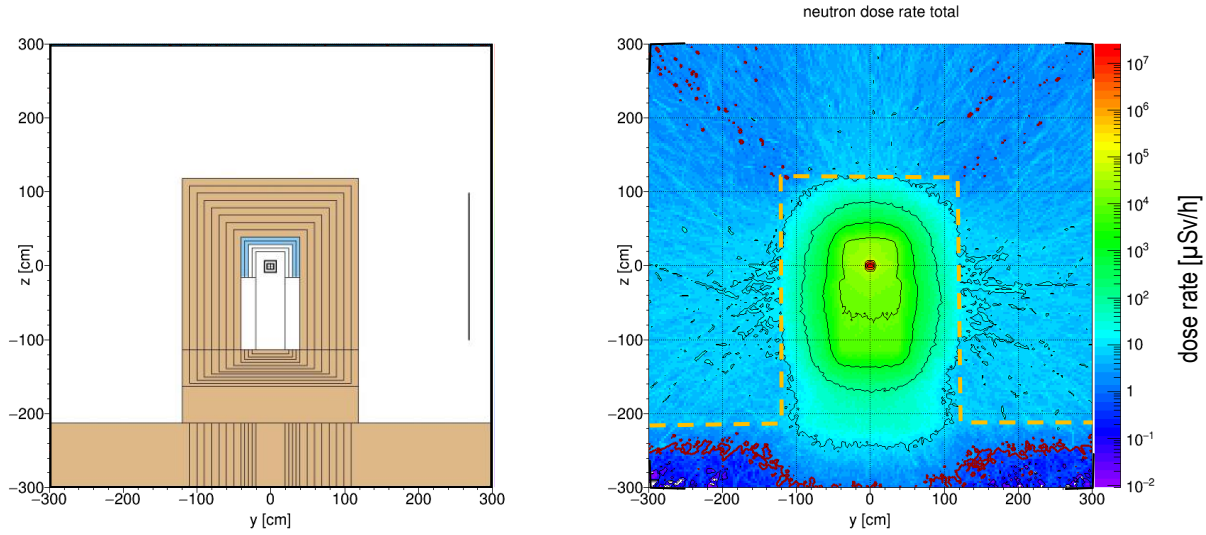

Fig. 77: Vertical plane through the Monte Carlo model of the guide shielding consisting of 10cm steel and 80cm ordinary concrete (40m from the focal point, left hand side) and neutron dose rate distribution in the plane (right hand side)

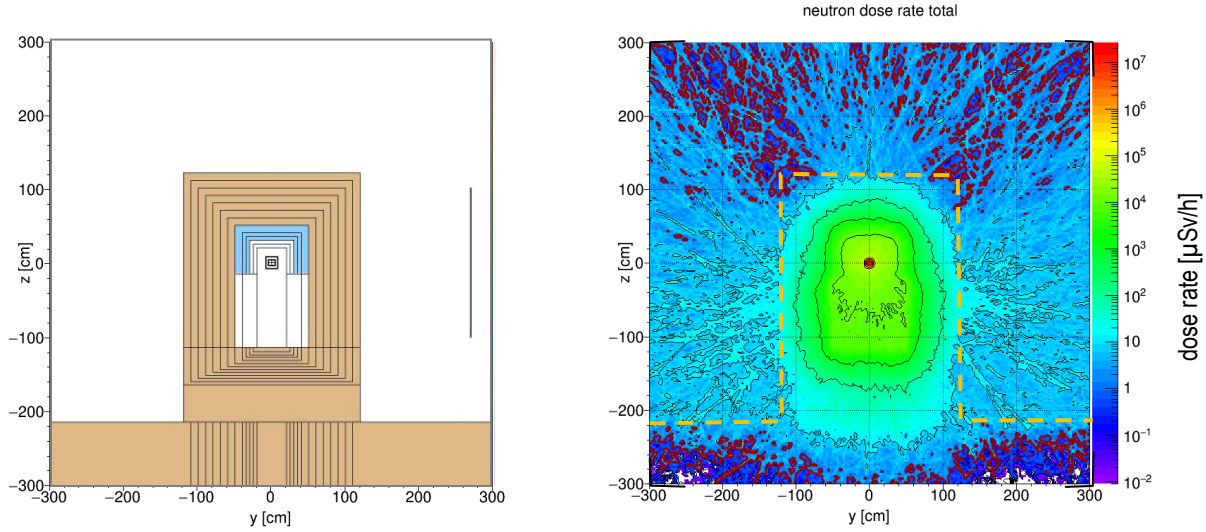

Fig. 78: Vertical plane through the Monte Carlo model of the guide shielding consisting of 20cm steel and 70cm ordinary concrete (40m from the focal point, left hand side) and neutron dose rate distribution in the plane (right hand side)

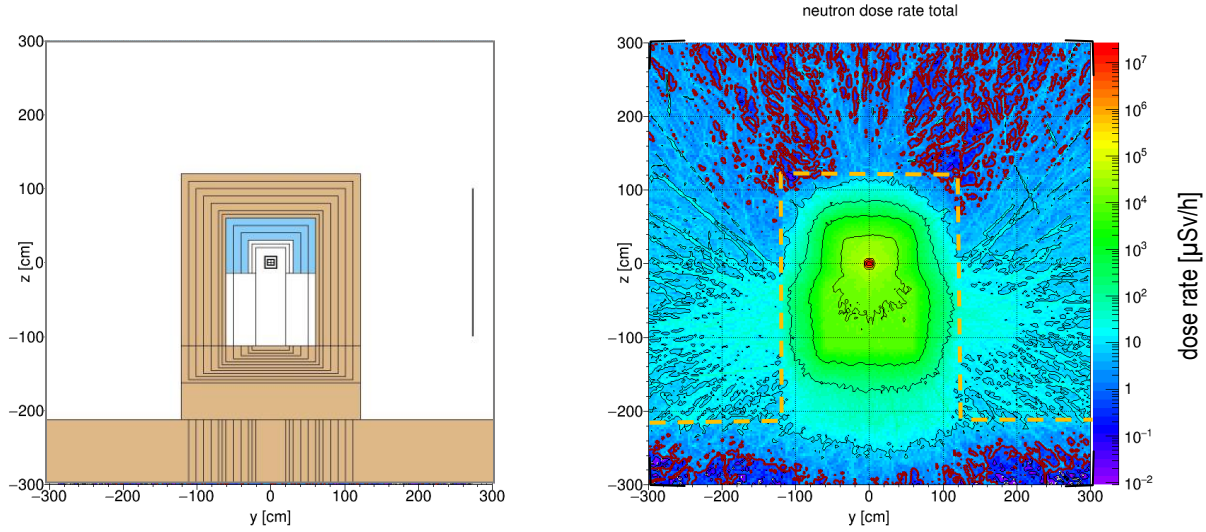

Fig. 79: Vertical plane through the Monte Carlo model of the guide shielding consisting of 30cm steel and 60cm ordinary concrete (40m from the focal point, left hand side) and neutron dose rate distribution in the plane (right hand side)

3.4.1 Conclusions

The neutron dose rate outside the shielding decreases with increasing steel thickness (which can be seen at the roof of the shielding) up to at least 30cm steel thickness but a leakage below the steel layer occurs which becomes more important for increasing steel thickness.

3.5 Influence of the vertical length of the steel layer

The inner steel layer of the shielding is not extended to the inner bottom of the shielding but ends at a height of z=-15cm respective to the beam axis. As shown in the last section a radiation leakage occurs below the steel layer. In the following sections results for steel liners ending at -15cm and at -100cm are compared for shieldings with different steel layer thicknesses. The concrete layer thickness t(conc) is in all cases t(conc)=90cm-t(steel).

3.5.1 10cm steel and 80cm ordinary concrete shielding

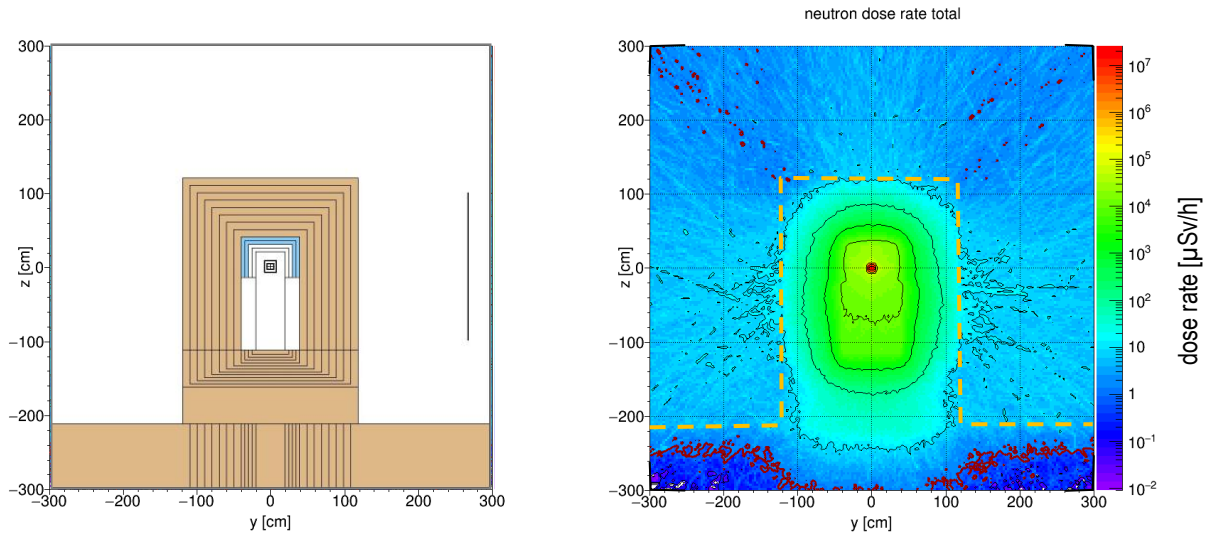

Fig. 80: Vertical plane through the Monte Carlo model of the guide shielding with a lower steel shielding border at -15cm below the beam axis (40m from the focal point, left hand side) and neutron dose rate distribution in the plane (right hand side)

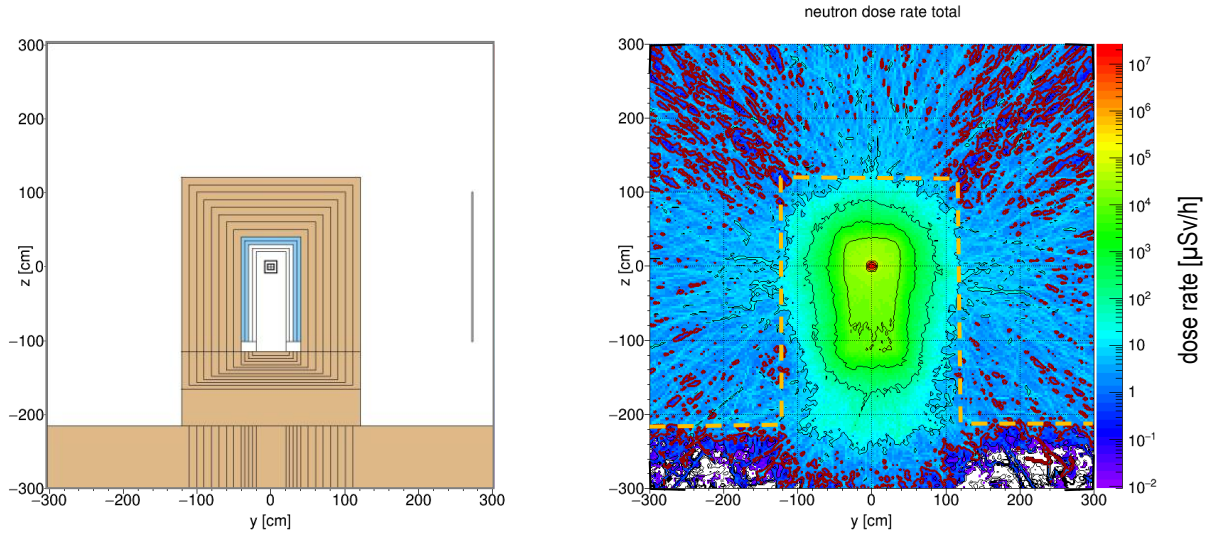

Fig. 81: Vertical plane through the Monte Carlo model of the guide shielding with a lower steel shielding border at -100cm below the beam axis (40m from the focal point, left hand side) and neutron dose rate distribution in the plane (right hand side)

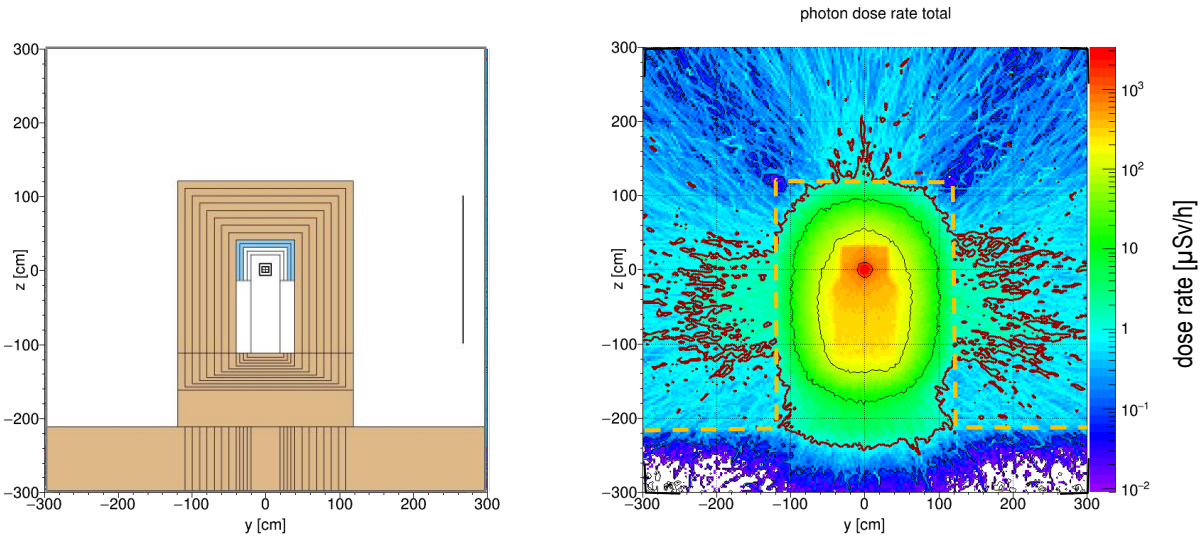

Fig. 82: Vertical plane through the Monte Carlo model of the guide shielding with a lower steel shielding border at -15cm below the beam axis (40m from the focal point, left hand side) and generated gamma dose rate distribution in the plane (right hand side)

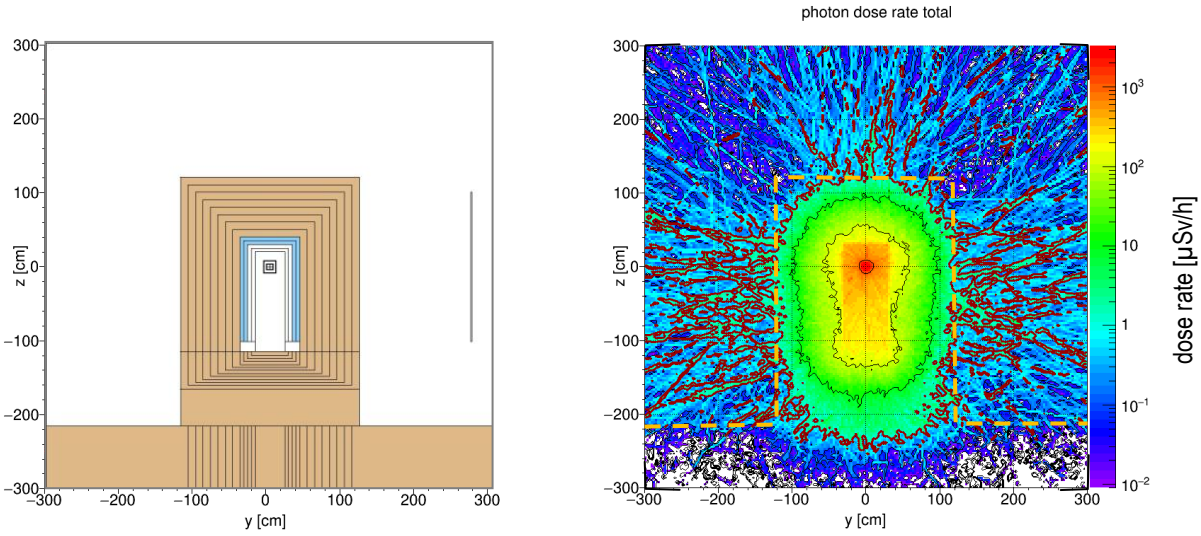

Fig. 83: Vertical plane through the Monte Carlo model of the guide shielding with a lower steel shielding border at -100cm below the beam axis (40m from the focal point, left hand side) and generated gamma dose rate distribution in the plane (right hand side)

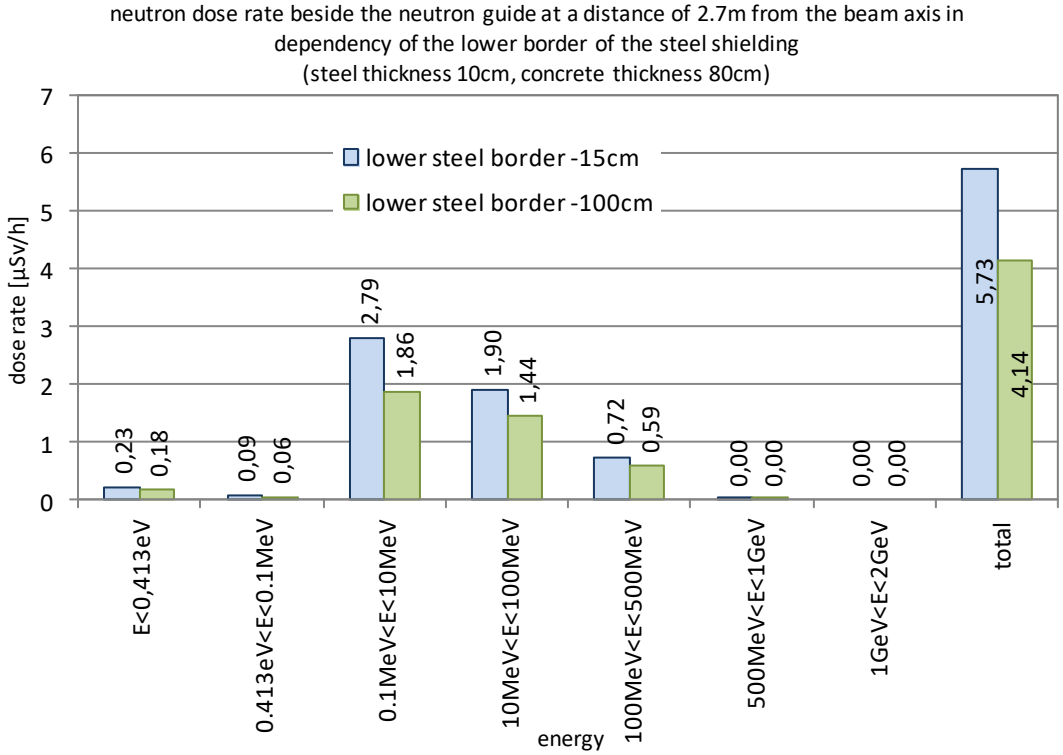

Fig. 84: neutron dose rate beside the neutron guide at a distance of 2.7m from the beam axis in dependency of the lower border of the steel shielding (steel thickness 10cm, concrete thickness 80cm)

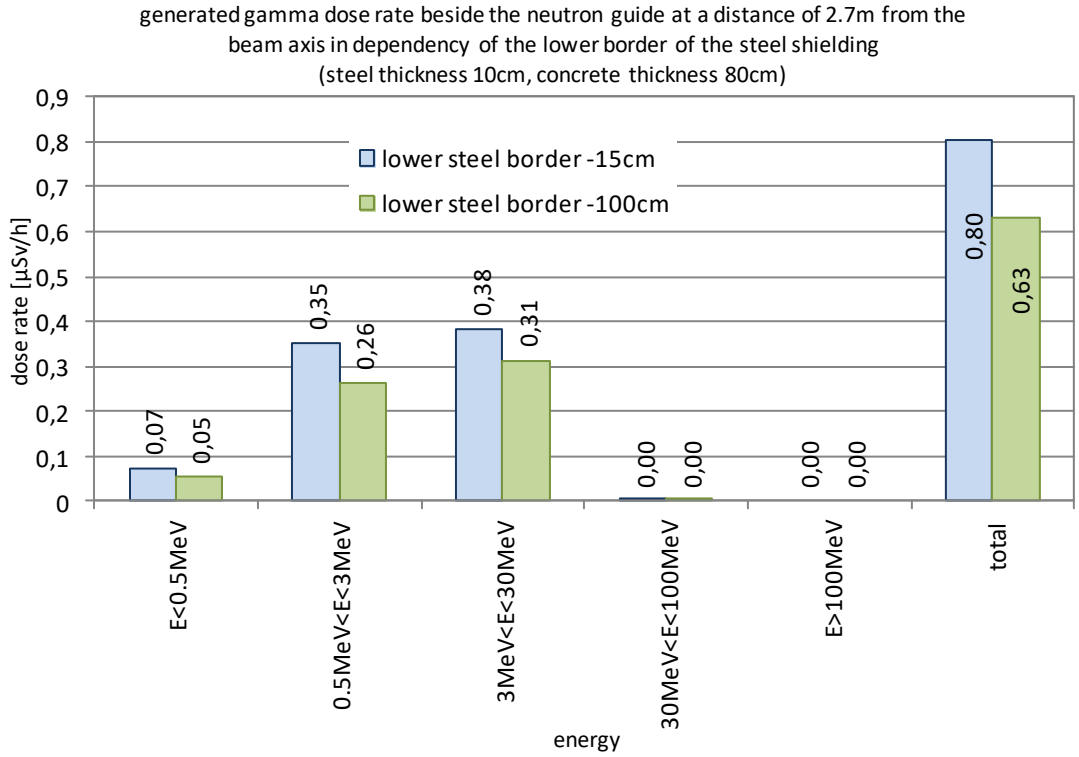

Fig. 85: generated gamma dose rate beside the neutron guide at a distance of 2.7m from the beam axis in dependency of the lower border of the steel shielding (steel thickness 10cm, concrete thickness 80cm)

3.5.2 20cm steel and 70cm ordinary concrete shielding

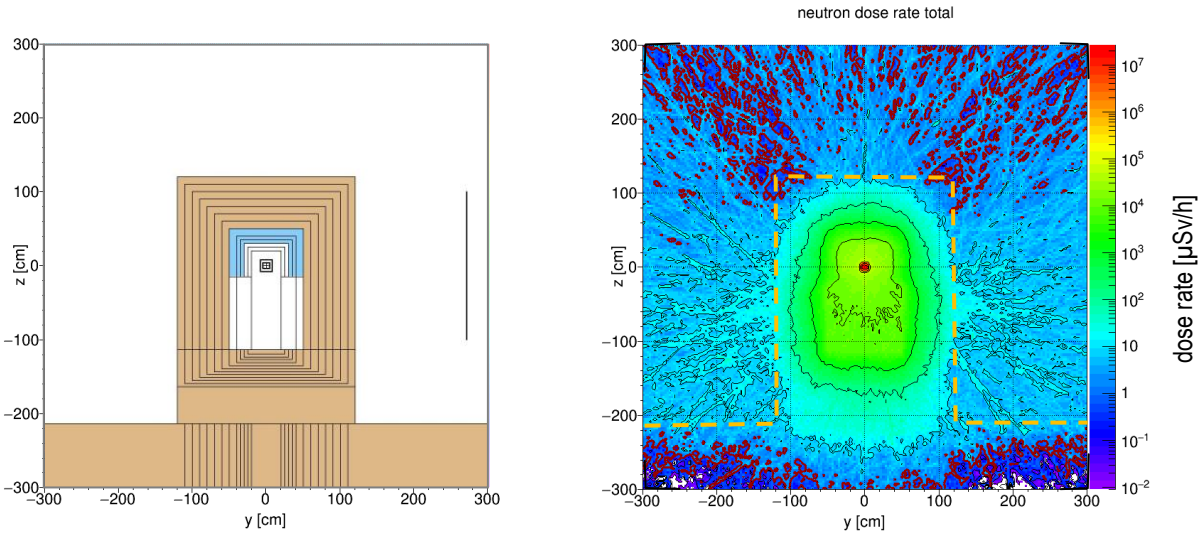

Fig. 86: Vertical plane through the Monte Carlo model of the guide shielding with a lower steel shielding border at -15cm below the beam axis (40m from the focal point, left hand side) and neutron dose rate distribution in the plane (right hand side)

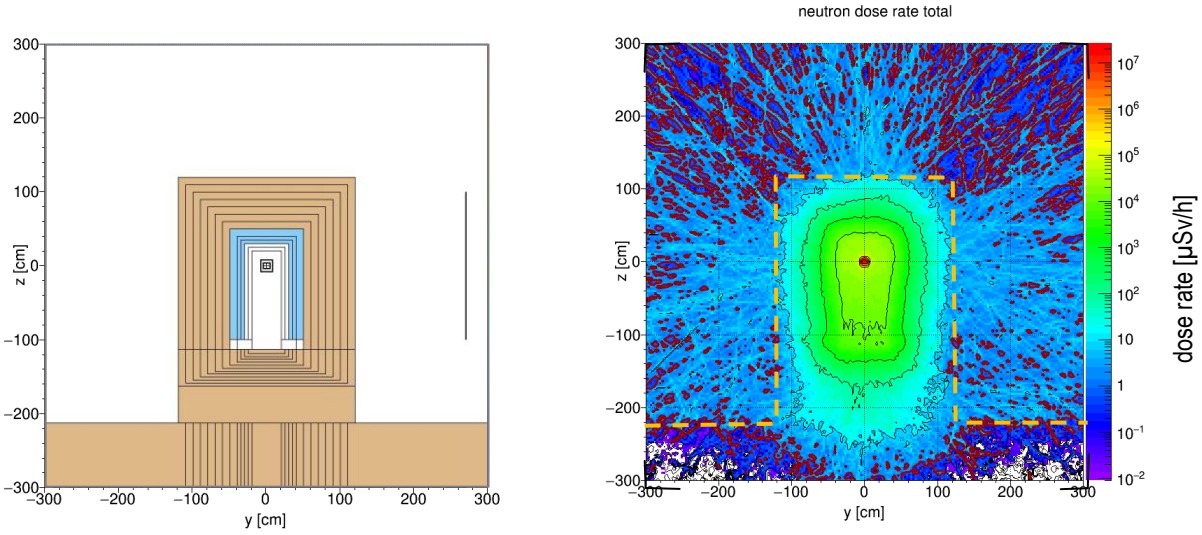

Fig. 87: Vertical plane through the Monte Carlo model of the guide shielding with a lower steel shielding border at -100cm below the beam axis (40m from the focal point, left hand side) and neutron dose rate distribution in the plane (right hand side)

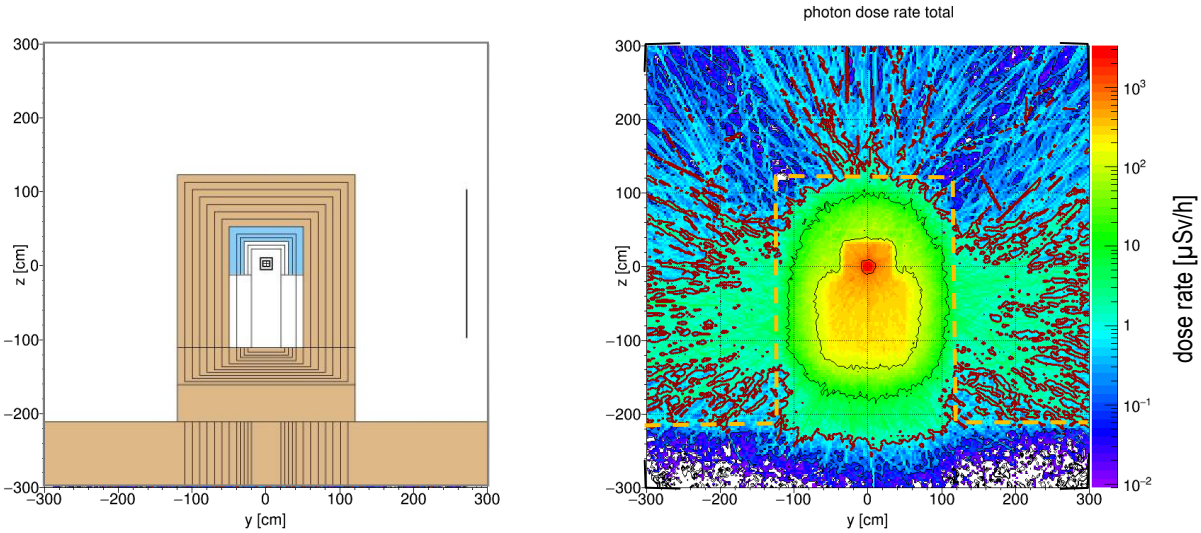

Fig. 88: Vertical plane through the Monte Carlo model of the guide shielding with a lower steel shielding border at -15cm below the beam axis (40m from the focal point, left hand side) and generated gamma dose rate distribution in the plane (right hand side)

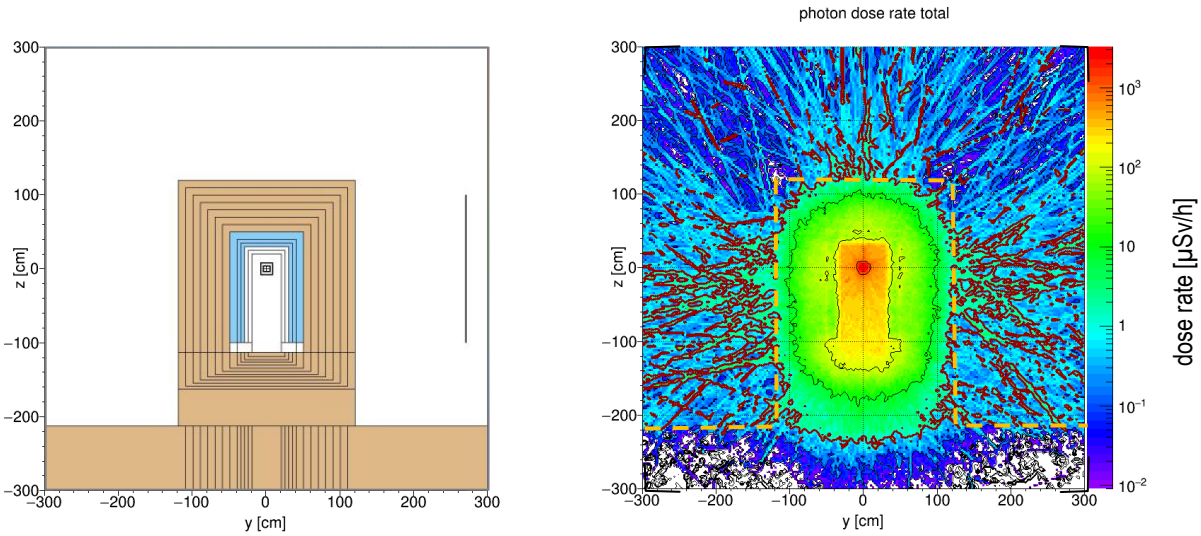

Fig. 89: Vertical plane through the Monte Carlo model of the guide shielding with a lower steel shielding border at -100cm below the beam axis (40m from the focal point, left hand side) and generated gamma dose rate distribution in the plane (right hand side)

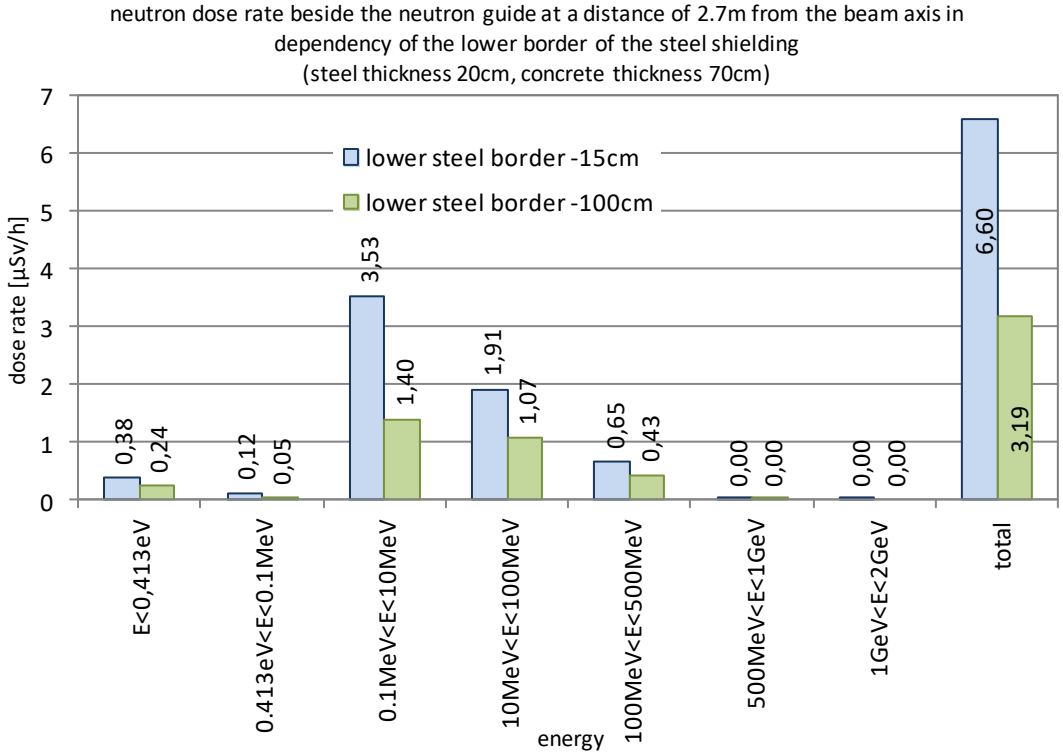

Fig. 90: neutron dose rate beside the neutron guide at a distance of 2.7m from the beam axis in dependency of the lower border of the steel shielding (steel thickness 20cm, concrete thickness 70cm)

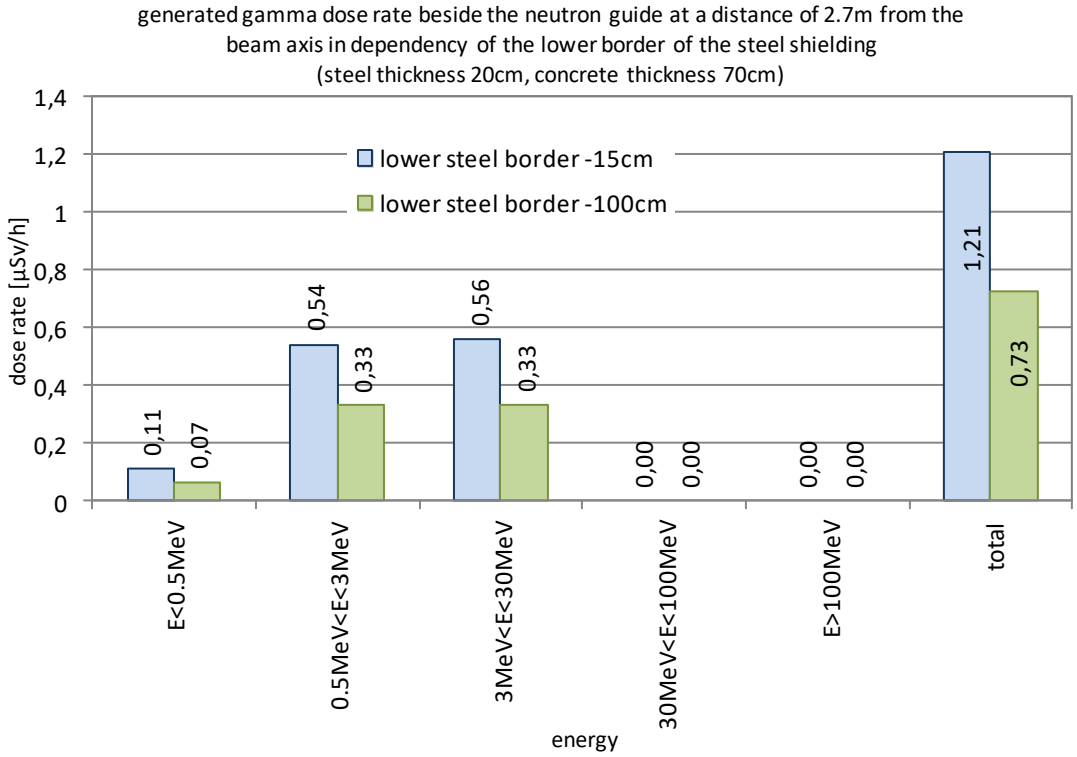

Fig. 91: generated gamma dose rate beside the neutron guide at a distance of 2.7m from the beam axis in dependency of the lower border of the steel shielding (steel thickness 20cm, concrete thickness 70cm)

3.5.3 Conclusions

For a shielding consisting of 10cm steel and 80cm concrete the neutron dose rate beside the guide is a factor 1.38 increased for the steel liner ending at z=-15cm. The corresponding factor for gamma radiation is 1.27.

However, the previous results show that it is beneficial to increase the steel thickness.

For a shielding consisting of 20cm steel and 70cm concrete the neutron dose rate beside the guide is a factor 2.1 increased for the steel liner ending at z=-15cm. The corresponding factor for gamma radiation is 1.65.

The effect on the gamma dose rate is lower as on the neutron dose rate because a big component of the gamma radiation is created in the shielding materials itself (as shown in previous chapters).

The dose rate beside the guide shielding can be decreased considerably by shifting the lower end of the steel shielding downwards. The actual concept (lower end at z=-15cm) should be reviewed therefore.

4 Preliminary common guide shielding version 3 (20cm Fe; 70cm conc.)

4.1 New fictive neutron source

The same fictive neutron source at location of the focal point (source area 6cm (w) x 3cm (h)) as described in the last chapter is applied for the simulations presented in this chapter. Only the source yield was changed: In the common guide shielding video conference on 19.10.2018 it was discussed that the CSPEC data contains a safety factor of 1.4 for simulation of the bunker roof. For the next simulations the CSPEC data is divided by 1.4. The neutron flux at 5.5m from the focal point decreases from $1.82 \cdot 10^{10}$ $cm^{-2}sec^{-1}$ to $1.30 \cdot 10^{10}$ $cm^{-2}sec^{-1}$.

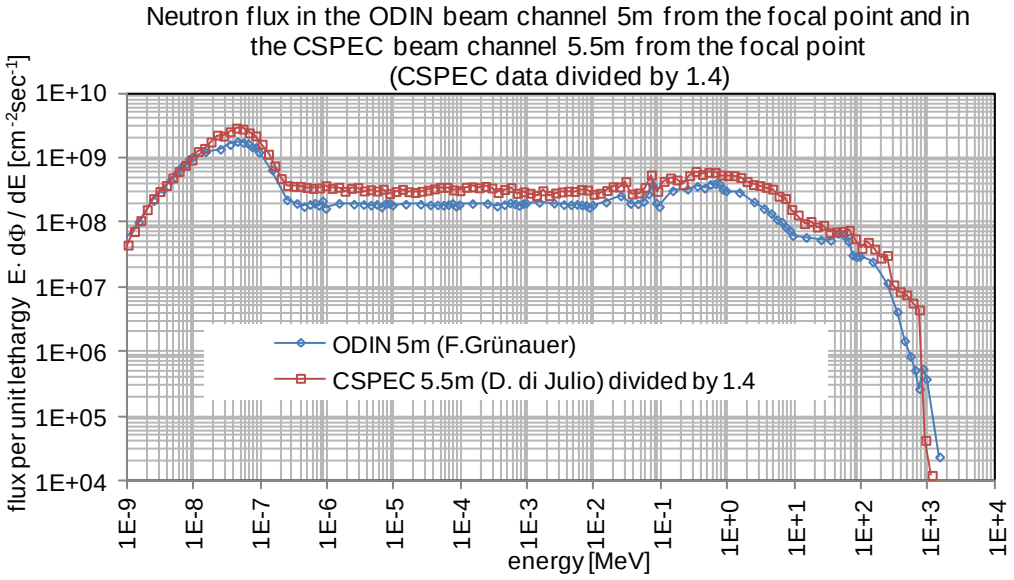

Fig. 92: Neutron flux in the ODIN beam channel 5m from the focal point and in the CSPEC beam channel 5.5m from the focal point (CSPEC data divided by 1.4)

4.2 Monte Carlo model

The Monte Carlo model of the common guide shielding version 3 is shown in the following images. It consists of a steel layer and an ordinary concrete layer. The steel layer has a thickness of 20cm and the concrete layer has a thickness of 70cm. Changes compared to the last version are:

1. The thickness of the inner borated concrete layers (set to vacuum in the simulations) was decreased from 10cm to 2cm. The inner width of the steel shielding around the guide is decreased from 60cm to 44cm therefore.
2. The inner width of the chopper pit was increased from 140.4cm to 160cm. The inner width of the steel shielding is now 164cm (borated concrete layers set to vacuum).
3. A 20cm steel layer was included below the neutron guide
4. The vertical steel layers in the chopper pit are extended to the floor of the pit.

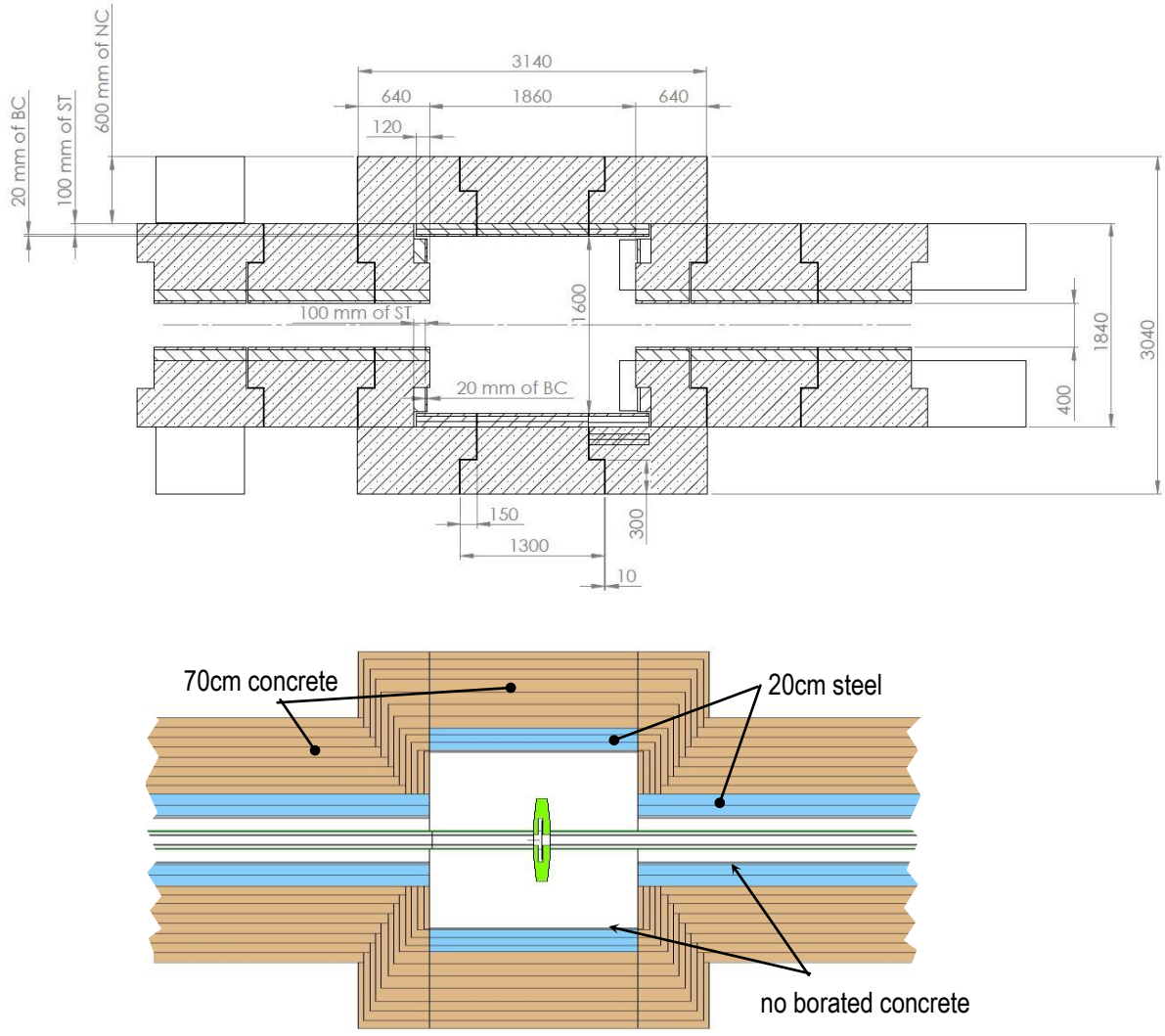

Fig. 93: Horizontal cut through the chopper pit. Top: Technical drawing. Bottom: Monte Carlo model (in the Monte Carlo model the shielding thickness is higher as in the drawing)

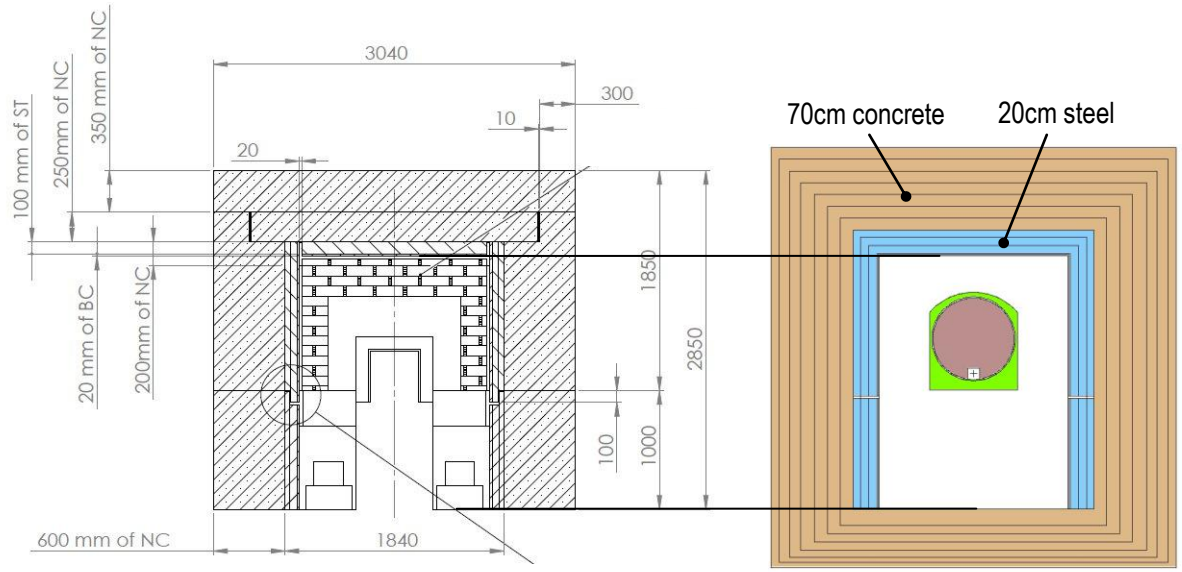

Fig. 94: Vertical cut through the chopper pit. Left hand side: Technical drawing. Right hand side: Monte Carlo model (in the Monte Carlo model the shielding thickness is higher as in the drawing)

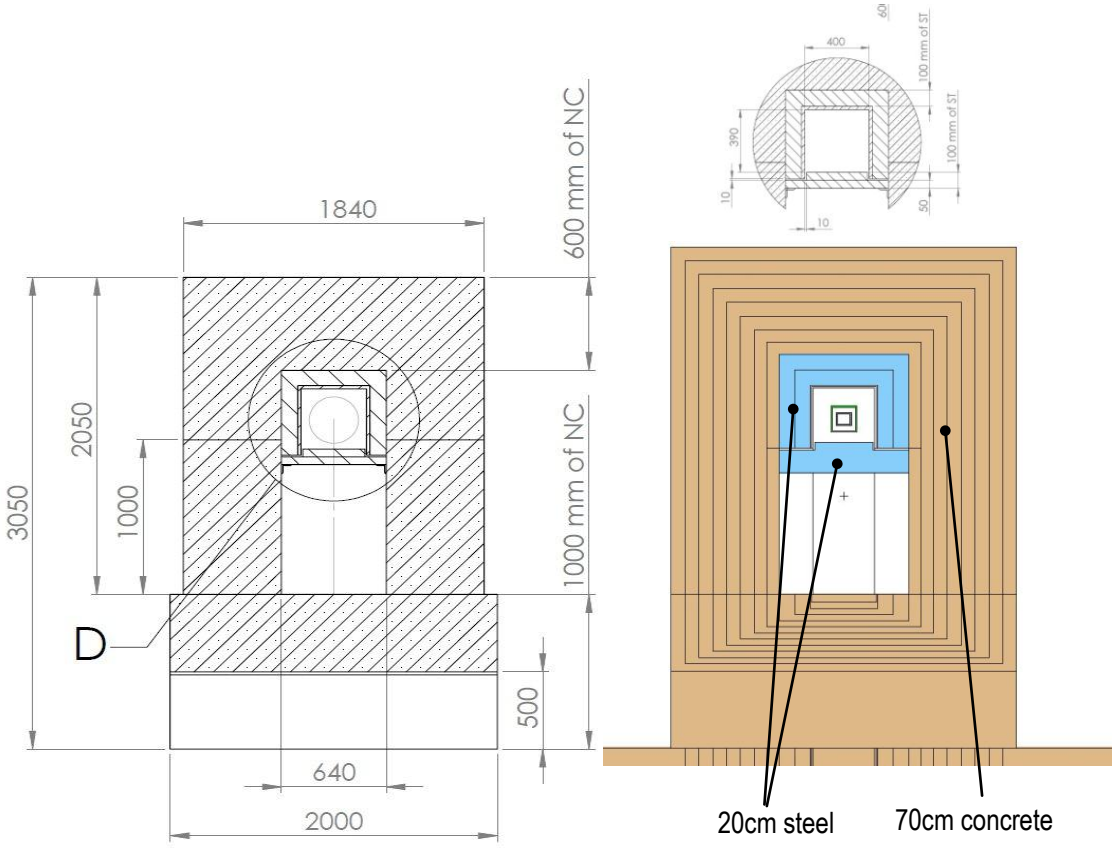

Fig. 95: Vertical cut through the guide shielding. Left hand side: Technical drawing. Right hand side: Monte Carlo model (in the Monte Carlo model the shielding thickness is higher as in the drawing)

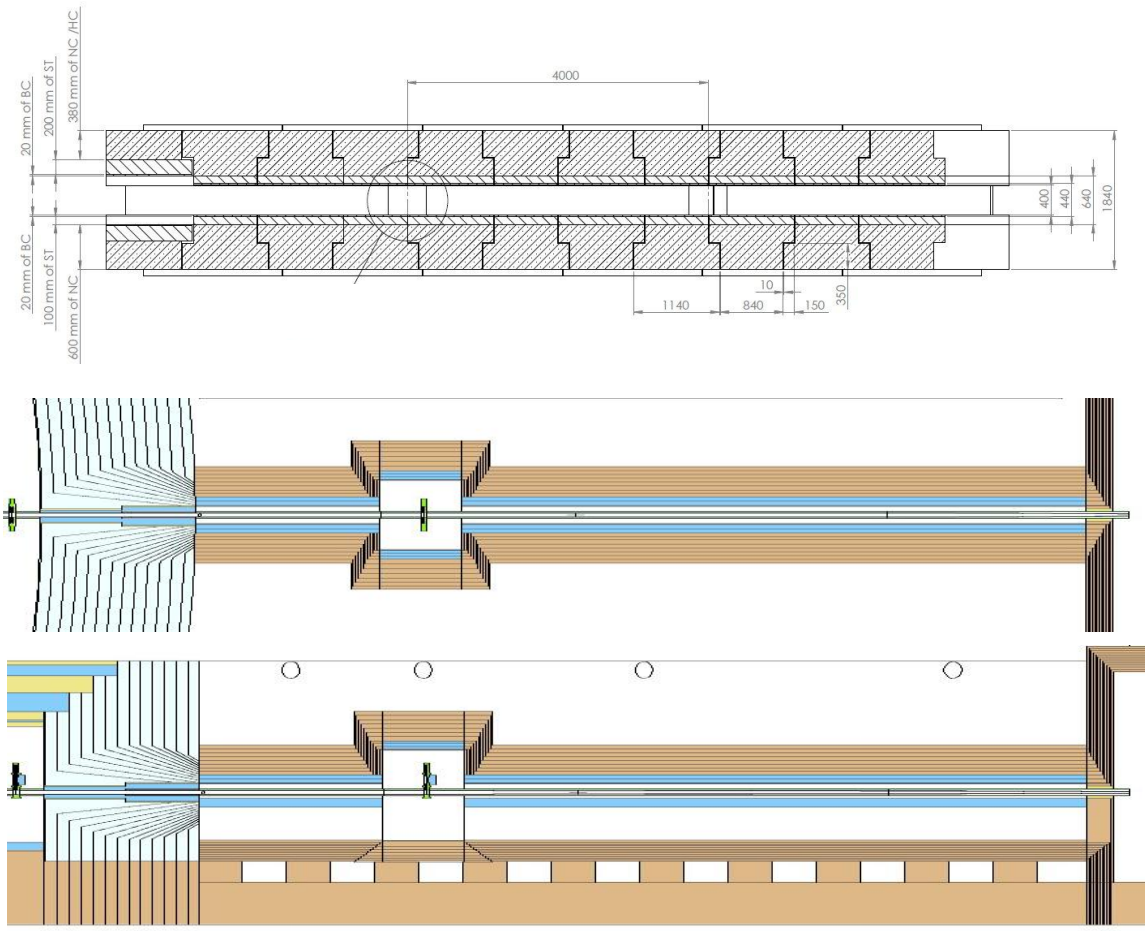

Fig. 96: Top: Horizontal cut through the guide shielding (drawing). Middle: Horizontal cut through the guide shielding (Monte Carlo model) Bottom: Vertical cut through the guide shielding (Monte Carlo model) (in the Monte Carlo model the shielding thickness is higher as in the drawing)

4.3 Dose rate distributions for the opened chopper FOC5

In this chapter the dose rate distributions for version 3 for the opened chopper FOC5 are shown.

4.3.1 Horizontal neutron dose rate distribution

The image below shows an horizontal area through the Monte Carlo model of the ODIN instrument for which the neutron dose rate distribution is presented in the following image.

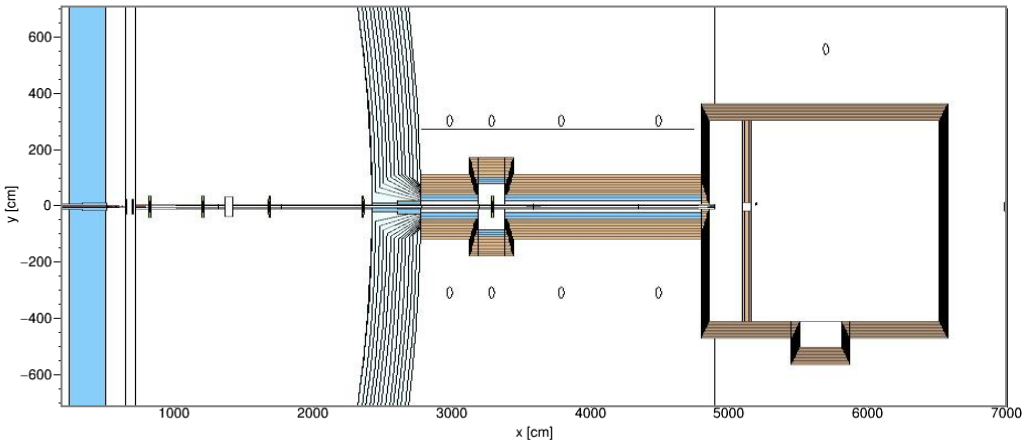

Fig. 97: Horizontal area through the Monte Carlo model of the ODIN instrument for which the radiation distribution is shown in the following image

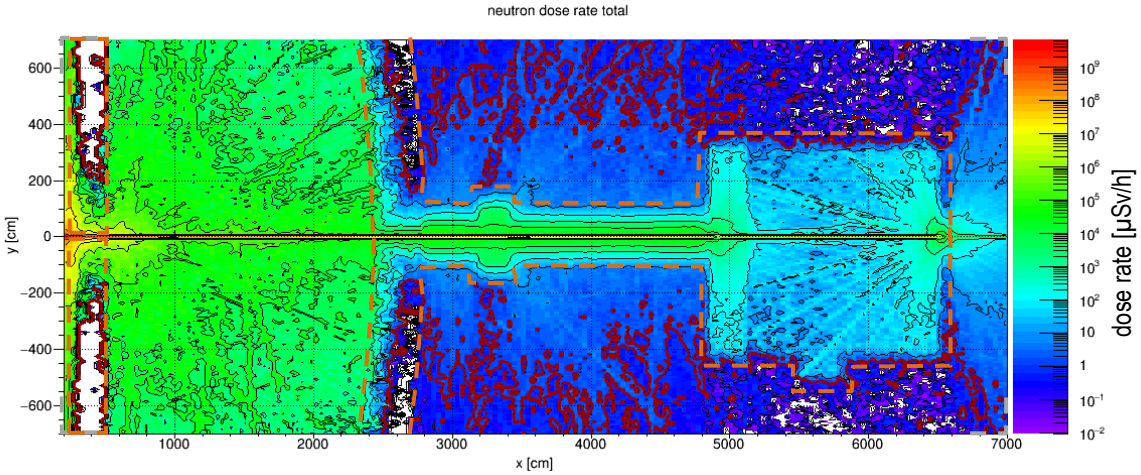

Fig. 98: Total neutron dose rate distribution in the horizontal area. The red line is the 1µSv/h border.

4.3.2 Horizontal generated gamma dose rate distribution

The image below shows an horizontal area through the Monte Carlo model of the ODIN instrument for which the generated gamma dose rate distribution is presented in the following image.

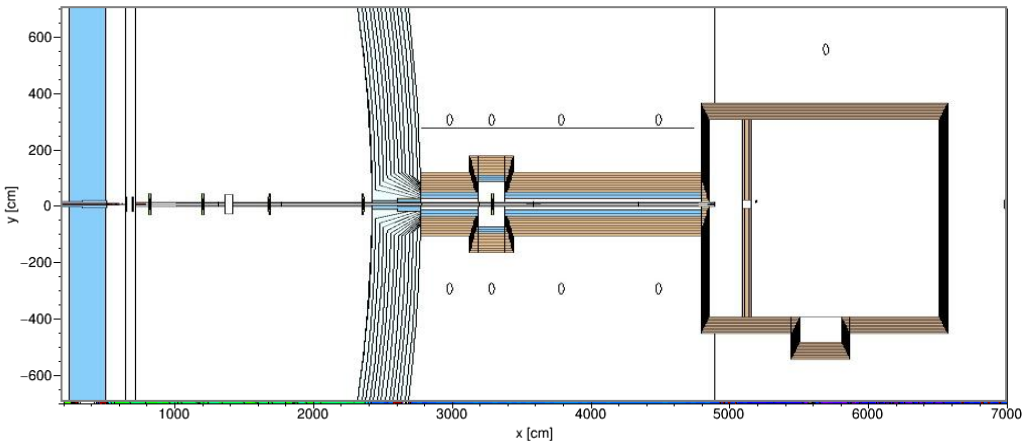

Fig. 99: Horizontal area through the Monte Carlo model of the ODIN instrument for which the radiation distribution is shown in the following image

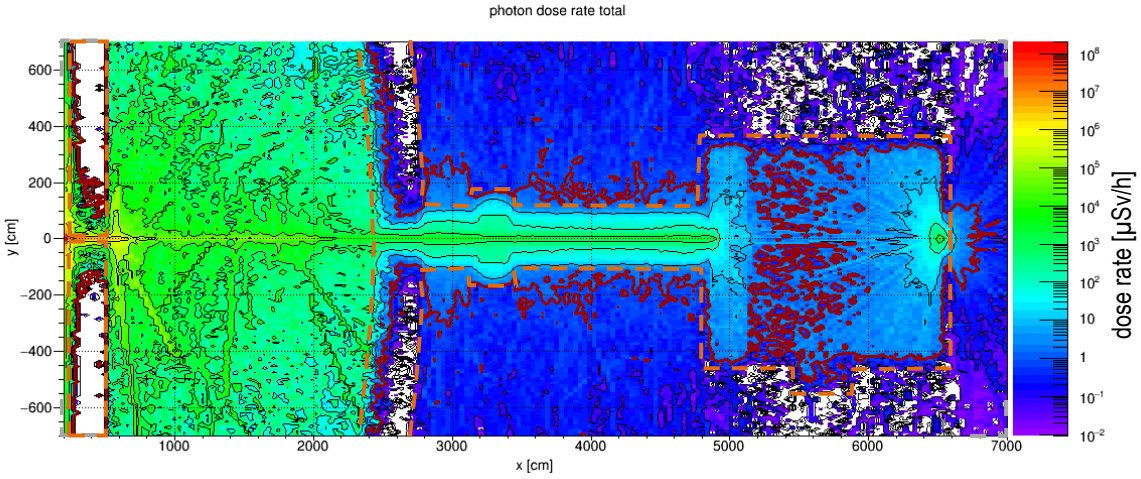

Fig. 100: Total generated gamma dose rate distribution in the horizontal area. The red line is the 1µSv/h border.

4.3.3 Vertical neutron dose rate distribution along the beam axis

The image below shows a vertical area through the Monte Carlo model of the ODIN instrument for which the neutron dose rate distribution is presented in the following image.

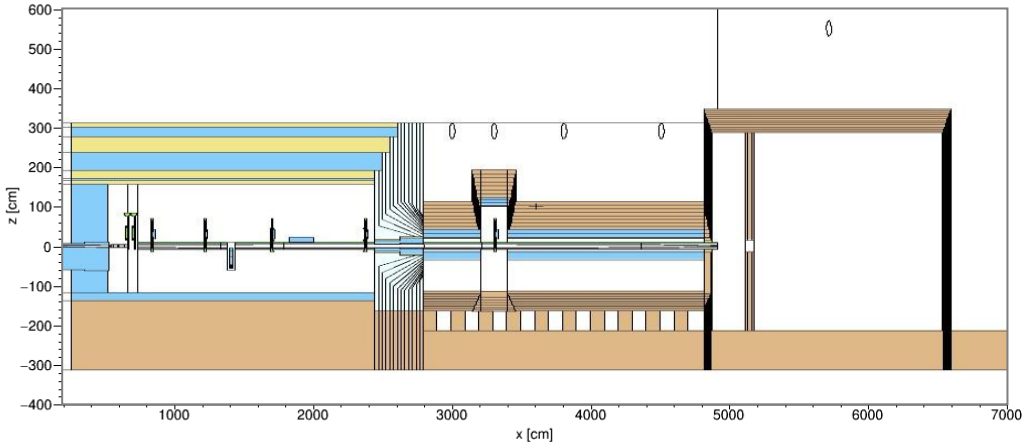

Fig. 101: Vertical area through the Monte Carlo model of the ODIN instrument for which the radiation distribution is shown in the following image

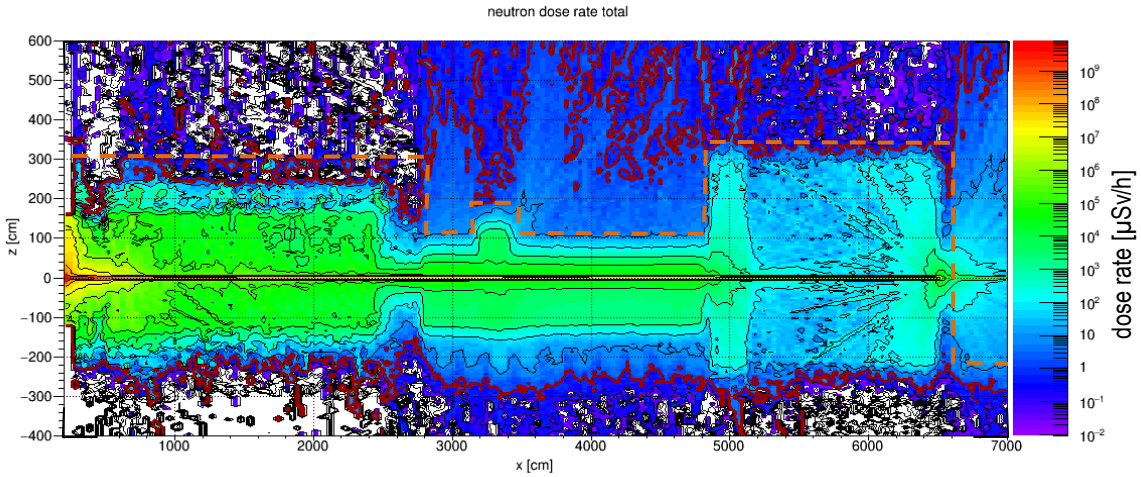

Fig. 102: Total neutron dose rate distribution in the horizontal area. The red line is the 1µSv/h border.

4.3.4 Vertical generated gamma dose rate distribution along the beam axis

The image below shows a vertical area through the Monte Carlo model of the ODIN instrument for which the generated gamma dose rate distribution is presented in the following image.

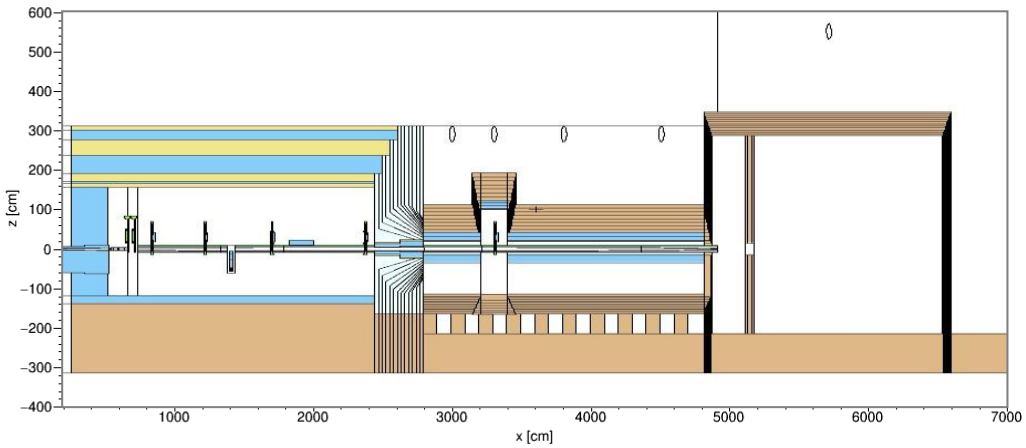

Fig. 103: Vertical area through the Monte Carlo model of the ODIN instrument for which the radiation distribution is shown in the following image

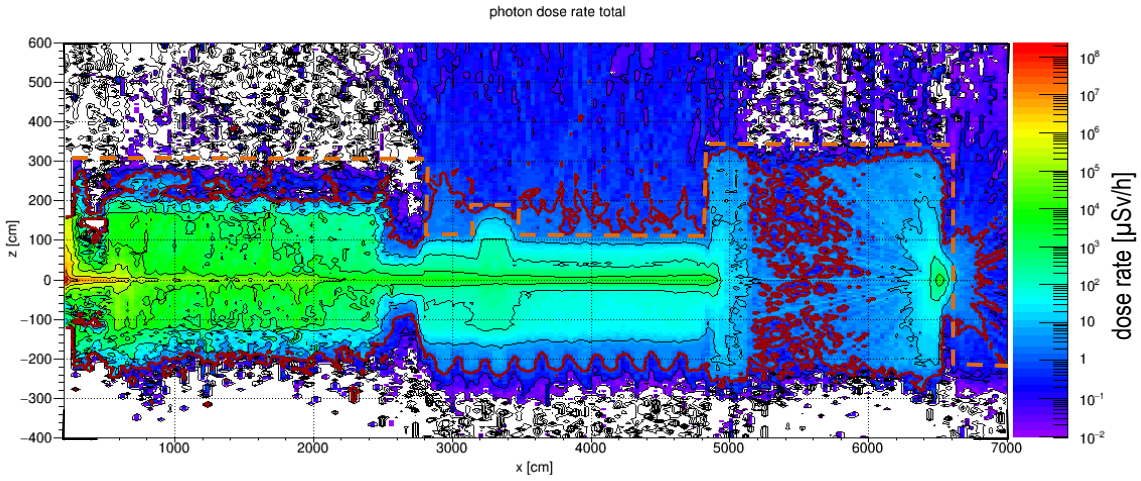

Fig. 104: Total generated gamma dose rate distribution in the vertical area. The red line is the 1µSv/h border.

4.3.5 Vertical neutron dose rate distribution through the guide shielding perpendicular to the beam axis

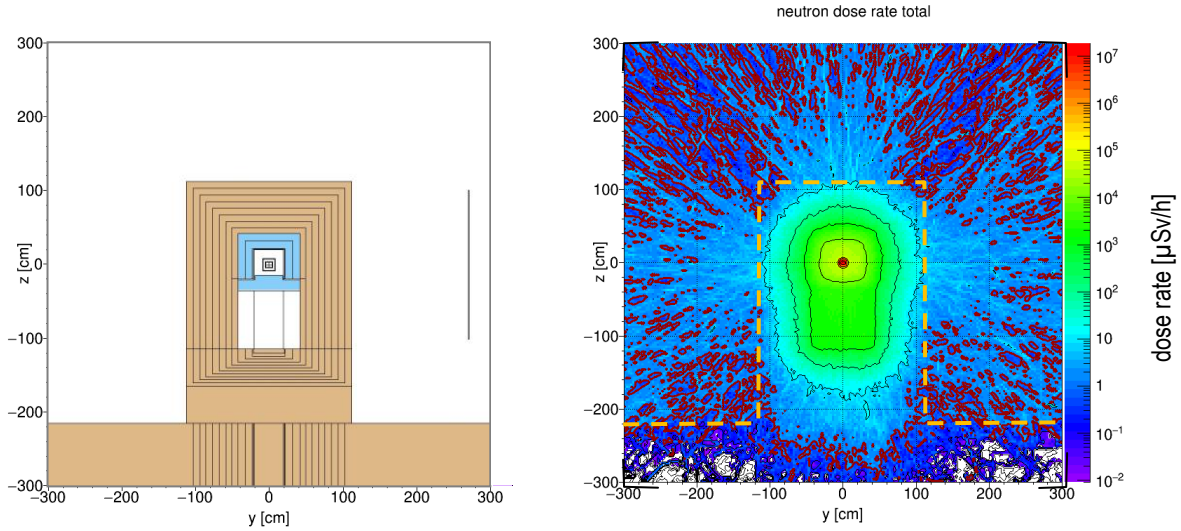

Fig. 105: Vertical neutron dose rate distribution through the guide shielding perpendicular to the beam axis (40m from the focal point). The red line is the 1µSv/h border.

4.3.6 Vertical generated gamma dose rate distribution through the guide shielding perpendicular to the beam axis

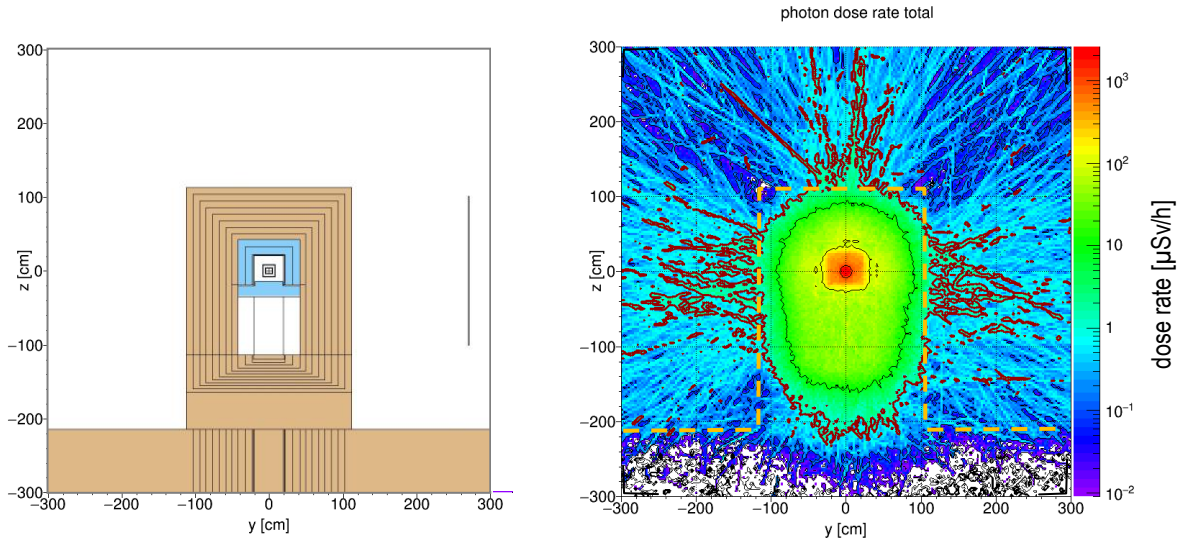

Fig. 106: Vertical generated gamma dose rate distribution through the guide shielding perpendicular to the beam axis (40m from the focal point). The red line is the 1µSv/h border.

4.3.7 Vertical neutron dose rate distribution through the chopper pit perpendicular to the beam axis

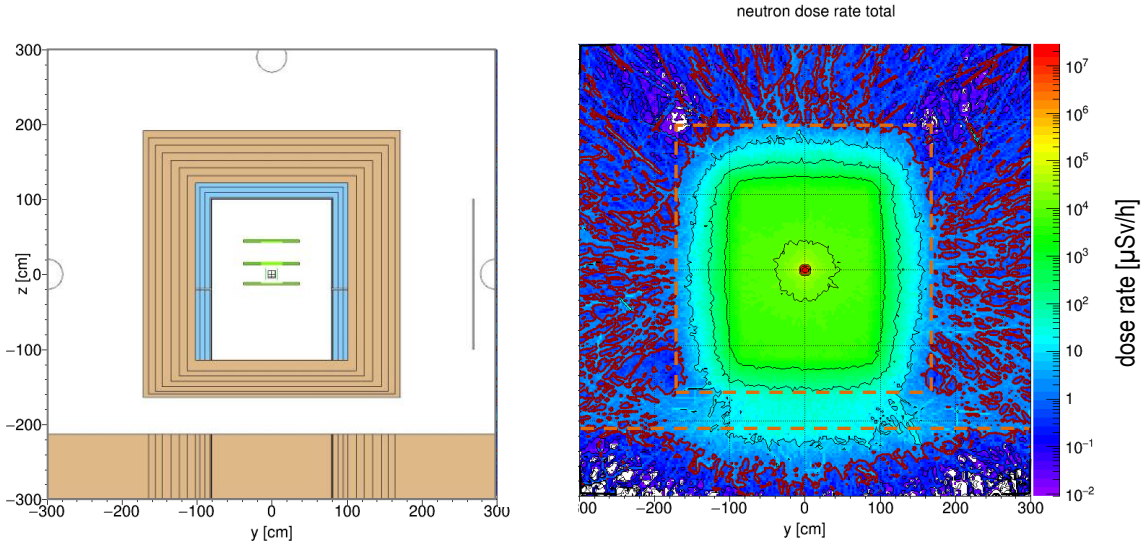

Fig. 107: Vertical neutron dose rate distribution through the chopper pit perpendicular to the beam axis. The red line is the 1µSv/h border.

4.3.8 Vertical neutron dose rate distribution through the chopper pit perpendicular to the beam axis

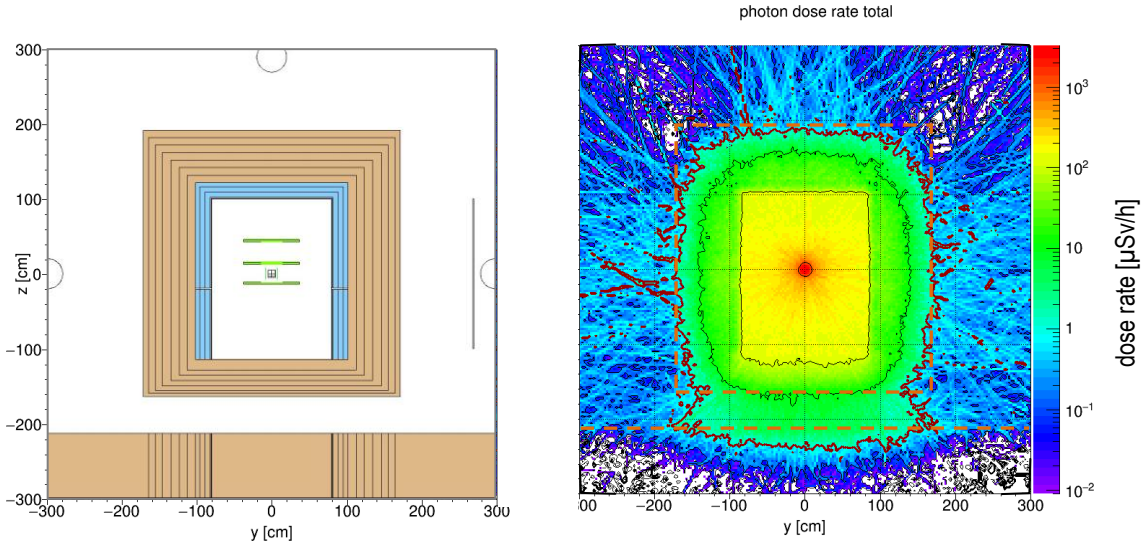

Fig. 108: Vertical generated gamma dose rate distribution through the chopper pit perpendicular to the beam axis. The red line is the 1µSv/h border.

4.3.9 Conclusions

With version 3 of the common guide shielding the desired dose rate level is still exceeded.

Although the source yield of the fictive neutron source was decreased by a factor 1.4 nearly the same dose rates on the outer surfaces of the shielding are reached as with version 2 with the extended steel layers.

Obviously the effect of the lower source yield is compensated by decreasing the inner width of the shielding.

4.4 Dose rate distributions for the closed chopper FOC5

In this chapter the dose rate distributions for version 3 for the closed chopper FOC5 are shown. A fictive cold/thermal neutron source is located in front of the chopper for the simulation.

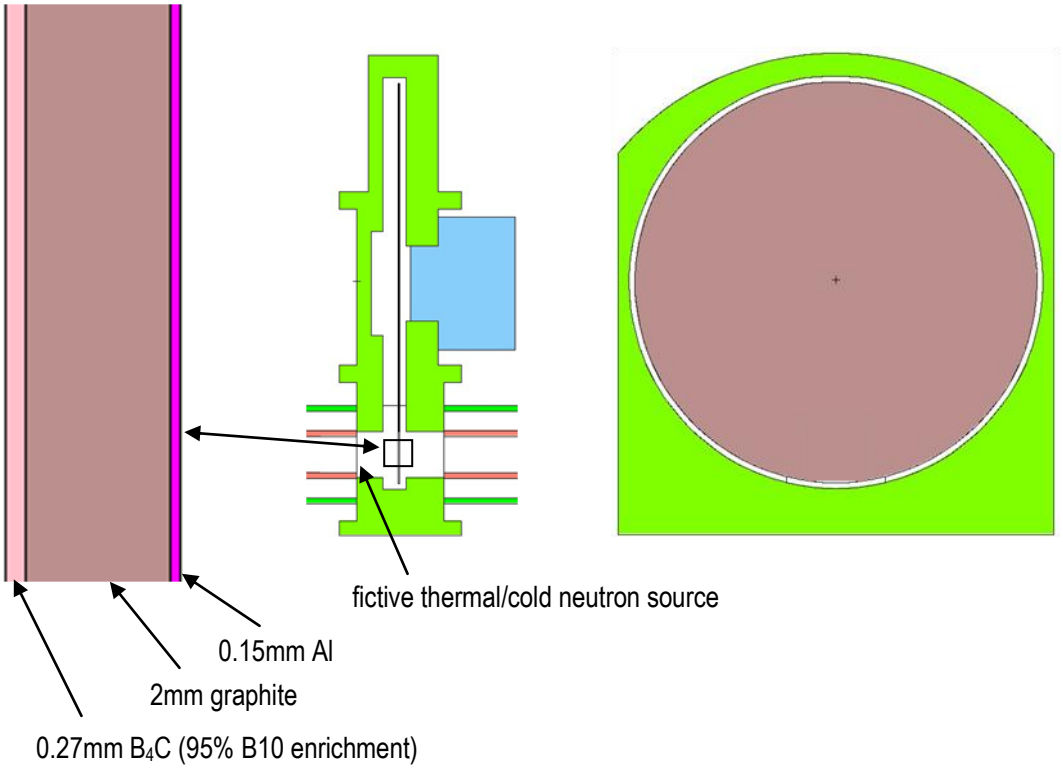

Fig. 109: Monte Carlo model of the chopper FOC5

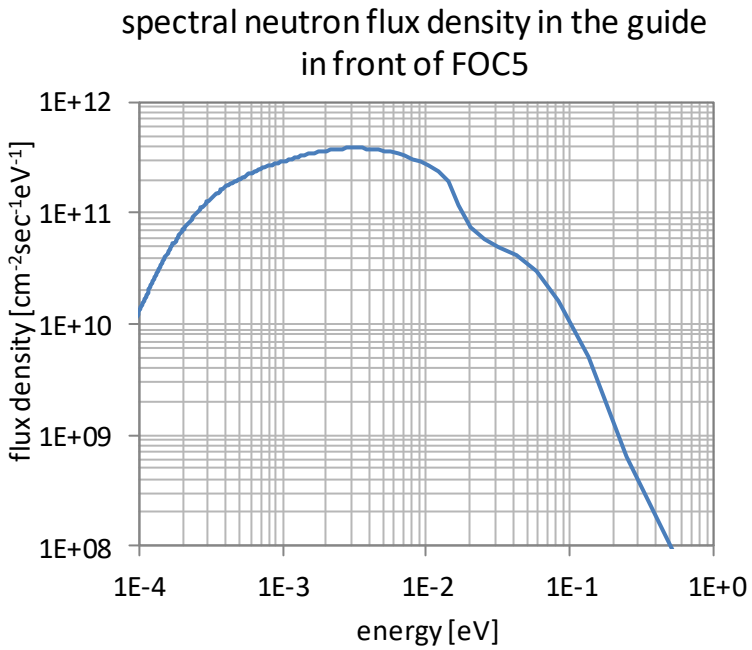

Fig. 110: Spectral neutron flux density in the guide in front of FOC5. The total thermal/cold neutron flux at this position is $8 \cdot 10^9$ $sec^{-1}cm^{-2}$.

4.4.1 Horizontal neutron dose rate distribution

The image below shows an horizontal area through the Monte Carlo model of the ODIN instrument for which the neutron dose rate distribution is presented in the following image.

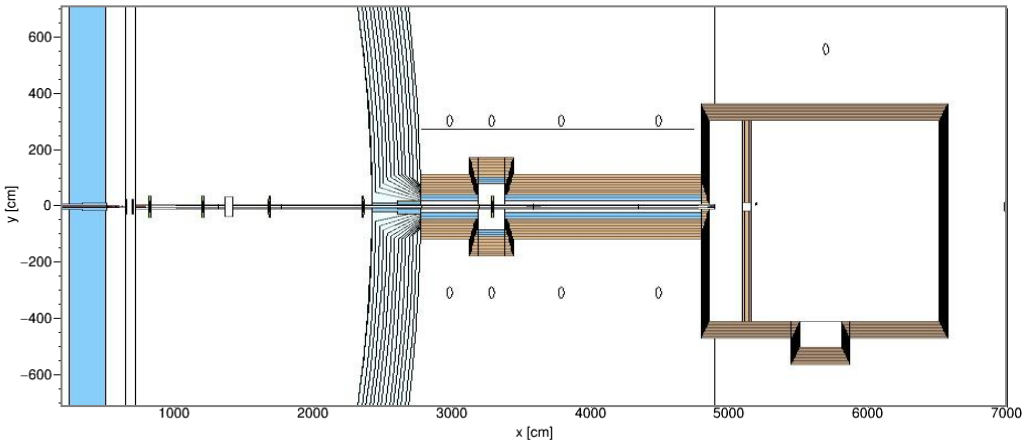

Fig. 111: Horizontal area through the Monte Carlo model of the ODIN instrument for which the radiation distribution is shown in the following image

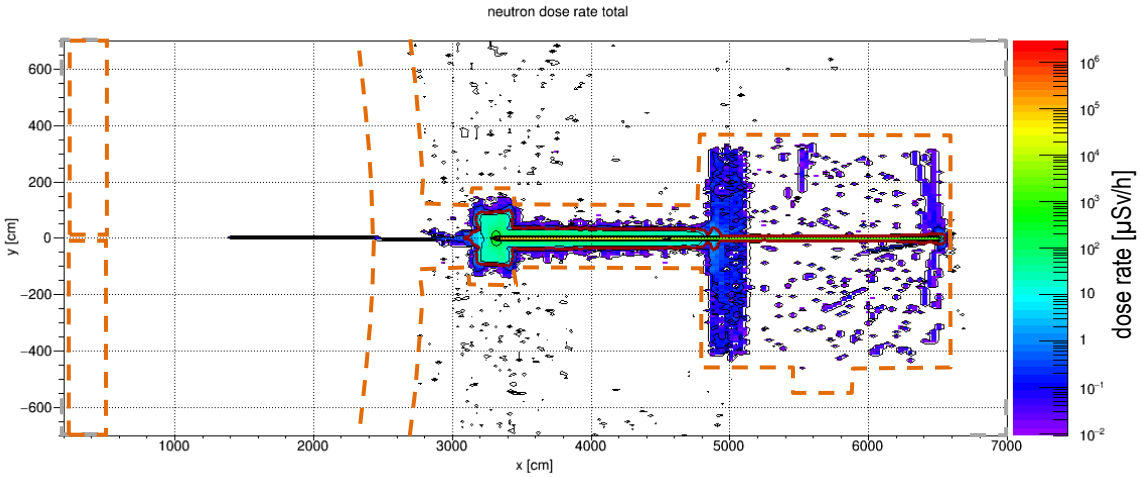

Fig. 112: Total neutron dose rate distribution in the horizontal area. The red line is the 1µSv/h border.

4.4.2 Horizontal generated gamma dose rate distribution

The image below shows an horizontal area through the Monte Carlo model of the ODIN instrument for which the generated gamma dose rate distribution is presented in the following image.

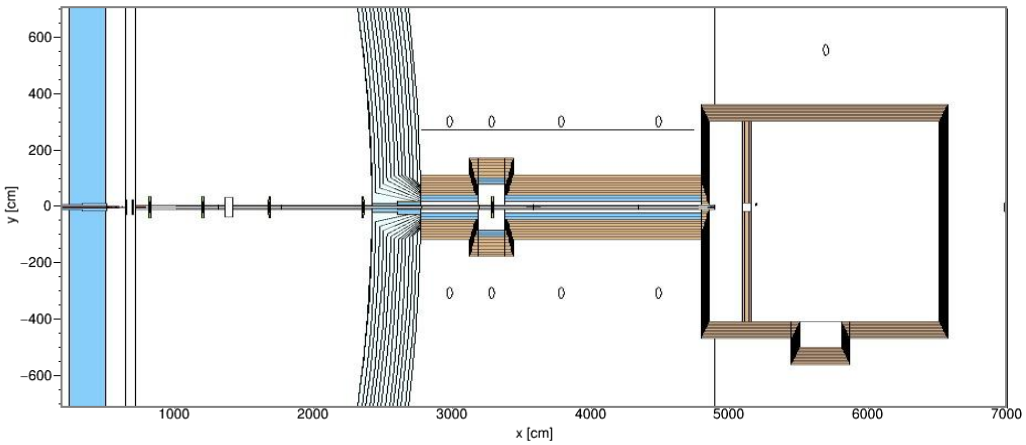

Fig. 113: Horizontal area through the Monte Carlo model of the ODIN instrument for which the radiation distribution is shown in the following image

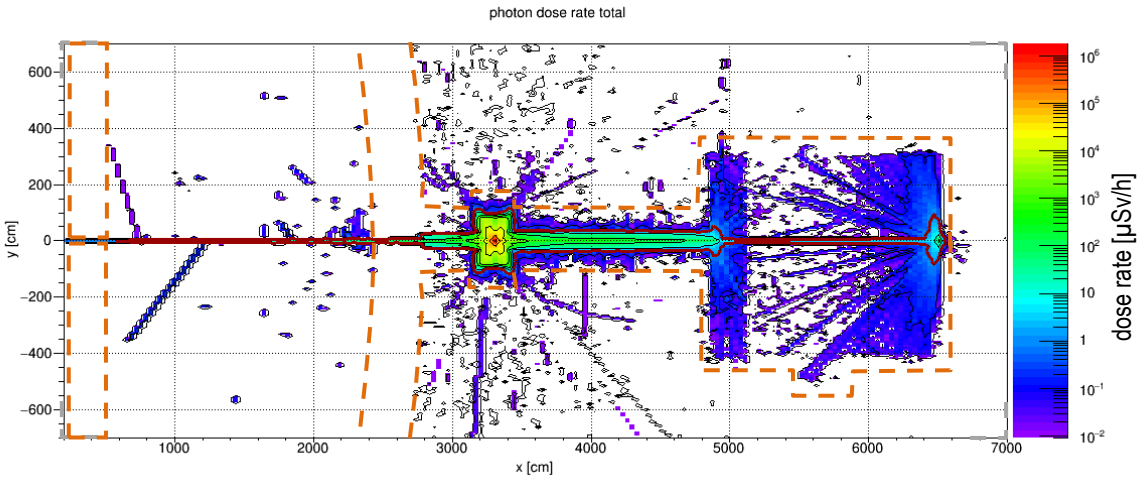

Fig. 114: Total generated gamma dose rate distribution in the horizontal area. The red line is the 1µSv/h border.

4.4.3 Vertical neutron dose rate distribution through the chopper pit perpendicular to the beam axis

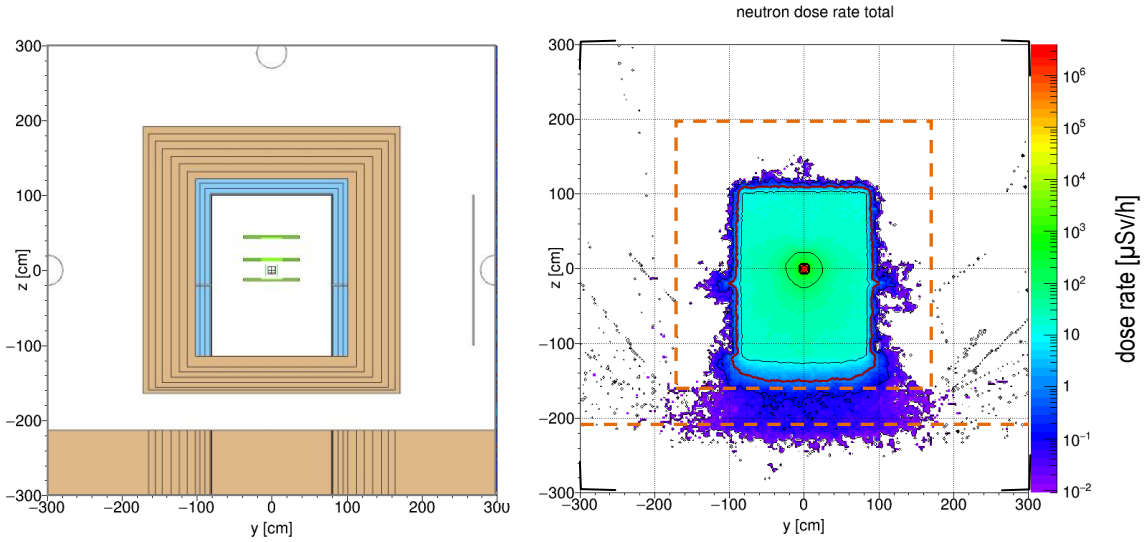

Fig. 115: Vertical neutron dose rate distribution through the chopper pit perpendicular to the beam axis. The red line is the 1µSv/h border.

4.4.4 Vertical generated gamma dose rate distribution through the chopper pit perpendicular to the beam axis

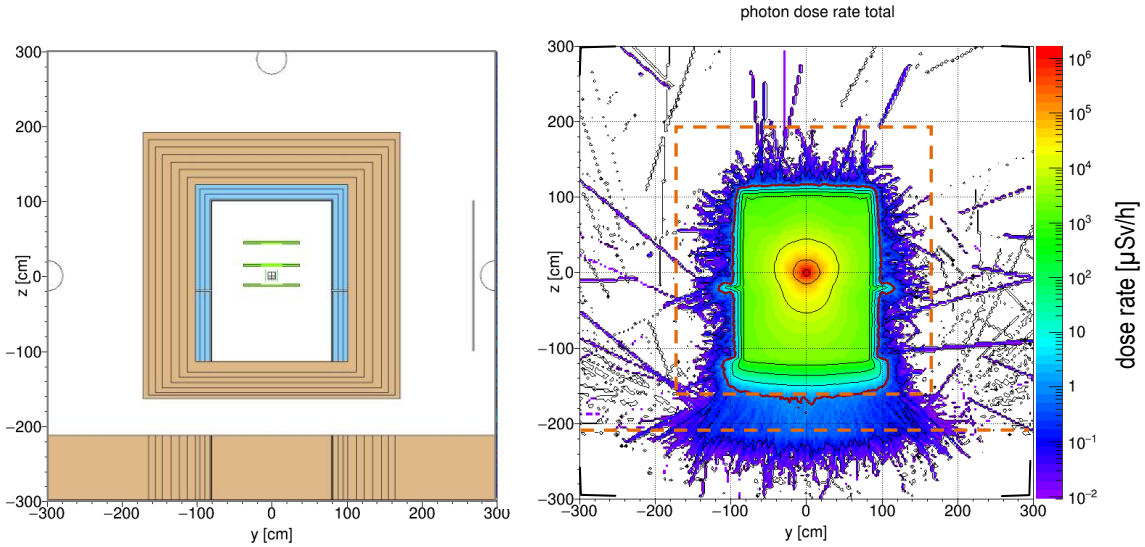

Fig. 116: Vertical total generated gamma dose rate distribution through the chopper pit perpendicular to the beam axis. The red line is the 1µSv/h border.

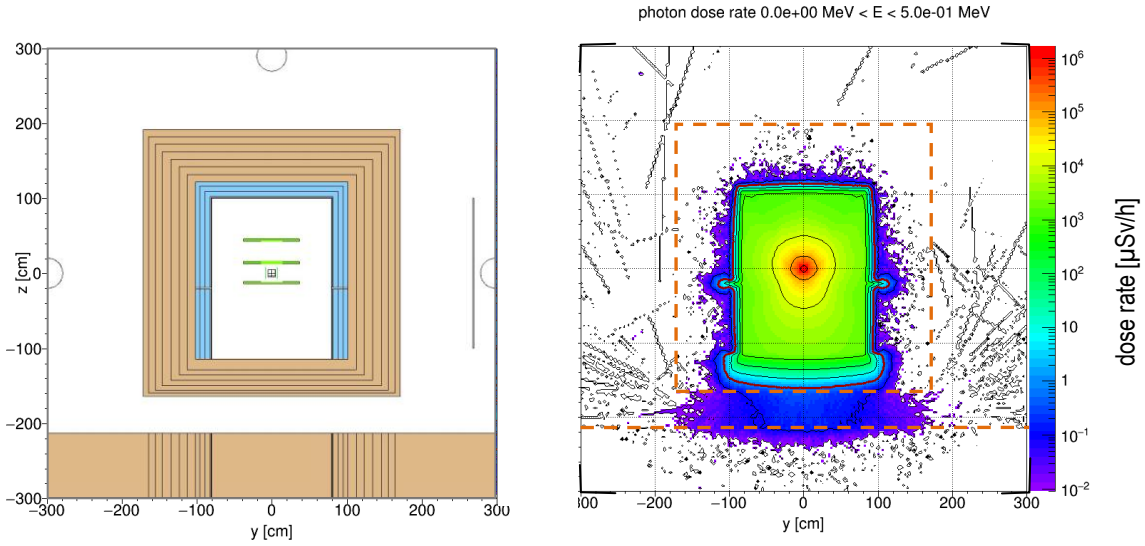

Fig. 117: Vertical generated gamma dose rate distribution through the chopper pit perpendicular to the beam axis in the energy region below 0.5MeV. The red line is the 1µSv/h border.

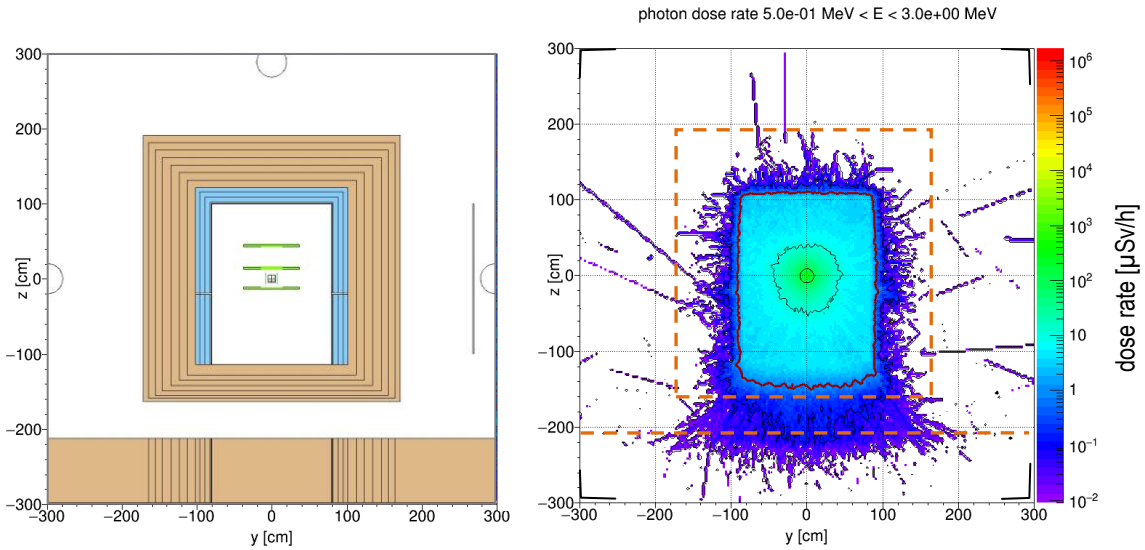

Fig. 118: Vertical generated gamma dose rate distribution through the chopper pit perpendicular to the beam axis in the energy region between 0.5MeV and 3MeV. The red line is the 1µSv/h border.

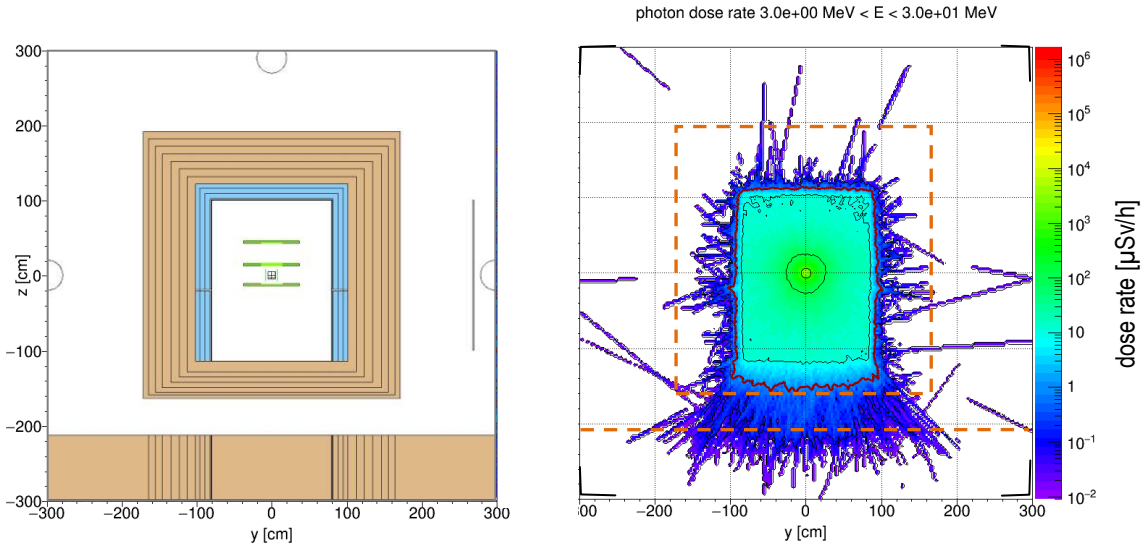

Fig. 119: Vertical generated gamma dose rate distribution through the chopper pit perpendicular to the beam axis in the energy region above 3MeV. The red line is the 1µSv/h border.

4.5 Conclusions

The dose rate in the chopper pit for the closed chopper is dominated by low energetic gamma radiation ($E\gamma$<0.5MeV). The 1µSv/h border is inside the shielding. The shielding attenuates the gamma radiation from the closed chopper far below 1µSv/h.

5 Variation of the thickness of the steel and concrete layers in version 3

5.1 Shielding version 3 consisting of 25cm steel and 70cm concrete

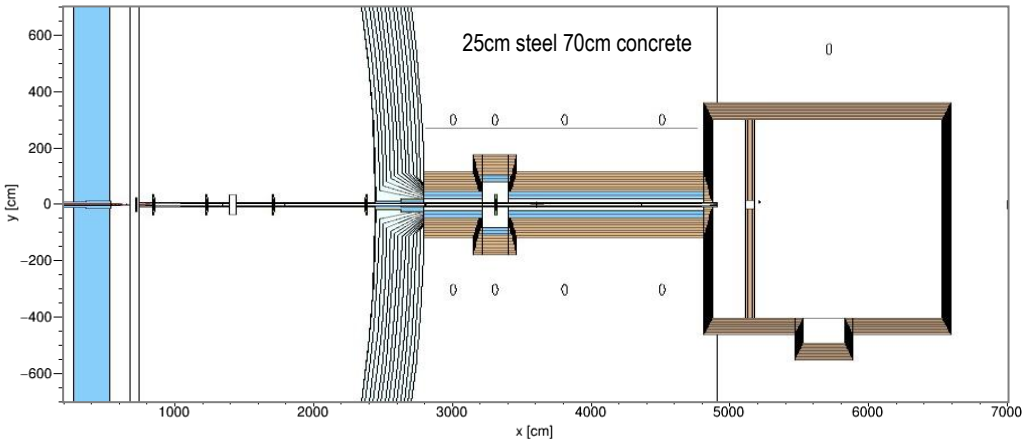

Fig. 120: Horizontal area through the Monte Carlo model of the ODIN instrument for which the radiation distribution is shown in the following image

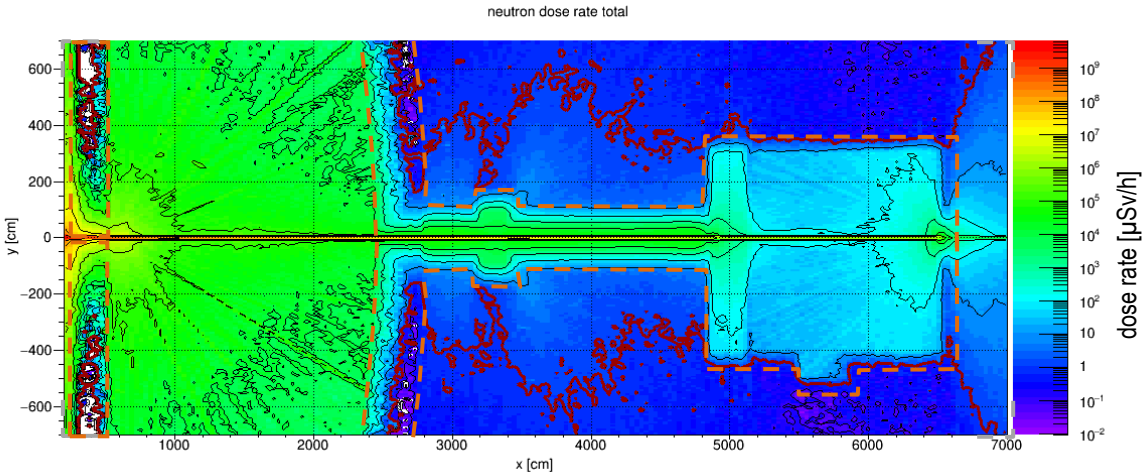

Fig. 121: Total neutron dose rate distribution in the horizontal area. The red line is the 1µSv/h border.

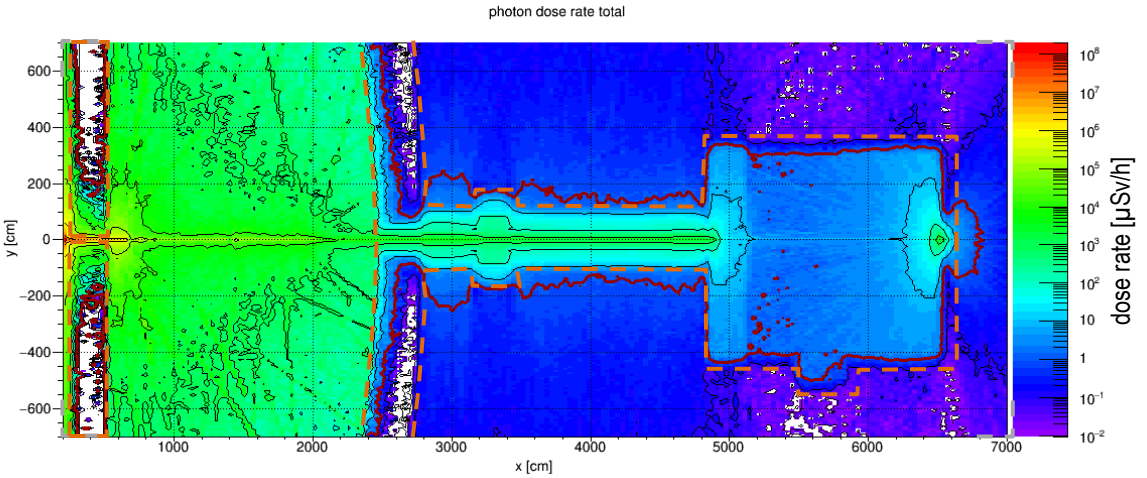

Fig. 122: Total generated gamma dose rate distribution in the horizontal area. The red line is the 1µSv/h border.

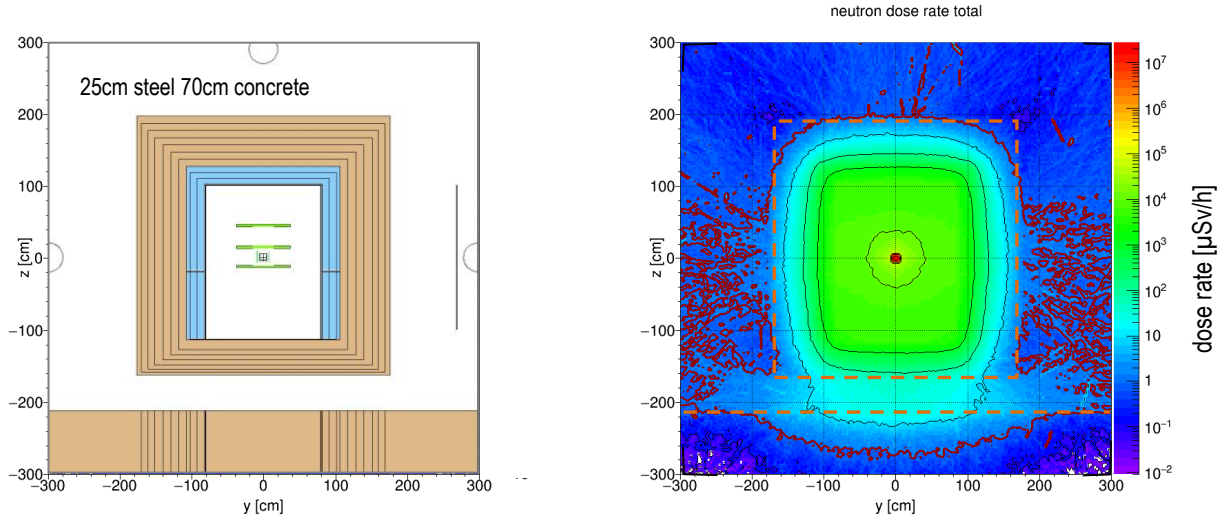

Fig. 123: Vertical neutron dose rate distribution through the chopper pit perpendicular to the beam axis. The red line is the 1µSv/h border.

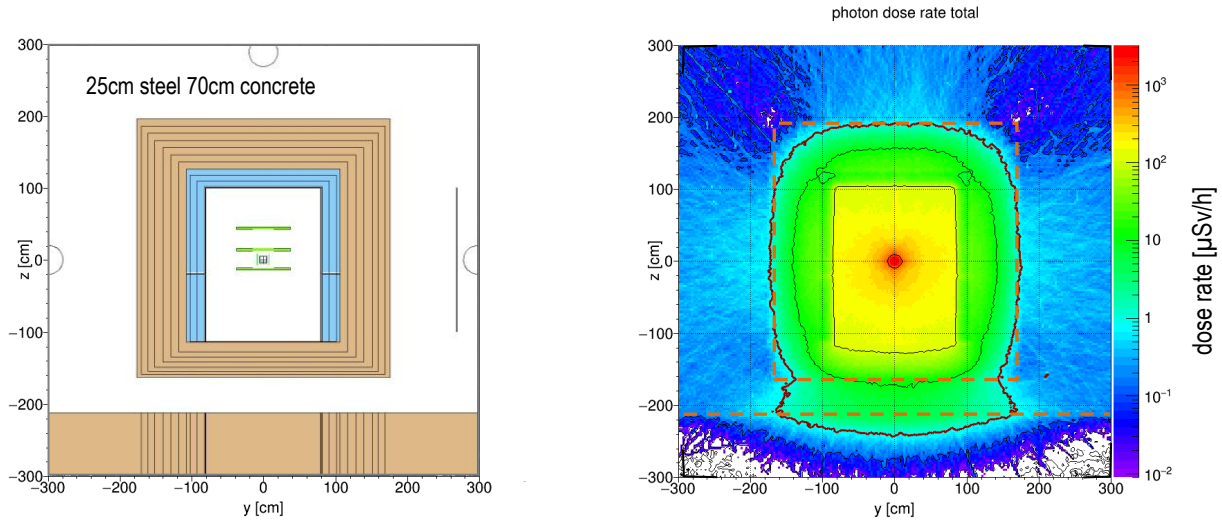

Fig. 124: Vertical generated gamma dose rate distribution through the chopper pit perpendicular to the beam axis. The red line is the 1µSv/h border.

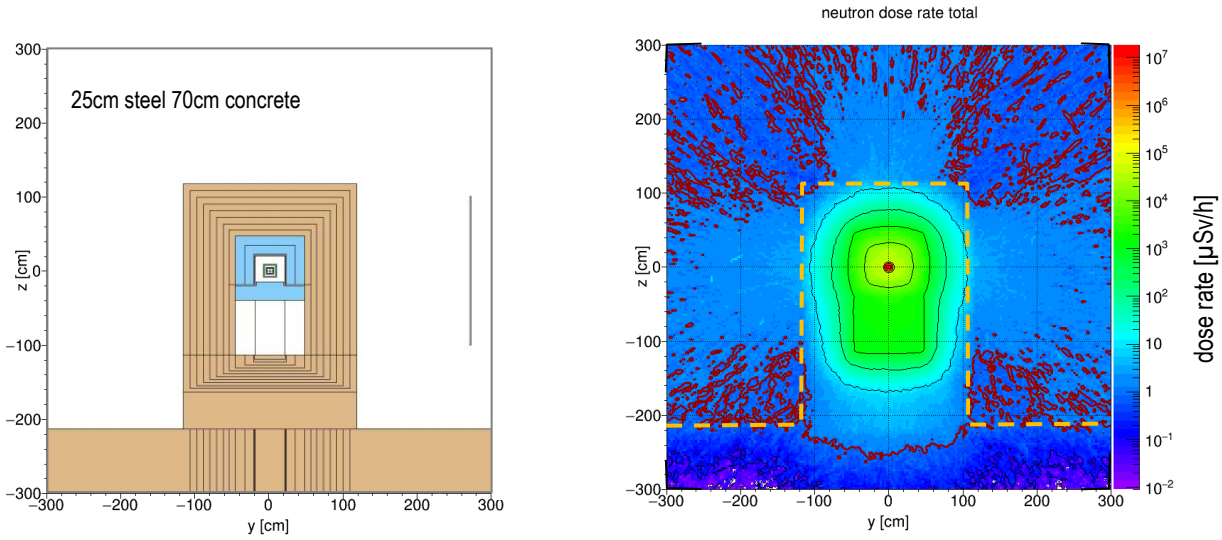

Fig. 125: Vertical neutron dose rate distribution through the guide shielding perpendicular to the beam axis (40m from the focal point). The red line is the 1µSv/h border.

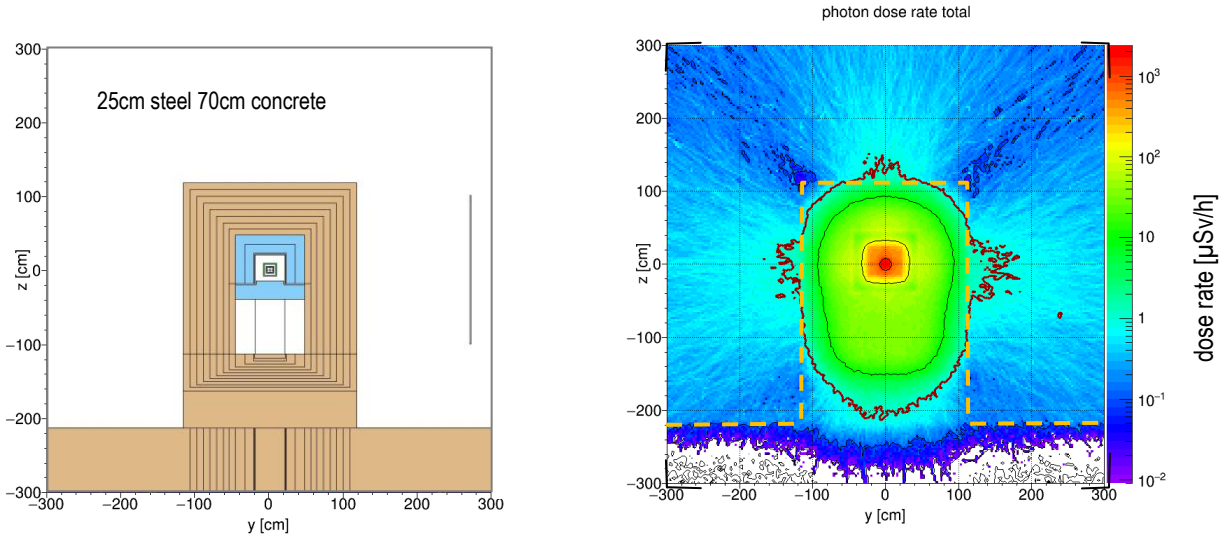

Fig. 126: Vertical generated gamma dose rate distribution through the guide shielding perpendicular to the beam axis (40m from the focal point). The red line is the 1µSv/h border.

5.2 Shielding version 3 consisting of 30cm steel and 70cm concrete

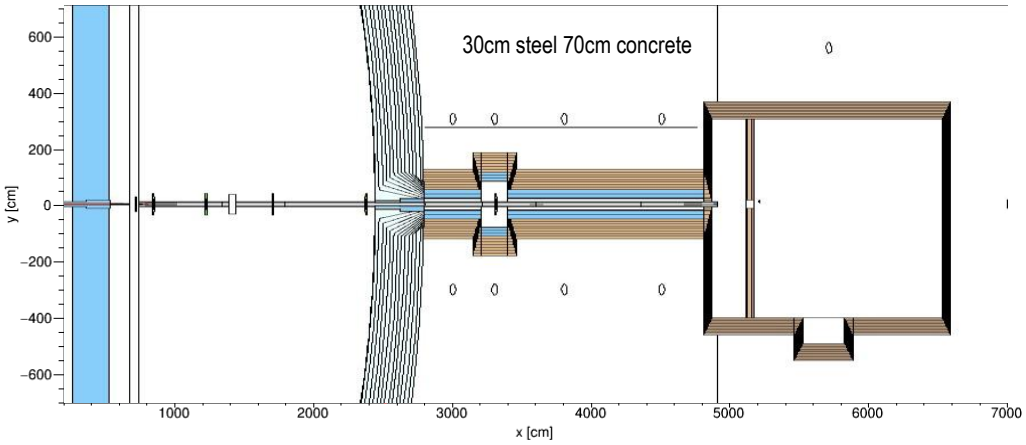

Fig. 127: Horizontal area through the Monte Carlo model of the ODIN instrument for which the radiation distribution is shown in the following image

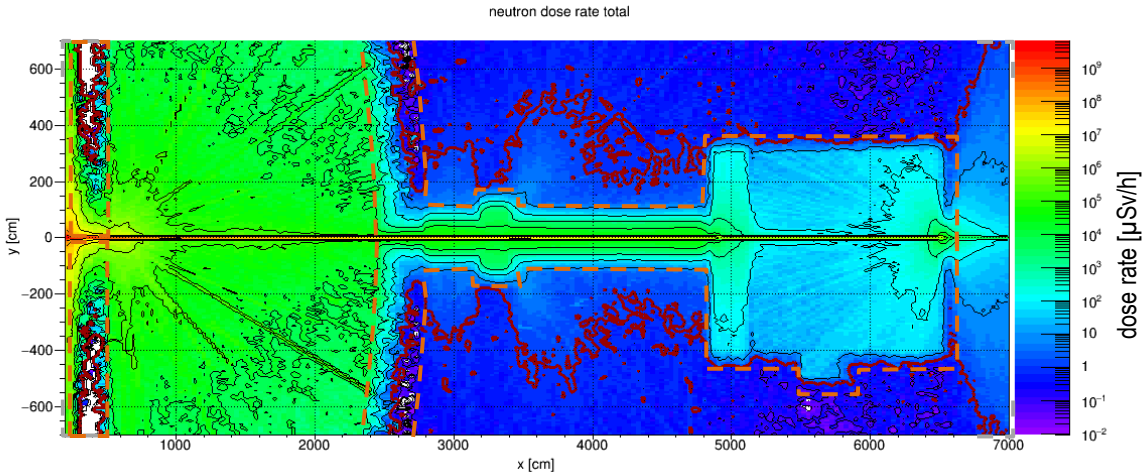

Fig. 128: Total neutron dose rate distribution in the horizontal area. The red line is the 1µSv/h border.

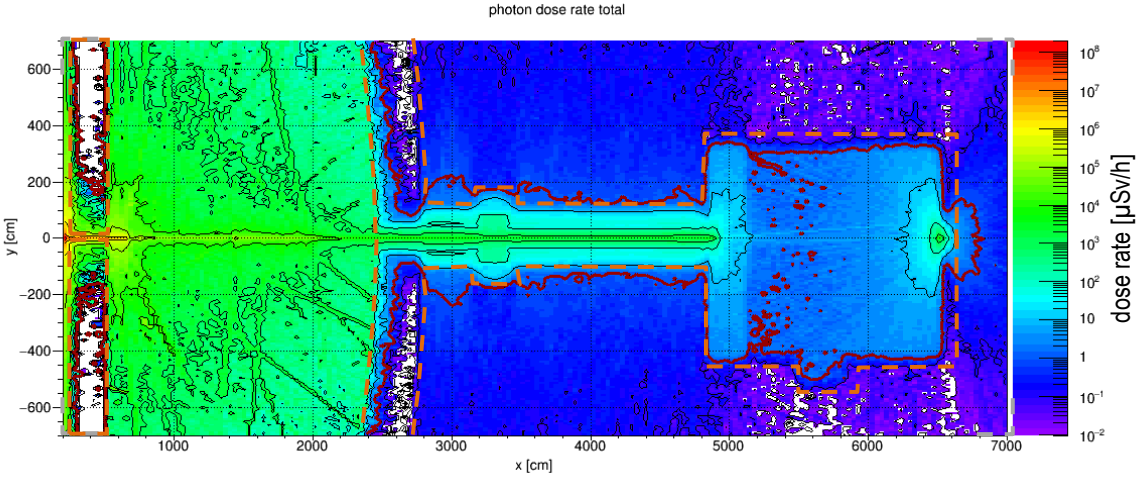

Fig. 129: Total generated gamma dose rate distribution in the horizontal area. The red line is the 1µSv/h border.

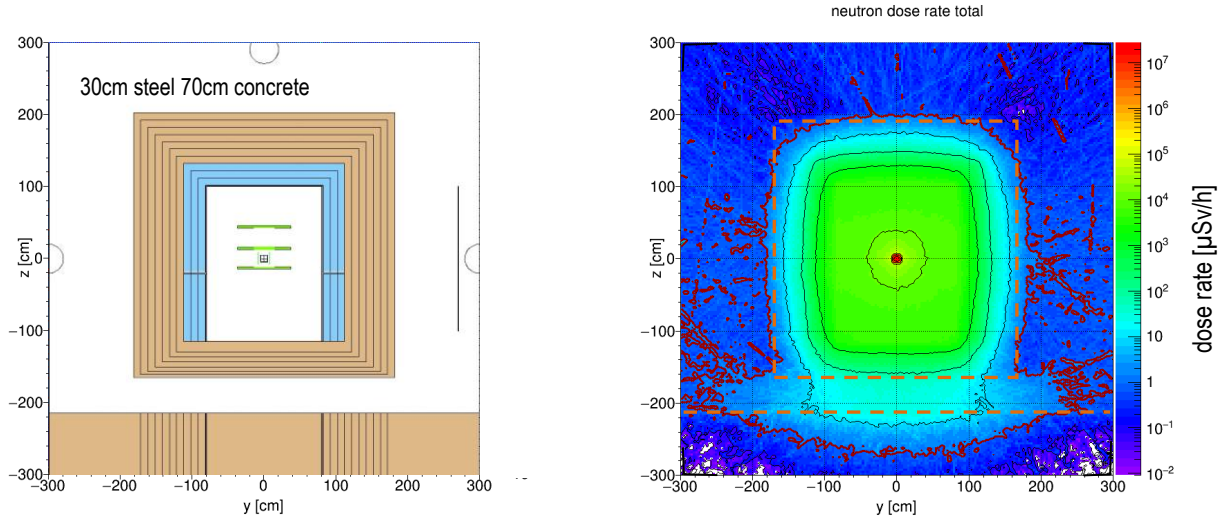

Fig. 130: Vertical neutron dose rate distribution through the chopper pit perpendicular to the beam axis. The red line is the 1µSv/h border.

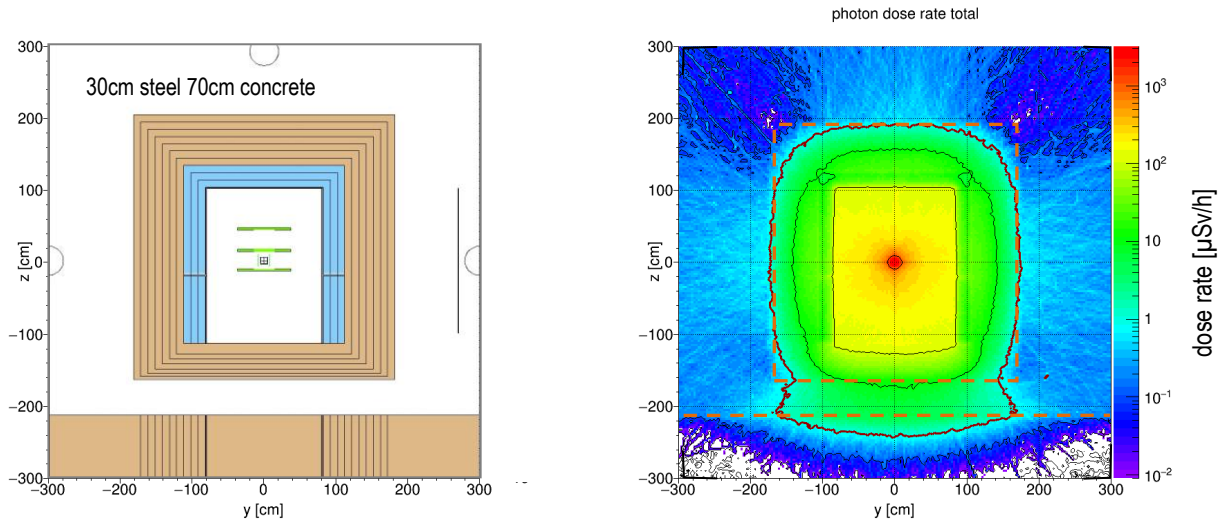

Fig. 131: Vertical generated gamma dose rate distribution through the chopper pit perpendicular to the beam axis. The red line is the 1µSv/h border.

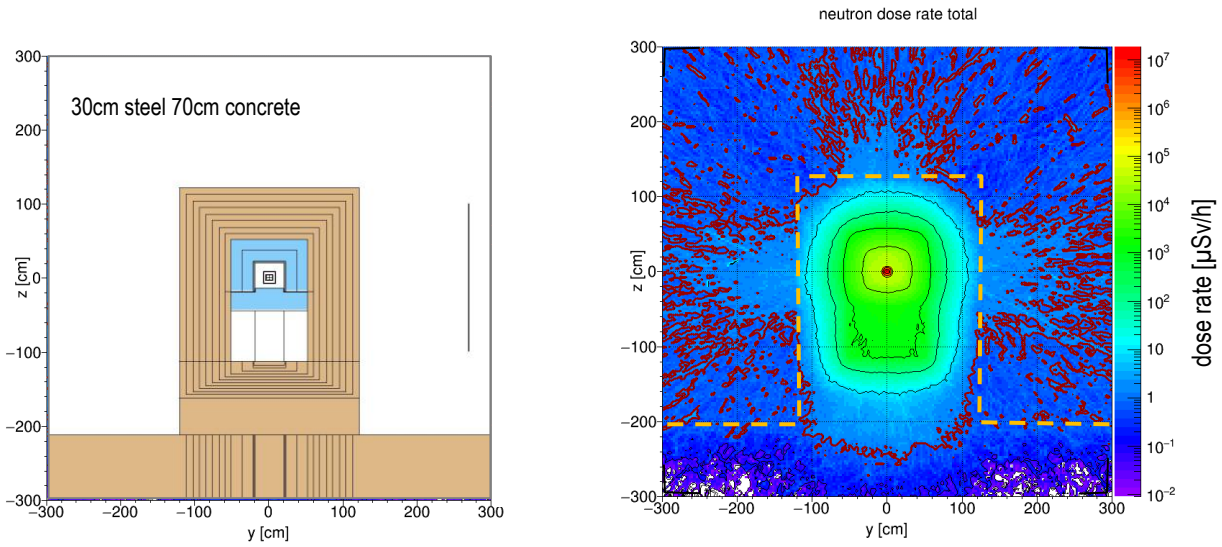

Fig. 132: Vertical neutron dose rate distribution through the guide shielding perpendicular to the beam axis (40m from the focal point). The red line is the 1µSv/h border.

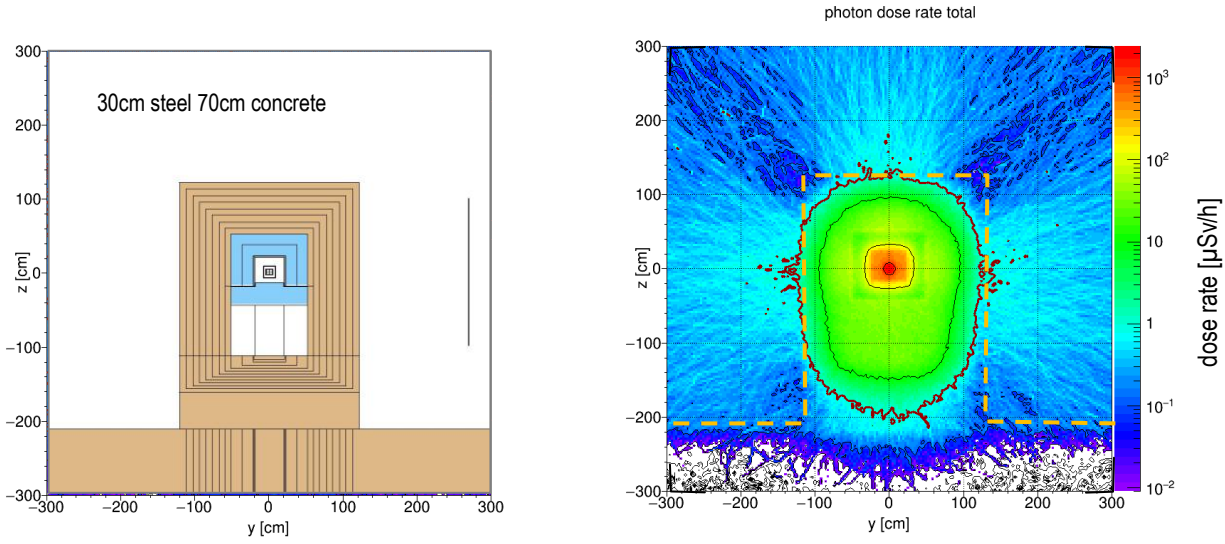

Fig. 133: Vertical generated gamma dose rate distribution through the guide shielding perpendicular to the beam axis (40m from the focal point). The red line is the 1µSv/h border.

5.3 Shielding version 3 consisting of 35cm steel and 70cm concrete

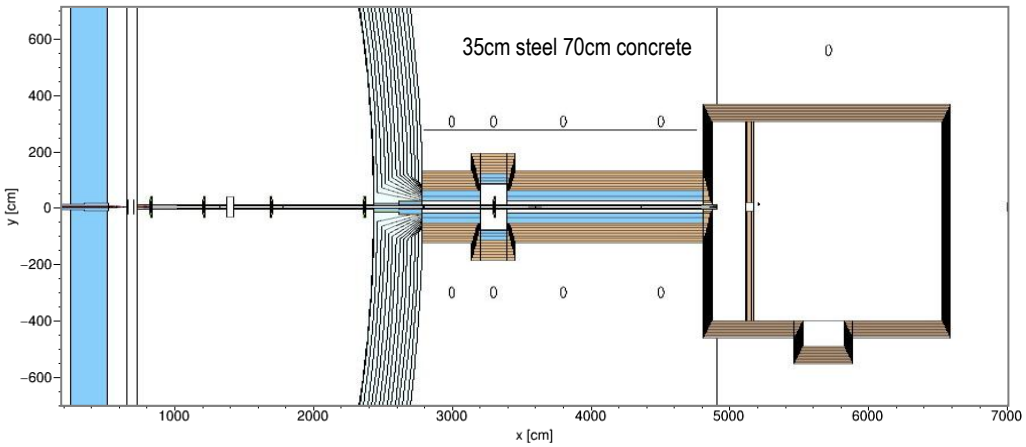

Fig. 134: Horizontal area through the Monte Carlo model of the ODIN instrument for which the radiation distribution is shown in the following image

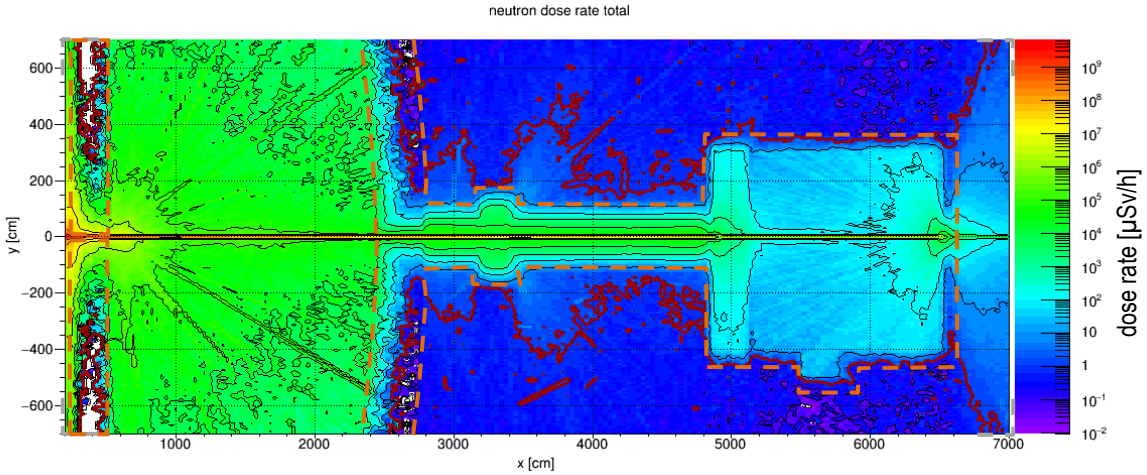

Fig. 135: Total neutron dose rate distribution in the horizontal area. The red line is the 1µSv/h border.

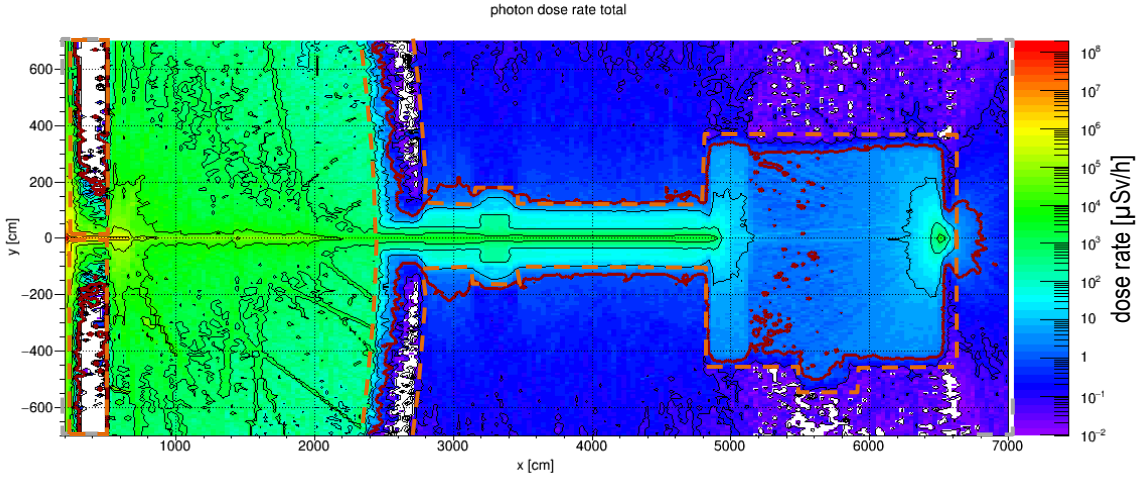

Fig. 136: Total generated gamma dose rate distribution in the horizontal area. The red line is the 1µSv/h border.

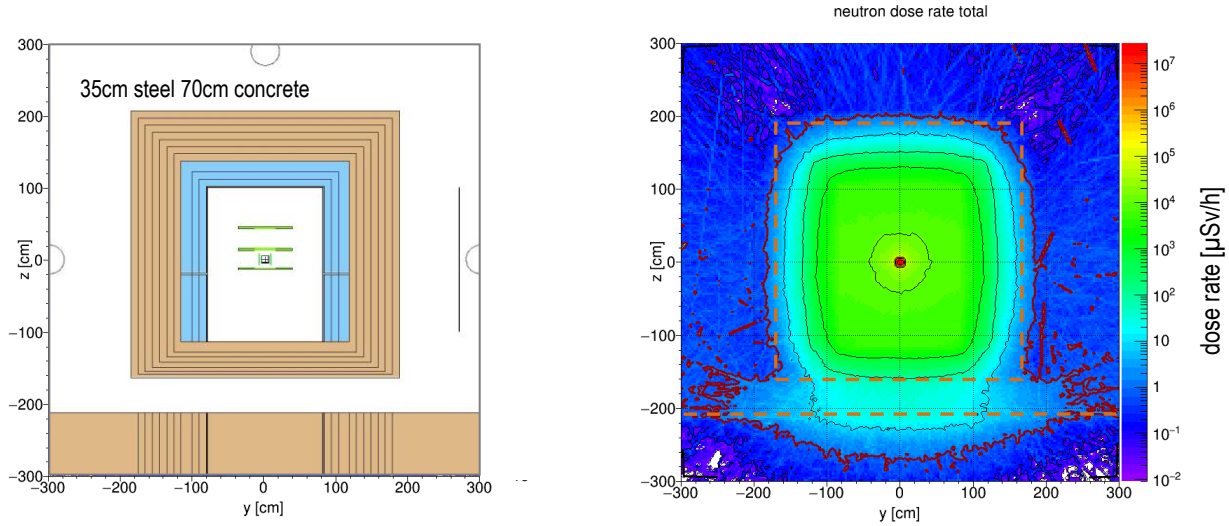

Fig. 137: Vertical neutron dose rate distribution through the chopper pit perpendicular to the beam axis. The red line is the 1µSv/h border.

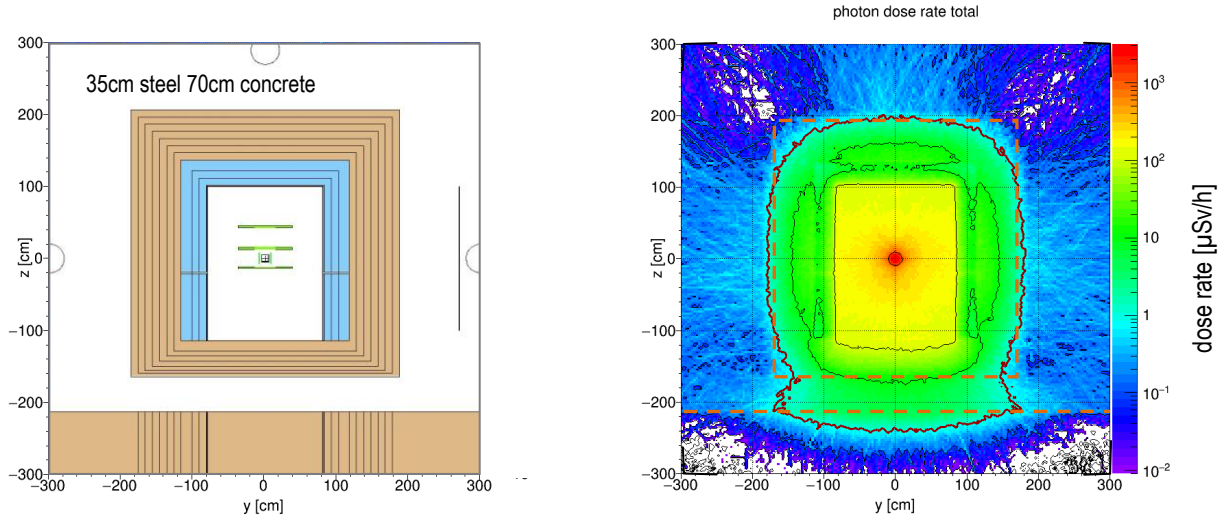

Fig. 138: Vertical generated gamma dose rate distribution through the chopper pit perpendicular to the beam axis. The red line is the 1µSv/h border.

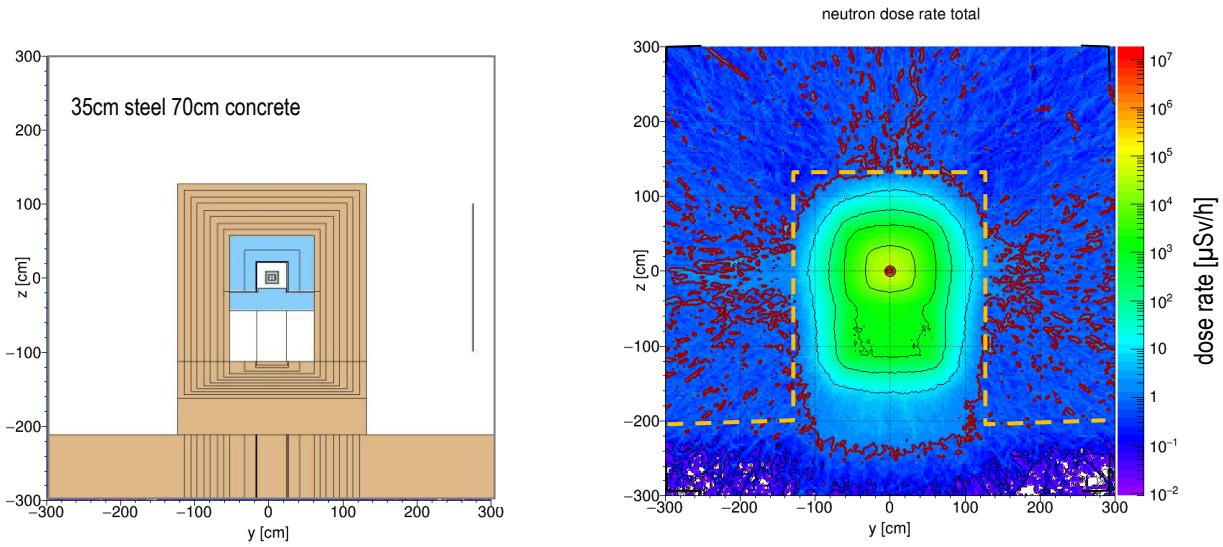

Fig. 139: Vertical neutron dose rate distribution through the guide shielding perpendicular to the beam axis (40m from the focal point). The red line is the 1µSv/h border.

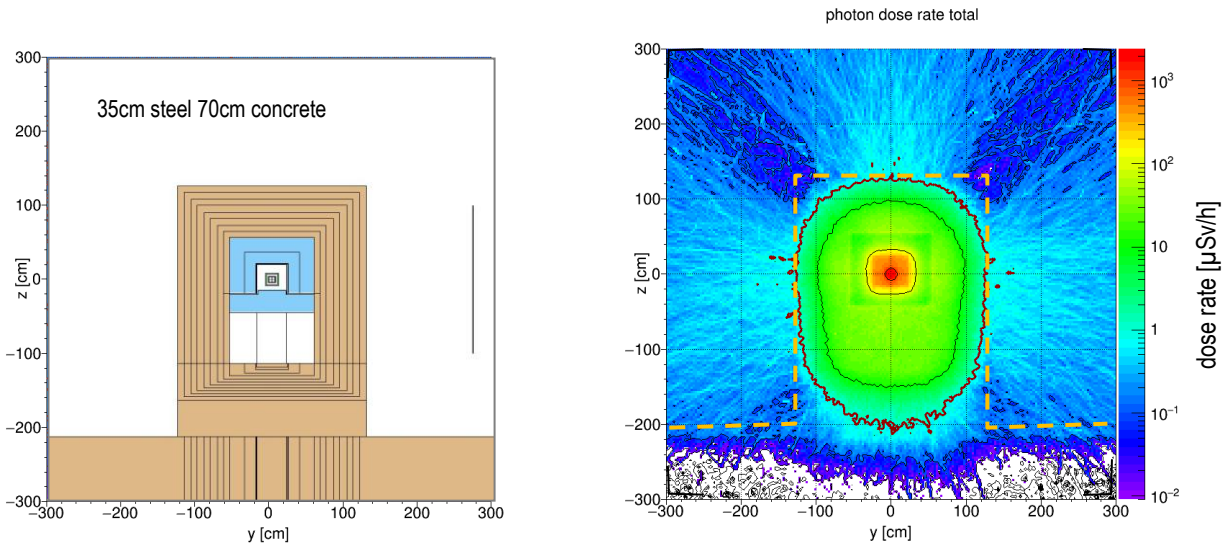

Fig. 140: Vertical generated gamma dose rate distribution through the guide shielding perpendicular to the beam axis (40m from the focal point). The red line is the 1µSv/h border.

5.4 Shielding version 3 consisting of 40cm steel and 70cm concrete

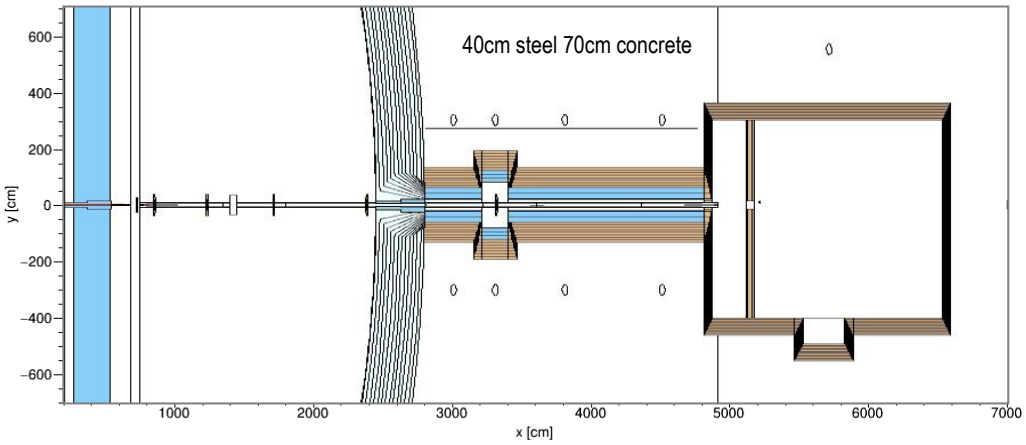

Fig. 141: Horizontal area through the Monte Carlo model of the ODIN instrument for which the radiation distribution is shown in the following image

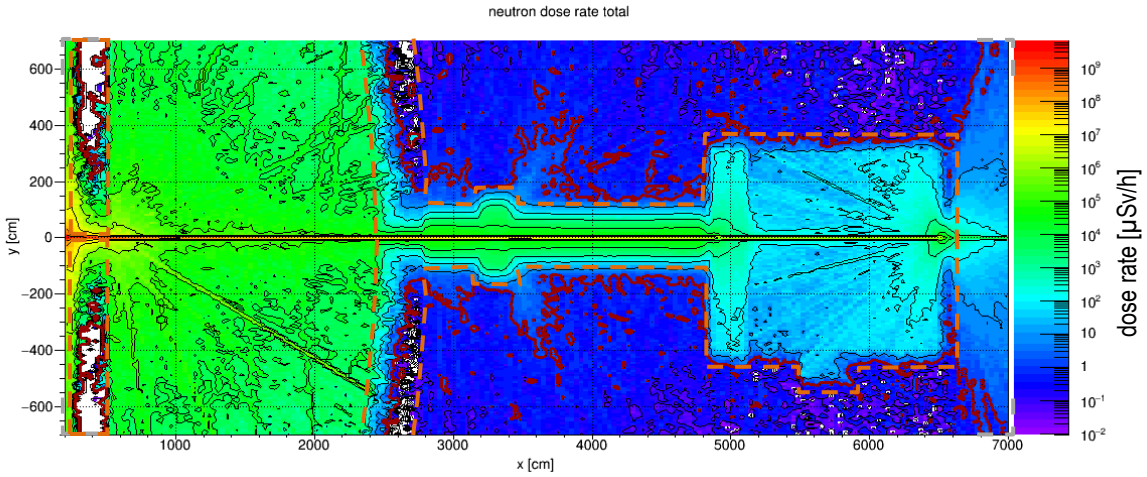

Fig. 142: Total neutron dose rate distribution in the horizontal area. The red line is the 1µSv/h border.

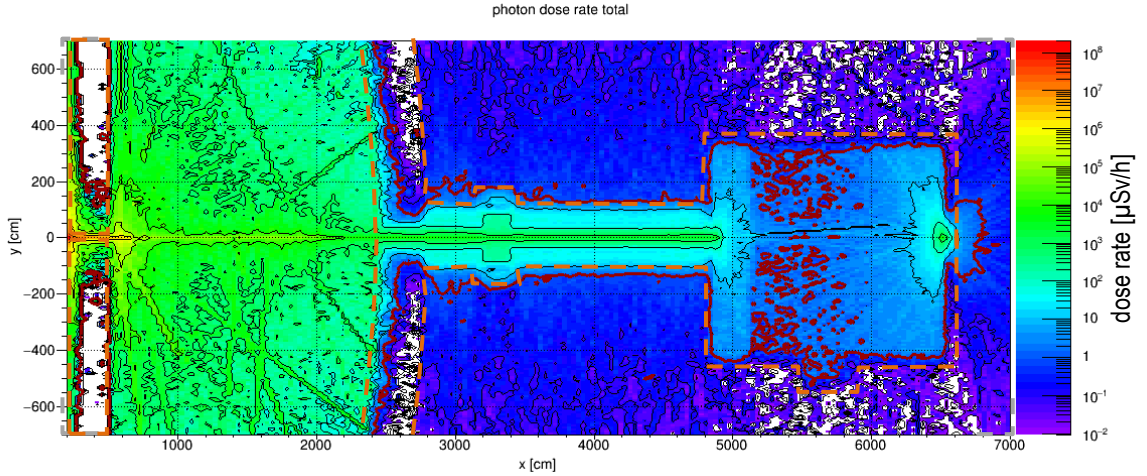

Fig. 143: Total generated gamma dose rate distribution in the horizontal area. The red line is the 1µSv/h border.

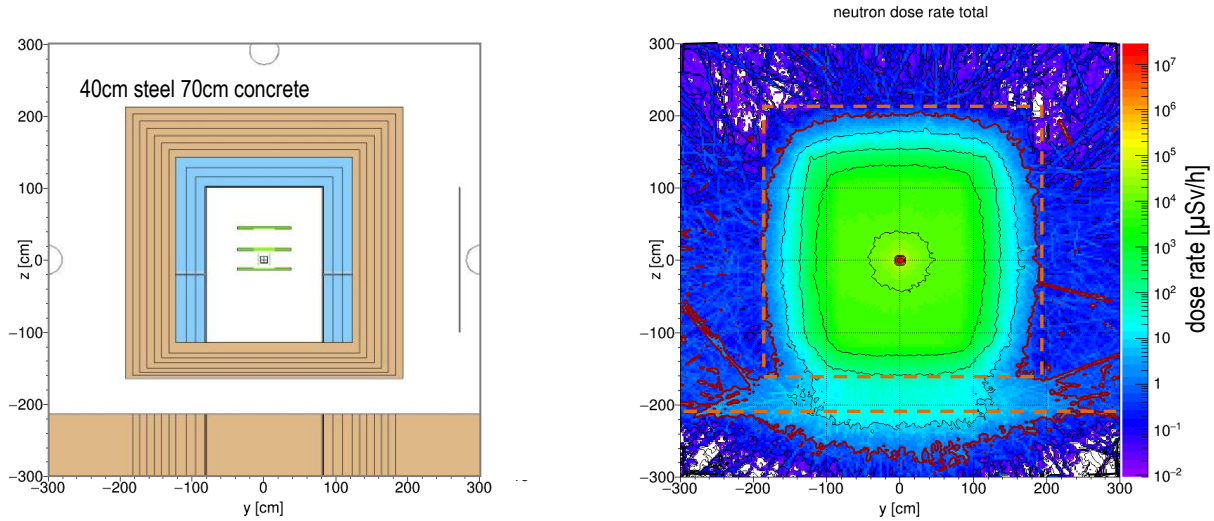

Fig. 144: Vertical neutron dose rate distribution through the chopper pit perpendicular to the beam axis. The red line is the 1µSv/h border.

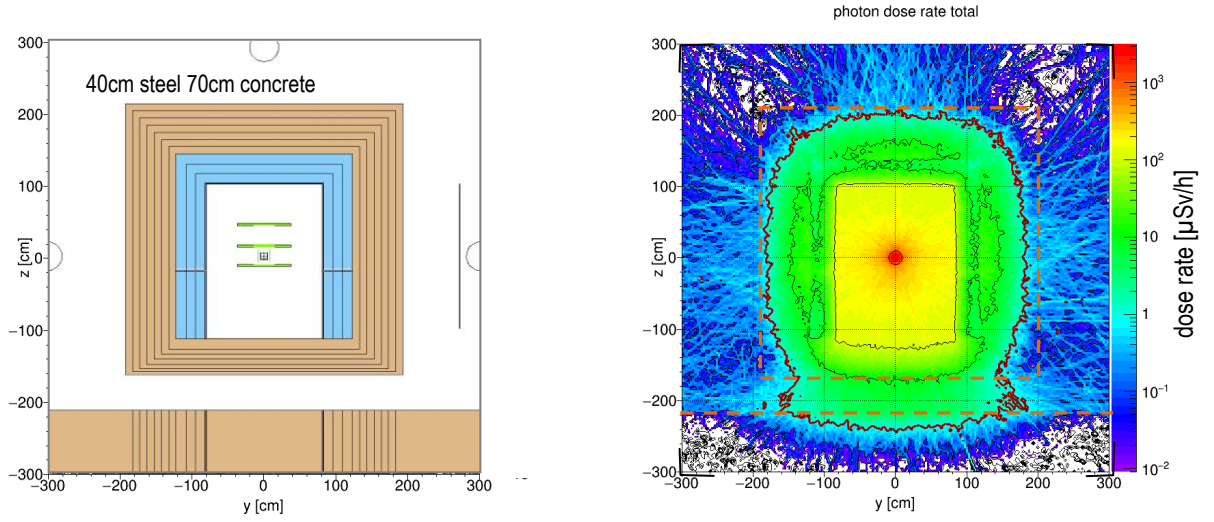

Fig. 145: Vertical generated gamma dose rate distribution through the chopper pit perpendicular to the beam axis. The red line is the 1µSv/h border.

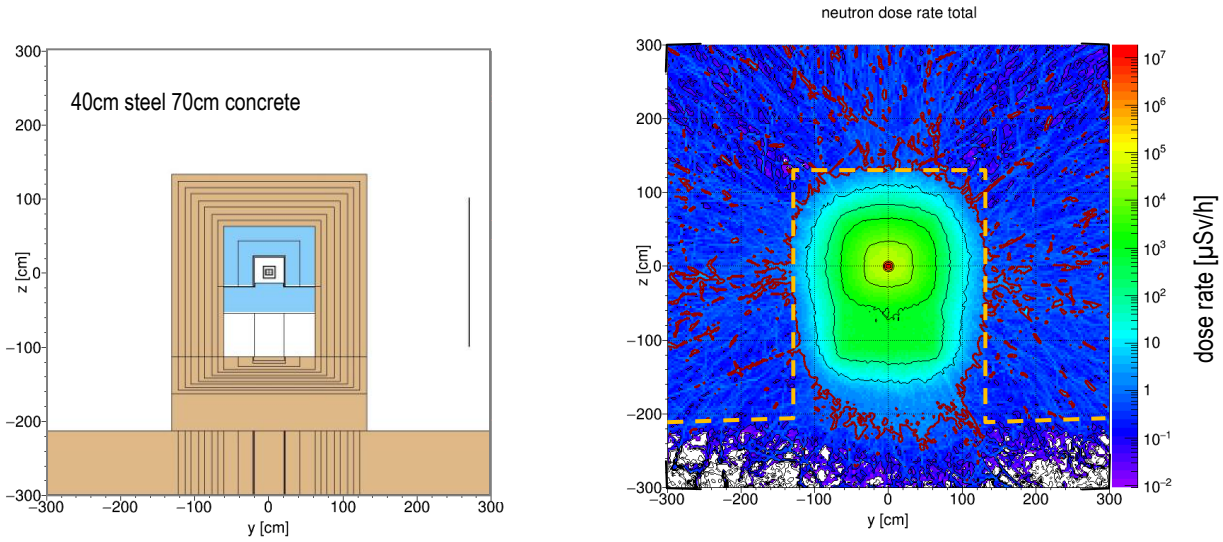

Fig. 146: Vertical neutron dose rate distribution through the guide shielding perpendicular to the beam axis (40m from the focal point). The red line is the 1µSv/h border.

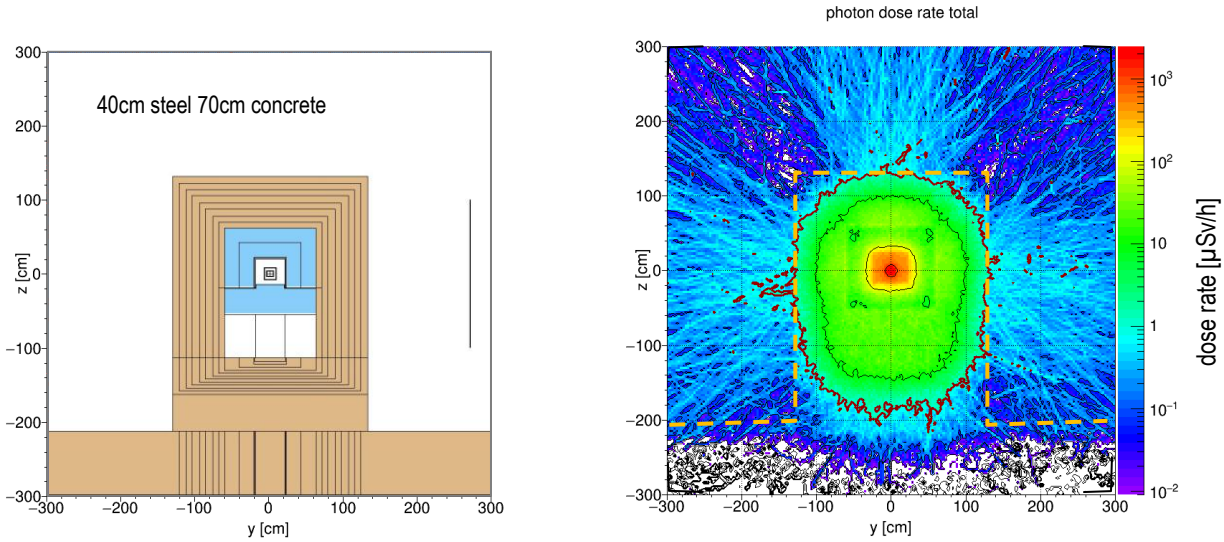

Fig. 147: Vertical generated gamma dose rate distribution through the guide shielding perpendicular to the beam axis (40m from the focal point). The red line is the 1µSv/h border.

5.5 Shielding version 3 consisting of 45cm steel and 70cm concrete

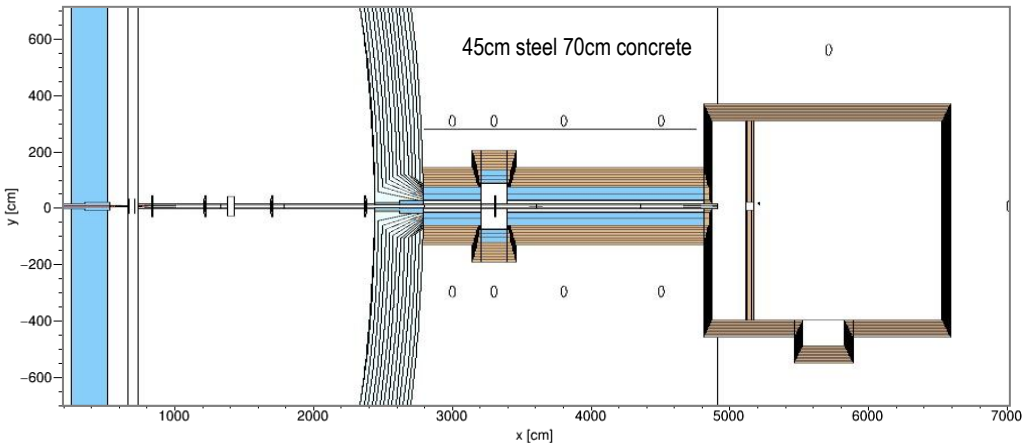

Fig. 148: Horizontal area through the Monte Carlo model of the ODIN instrument for which the radiation distribution is shown in the following image

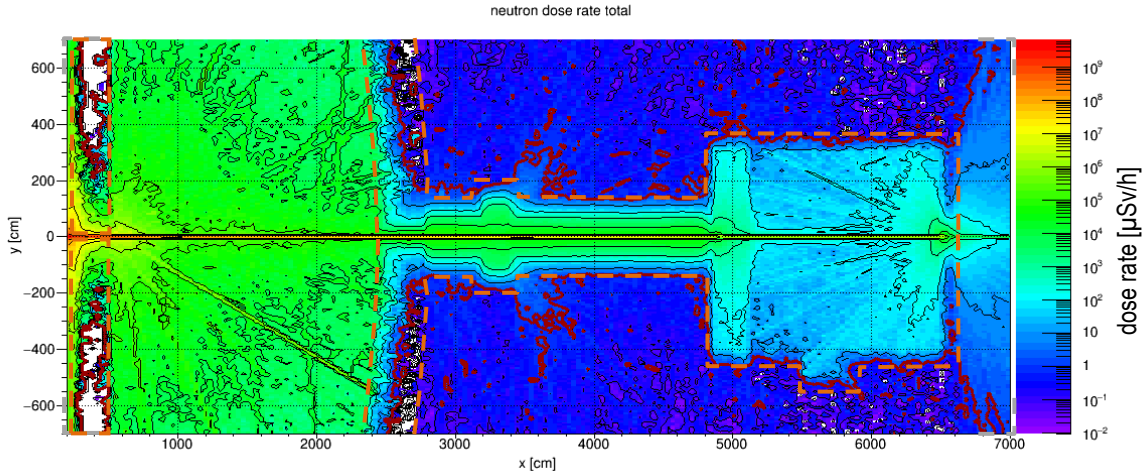

Fig. 149: Total neutron dose rate distribution in the horizontal area. The red line is the 1µSv/h border.

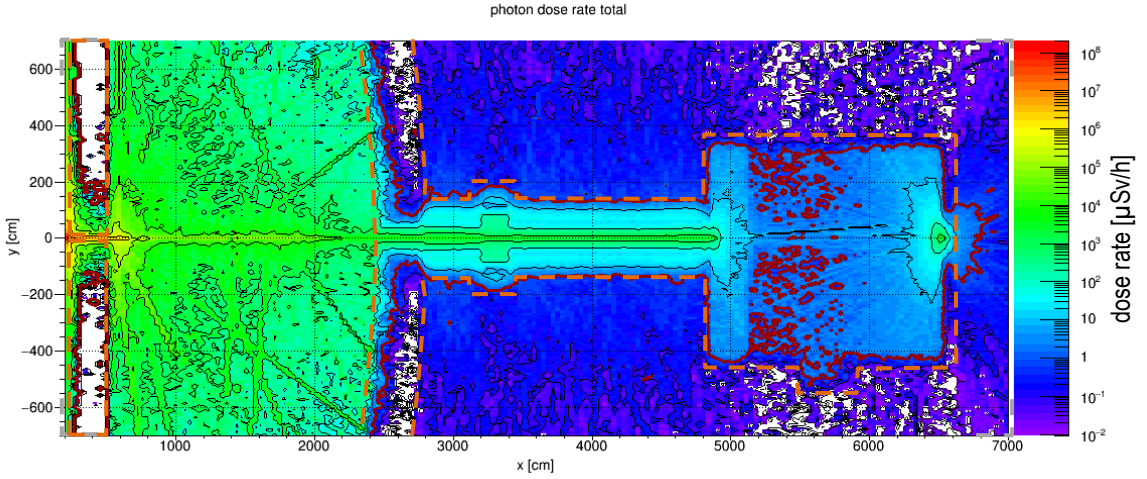

Fig. 150: Total generated gamma dose rate distribution in the horizontal area. The red line is the 1µSv/h border.

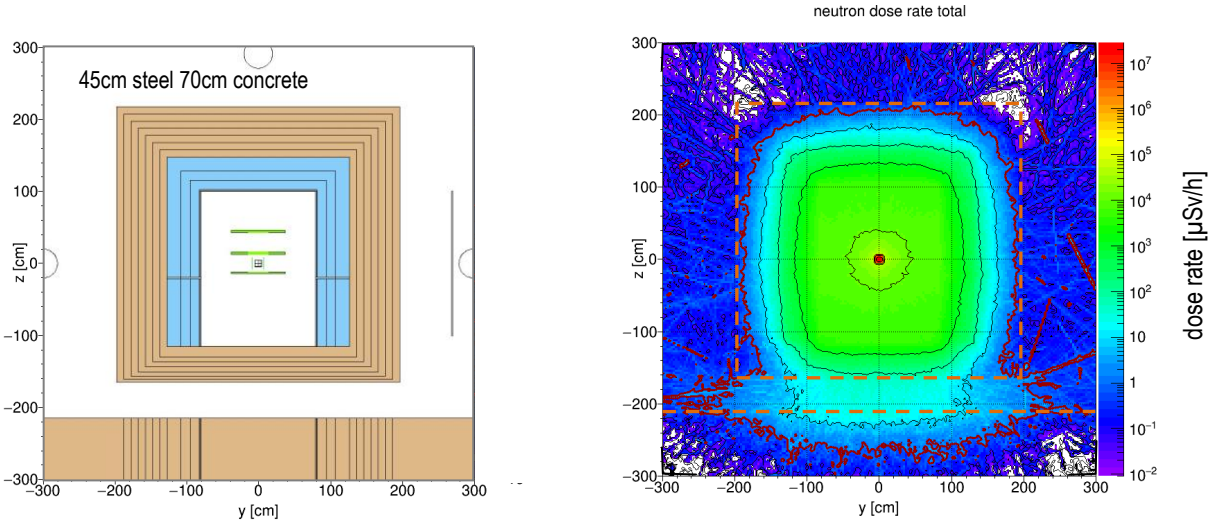

Fig. 151: Vertical neutron dose rate distribution through the chopper pit perpendicular to the beam axis. The red line is the 1µSv/h border.

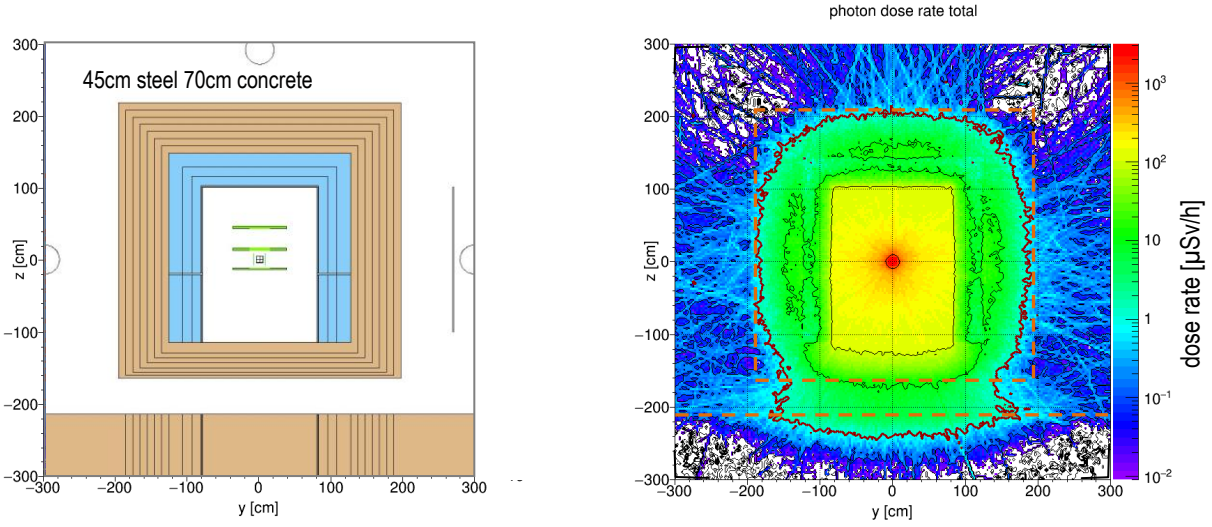

Fig. 152: Vertical generated gamma dose rate distribution through the chopper pit perpendicular to the beam axis. The red line is the 1µSv/h border.

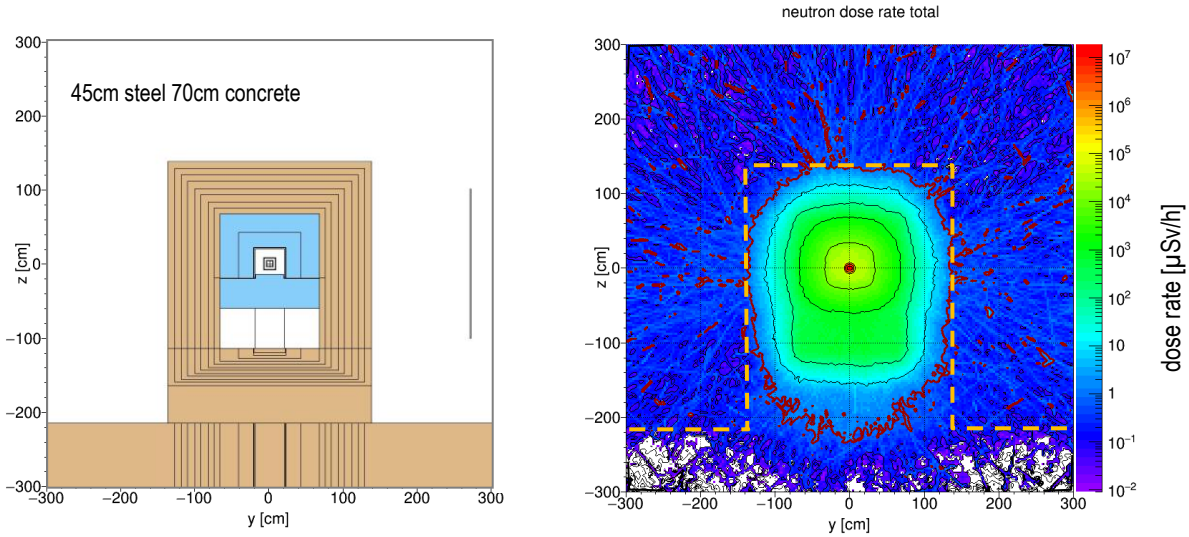

Fig. 153: Vertical neutron dose rate distribution through the guide shielding perpendicular to the beam axis (40m from the focal point). The red line is the 1µSv/h border.

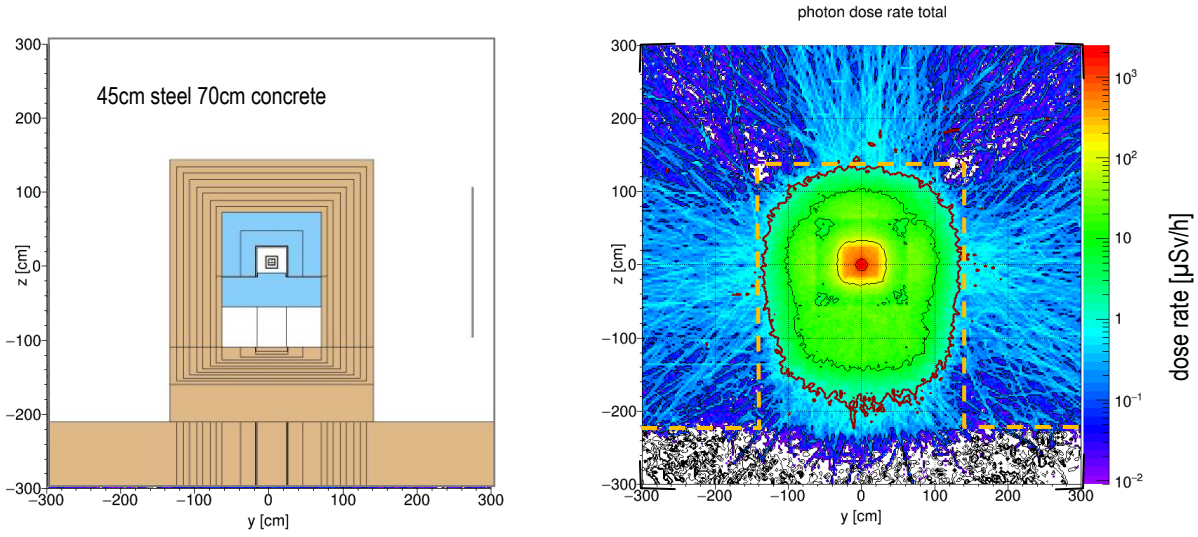

Fig. 154: Vertical generated gamma dose rate distribution through the guide shielding perpendicular to the beam axis (40m from the focal point). The red line is the 1µSv/h border.

5.6 Shielding version 3 consisting of 30cm steel and 80cm concrete

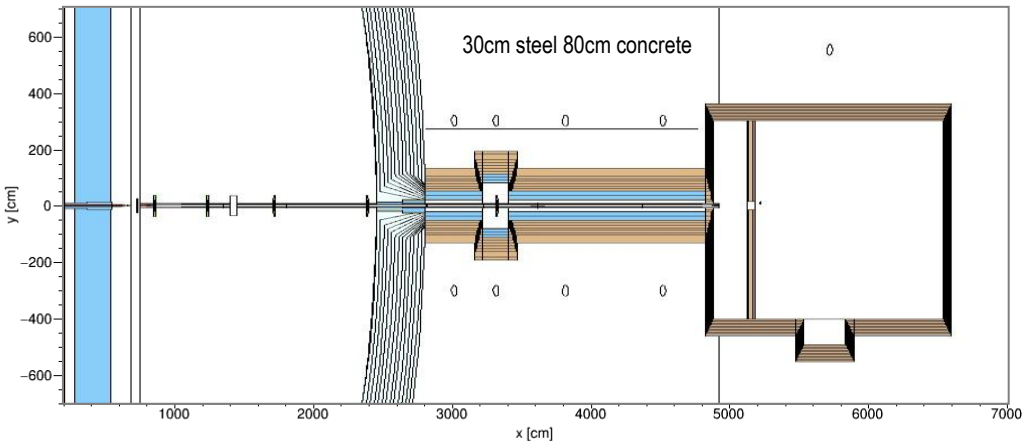

Fig. 155: Horizontal area through the Monte Carlo model of the ODIN instrument for which the radiation distribution is shown in the following image

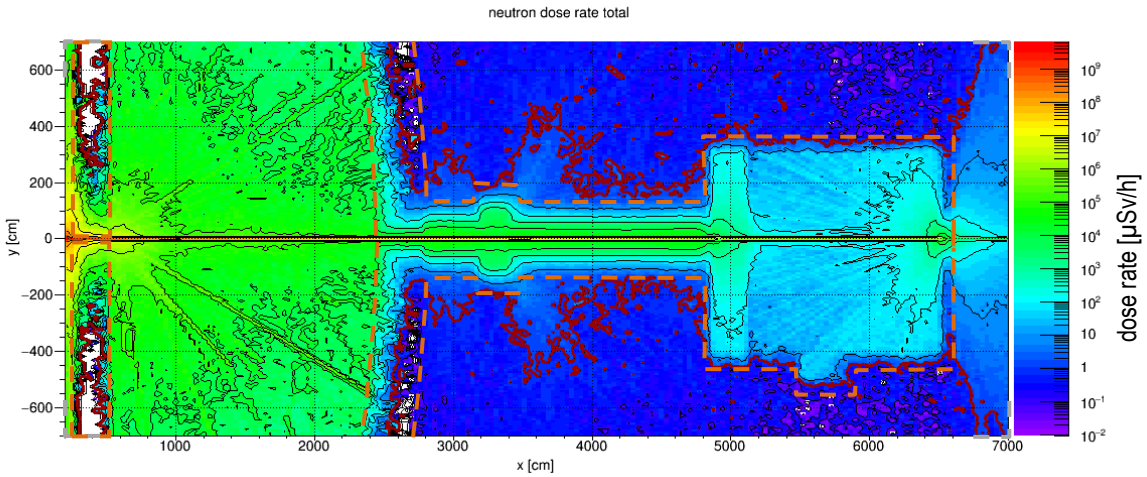

Fig. 156: Total neutron dose rate distribution in the horizontal area. The red line is the 1µSv/h border.

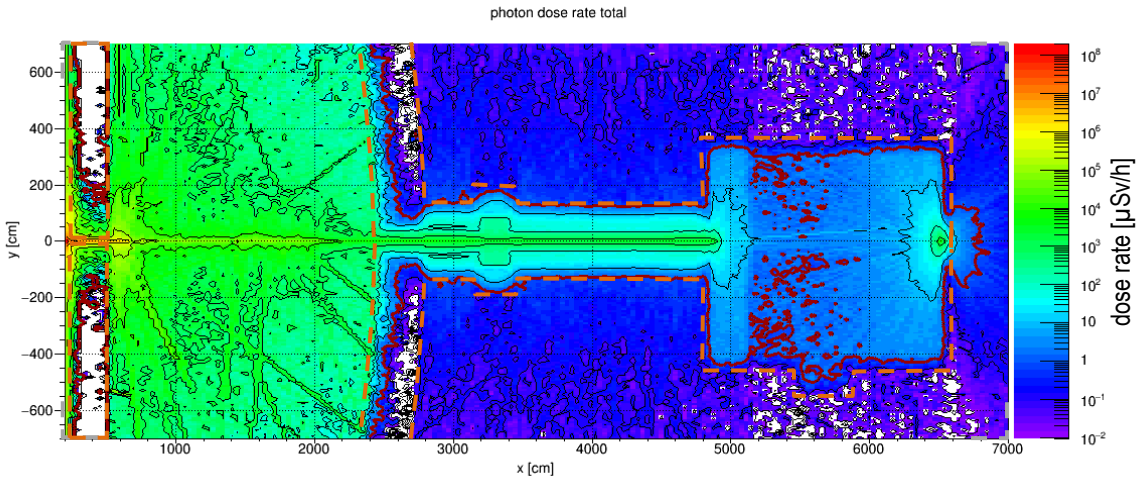

Fig. 157: Total generated gamma dose rate distribution in the horizontal area. The red line is the 1µSv/h border.

5.7 Shielding version 3 consisting of 30cm steel and 90cm concrete

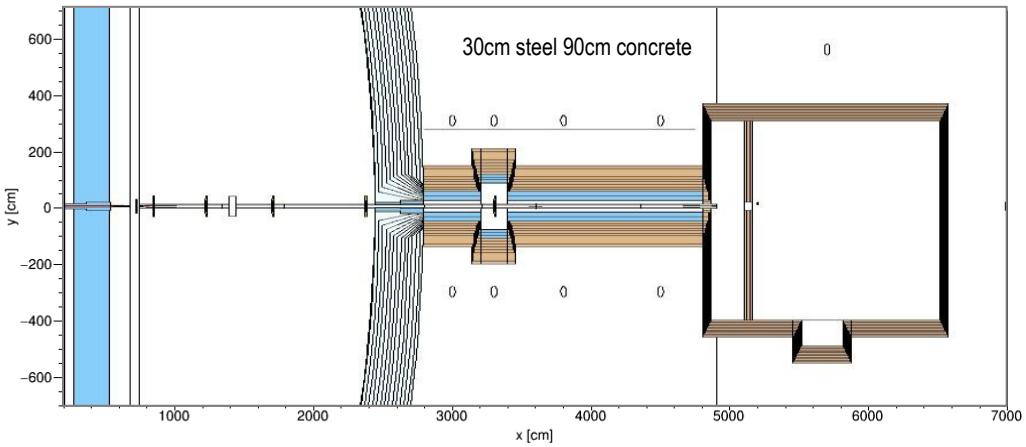

Fig. 158: Horizontal area through the Monte Carlo model of the ODIN instrument for which the radiation distribution is shown in the following image

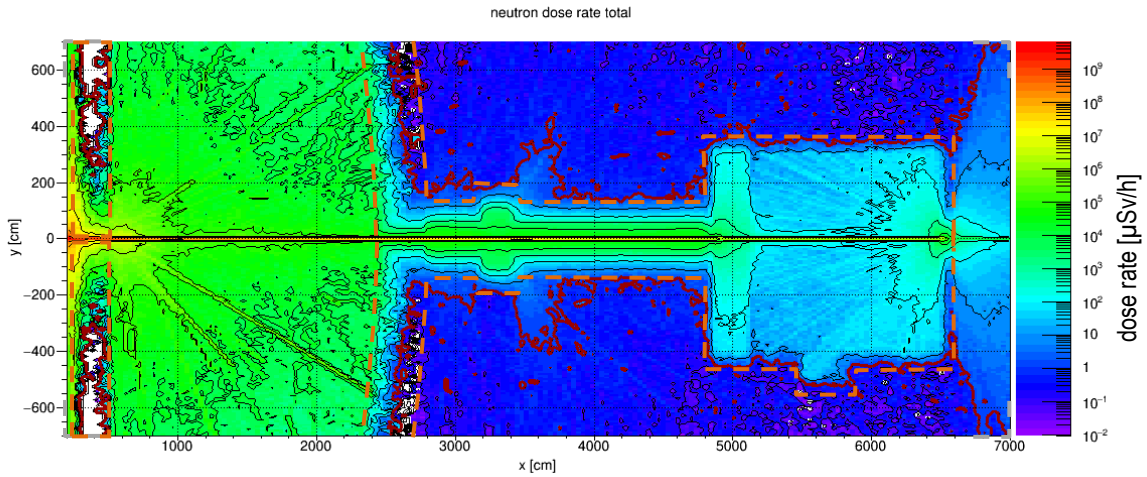

Fig. 159: Total neutron dose rate distribution in the horizontal area. The red line is the 1µSv/h border.

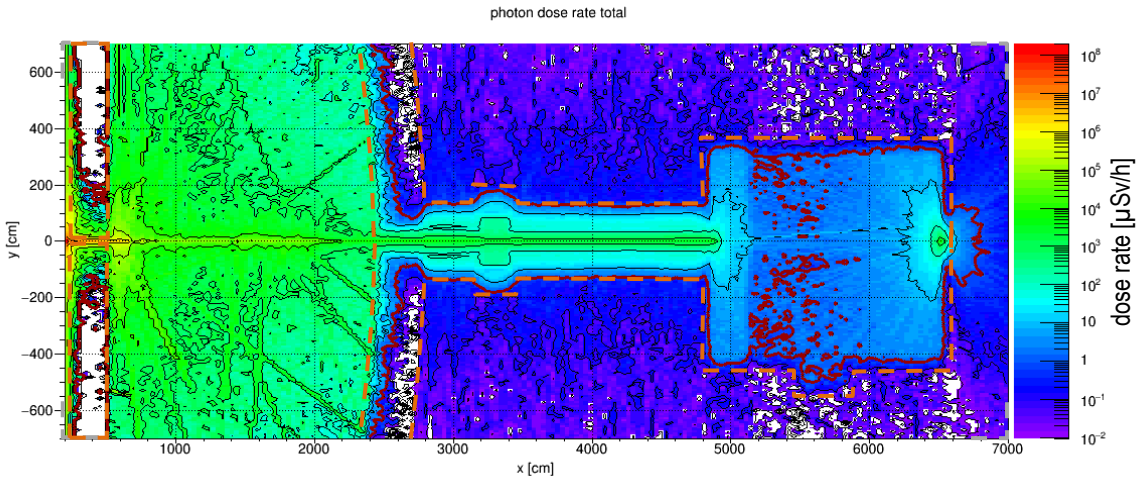

Fig. 160: Total generated gamma dose rate distribution in the horizontal area. The red line is the 1µSv/h border.

5.8 Shielding version 3 consisting of 30cm steel and 100cm concrete

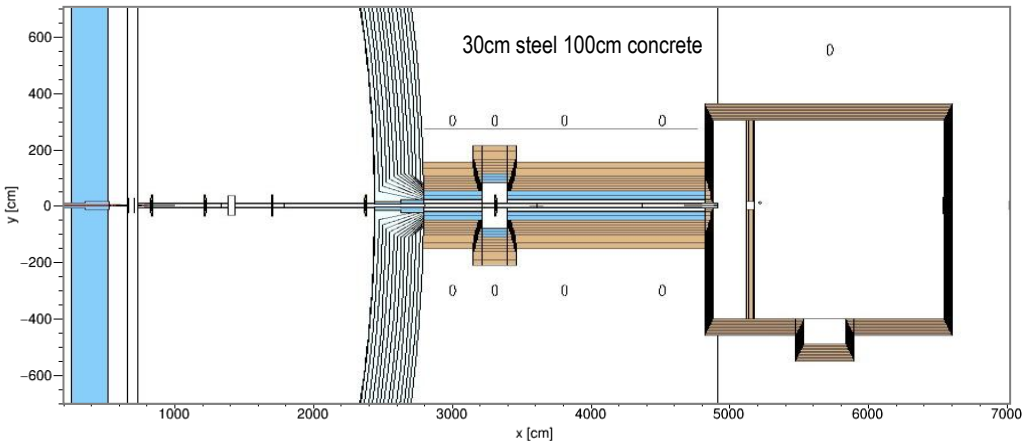

Fig. 161: Horizontal area through the Monte Carlo model of the ODIN instrument for which the radiation distribution is shown in the following image

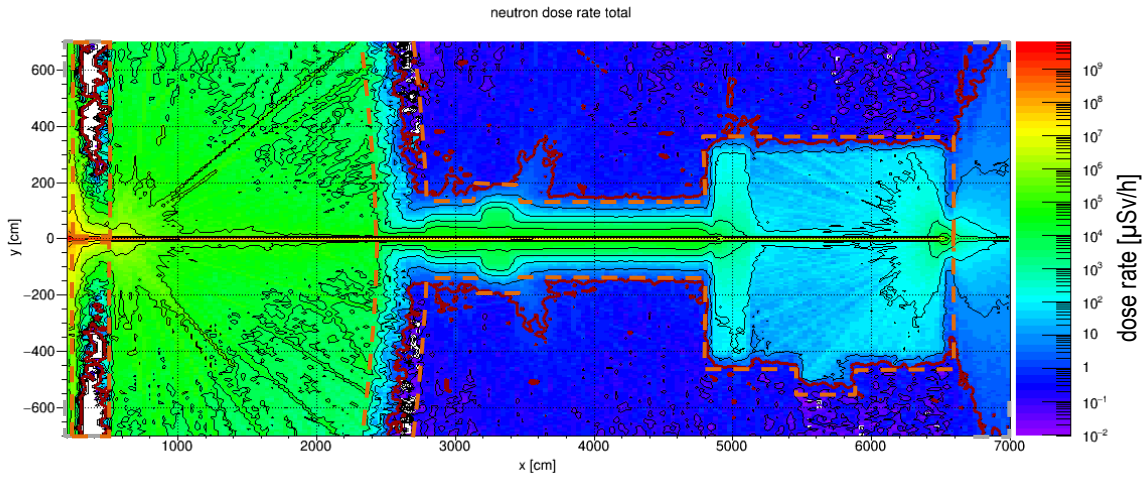

Fig. 162: Total neutron dose rate distribution in the horizontal area. The red line is the 1µSv/h border.

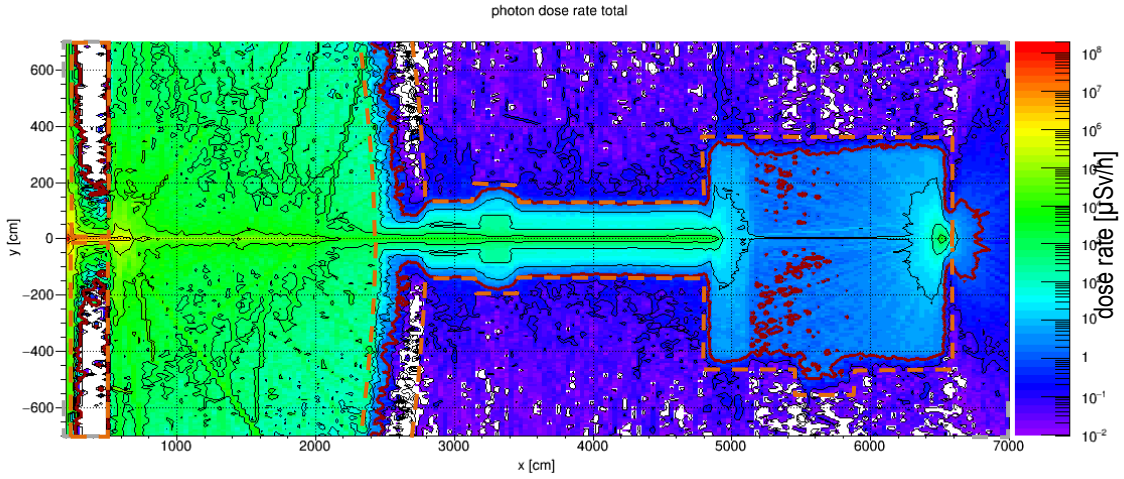

Fig. 163: Total generated gamma dose rate distribution in the horizontal area. The red line is the 1µSv/h border.

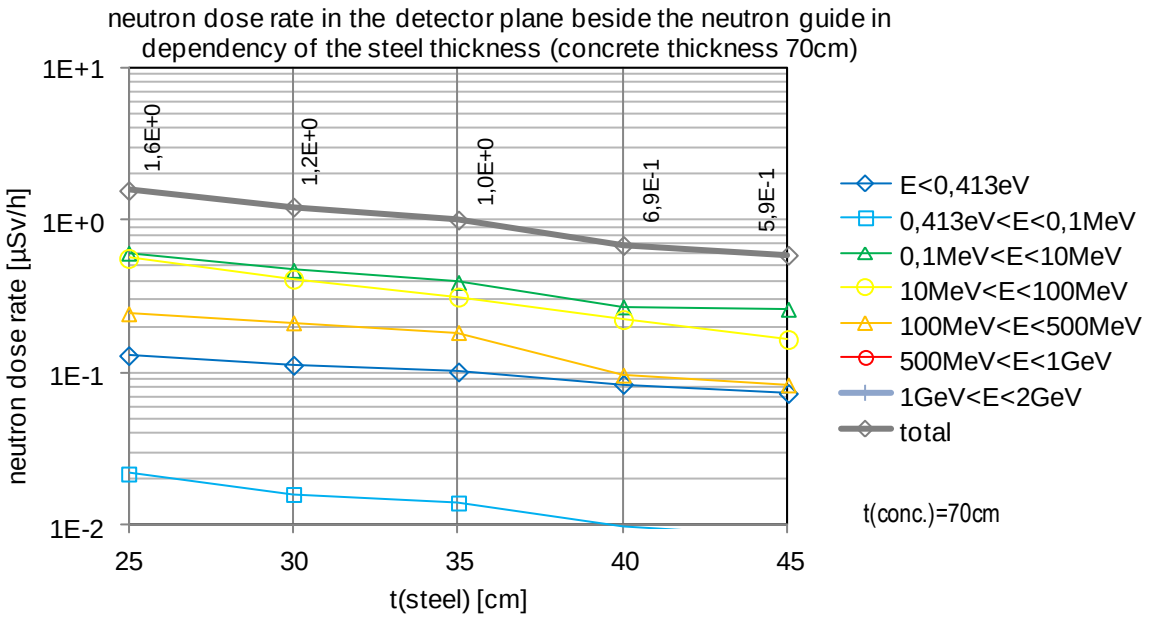

Fig. 164: neutron dose rate in the detector plane beside the neutron guide in dependency of the steel thickness (concrete thickness 70cm)

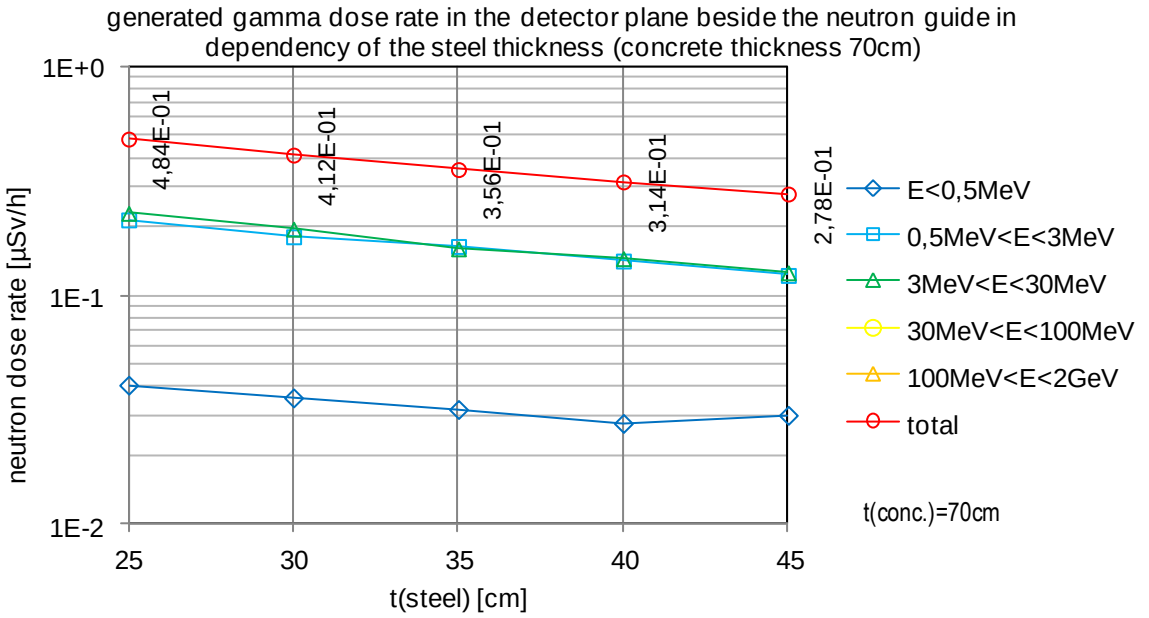

Fig. 165: generated gamma dose rate in the detector plane beside the neutron guide in dependency of the steel thickness (concrete thickness 70cm)

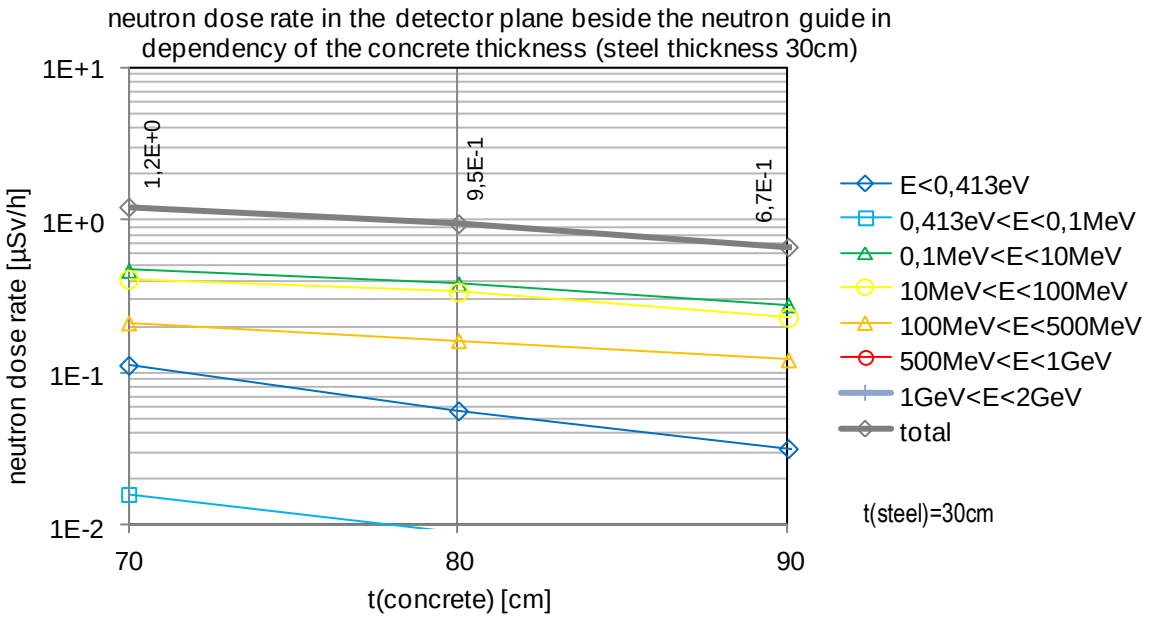

Fig. 166: neutron dose rate in the detector plane beside the neutron guide in dependency of the concrete thickness (steel thickness 30cm)

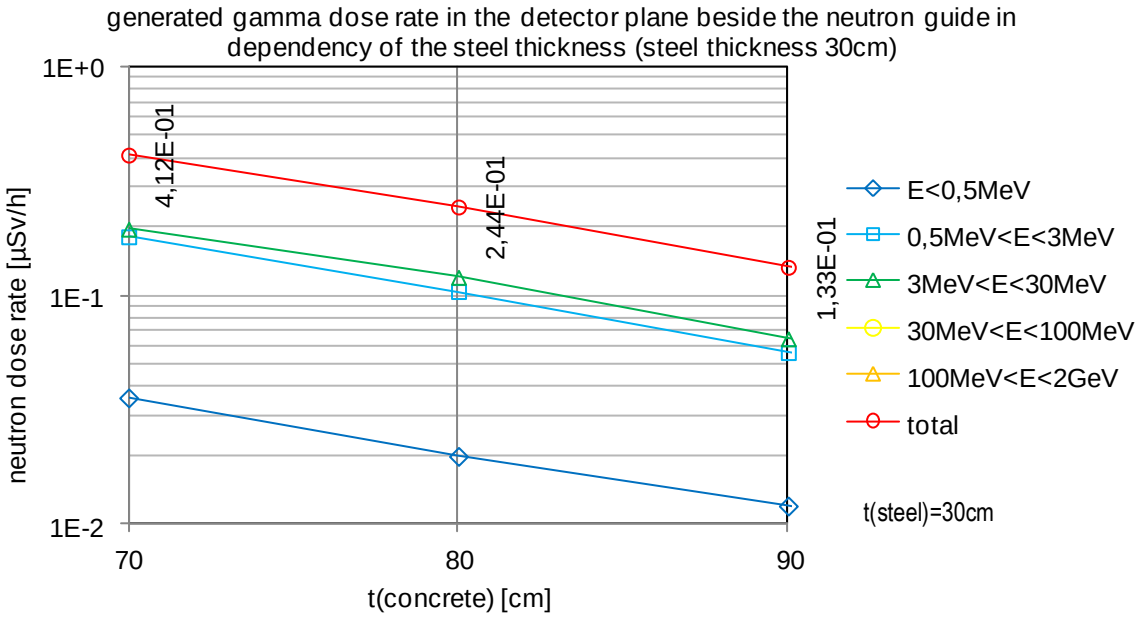

Fig. 167: generated gamma dose rate in the detector plane beside the neutron guide in dependency of the steel thickness (steel thickness 30cm)

6 Radiography of the moderator and its surrounding

Problem: Can the neutron flux in the channels be scaled by the area of the entrance window of the NBOA when the window size is changed? This would be the case if the moderator and its surrounding act as a big homogenous source (bigger than the entrance window). In order to answer this question a radiography of the moderator and its surrounding was performed. A layer of an ideal absorber was placed outside the NBOA at the ODIN (mirror) channel 5.5m from the focal point. The aperture in the layer has a radius of 1mm and a DXRAN sphere was placed in it. The hydrogen cross section table was changed from 1001.70c (upper energy border of tables: 20MeV) to 1001.66c (upper energy border of tables: 150MeV). Above the upper energy border of tables models are used in MCNP which cause errors in combination with next event estimators and DXTRAN spheres. However, up to 150MeV a projection of the source yield of the moderator and its surrounding can be obtained in this way. For the guide shielding the neutron energy group between 0.1MeV and 100MeV is most important.

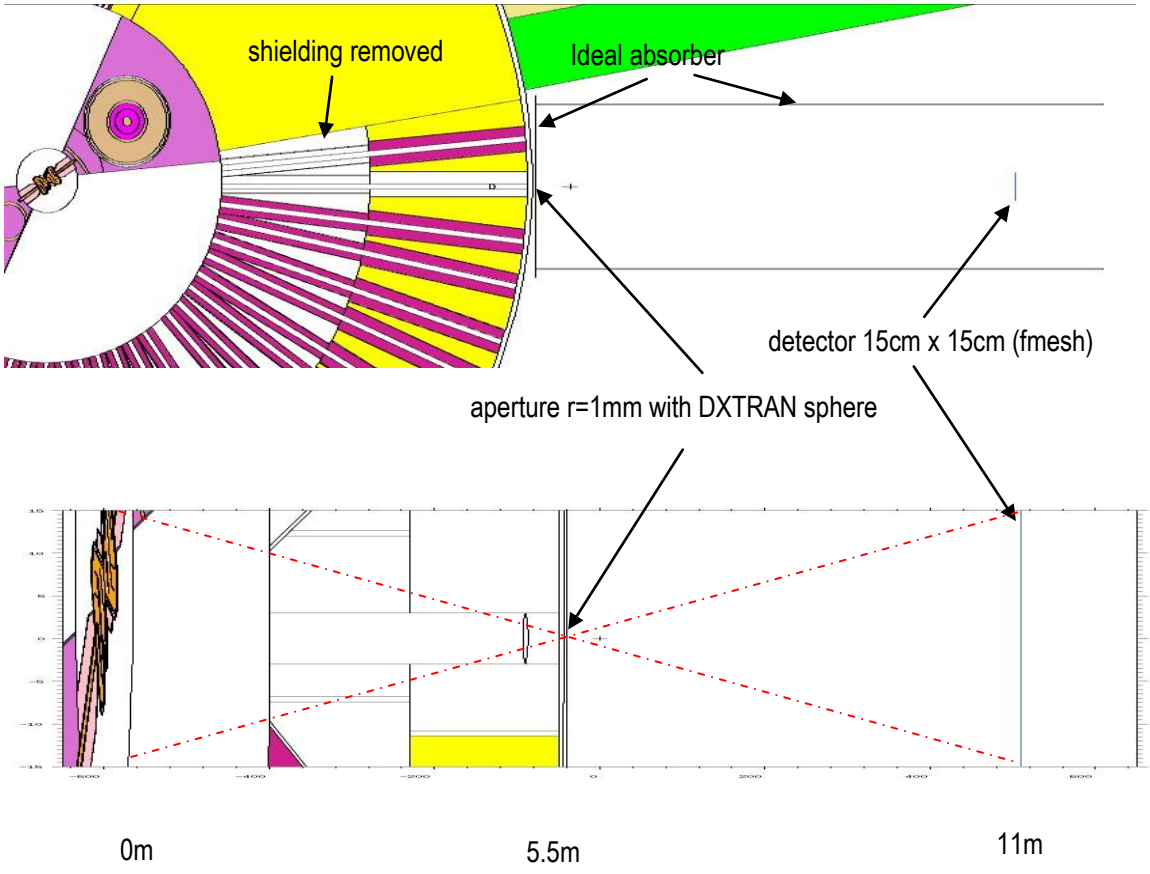

Fig. 168: Horizontal cut through the Monte Carlo model for radiography of the target

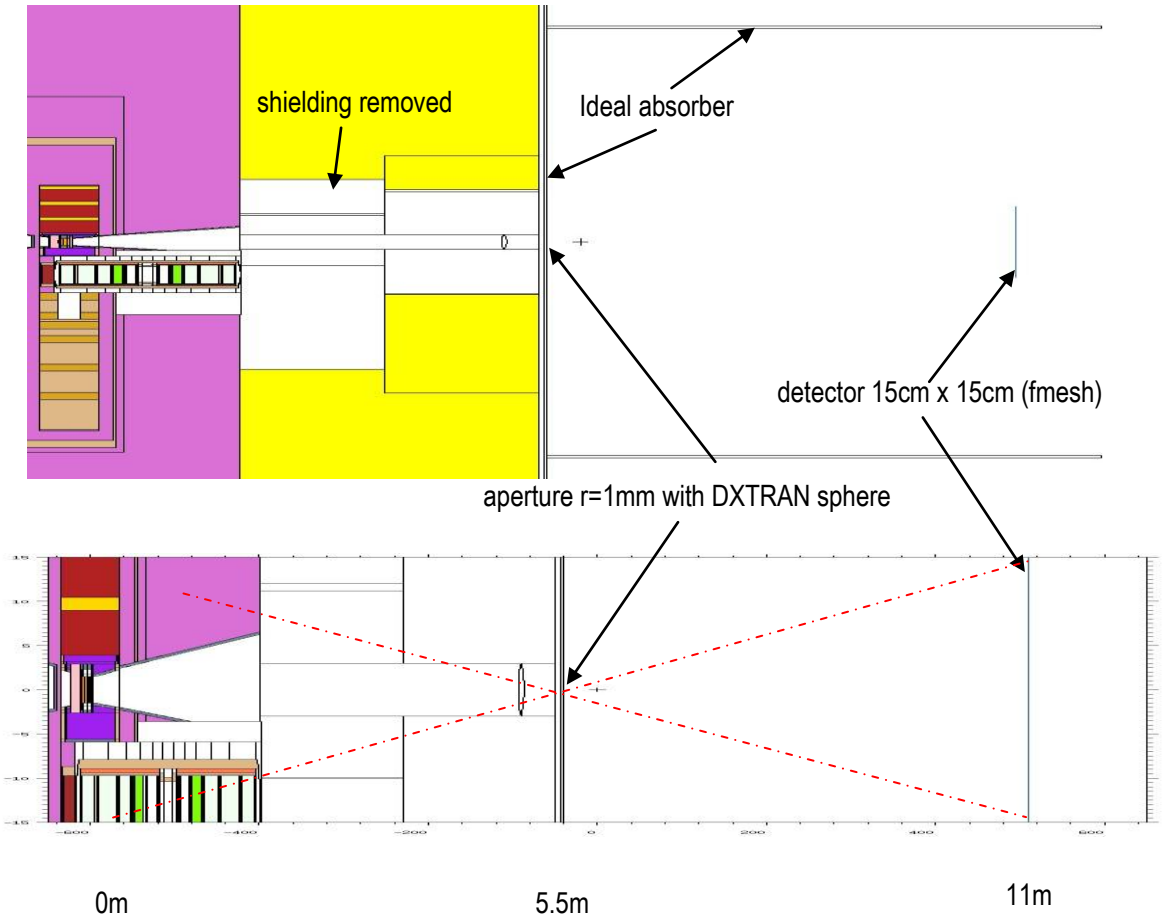

Fig. 169: Vertical cut through the Monte Carlo model for radiography of the target

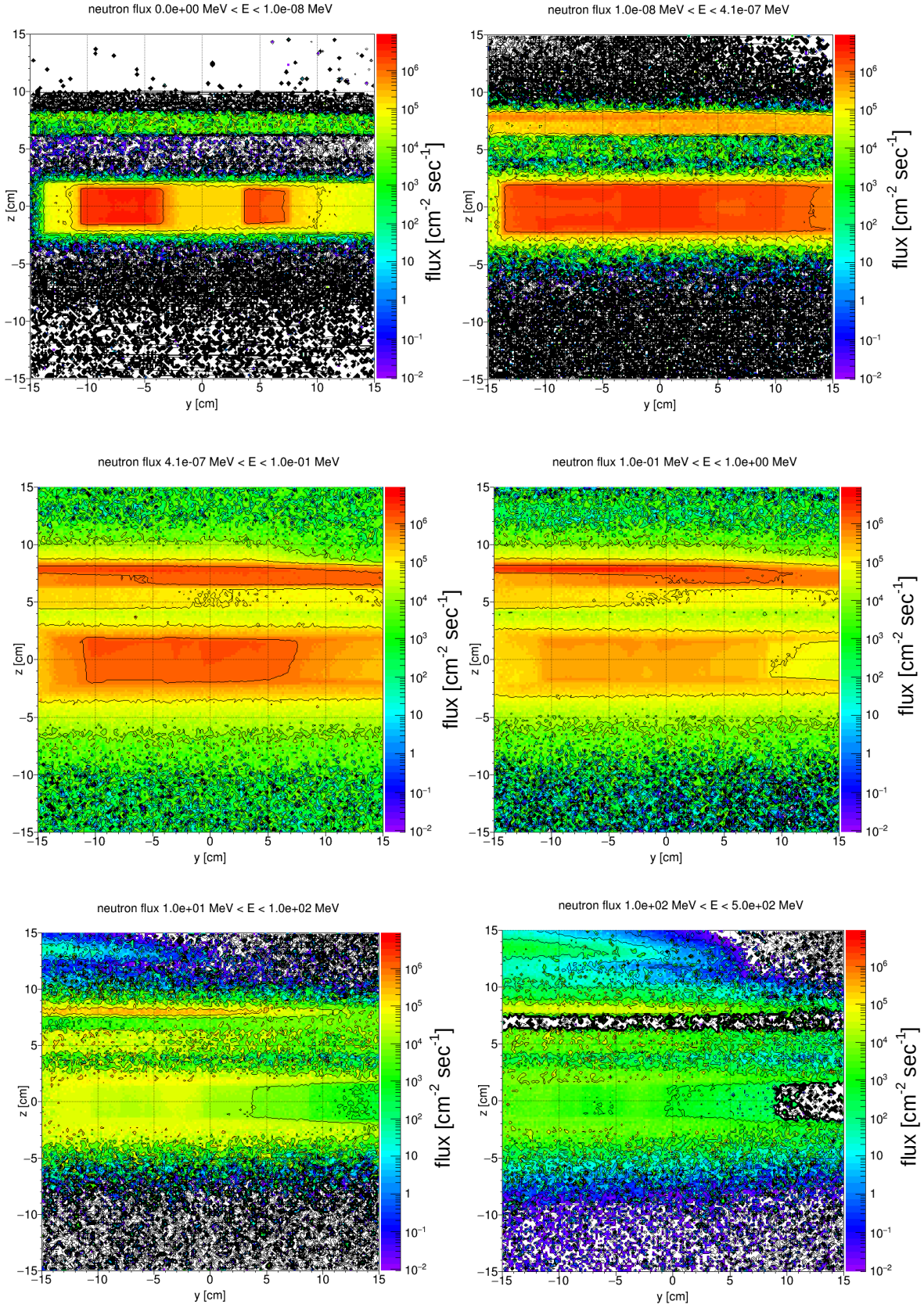

Fig. 170: Neutron flux in the detector plane in different energy groups. The flux values present a mirrored projection of the source yield

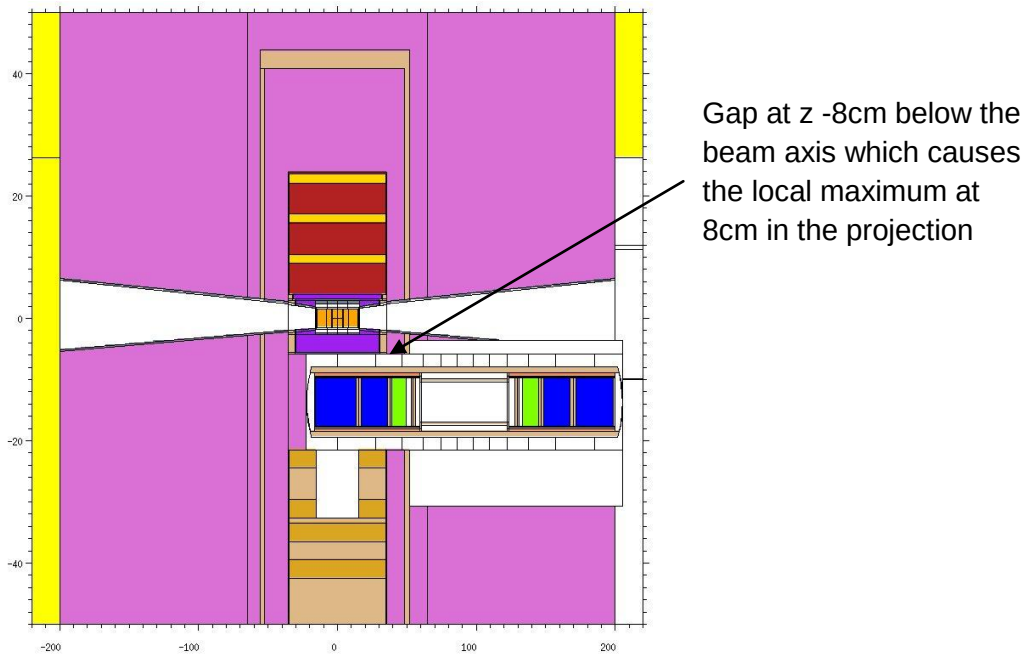

Fig. 171: Vertical cut through the Monte Carlo model for radiography of the target

7 New fictive neutron source

For the following presented simulations no longer the CSPEC source data was used but the own source data obtained by a f4 (track length estimator) simulation for the ODIN channel with the ESS target model. In the simulation a channel size of 6cm x 6cm was applied. An additional f5 simulation with the neutron guide showed that the flux is decreased by the neutron guide (no total reflection considered) by only 31%. For safety reasons the values for the 6cm x 6 cm channel are used for the fictive source in the area of the focal point. The source area was increased to 4cm (h) x 10cm (w) due to the radiography results presented in the last chapter. The higher beam divergency causes also a decrease in neutron flux at 28m. The total neutron flux at 5m from the focal point is $8.53 \cdot 10^{9} cm^{-2} sec^{-1}$.

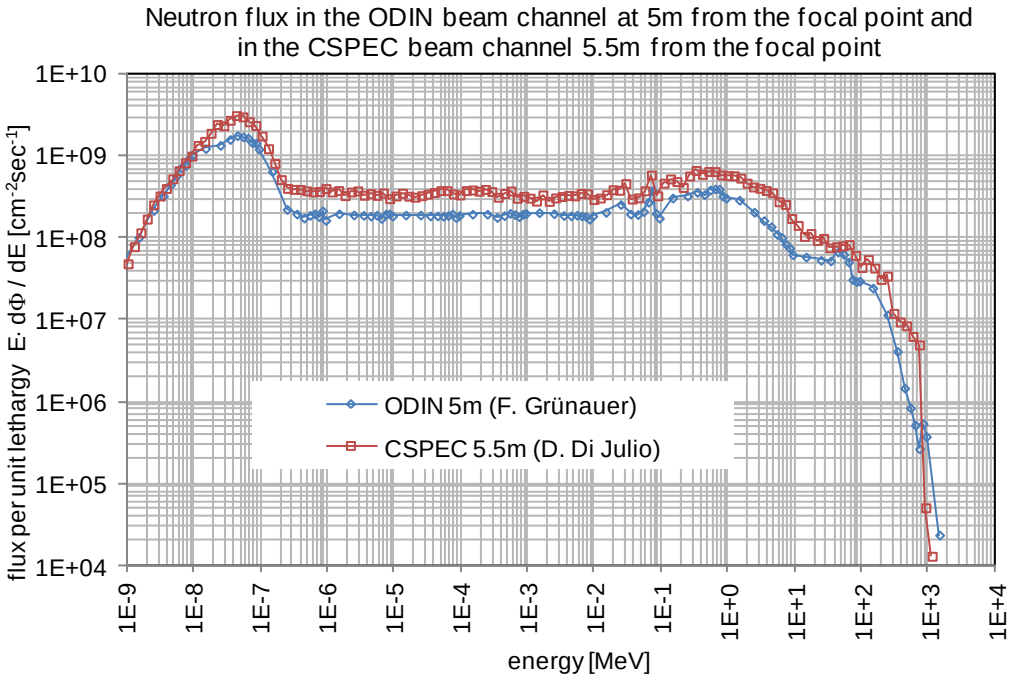

Fig. 172: Neutron flux in the ODIN beam channel at 5m from the focal point and in the CSPEC beam channel 5.5m from the focal point

7.1 Shielding version 3 consisting of 25cm steel and 70cm concrete

The simulation for the common guide shielding version 3 with 25cm steel and 70cm ordinary concrete was repeated with the ODIN source data. The results are shown in the following figures. For comparison the results with the old CSPEC source data are also shown. With the new ODIN source data the shielding version 3 with 25cm steel and 70cm ordinary concrete attenuates the radiation to the desired level.

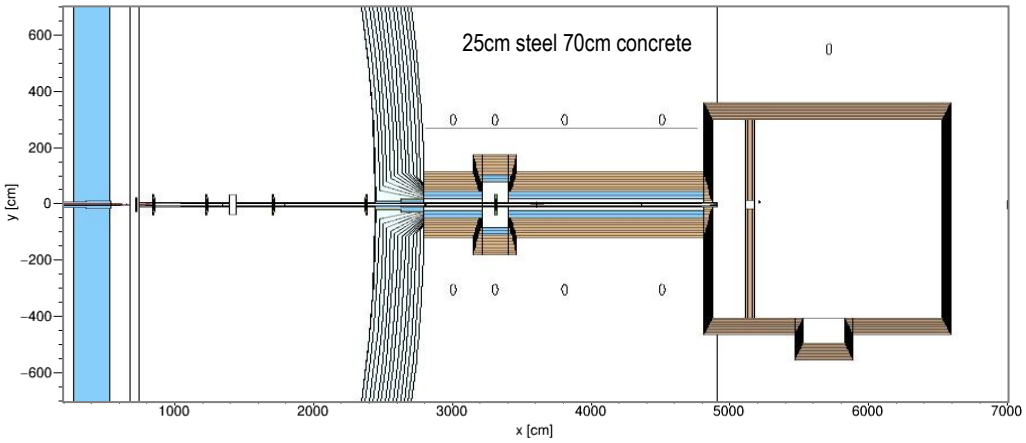

Fig. 173: Horizontal area through the Monte Carlo model of the ODIN instrument for which the radiation distribution is shown in the following image

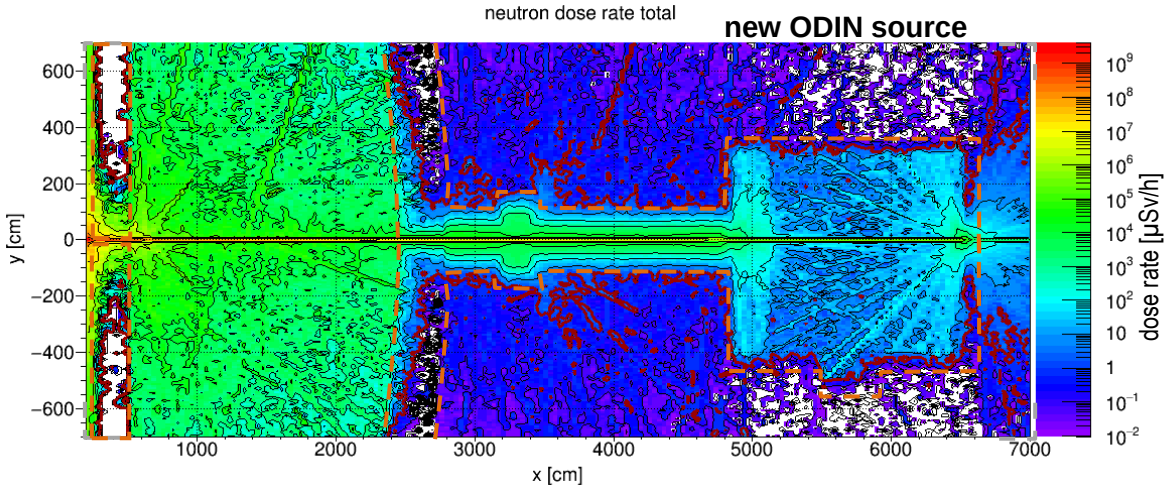

Fig. 174: Total neutron dose rate distribution in the horizontal area obtained **with the ODIN source data**. *The red line is the 1µSv/h border.*

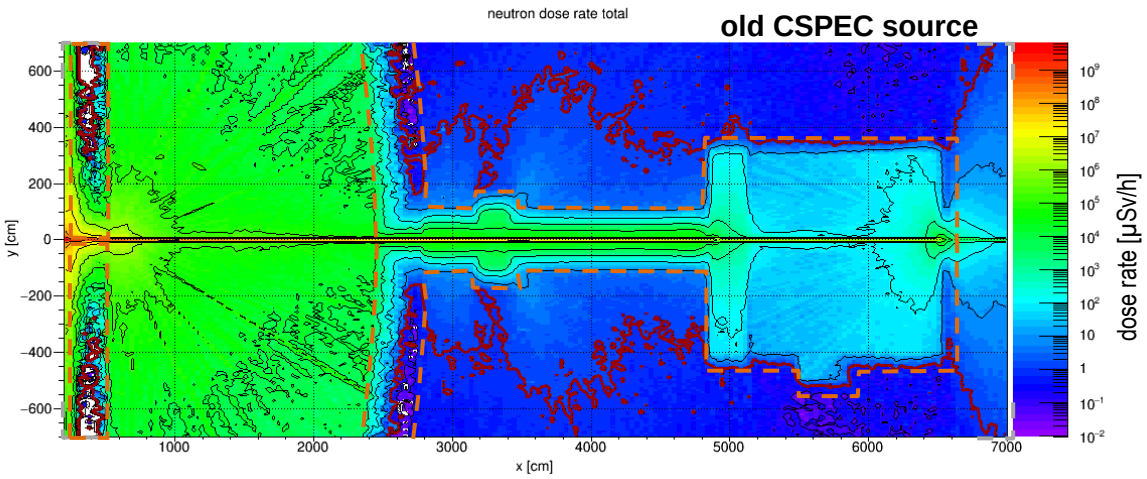

Fig. 175: For comparison: Total neutron dose rate distribution in the horizontal area obtained **with the old CSPEC source data**. *The red line is the 1µSv/h border.*

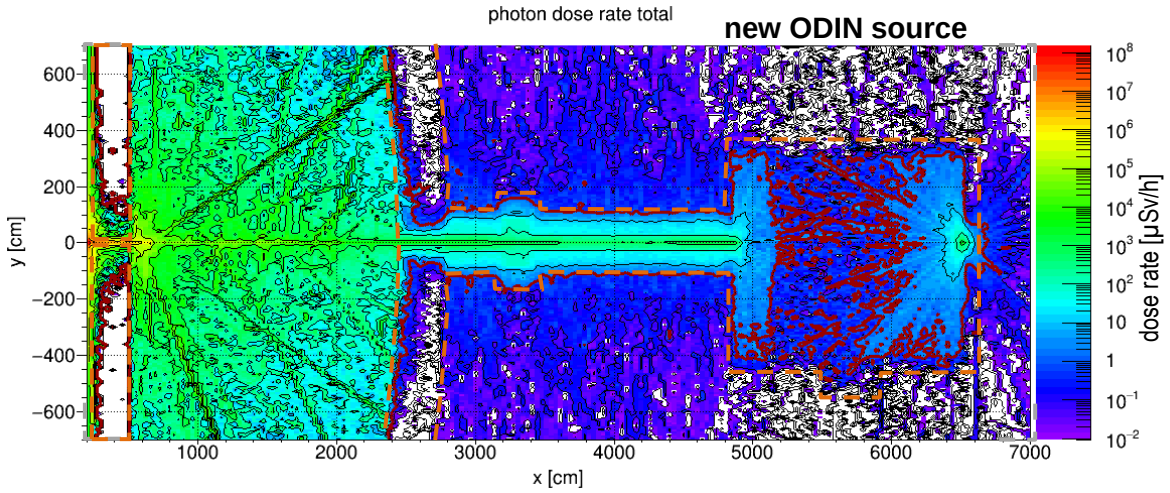

Fig. 176: Total generated gamma dose rate distribution in the horizontal area obtained **with the ODIN source data**. *The red line is the 1µSv/h border.*

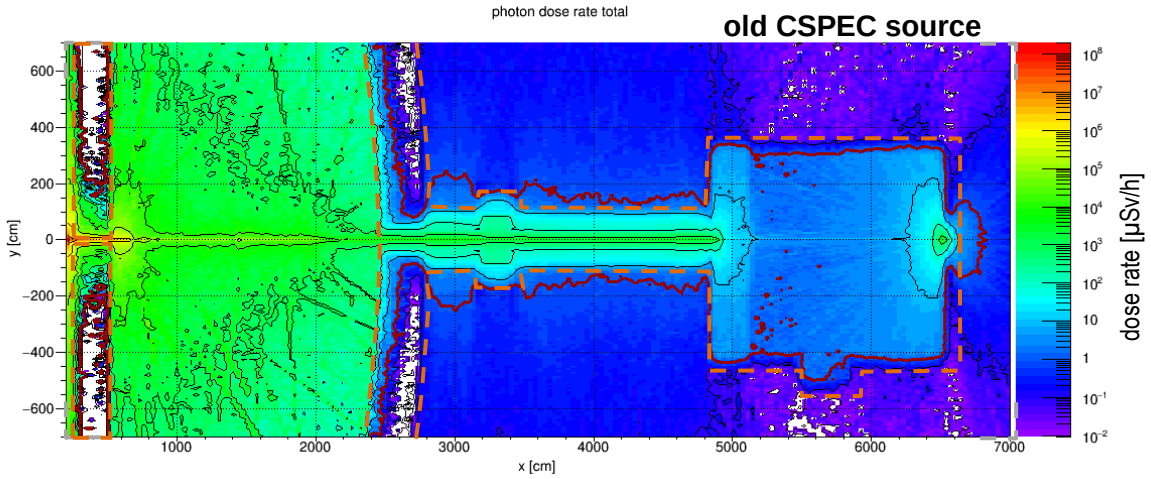

Fig. 177: For comparison: Total generated gamma dose rate distribution in the horizontal area obtained **with the old CSPEC source data**. *The red line is the 1µSv/h border.*

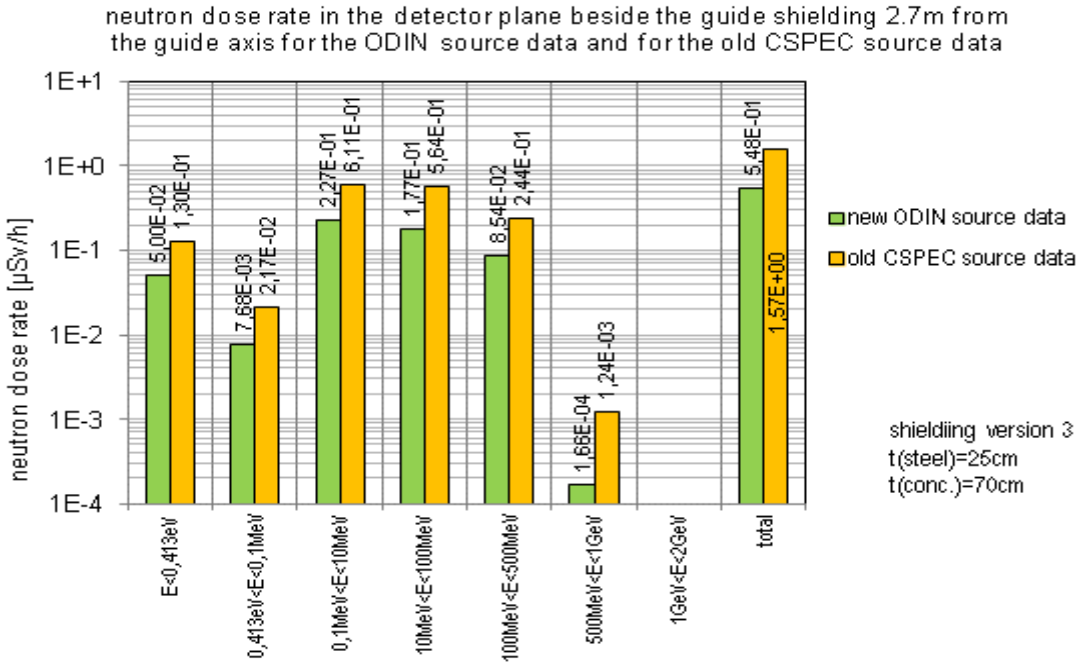

Fig. 178: Neutron dose rate in the detector plane beside the guide shielding 2.7m from the guide axis for the ODIN source data and for the old CSPEC source data

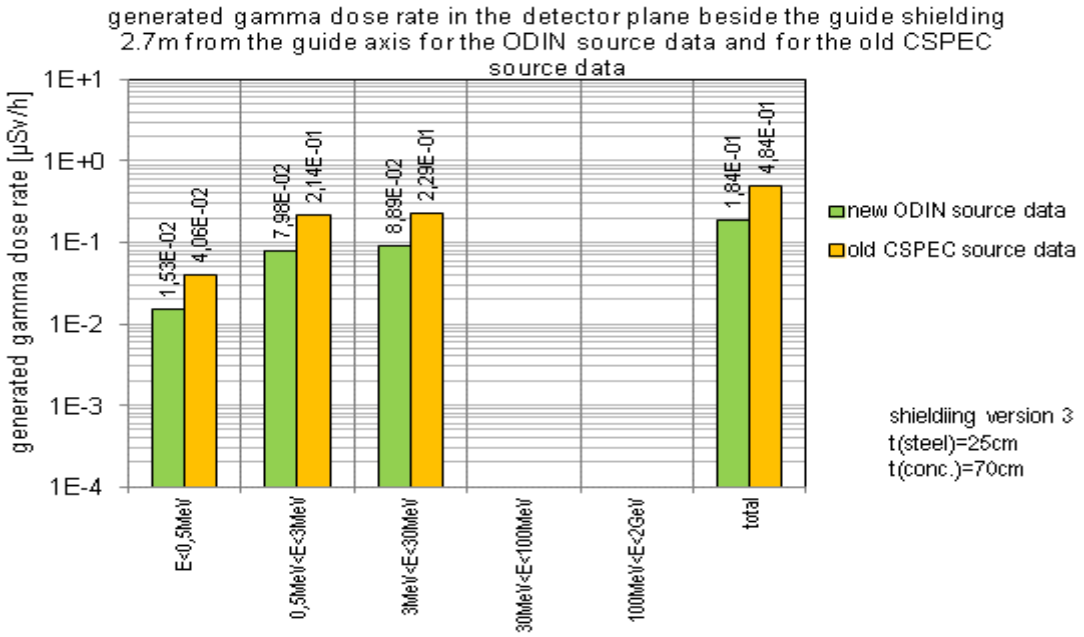

Fig. 179: Generated gamma dose rate in the detector plane beside the guide shielding 2.7m from the guide axis for the ODIN source data and for the old CSPEC source data

7.1.1 Conclusion

The neutron dose is reduced by nearly a factor of three by using the new fictive neutron source. In the next chapter a reduction of the shielding thickness is considered therefore.

7.2 The influence of the ordinary concrete composition

The composition of ordinary concrete is not fixed but varying. The influence of the different concrete compositions given on the ESS common guide shielding confluence page and given by DIN25413 Teil 1 on the dose rate outside the shielding was tested by simulation with shielding version 3 with a steel thickness of 15cm and a concrete thickness of 60cm. The ESS composition contains trace elements which were not considered in the simulation. Only the elements shown in the figure below were considered.

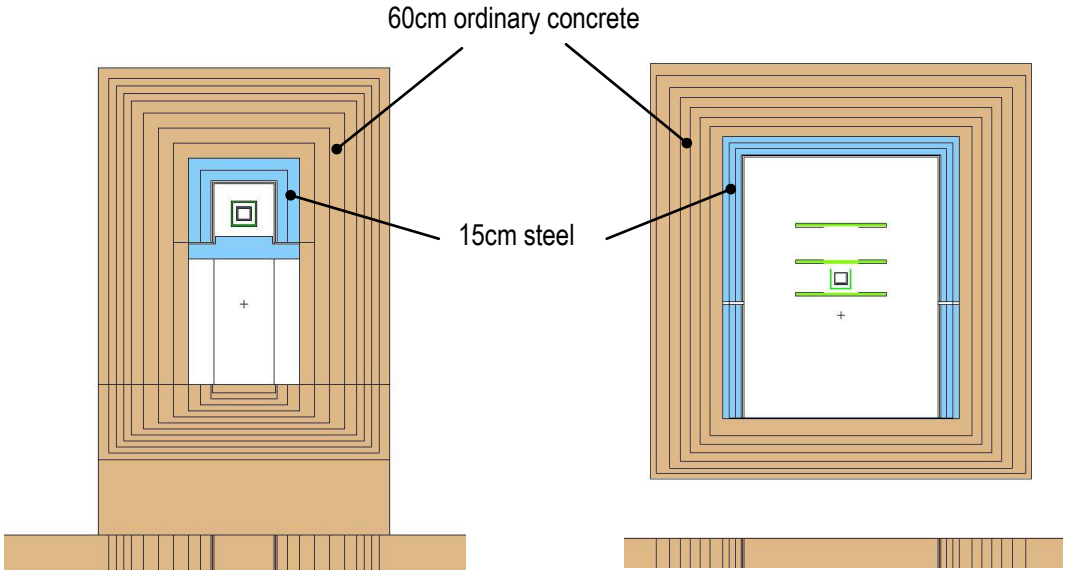

Fig. 180: Vertical cut through the Monte Carlo model of the guide shielding (left hand side) and the chopper pit (right hand side)

A comparison of the DIN25413 Teil 1 ordinary concrete composition and the ESS ordinary concrete composition is shown in the figure below.

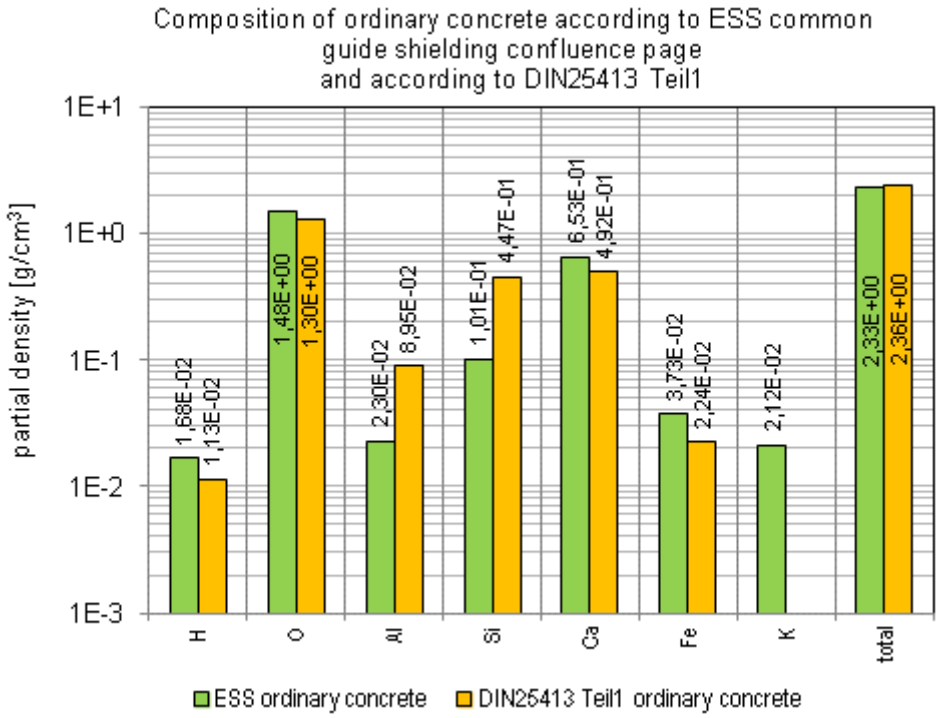

Fig. 181: Composition of ordinary concrete according to ESS common guide shielding confluence page and according to DIN25413 Teil1

The neutron dose rate and the generated gamma dose rate obtained in the detector plane 2.7m beside the guide axis is shown in the next figures for application of both concrete compositions.

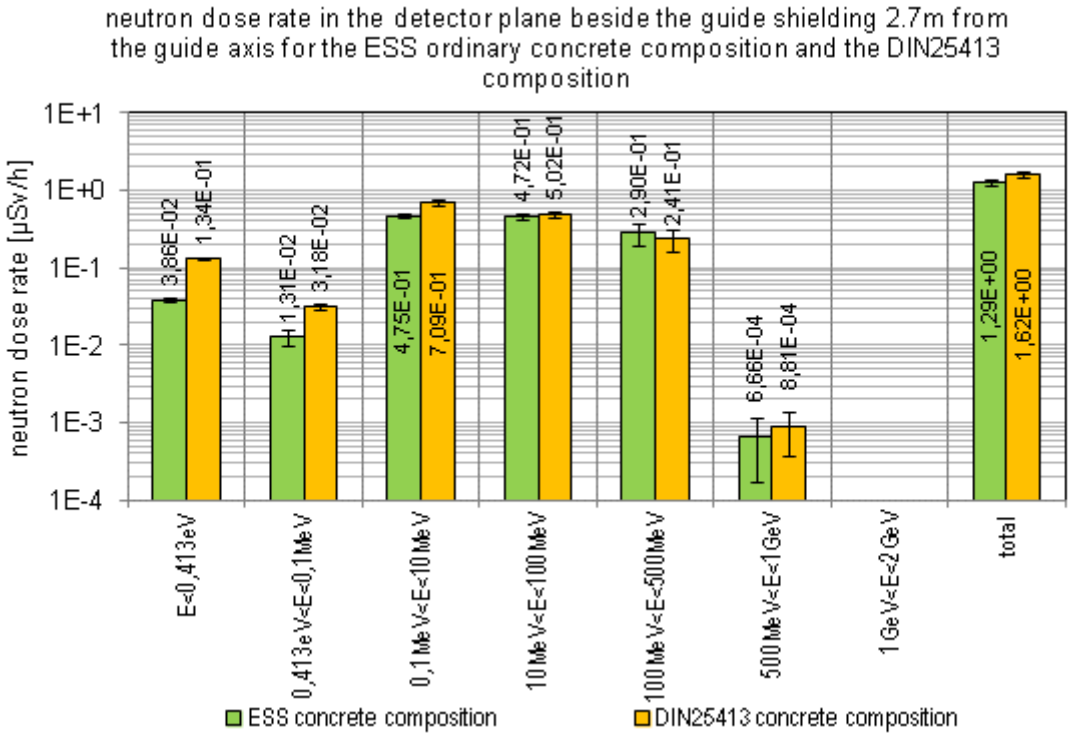

Fig. 182: Neutron dose rate in the detector plane beside the guide shielding 2.7m from the guide axis for the ESS ordinary concrete composition and the DIN25413 composition

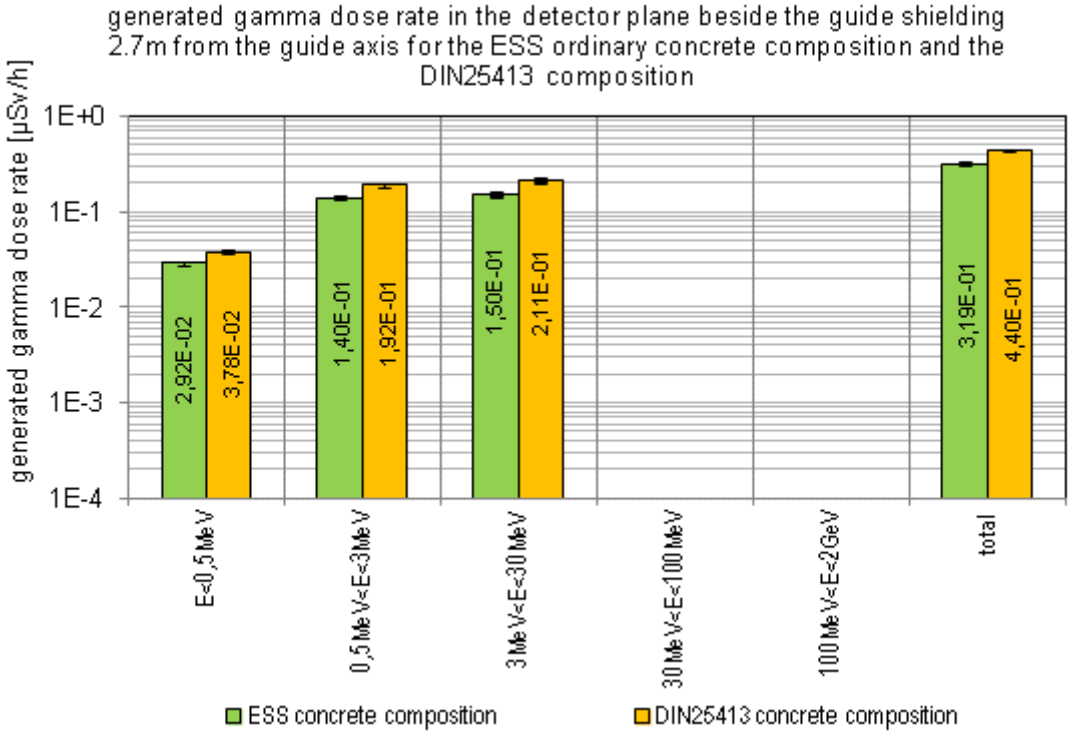

Fig. 183: Generated gamma dose rate in the detector plane beside the guide shielding 2.7m from the guide axis for the ESS ordinary concrete composition and the DIN25413 composition

7.2.1 Conclusion

With the ESS concrete composition lower dose rates are obtained.

7.3 Shielding version 3B consisting of 20cm steel and 70cm ESS ordinary concrete

As shown in the last chapter the ESS ordinary concrete composition causes a higher attenuation compared to the DIN 25413 composition that was used in the simulations presented in the previous chapters. Therefore the question arises if the steel layer of the shielding can be reduced by 5cm to 20cm. The steel shielding below the guide was introduced because a leakage occurred for bigger steel layers. It is omitted in the shielding version presented here.

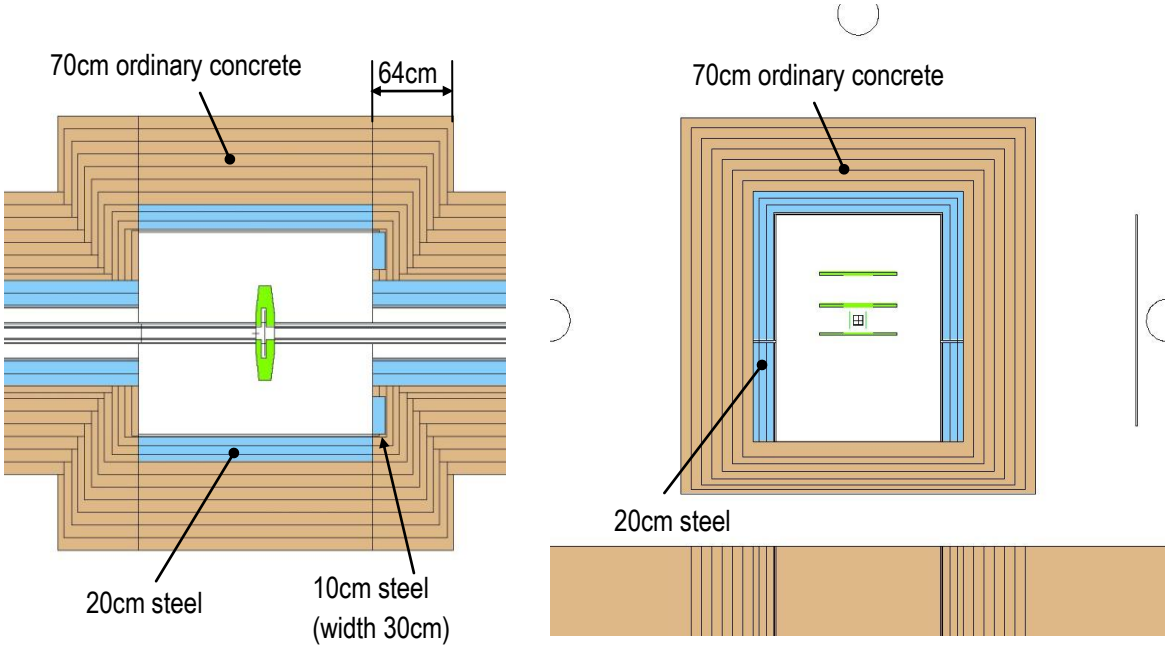

Fig. 184: Horizontal cut (left hand side) and vertical cut (right hand side) through the Monte Carlo model of the chopper pit.

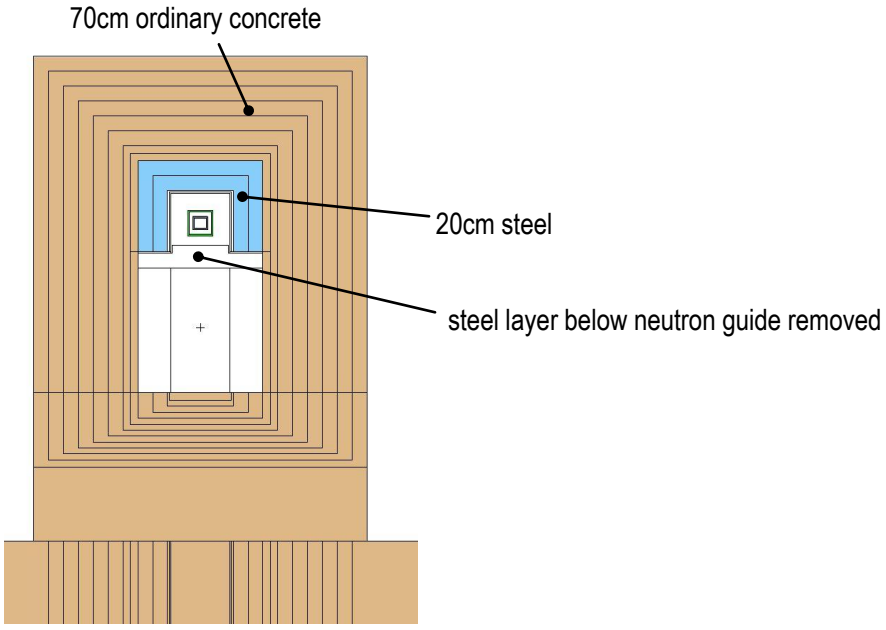

Fig. 185: Vertical cut through the Monte Carlo model of the guide shielding.

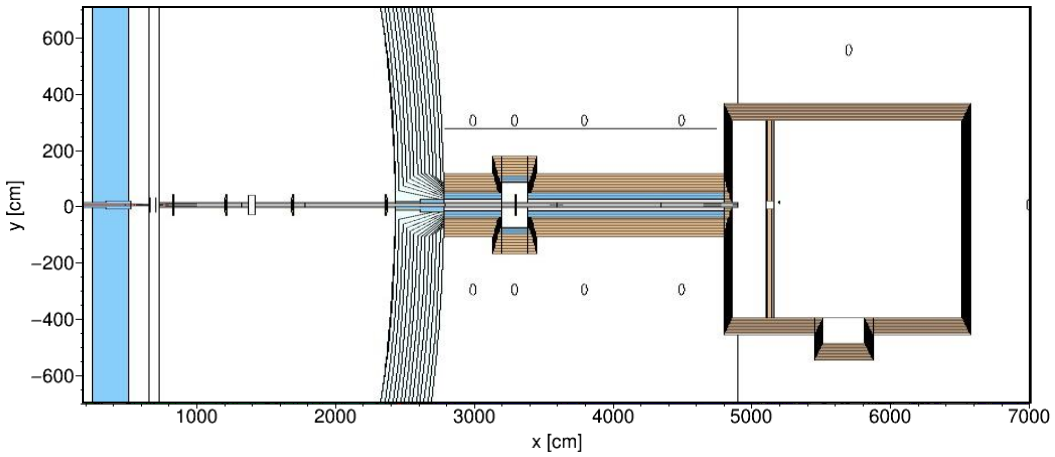

Fig. 186: Horizontal area through the Monte Carlo model of the ODIN instrument for which the radiation distribution is shown in the following image

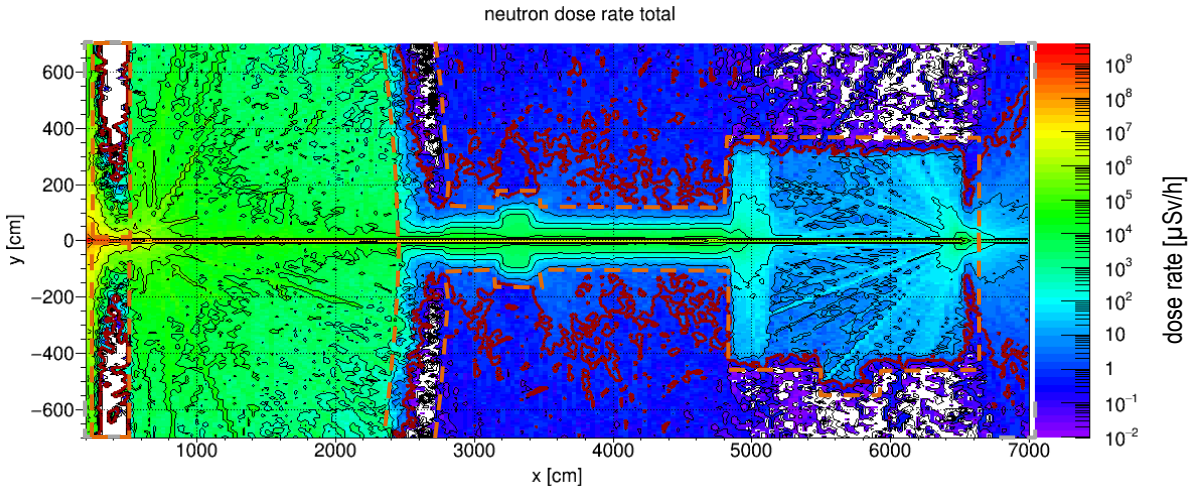

Fig. 187: Total neutron dose rate distribution in the horizontal area. The red line is the 1µSv/h border.

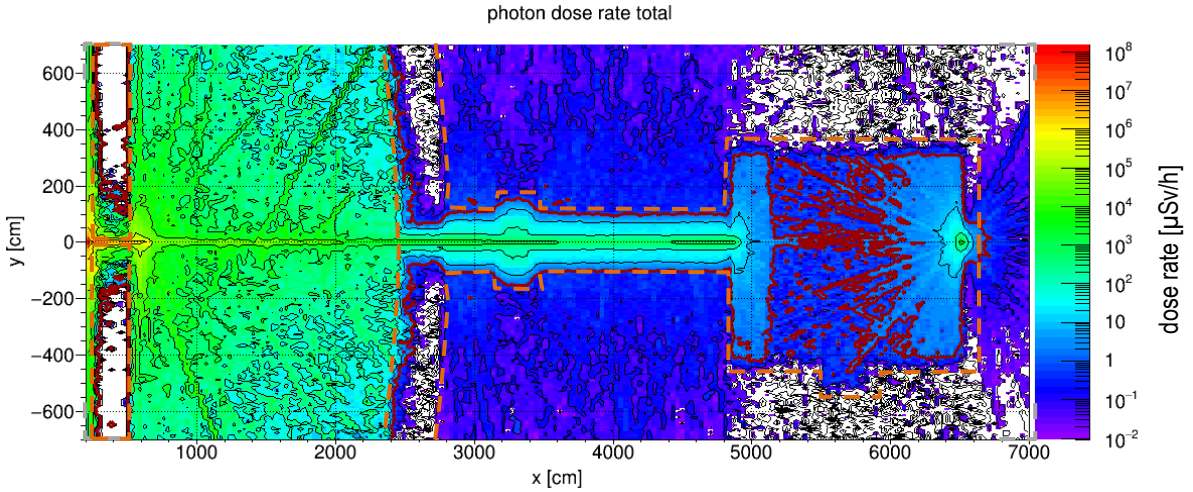

Fig. 188: Total generated gamma dose rate distribution in the horizontal area. The red line is the 1µSv/h border.

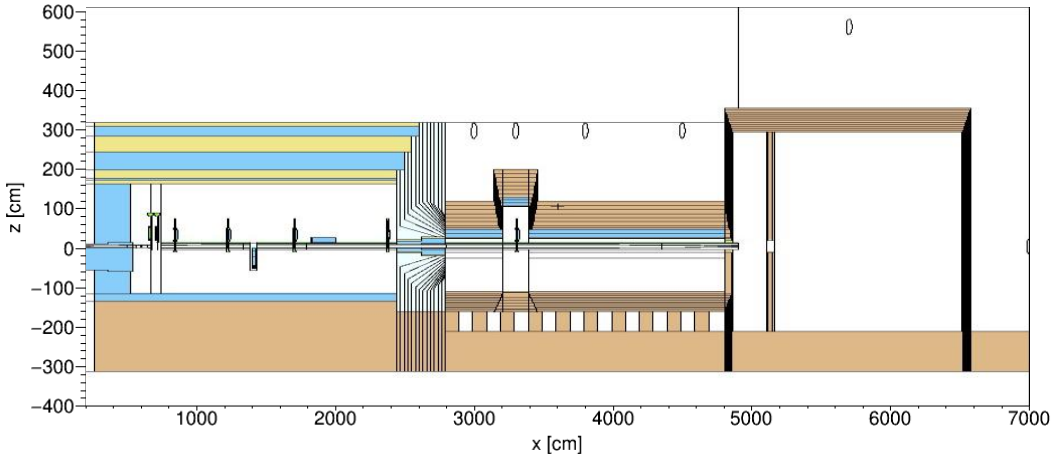

Fig. 189: Vertical area through the Monte Carlo model of the ODIN instrument for which the radiation distribution is shown in the following image

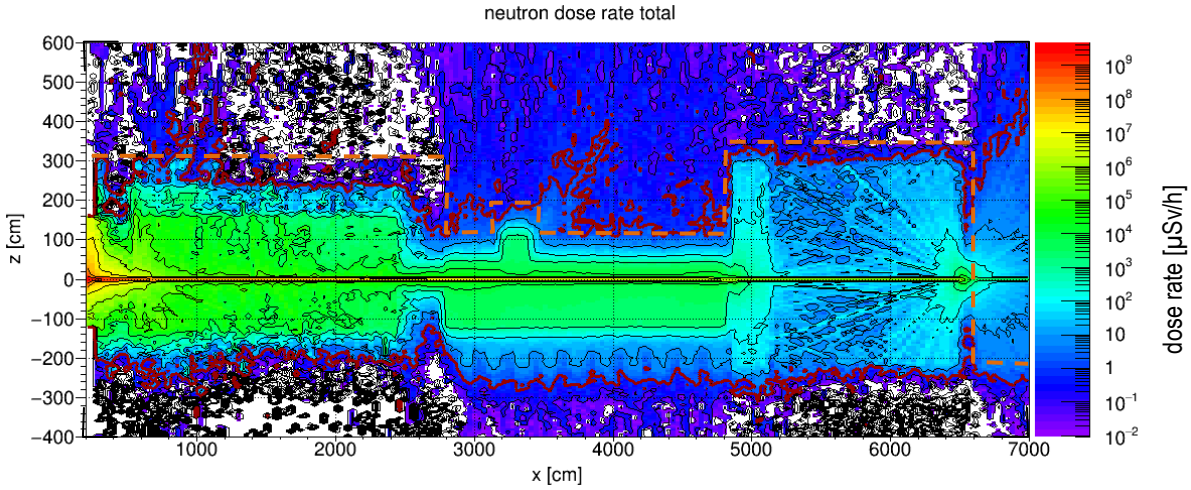

Fig. 190: Total neutron dose rate distribution in the vertical area. The red line is the 1µSv/h border.

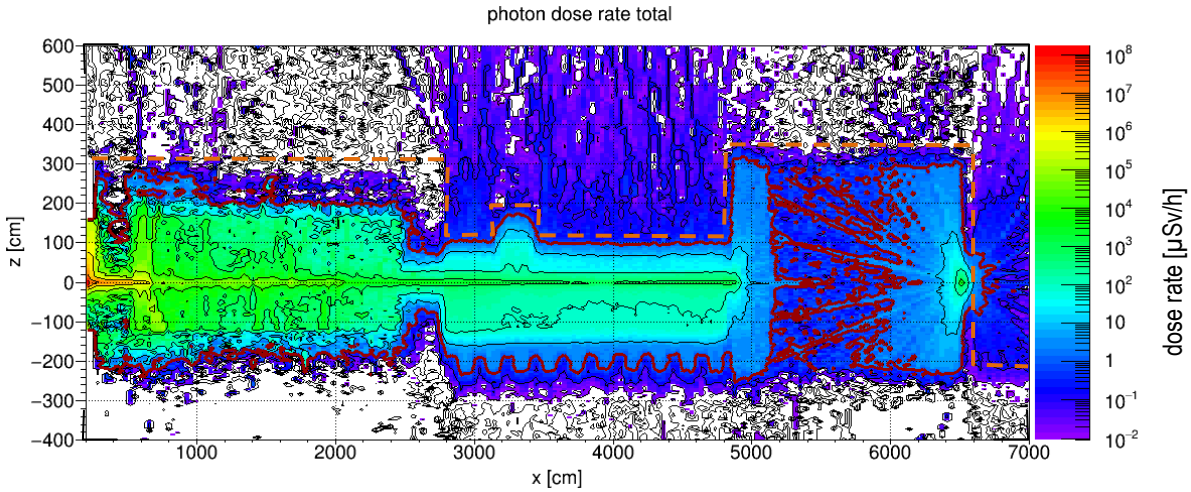

Fig. 191: Total generated gamma dose rate distribution in the vertical area. The red line is the 1µSv/h border.

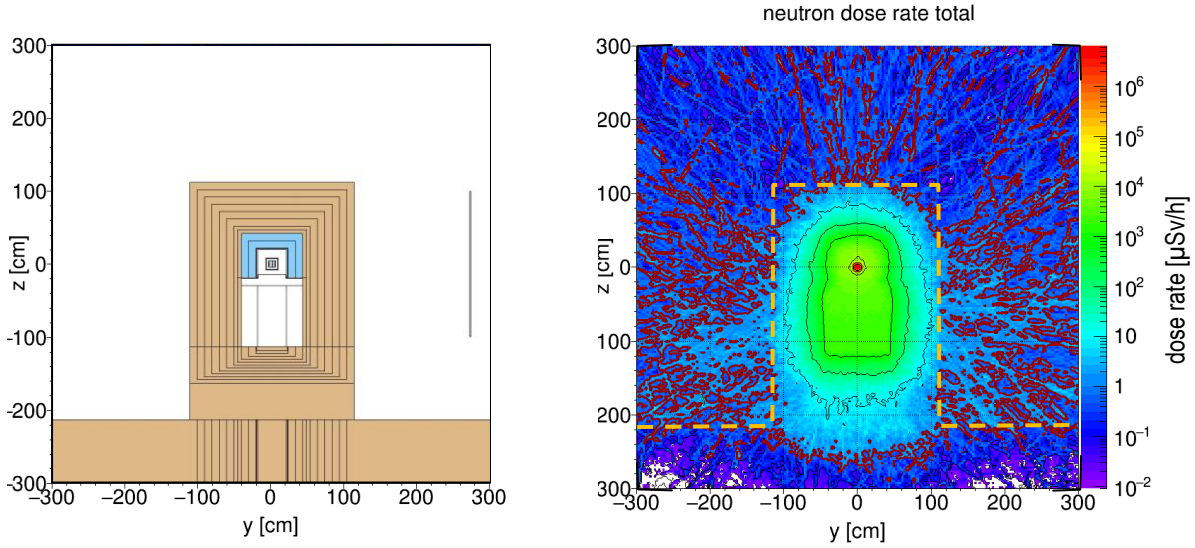

Fig. 192: Vertical neutron dose rate distribution through the guide shielding perpendicular to the beam axis (40m from the focal point). The red line is the 1µSv/h border.

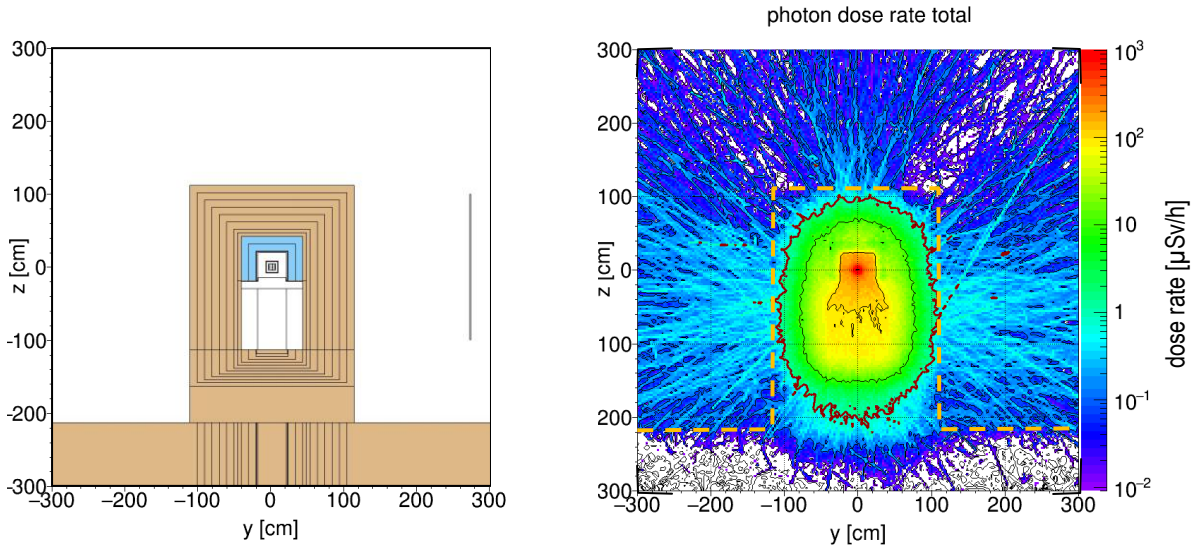

Fig. 193: Vertical generated gamma dose rate distribution through the guide shielding perpendicular to the beam axis (40m from the focal point). The red line is the 1µSv/h border.

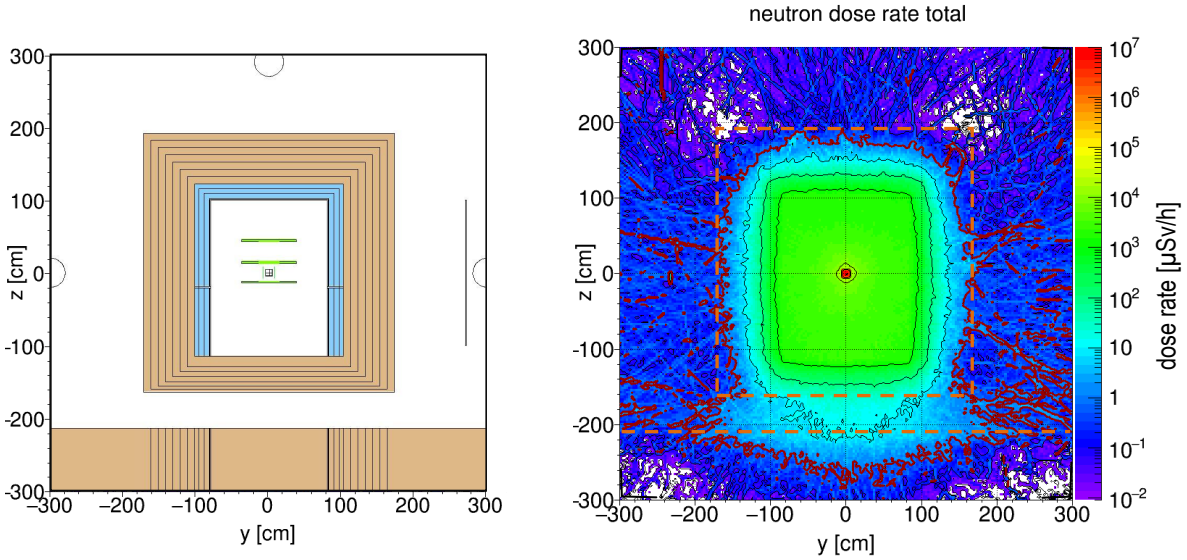

Fig. 194: Vertical neutron dose rate distribution through the chopper pit perpendicular to the beam axis. The red line is the 1µSv/h border.

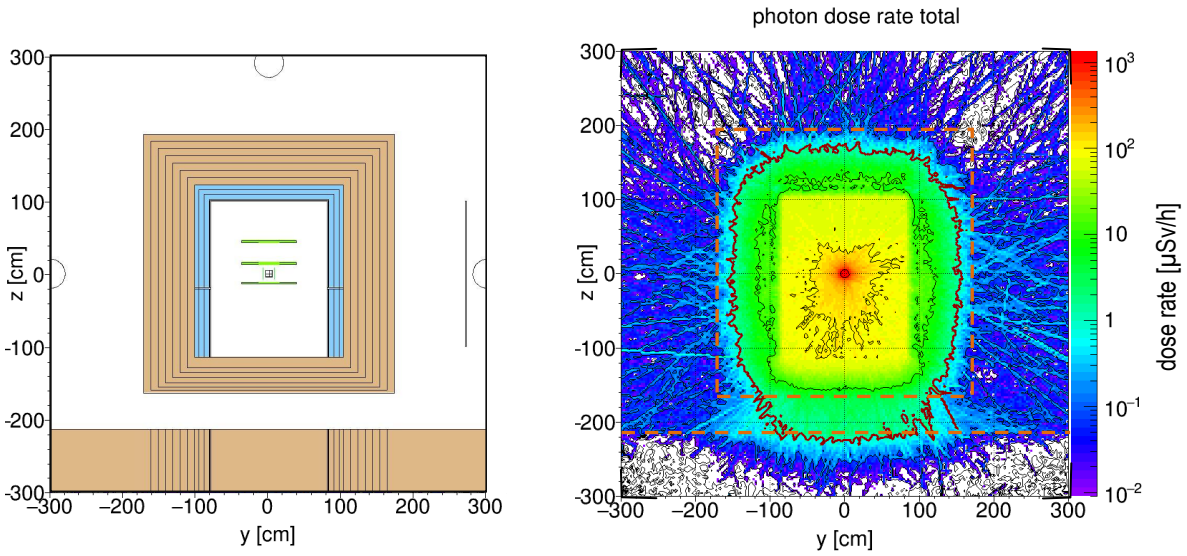

Fig. 195: Vertical generated gamma dose rate distribution through the chopper pit perpendicular to the beam axis. The red line is the 1µSv/h border.

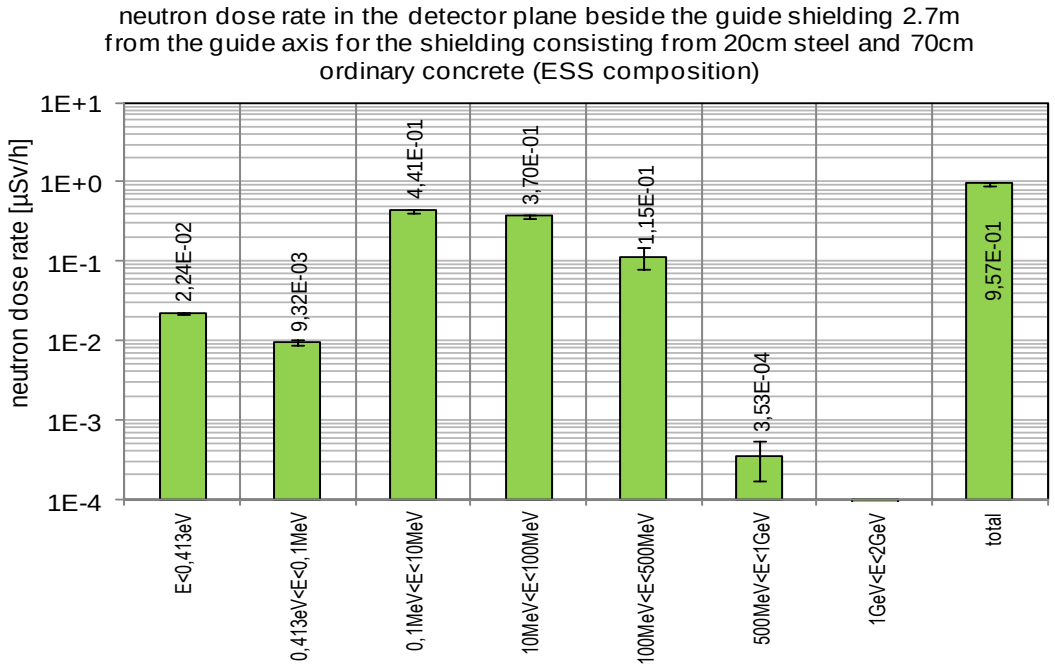

Fig. 196: Neutron dose rate in the detector plane beside the guide shielding 2.7m from the guide axis for the shielding consisting from 20cm steel and 70cm ordinary concrete (ESS composition)

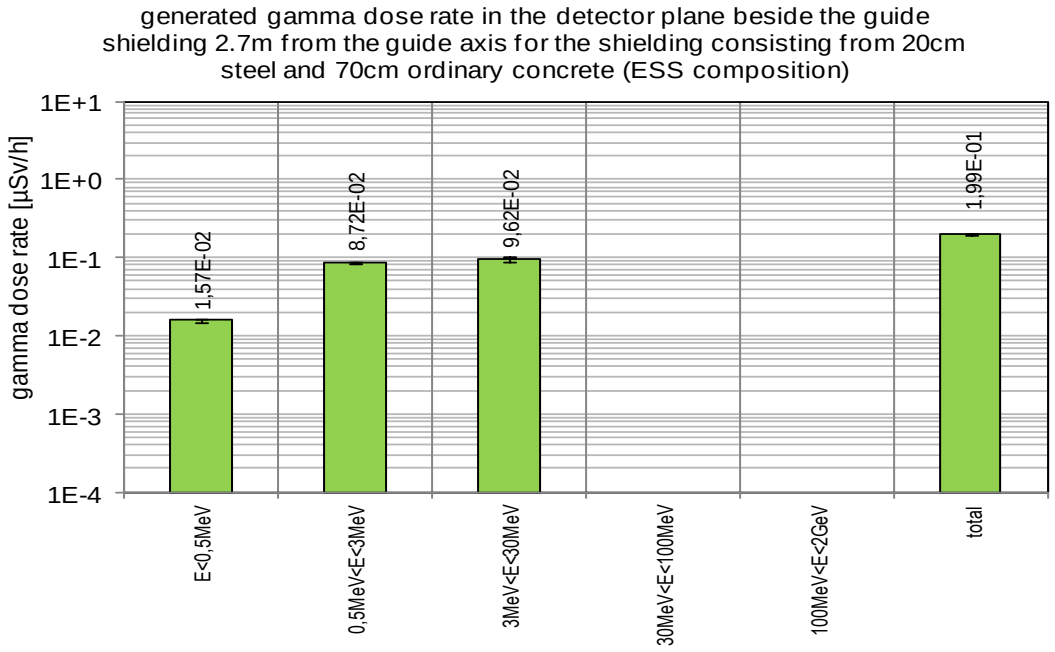

Fig. 197: Generated gamma dose rate in the detector plane beside the guide shielding 2.7m from the guide axis for the shielding consisting from 20cm steel and 70cm ordinary concrete (ESS composition)

7.3.1 Conclusion

The dose rate on the outer surface of the shielding around the neutron guide is too high (above 1.5µSv/h). A considerable leakage below the steel layer can be observed.

7.4 The influence of polyethylene

The influence of polyethylene was tested by replacing 20cm of concrete by pure polyethylene in the model described in the previous chapter.

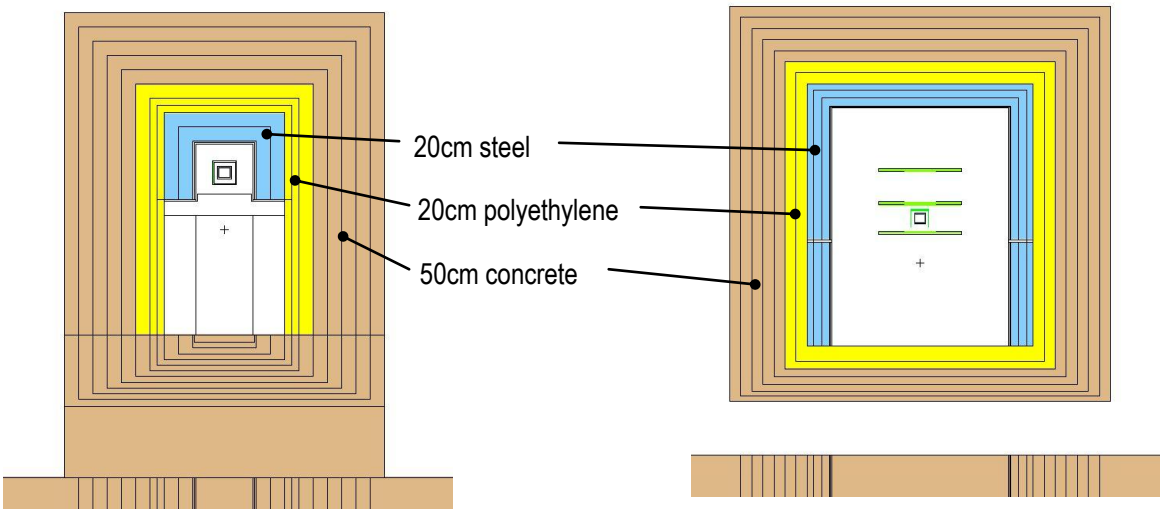

Fig. 198: Vertical cut through the Monte Carlo model of the guide shielding (left hand side) and the chopper pit (right hand side)

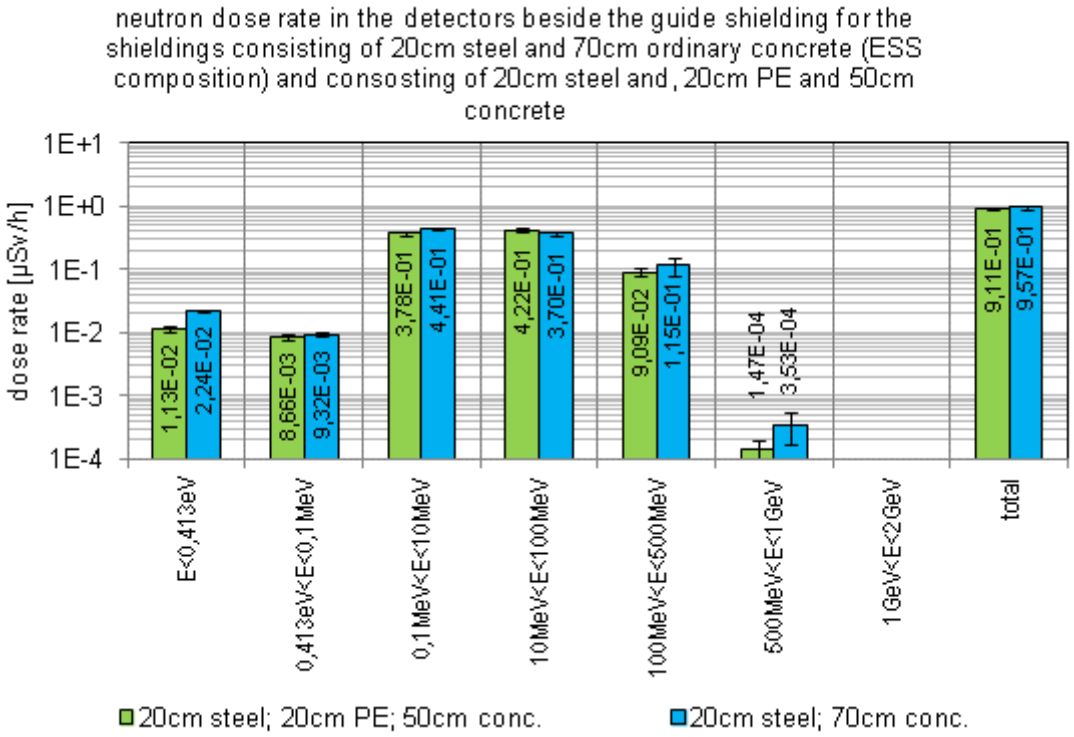

Fig. 199: neutron dose rate in the detectors beside the guide shielding for the shieldings consisting of 20cm steel and 70cm ordinary concrete (ESS composition) and consosting of 20cm steel and, 20cm PE and 50cm concrete

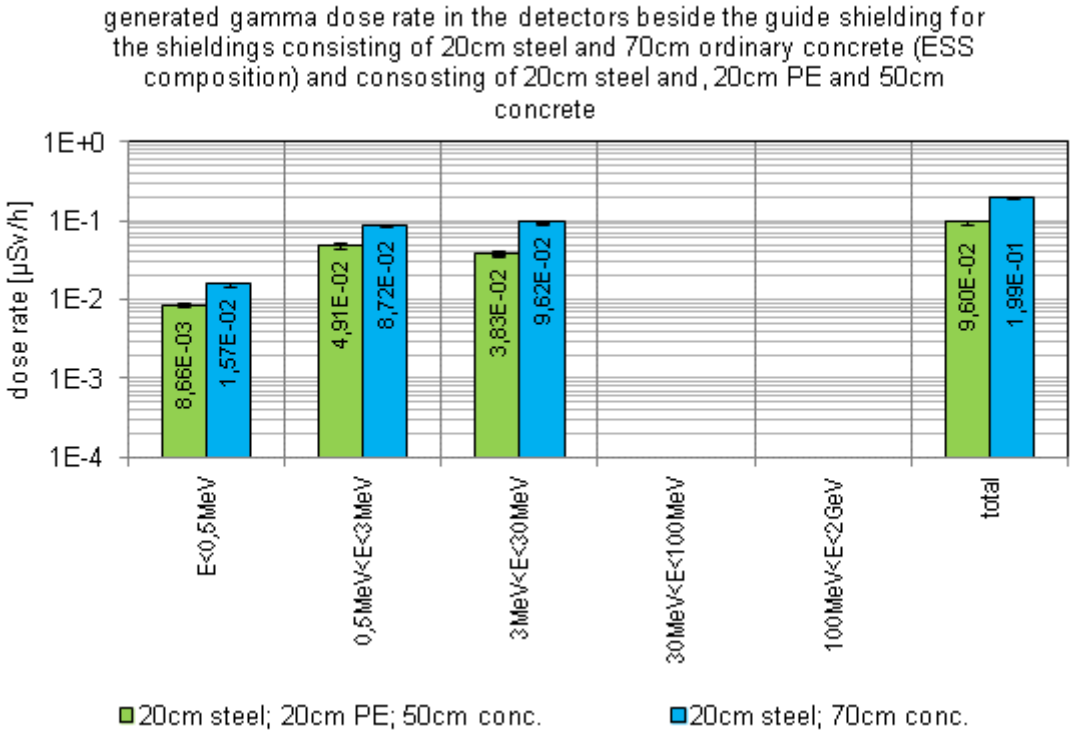

Fig. 200: Generated gamma dose rate in the detectors beside the guide shielding for the shieldings consisting of 20cm steel and 70cm ordinary concrete (ESS composition) and consosting of 20cm steel and, 20cm PE and 50cm concrete

7.4.1 Conclusion

The influence of replacing concrete by polyethylene is rather low. The neutron dose rate is reduced in the energy region between 0.1MeV and 10MeV but is increased in the energy region between 10MeV and 100MeV. Obviously the content of elements above oxygene in concrete is beneficial for shielding high energetic neutron radiation. However the thermal neutron dose rate is decreased by ca. factor of two outside the shielding by polyethylene. Hence the generation of gamma radiation in the outer layers of the shielding is reduced. Of course for reduction of the gamma dose rate outside the shielding absorber layers containing boron would be more efficient than the polyethylene layer.

7.5 Shielding version 3C consisting of 20cm steel and 80cm ESS ordinary concrete (chopper pit: 20cm steel and 70cm ordinary concrete)

In this version of the shielding 20cm steel and 80cm ordinary concrete (ESS composition) is used around the neutron guide. 20cm steel and 70cm ordinary concrete is used as side walls and roof for the chopper pit. The front and rear wall of the chopper pit is 64cm thick (10cm steel, 54cm concrete, see previous version). The inner width of the guide shielding is 44cm. The inner width of the chopper pit is 164.4cm. Detectors on the outer surfaces of the shielding are included in the model as shown in the figures below.

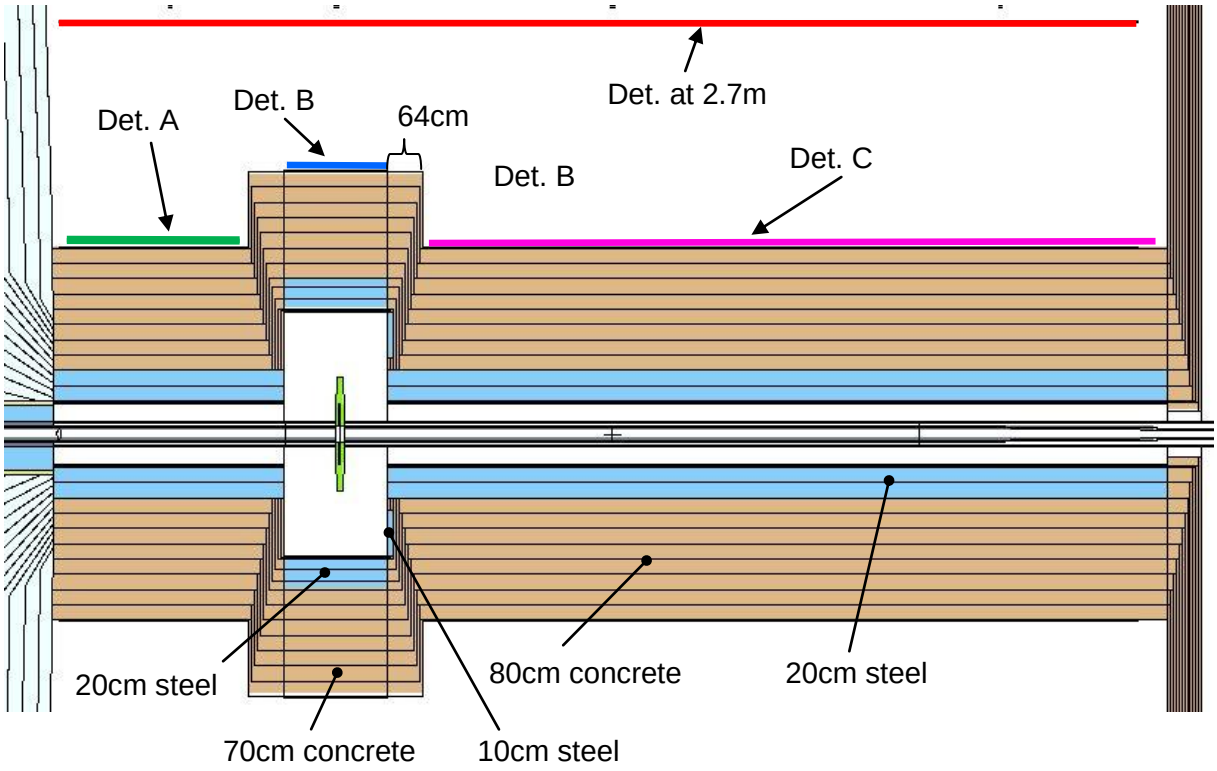

Fig. 201: Horizontal cut through the Monte Carlo model of the guide shielding

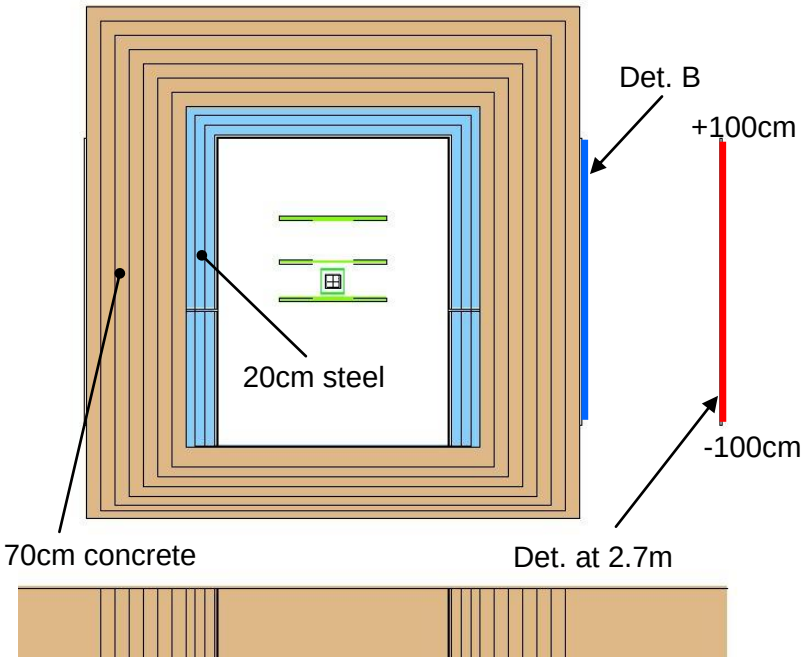

Fig. 202: Vertical cut through the Monte Carlo model of the chopper pit

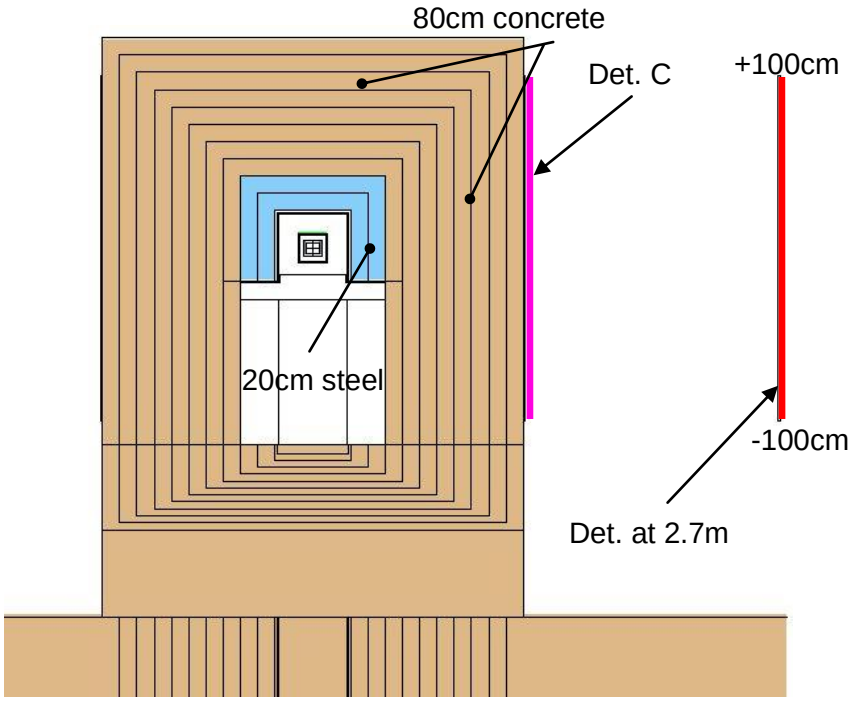

Fig. 203: Vertical cut through the Monte Carlo model of the guide shielding

The dose rates in the detectors are shown in the following figures.

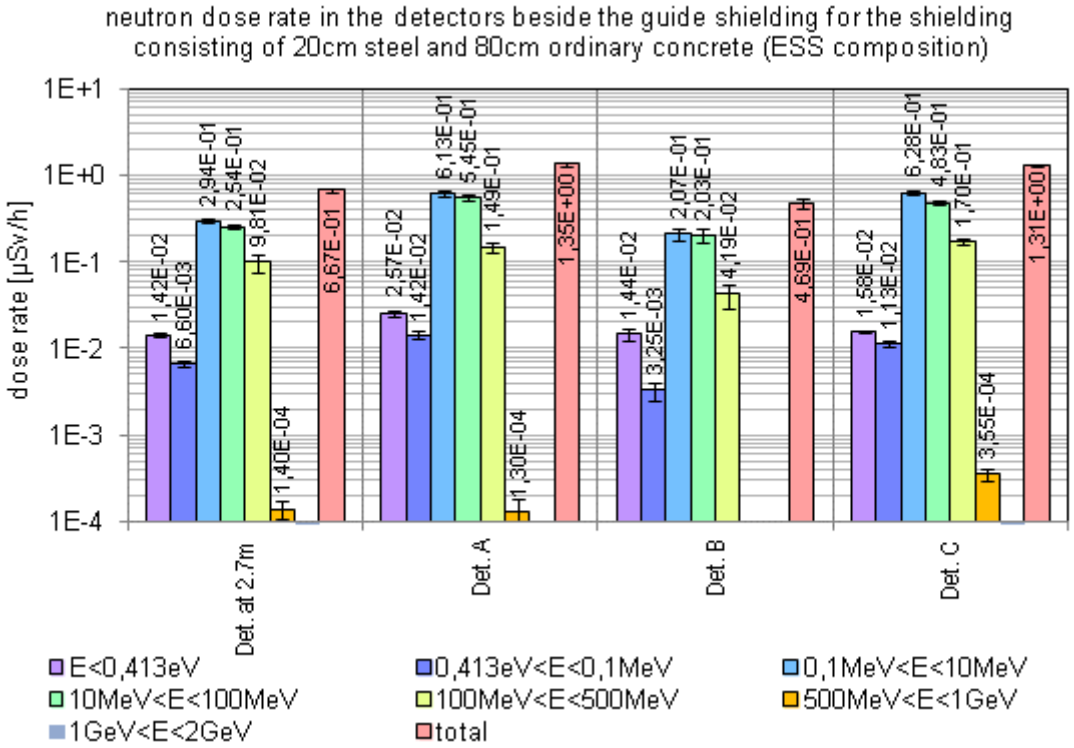

Fig. 204: Neutron dose rate in the detectors beside the guide shielding for the shielding consisting of 20cm steel and 80cm ordinary concrete (ESS composition) (chopper pit 20cm: steel and 70cm ordinary concrete)

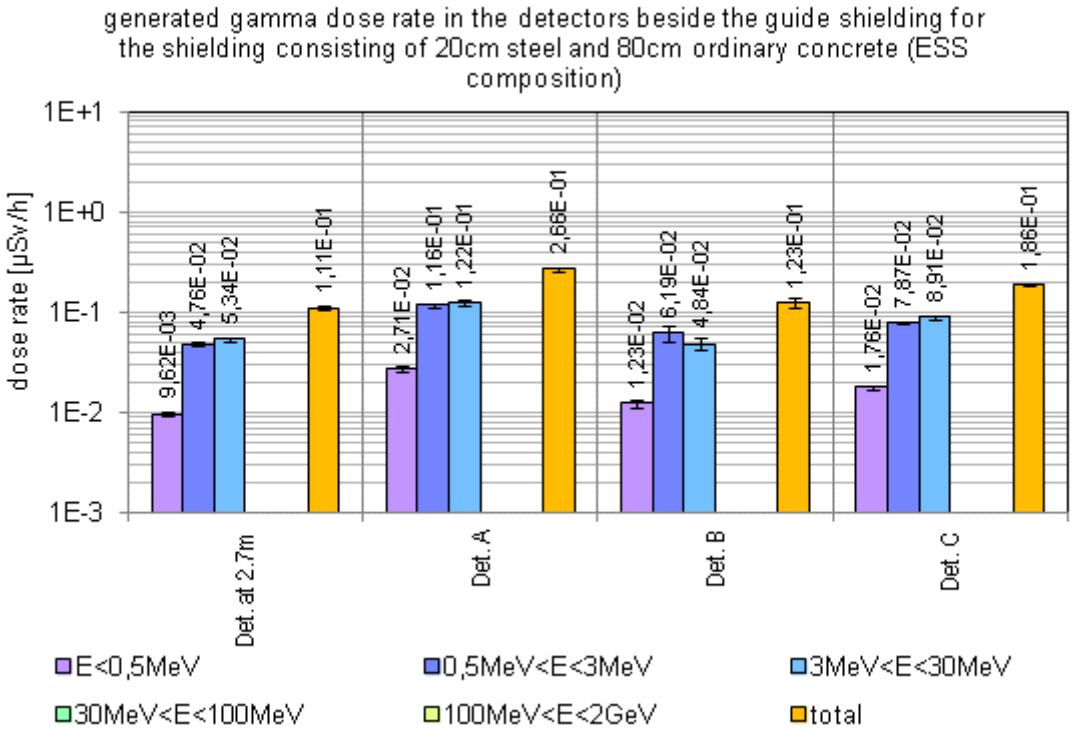

Fig. 205: Generated gamma dose rate in the detectors beside the guide shielding for the shielding consisting of 20cm steel and 80cm ordinary concrete (ESS composition) (chopper pit 20cm: steel and 70cm ordinary concrete)

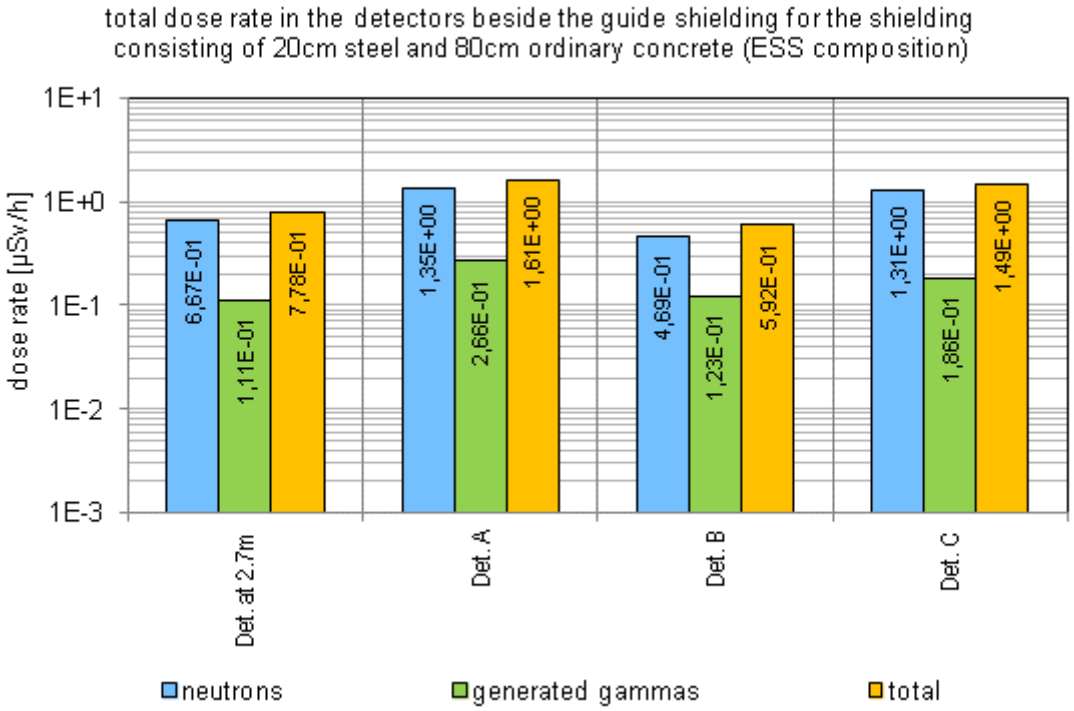

Fig. 206: Total dose rate in the detectors beside the guide shielding for the shielding consisting of 20cm steel and 80cm ordinary concrete (ESS composition)

The dose rate distributions in horizontal and vertical planes through the shielding are shown in the following images.

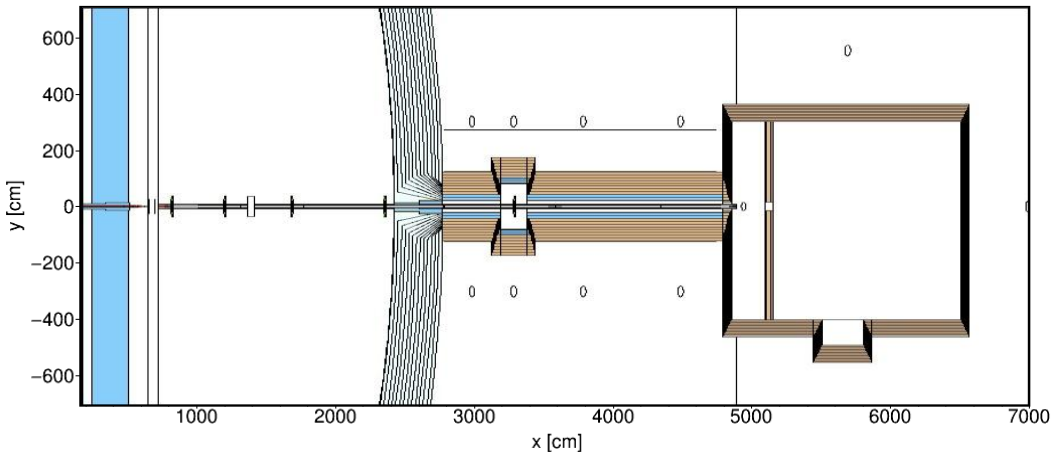

Fig. 207: Horizontal area through the Monte Carlo model of the ODIN instrument for which the radiation distribution is shown in the following image

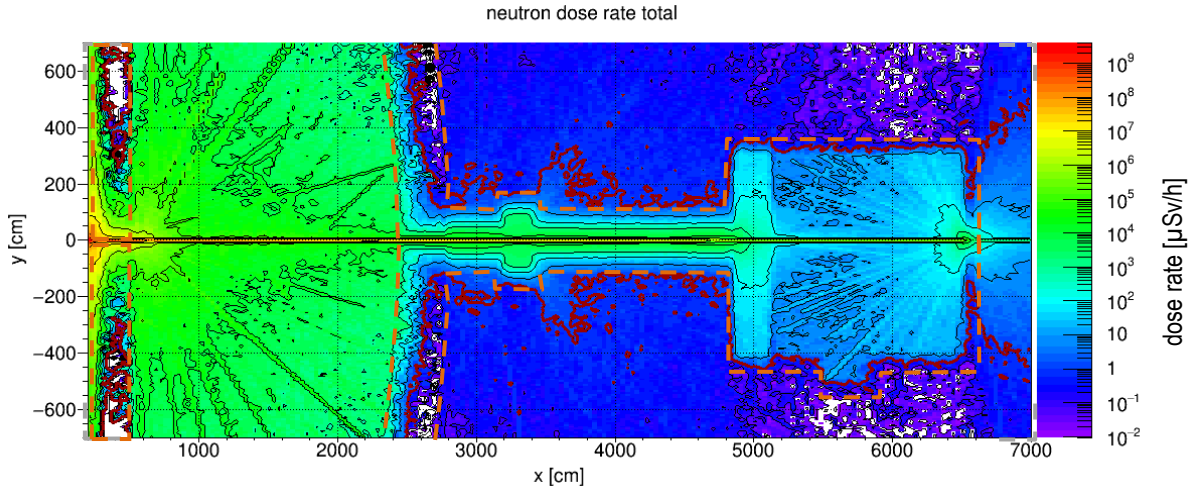

Fig. 208: Total neutron dose rate distribution in the horizontal area. The red line is the 1µSv/h border.

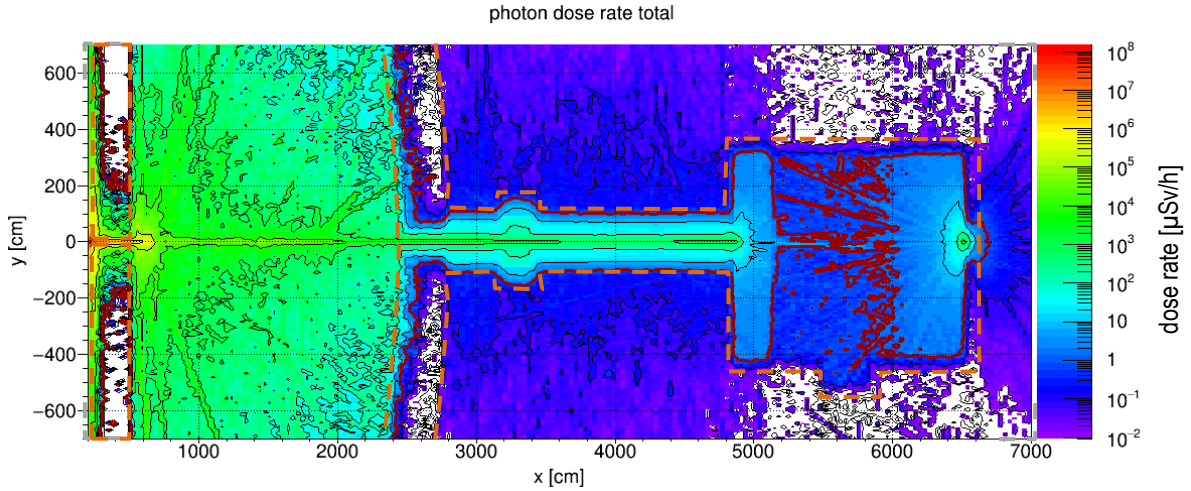

Fig. 209: Total generated gamma dose rate distribution in the horizontal area. The red line is the 1µSv/h border.

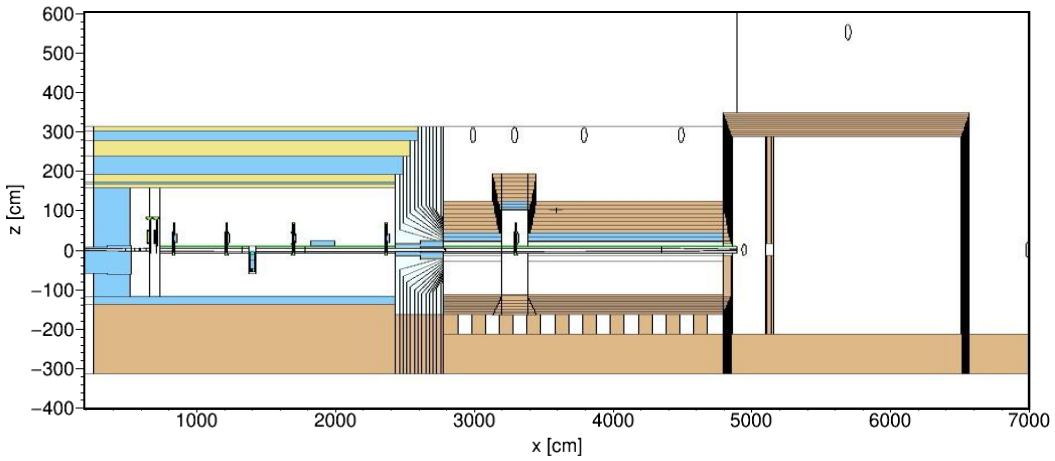

Fig. 210: Vertical area through the Monte Carlo model of the ODIN instrument for which the radiation distribution is shown in the following image

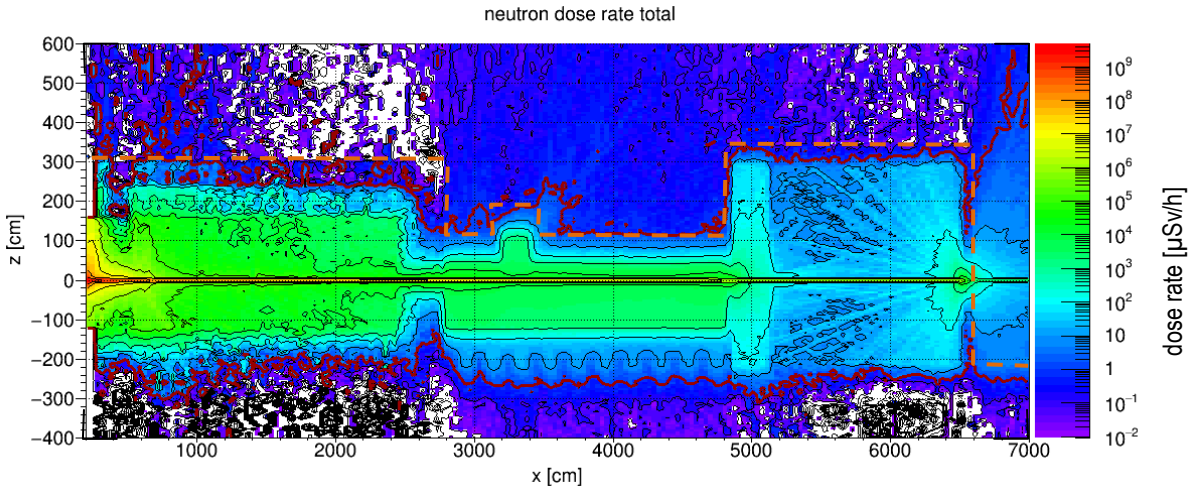

Fig. 211: Total neutron dose rate distribution in the vertical area. The red line is the 1µSv/h border.

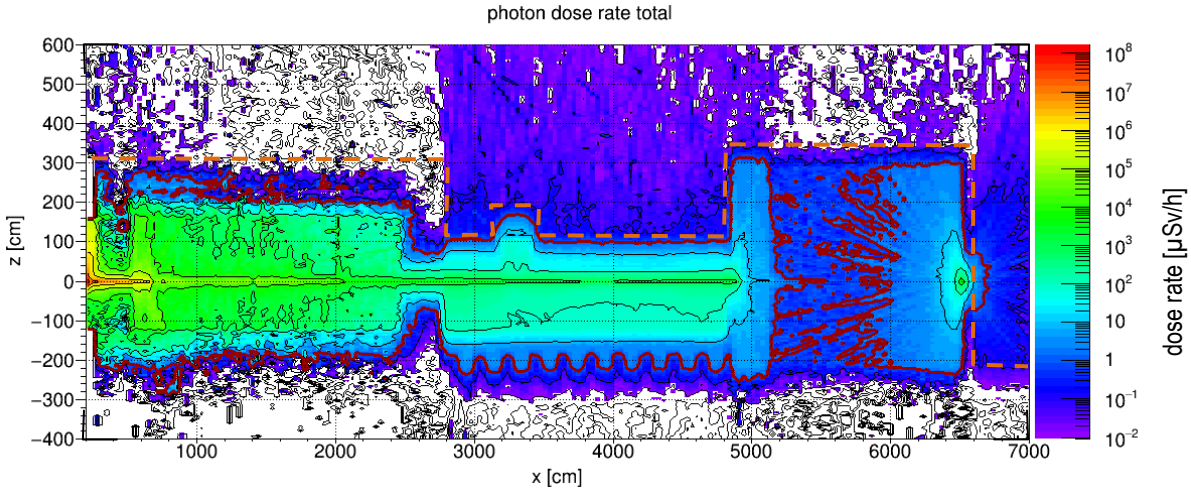

Fig. 212: Total generated gamma dose rate distribution in the vertical area. The red line is the 1µSv/h border.

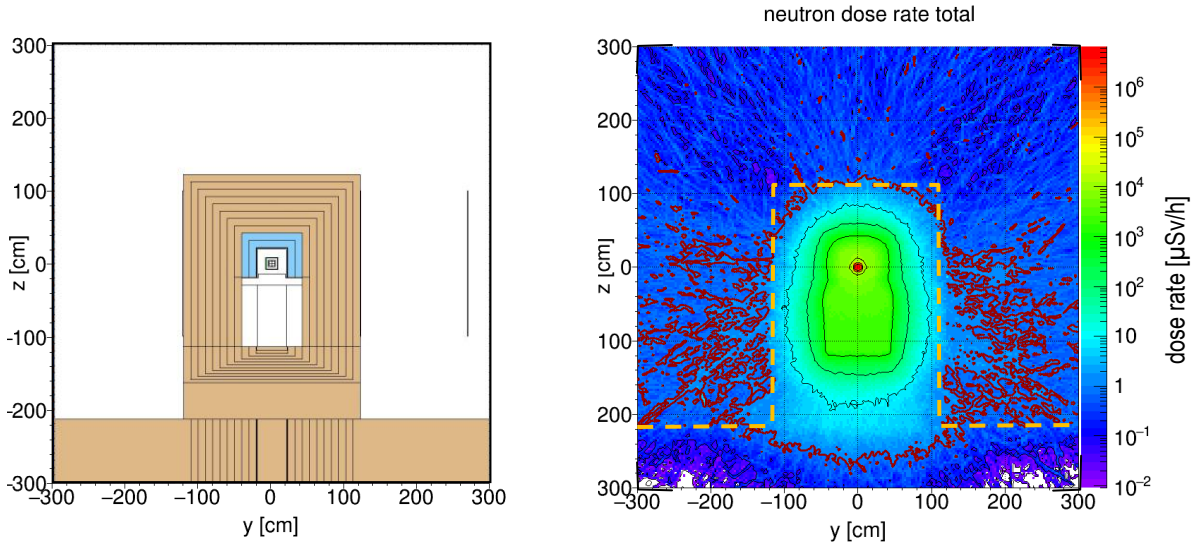

Fig. 213: Vertical neutron dose rate distribution through the guide shielding perpendicular to the beam axis (40m from the focal point). The red line is the 1µSv/h border.

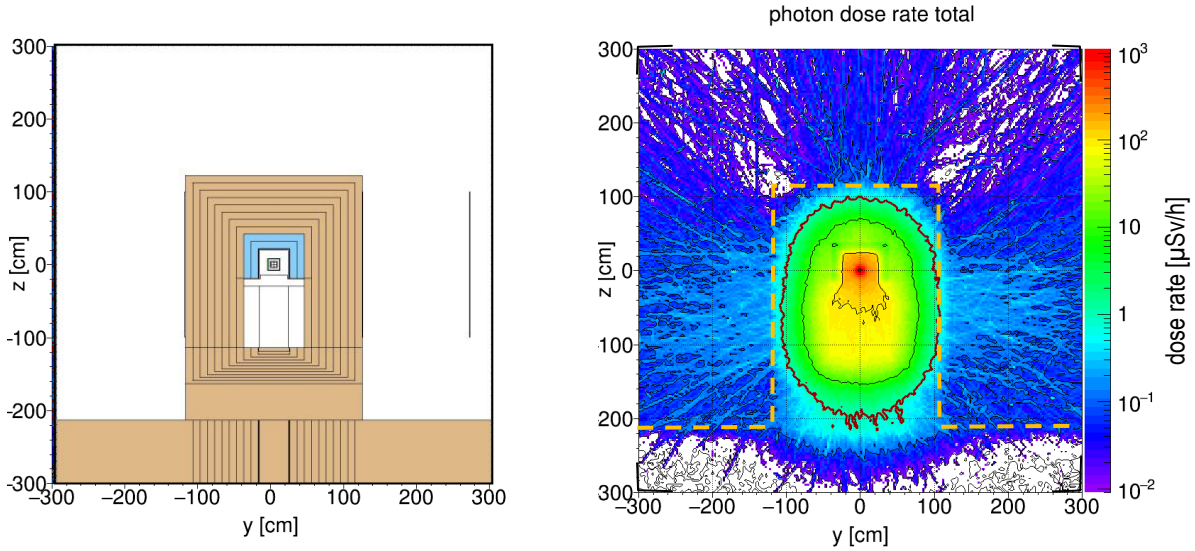

Fig. 214: Vertical generated gamma dose rate distribution through the guide shielding perpendicular to the beam axis (40m from the focal point). The red line is the 1µSv/h border.

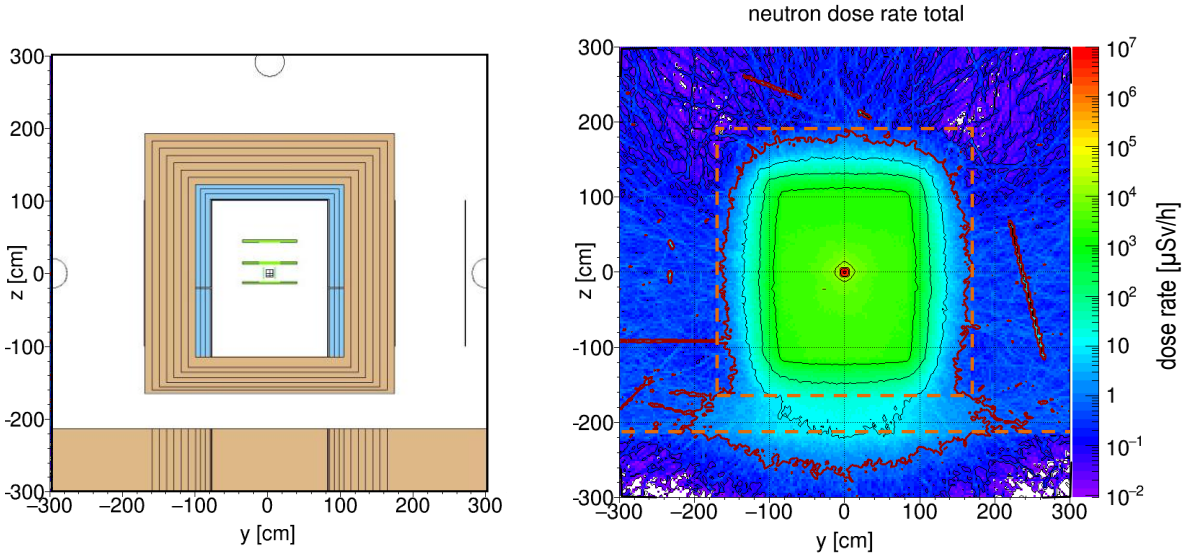

Fig. 215: Vertical neutron dose rate distribution through the chopper pit perpendicular to the beam axis. The red line is the 1µSv/h border.

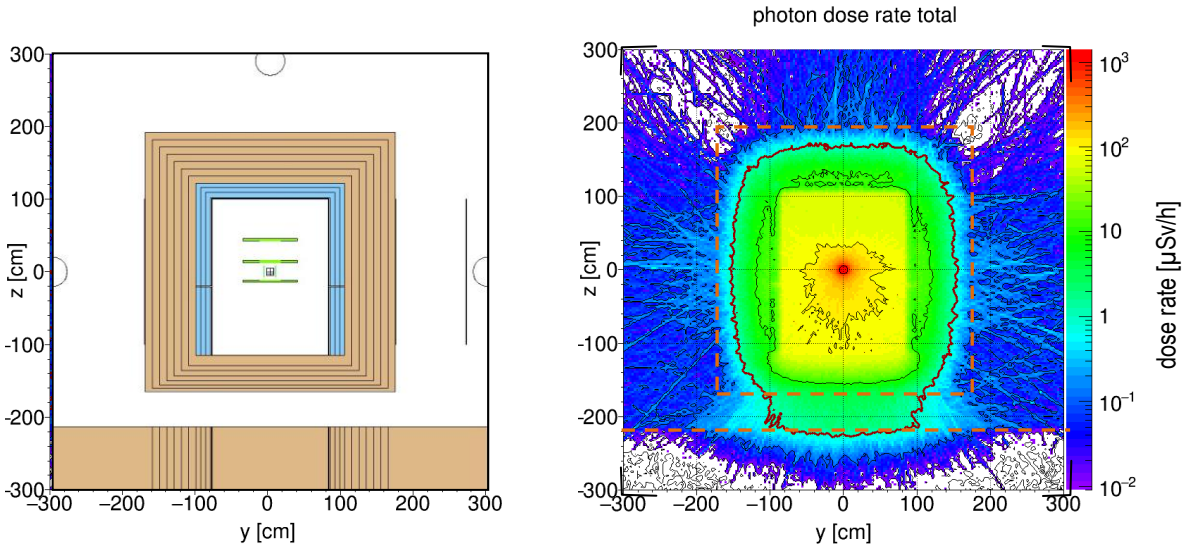

Fig. 216: Vertical generated gamma dose rate distribution through the chopper pit perpendicular to the beam axis. The red line is the 1µSv/h border.

7.5.1 Closed chopper FOC5

The gamma dose rate distribution for a chopper pit shielding consisting of 20cm steel and 70cm concrete was already presented in previous chapters. The shielding is sufficient for this case.

7.5.2 Conclusion

On the outer surface of the shielding around the neutron guide behind the chopper pit a total dose rate of 1.49µSv/h is reached (which is very close to the desired level of 1.5µSv/h). On the outer surfaces of the chopper pit side walls a total dose rate of 0.6µSv/h is reached (this holds for the opened chopper; of course the dose rate for the closed chopper has also to be considered, but as shown in previous chapters this contribution is much smaller for this shielding layout). Outside the rear wall of the chopper pit the dose rate is still above the desired level of 1.5µSv/h. On the outer surface of the guide shielding before the chopper pit a dose rate of 1.6µSv/h is obtained which is close to but above the desired dose rate level of 1.5µSv/h. A leakage below the inner steel shielding can still be observed.

7.6 Shielding version 3D consisting of 20cm steel and 80cm ESS ordinary concrete and a 10cm steel layer below the neutron guide (chopper pit: 20cm steel and 70cm ordinary concrete)

In the last chapter it was shown that the neutron dose rate beside the neutron guide before the chopper pit is still too high (1.6µSv/h) and that still a leakage below the inner steel shielding exists. Therefore a steel layer below the neutron guide is introduced again in this version but its thickness is only 10cm.

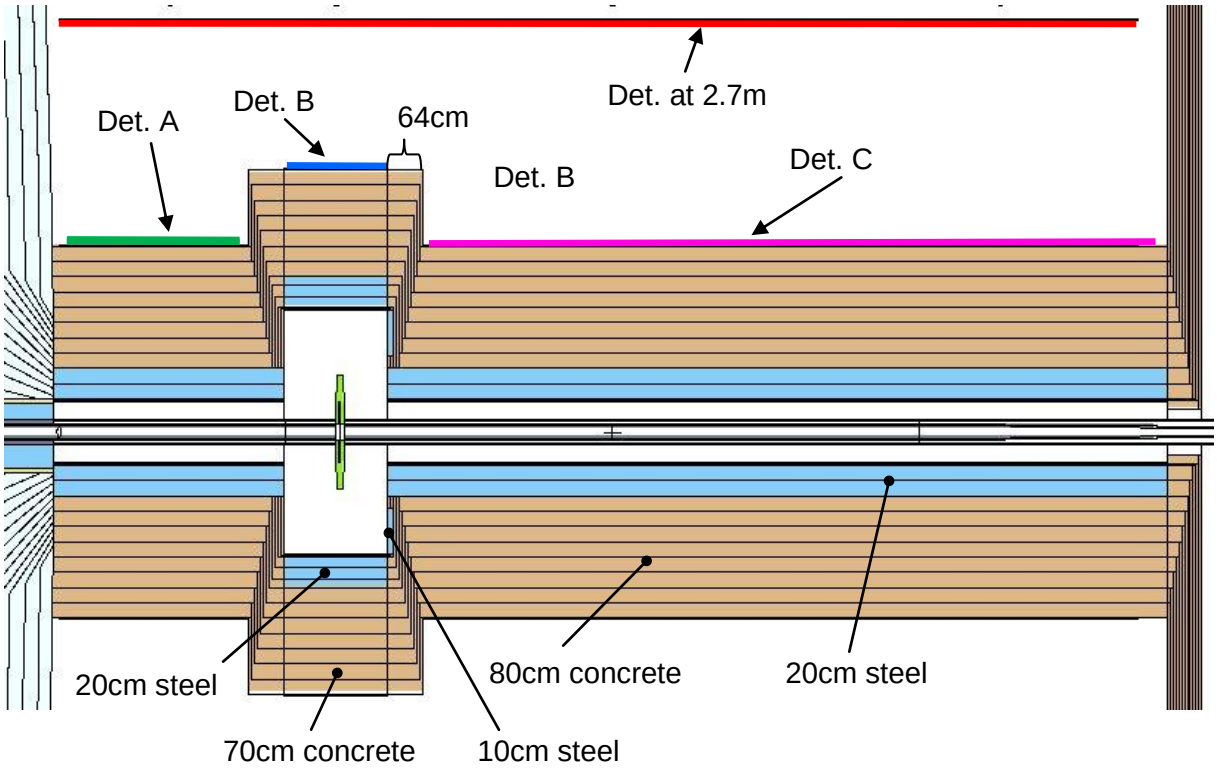

Fig. 217: Horizontal cut through the Monte Carlo model of the guide shielding

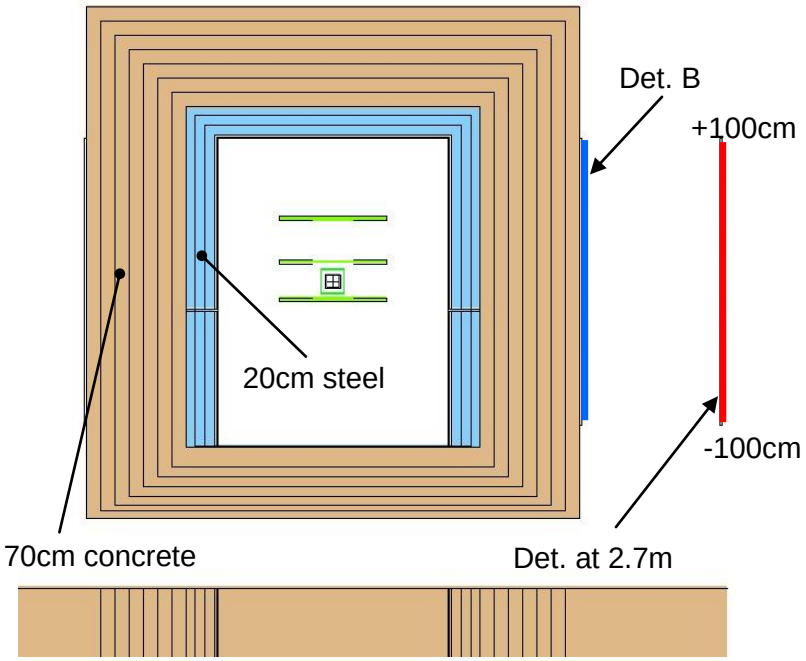

Fig. 218: Vertical cut through the Monte Carlo model of the chopper pit

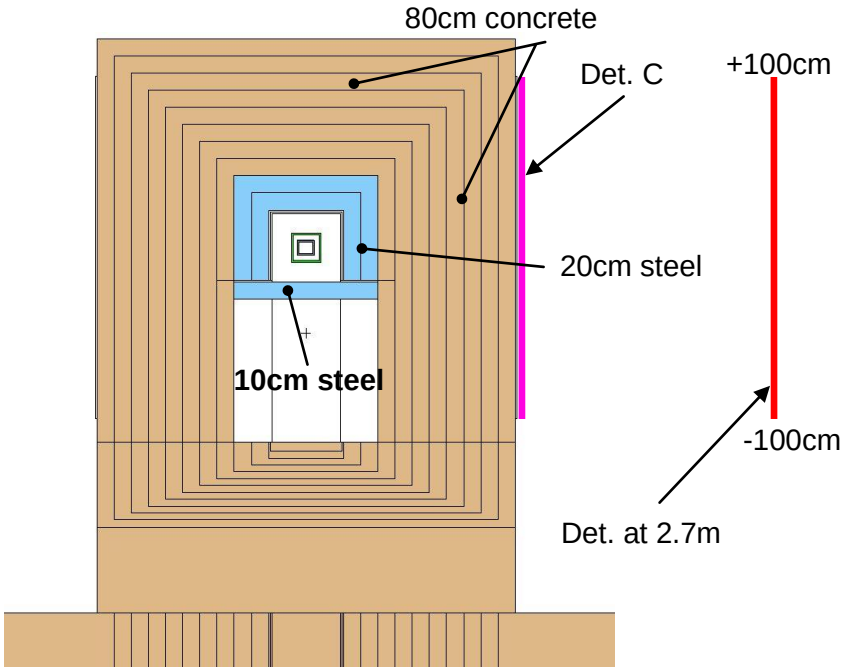

Fig. 219: Vertical cut through the Monte Carlo model of the guide shielding

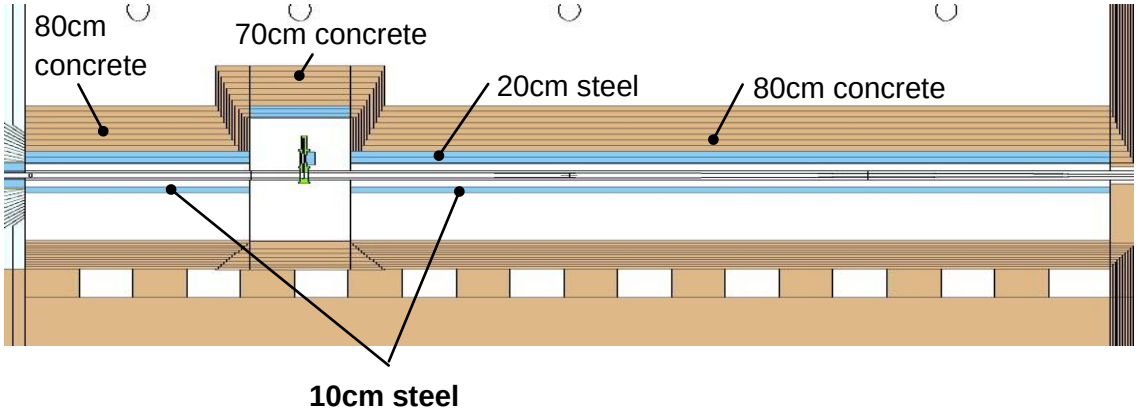

The dose rates in the detectors are shown in the following figures.

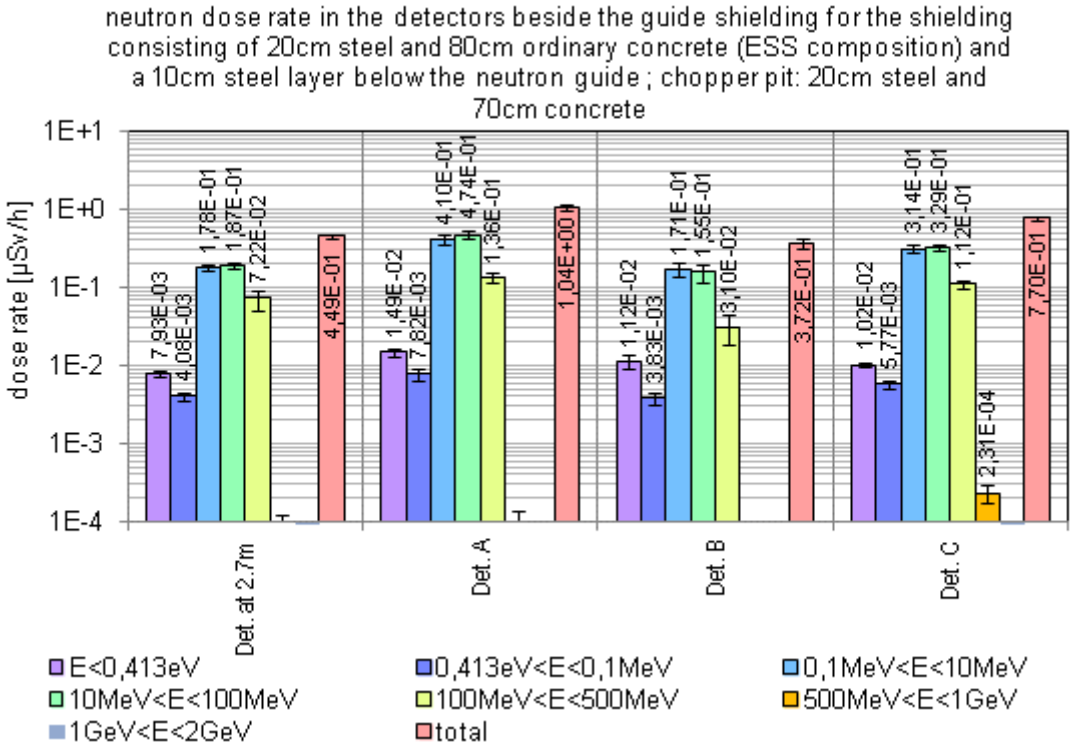

Fig. 220: neutron dose rate in the detectors beside the guide shielding for the shielding consisting of 20cm steel and 80cm ordinary concrete (ESS composition) and a 10cm steel layer below the neutron guide ; chopper pit: 20cm steel and 70cm concrete

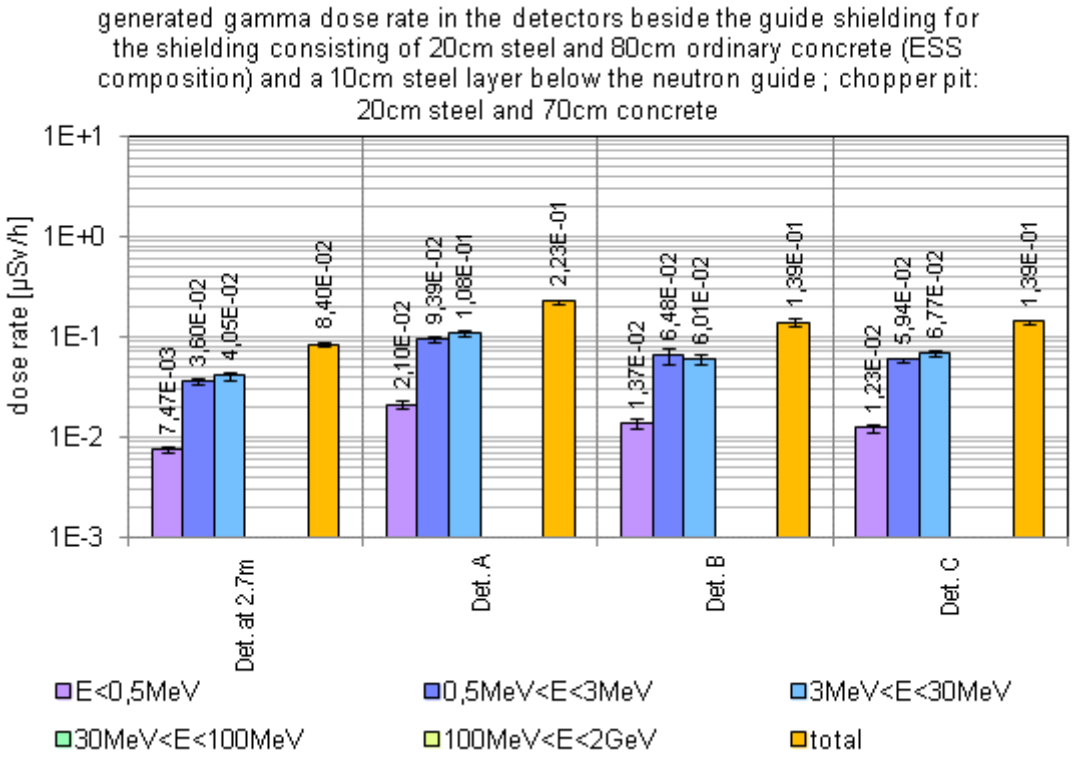

Fig. 221: Generated gamma dose rate in the detectors beside the guide shielding for the shielding consisting of 20cm steel and 80cm ordinary concrete (ESS composition) and a 10cm steel layer below the neutron guide ; chopper pit: 20cm steel and 70cm concrete

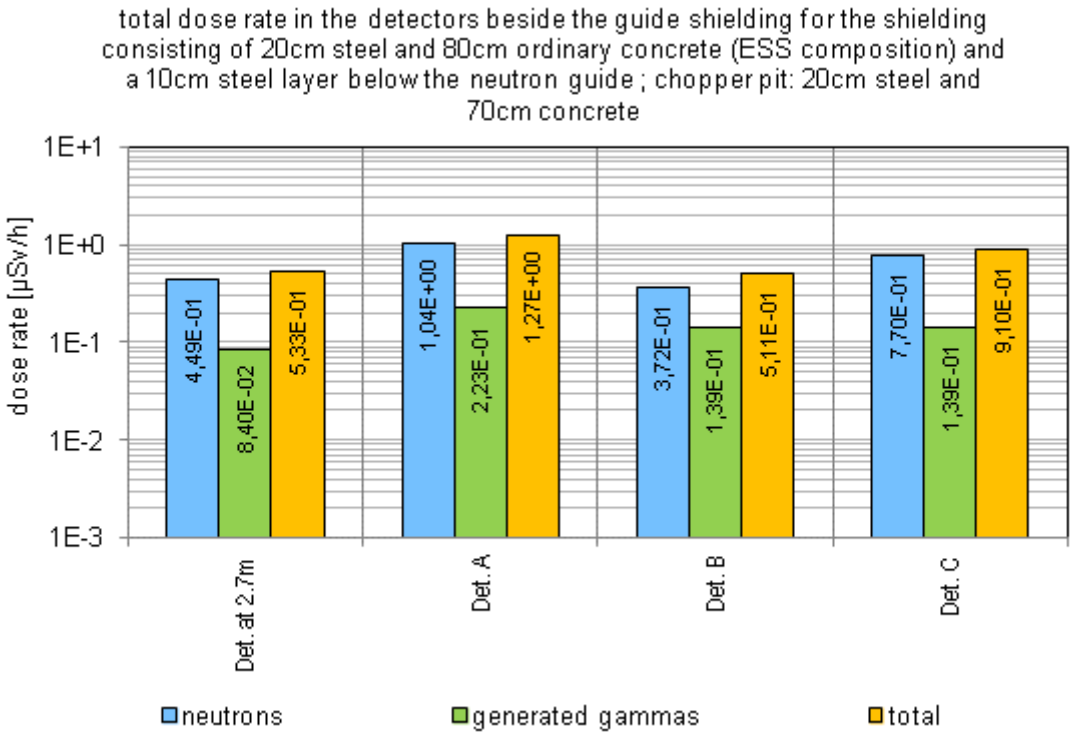

Fig. 222: Total dose rate in the detectors beside the guide shielding for the shielding consisting of 20cm steel and 80cm ordinary concrete (ESS composition) and a 10cm steel layer below the neutron guide ; chopper pit: 20cm steel and 70cm concrete

The dose rate distributions in horizontal and vertical planes through the shielding are shown in the following images.

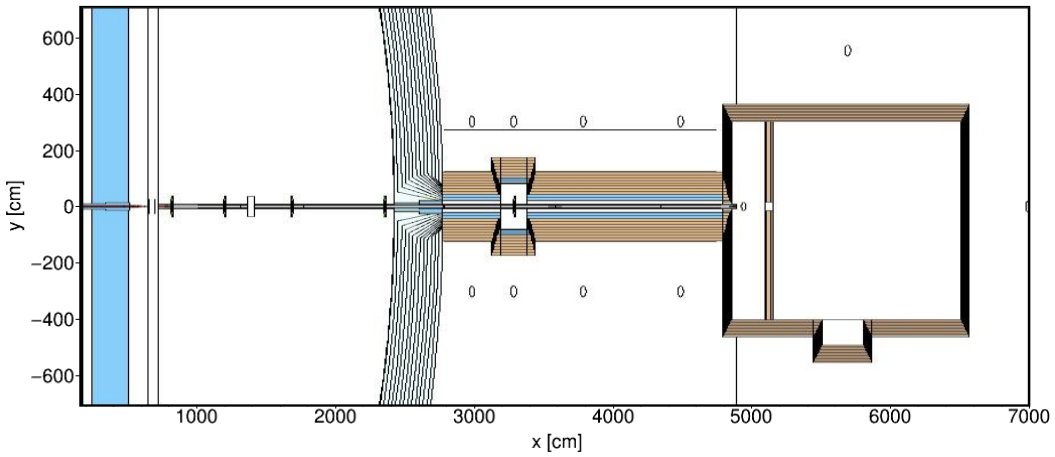

Fig. 223: Horizontal area through the Monte Carlo model of the ODIN instrument for which the radiation distribution is shown in the following image

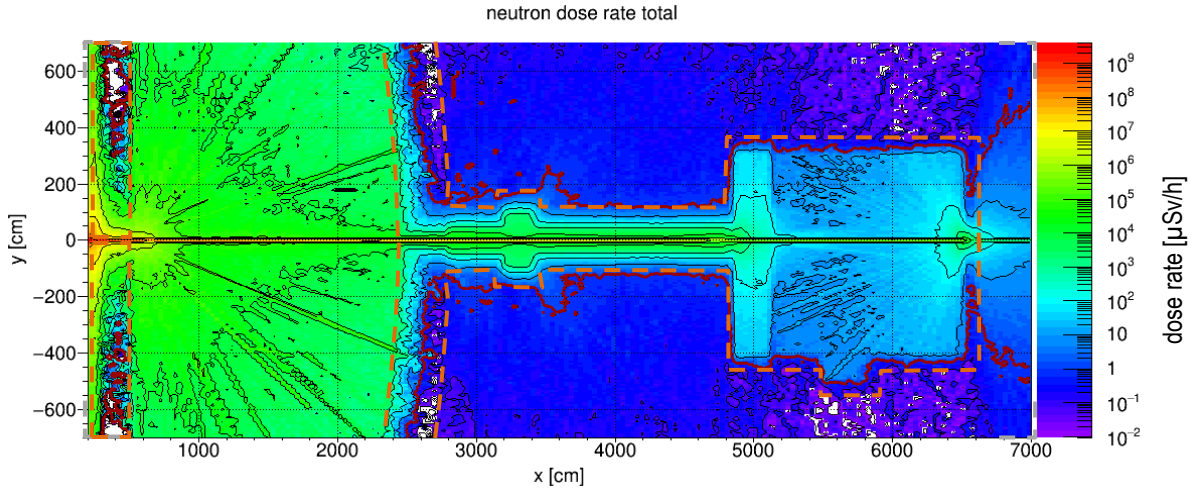

Fig. 224: Total neutron dose rate distribution in the horizontal area. The red line is the 1µSv/h border.

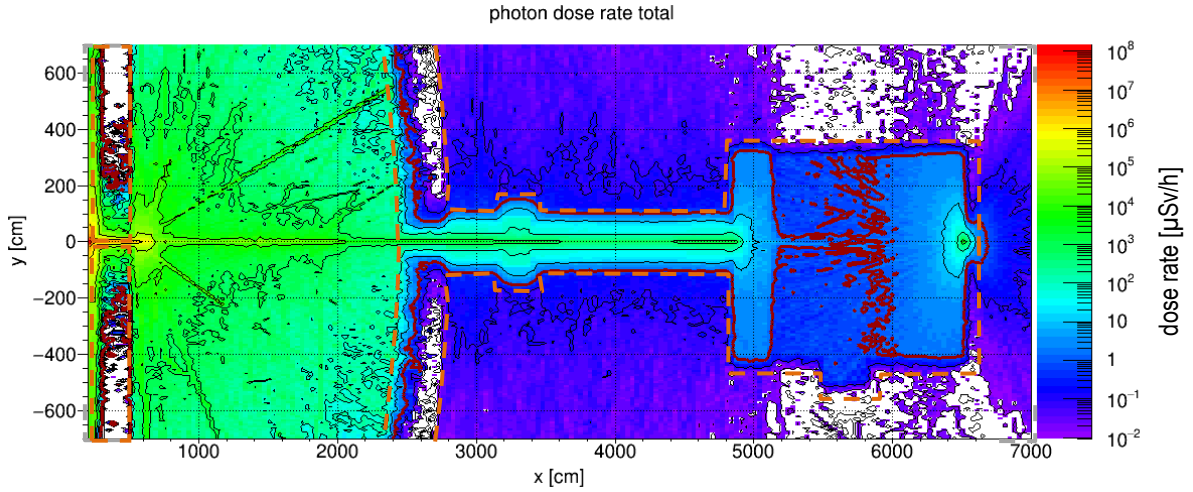

Fig. 225: Total generated gamma dose rate distribution in the horizontal area. The red line is the 1µSv/h border.

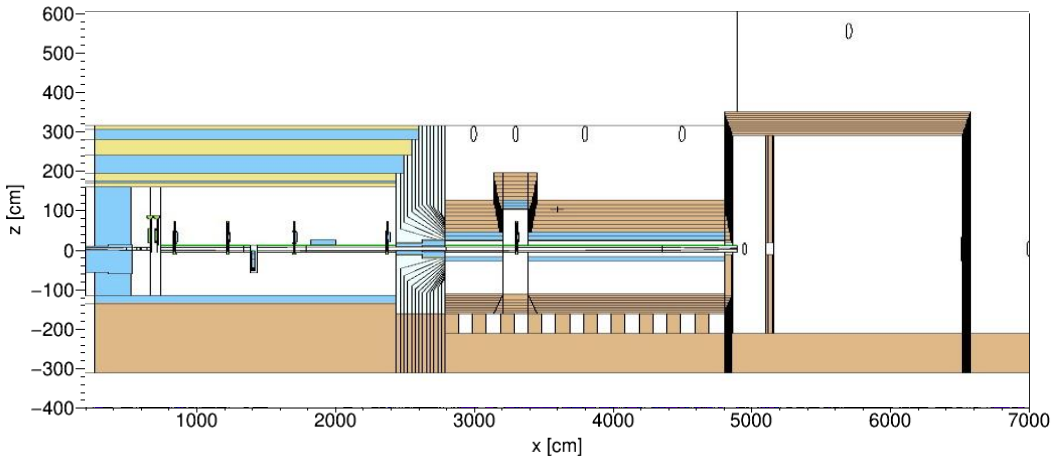

Fig. 226: Vertical area through the Monte Carlo model of the ODIN instrument for which the radiation distribution is shown in the following image

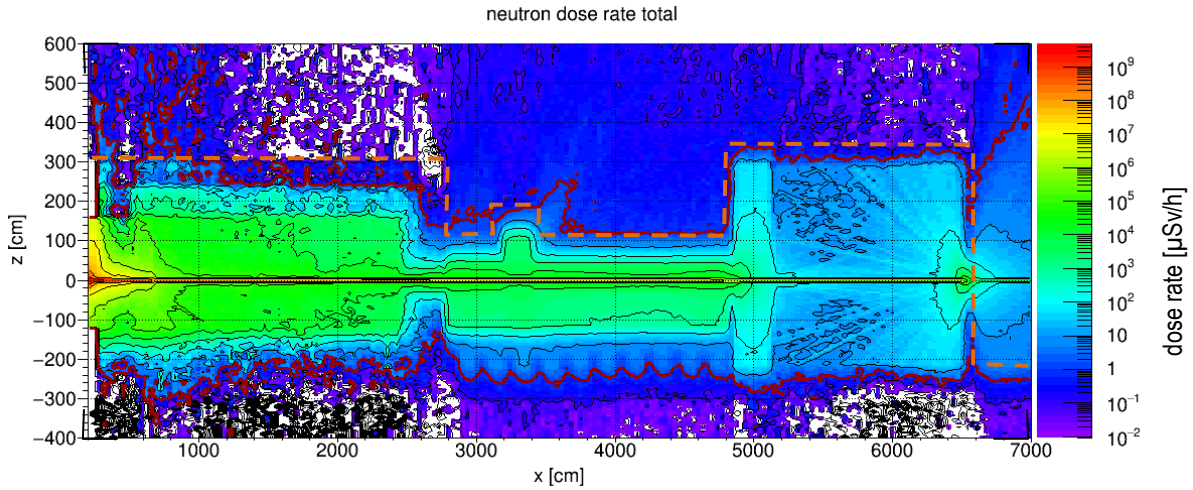

Fig. 227: Total neutron dose rate distribution in the vertical area. The red line is the 1µSv/h border.

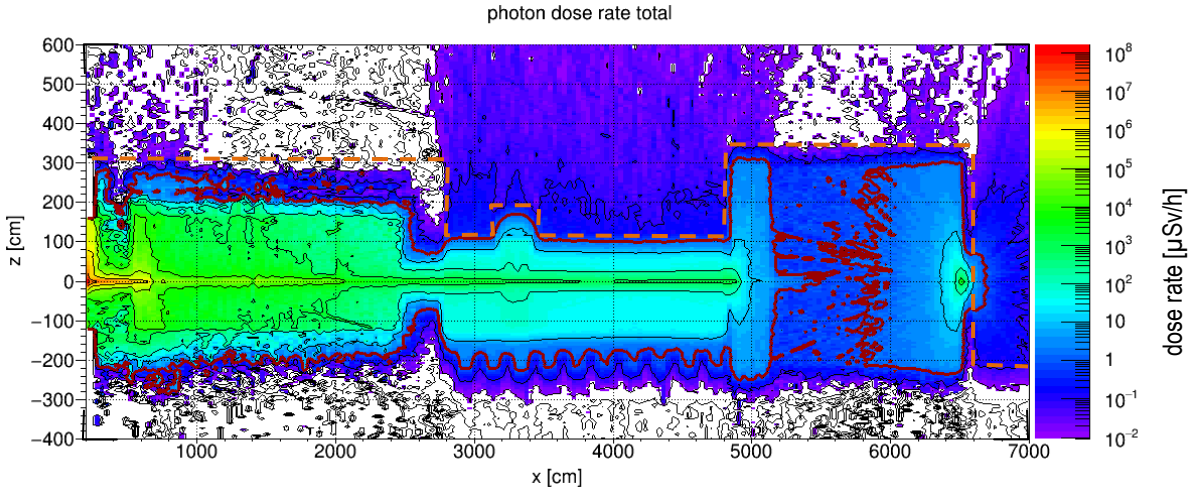

Fig. 228: Total generated gamma dose rate distribution in the vertical area. The red line is the 1µSv/h border.

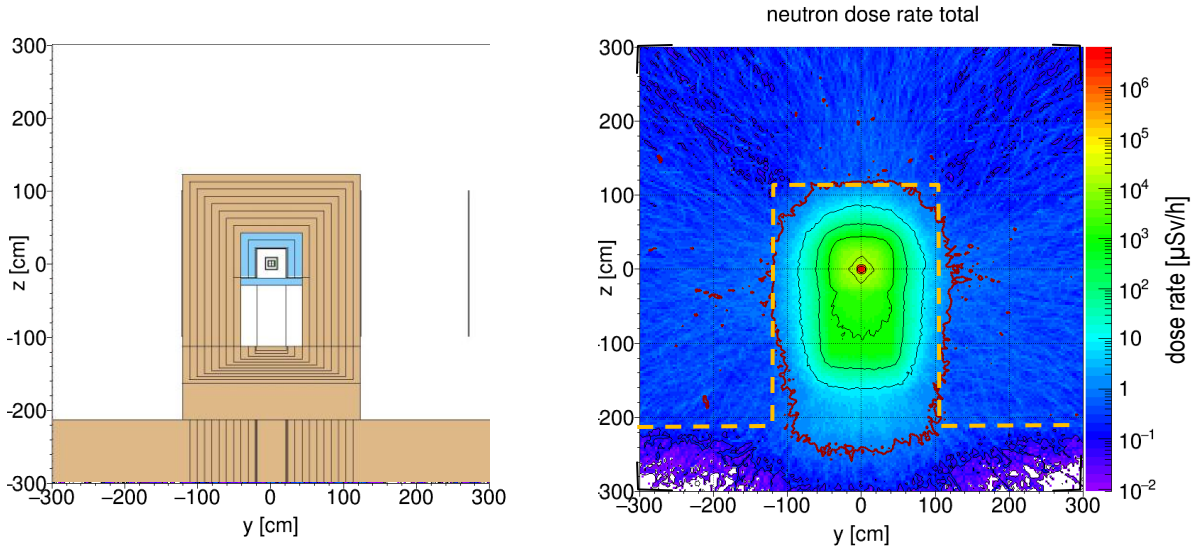

Fig. 229: Vertical neutron dose rate distribution through the guide shielding perpendicular to the beam axis (40m from the focal point). The red line is the 1µSv/h border.

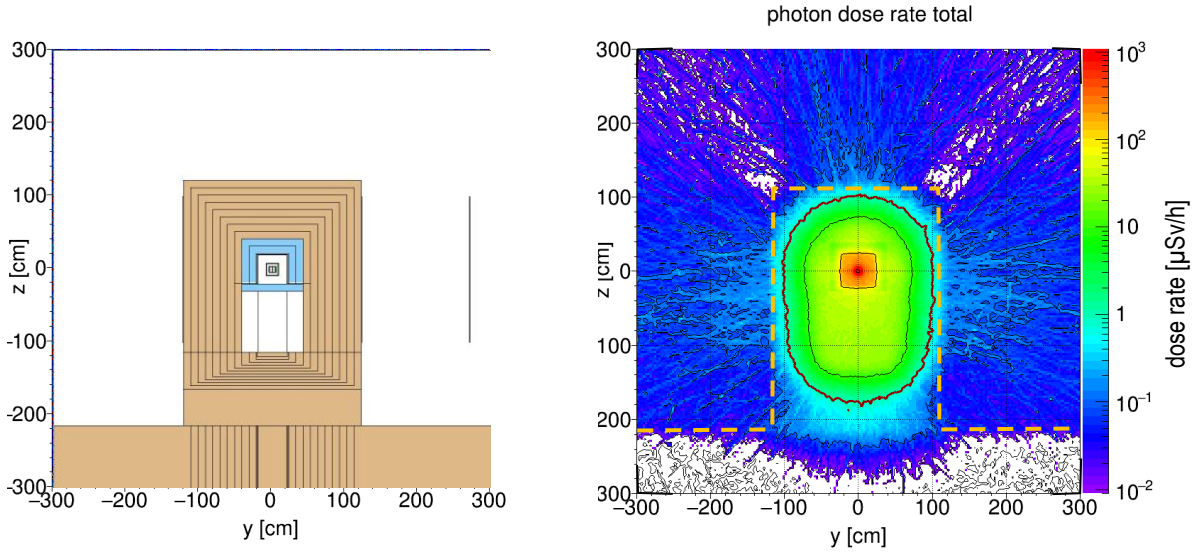

Fig. 230: Vertical generated gamma dose rate distribution through the guide shielding perpendicular to the beam axis (40m from the focal point). The red line is the 1µSv/h border.

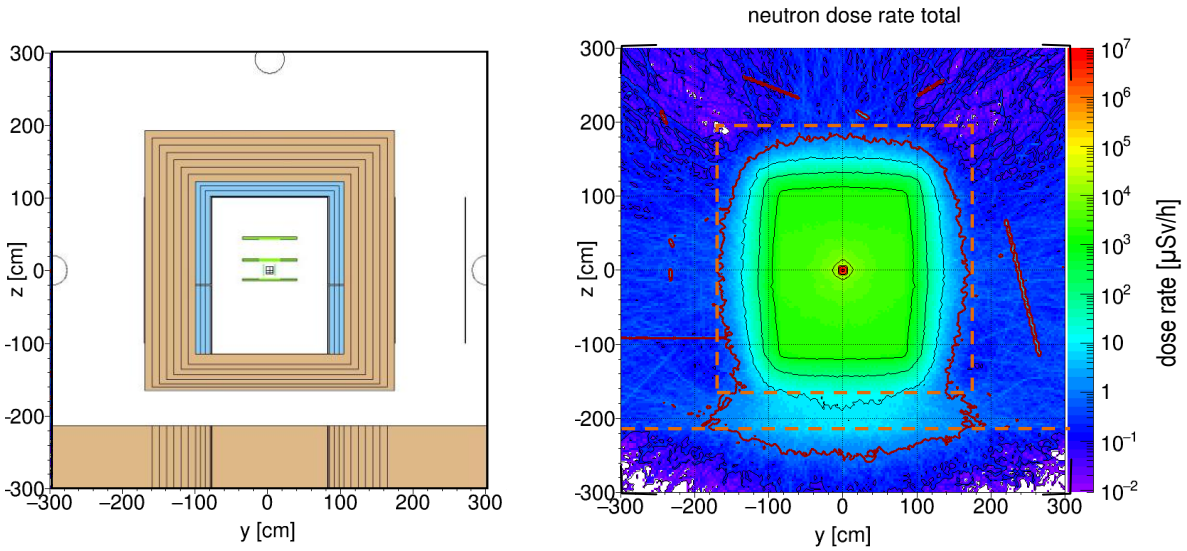

Fig. 231: Vertical neutron dose rate distribution through the chopper pit perpendicular to the beam axis. The red line is the 1µSv/h border.

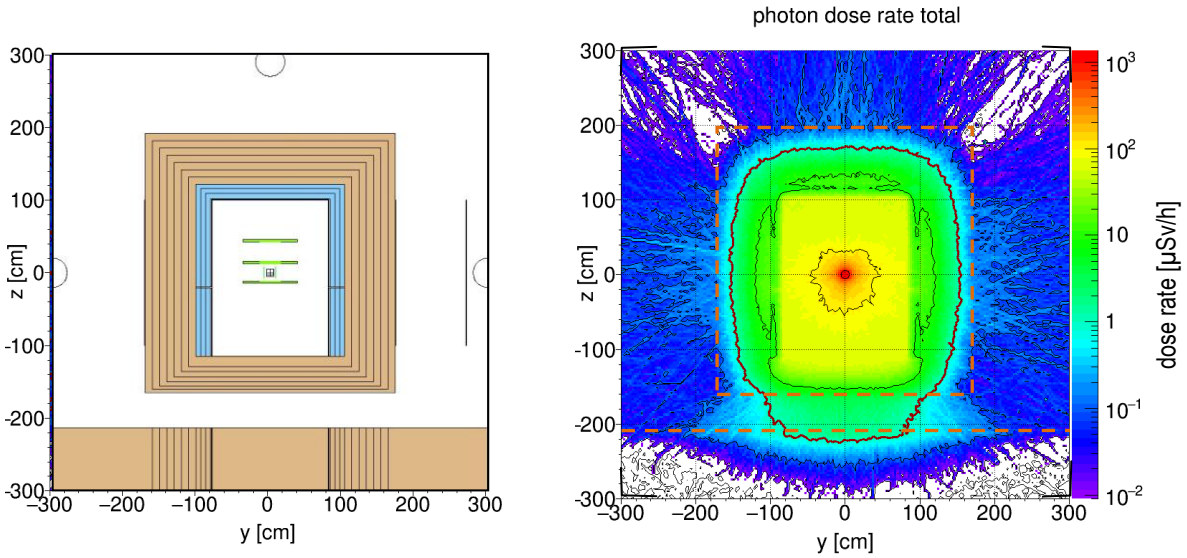

Fig. 232: Vertical generated gamma dose rate distribution through the chopper pit perpendicular to the beam axis. The red line is the 1µSv/h border.

7.6.1 Closed chopper FOC5

The gamma dose rate distribution for a chopper pit shielding consisting of 20cm steel and 70cm concrete was already presented in previous chapters. The shielding is sufficient for this case.

7.6.2 Conclusion

With this version on all outer surfaces the desired dose rate level of 1.5µSv/h is not exceeded. The leakage below the inner steel layer of the shielding (20cm) is eliminated by the 10cm steel layer below the neutron guide.

7.7 Shielding version 3E consisting of 20cm steel and 80cm ESS ordinary concrete and a 5cm steel layer below the neutron guide (chopper pit: 20cm steel and 70cm ordinary concrete)

In the last chapter a 10cm steel layer below the neutron guide was introduced in order to prevent the leakage below the steel layer at the side walls. In the version in this chapter it is tested if a steel layer of 5cm is also sufficient below the neutron guide. In addition the thickness of the steel layers at the rear wall of the chopper pit are increased to 30cm.

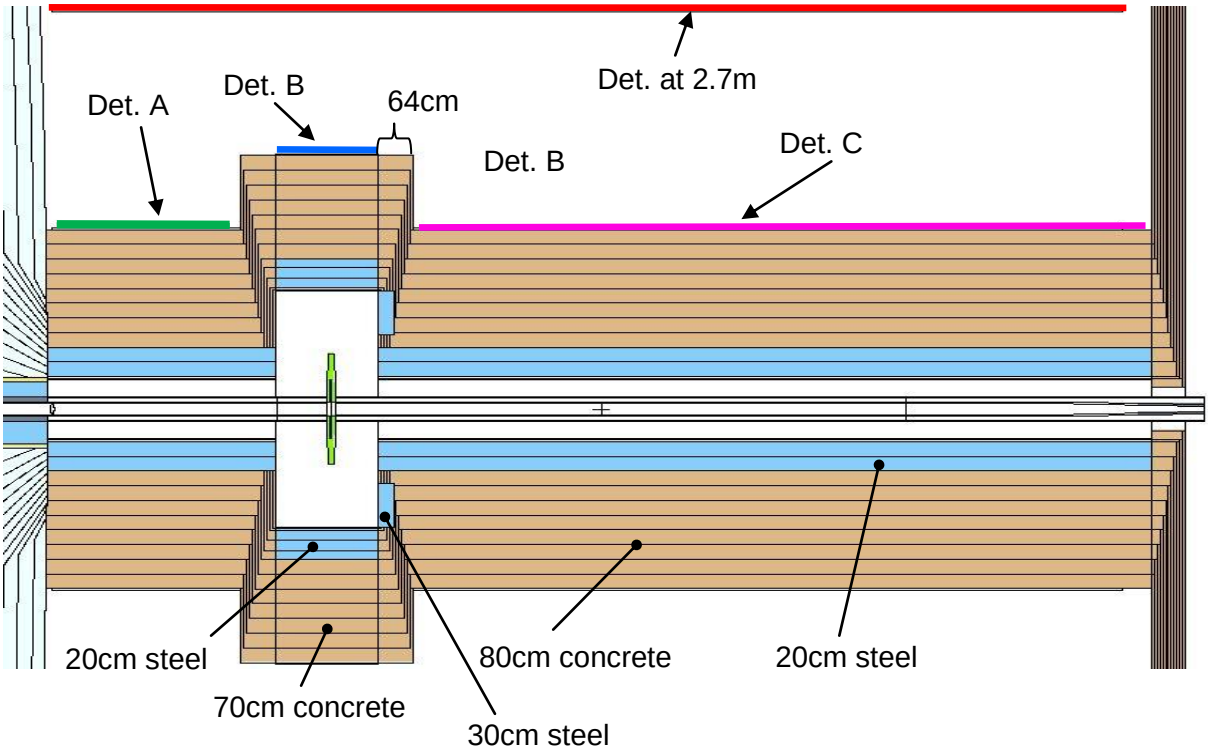

Fig. 233: Horizontal cut through the Monte Carlo model of the guide shielding

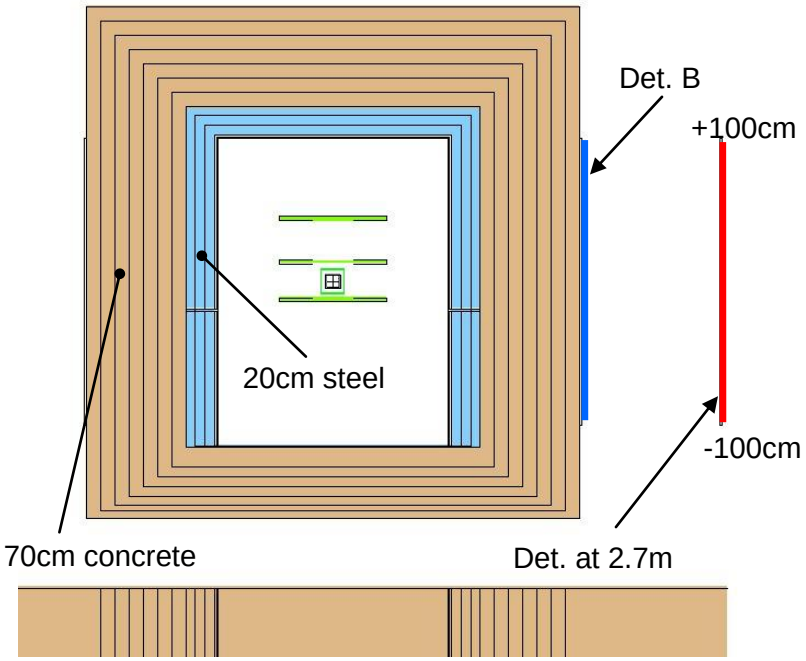

Fig. 234: Vertical cut through the Monte Carlo model of the chopper pit

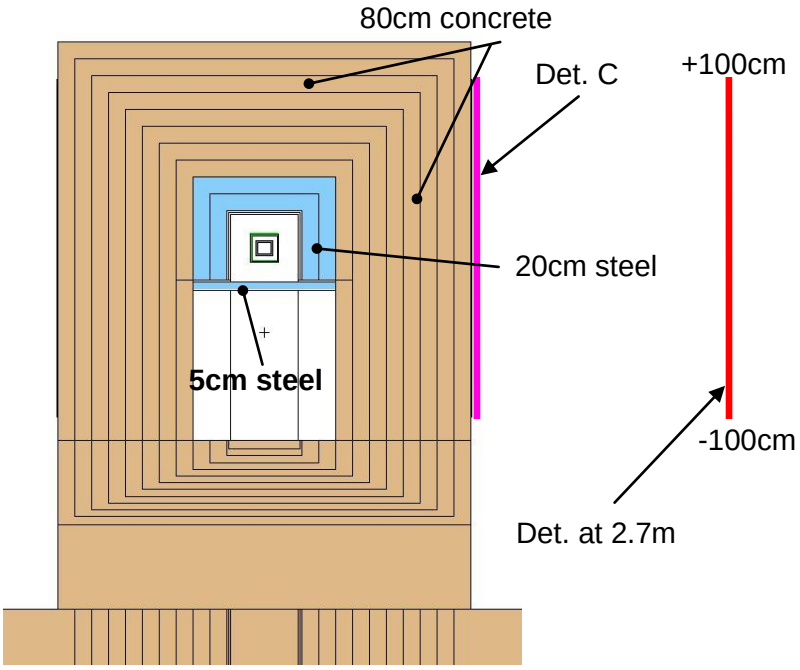

Fig. 235: Vertical cut through the Monte Carlo model of the guide shielding

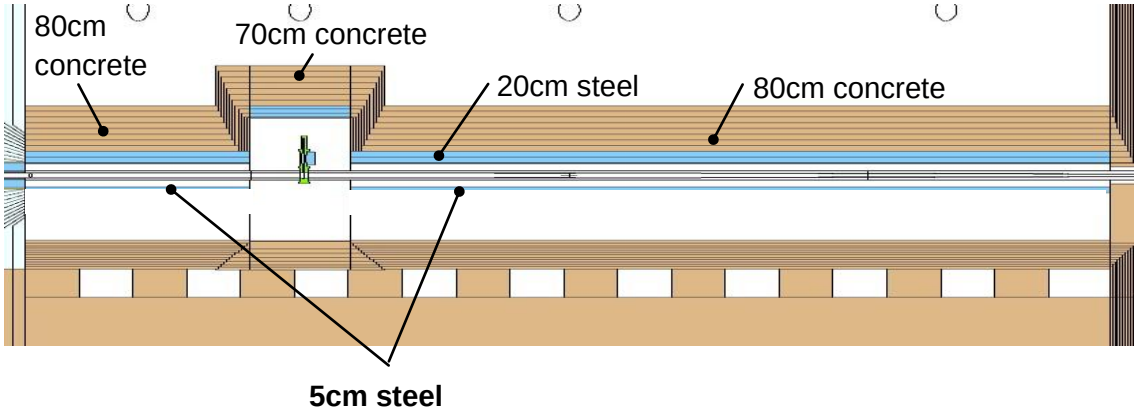

Fig. 236: Vertical cut through the Monte Carlo model of the guide shielding along the guide axis

The dose rates in the detectors are shown in the following figures.

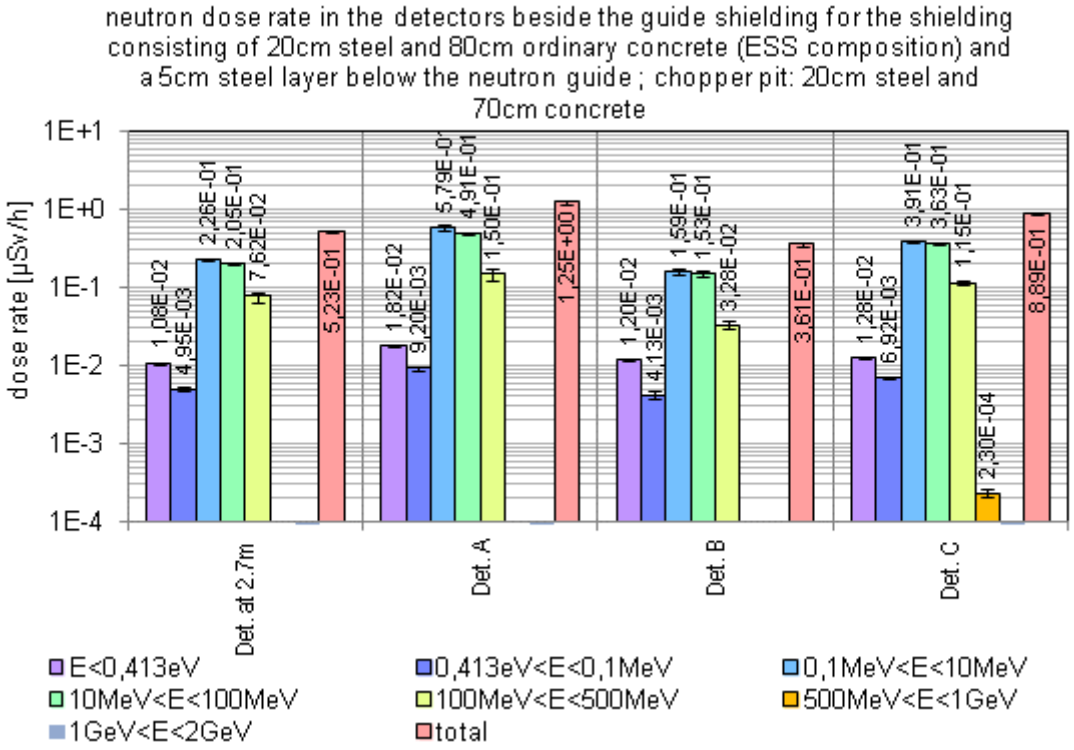

Fig. 237: neutron dose rate in the detectors beside the guide shielding for the shielding consisting of 20cm steel and 80cm ordinary concrete (ESS composition) and a 5cm steel layer below the neutron guide ; chopper pit: 20cm steel and 70cm concrete

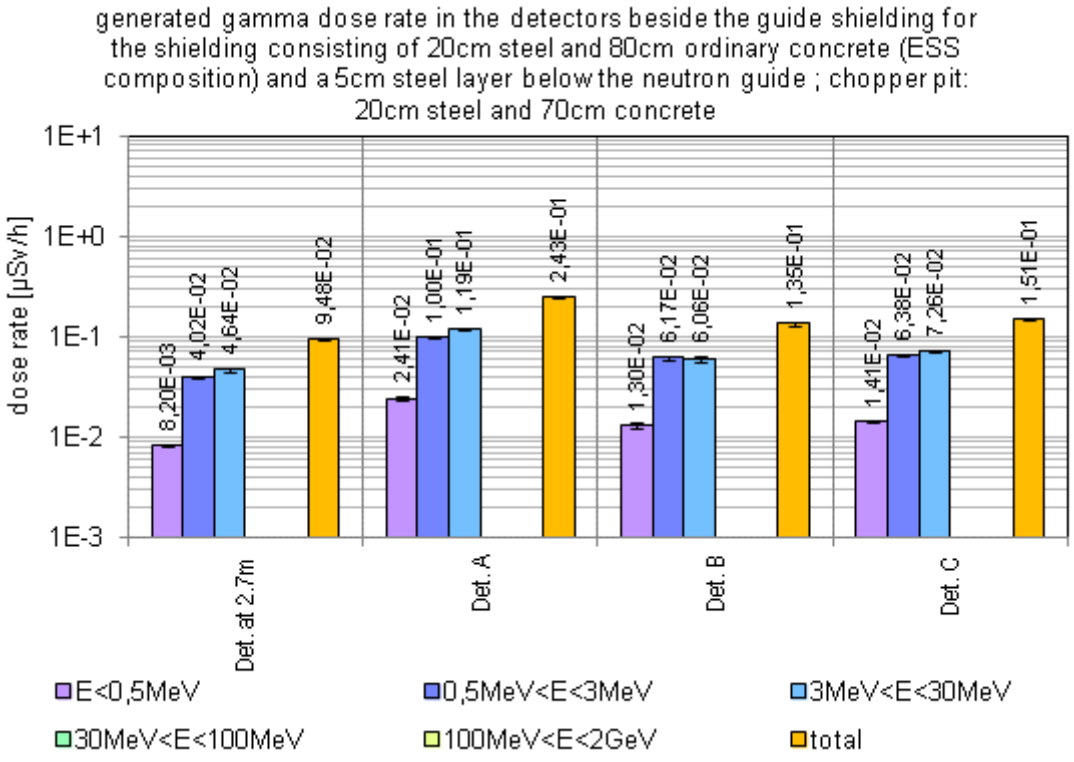

Fig. 238: Generated gamma dose rate in the detectors beside the guide shielding for the shielding consisting of 20cm steel and 80cm ordinary concrete (ESS composition) and a 5cm steel layer below the neutron guide ; chopper pit: 20cm steel and 70cm concrete

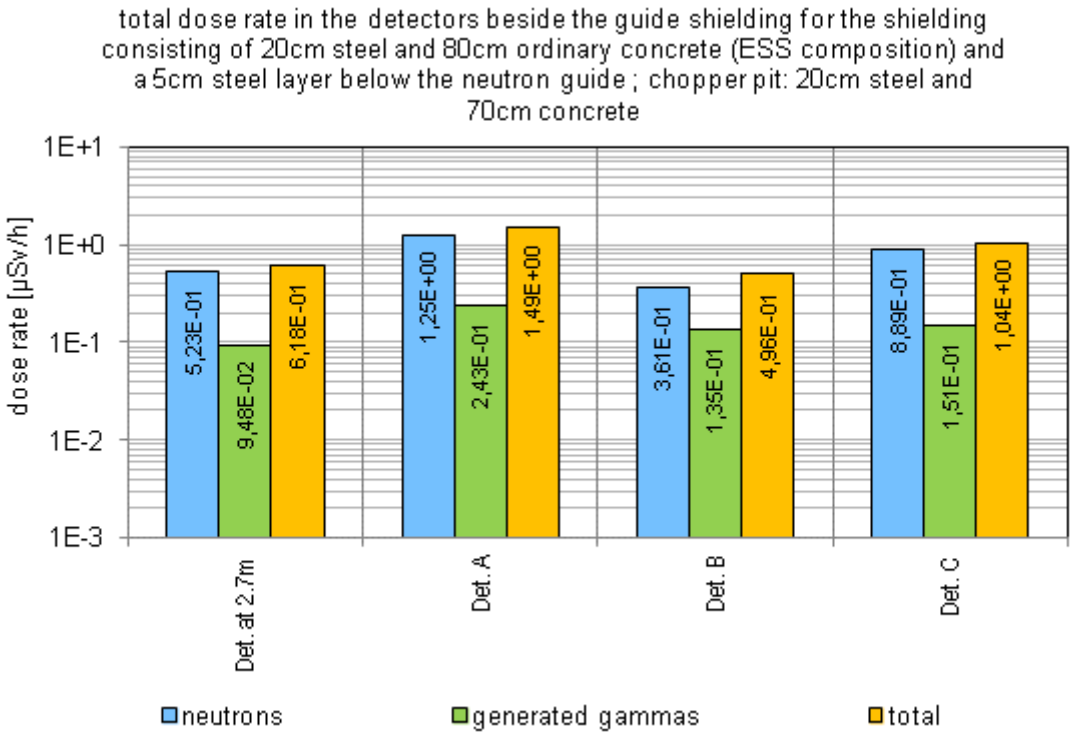

Fig. 239: Total dose rate in the detectors beside the guide shielding for the shielding consisting of 20cm steel and 80cm ordinary concrete (ESS composition) and a 5cm steel layer below the neutron guide ; chopper pit: 20cm steel and 70cm concrete

The dose rate distributions in horizontal and vertical planes through the shielding are shown in the following images.

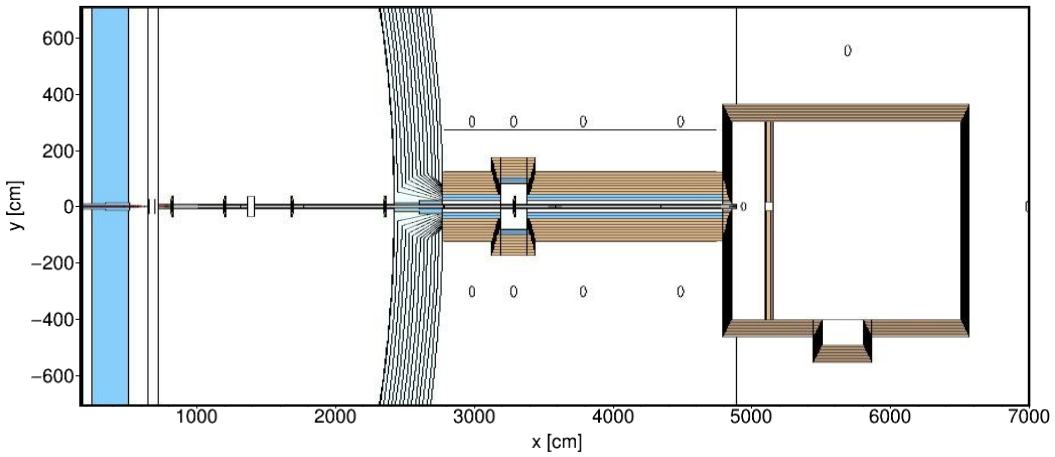

Fig. 240: Horizontal area through the Monte Carlo model of the ODIN instrument for which the radiation distribution is shown in the following image

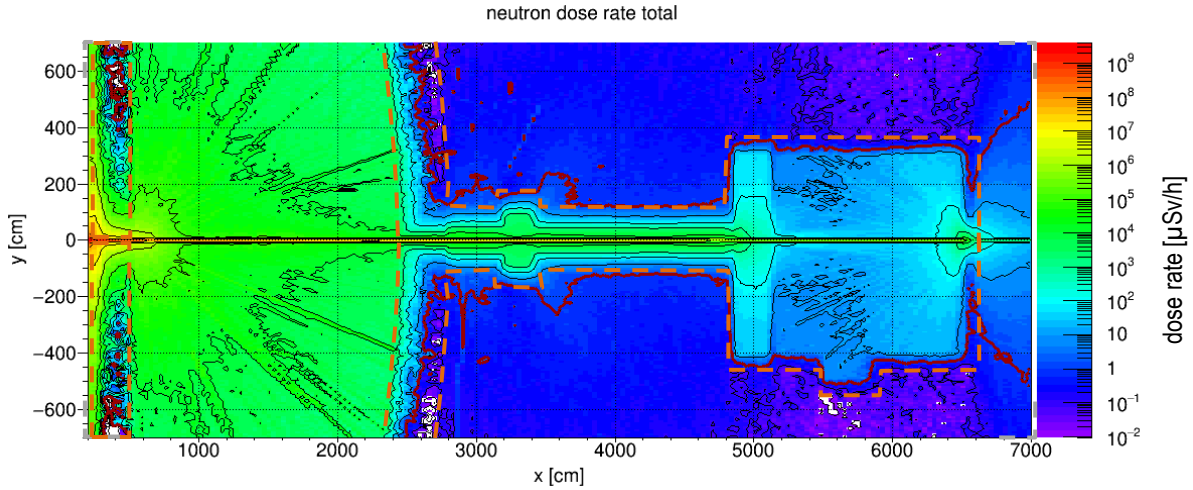

Fig. 241: Total neutron dose rate distribution in the horizontal area. The red line is the 1µSv/h border.

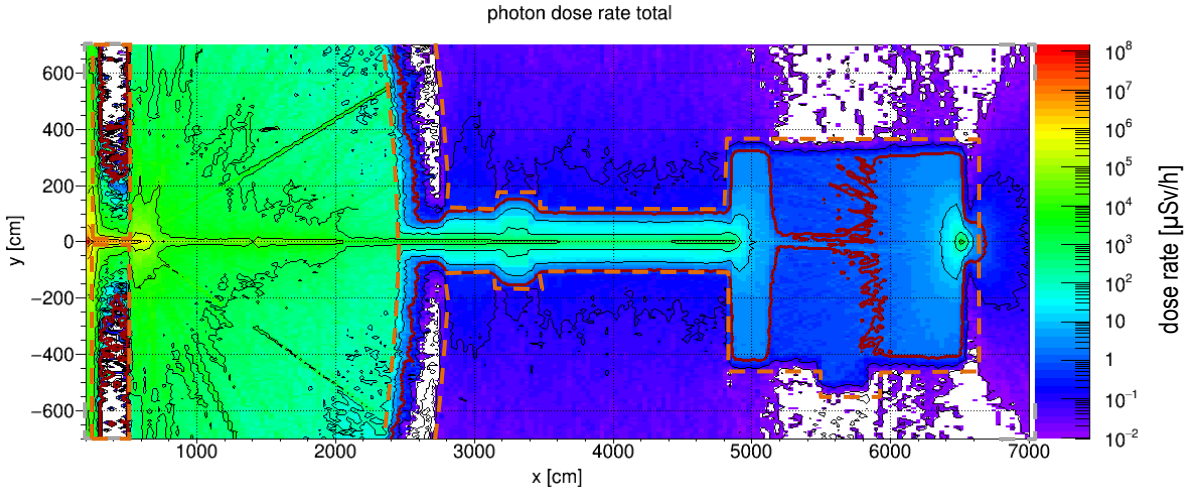

Fig. 242: Total generated gamma dose rate distribution in the horizontal area. The red line is the 1µSv/h border.

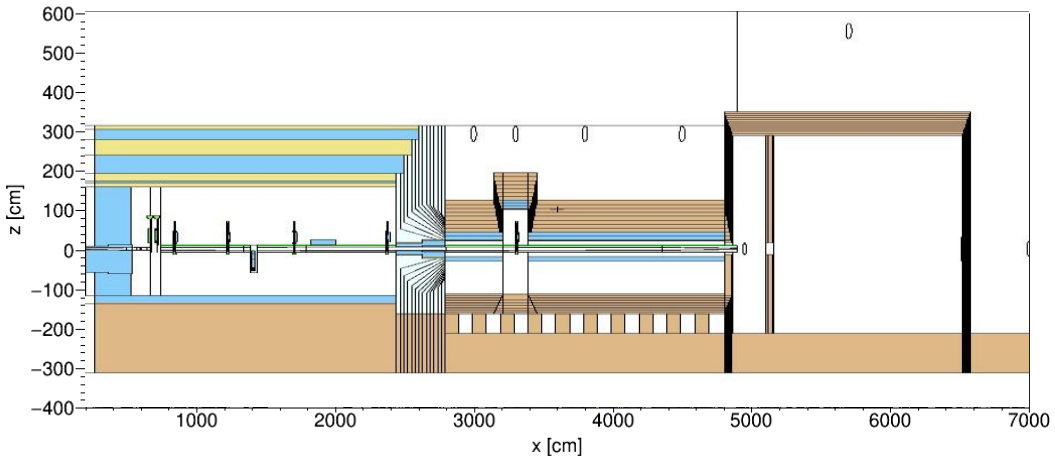

Fig. 243: Vertical area through the Monte Carlo model of the ODIN instrument for which the radiation distribution is shown in the following image

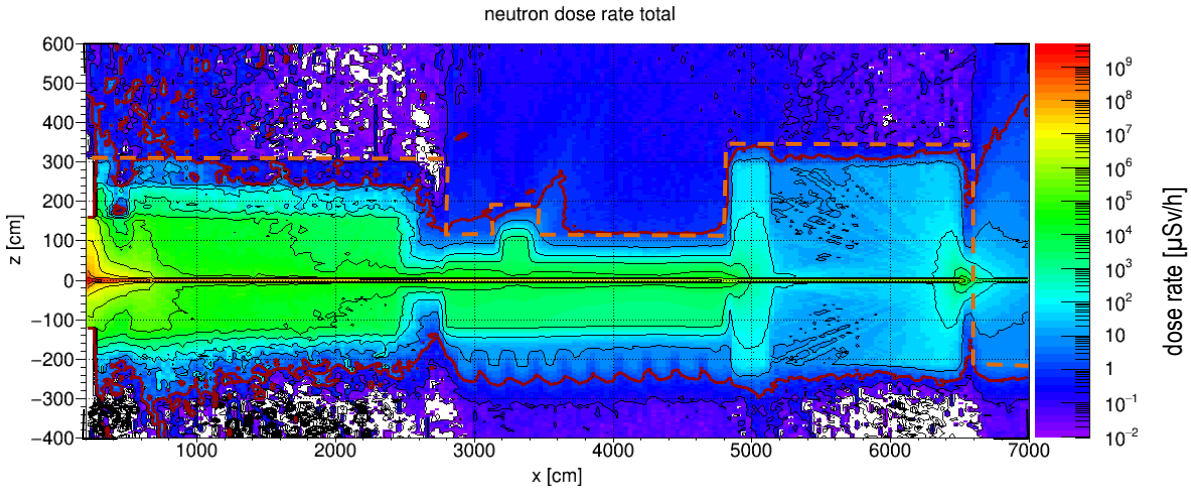

Fig. 244: Total neutron dose rate distribution in the vertical area. The red line is the 1µSv/h border.

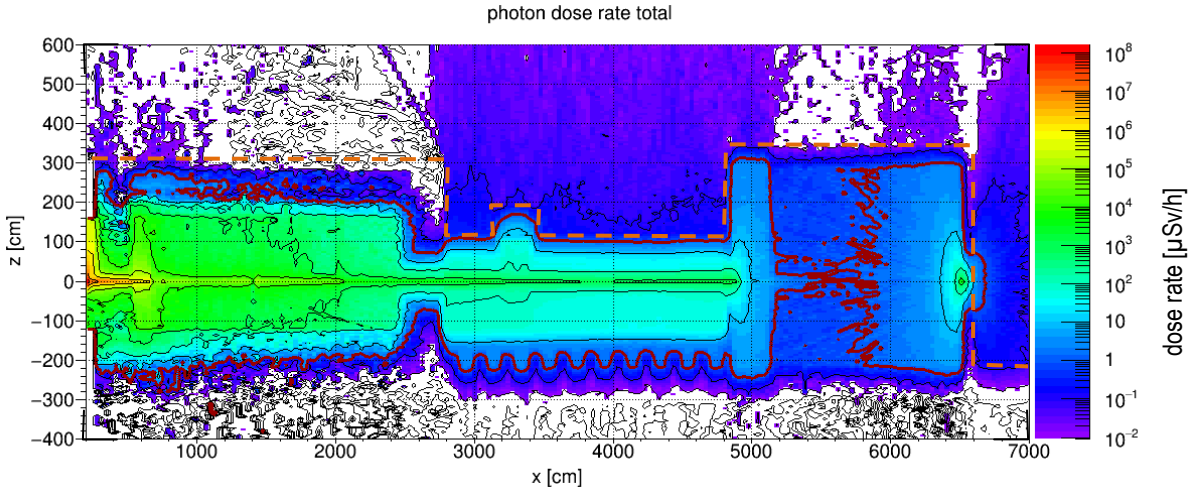

Fig. 245: Total generated gamma dose rate distribution in the vertical area. The red line is the 1µSv/h border.

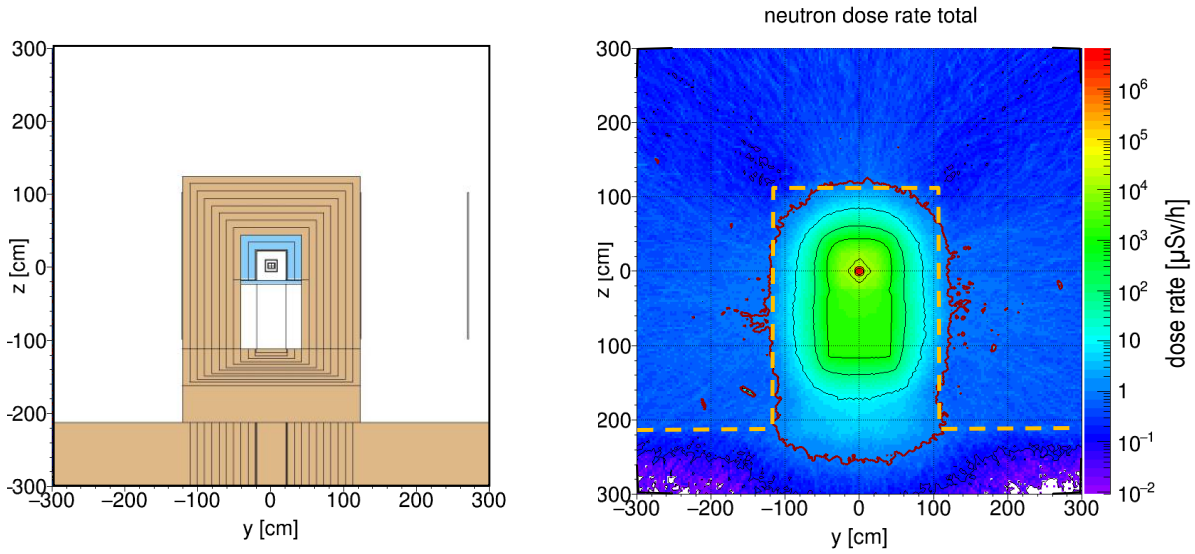

Fig. 246: Vertical neutron dose rate distribution through the guide shielding perpendicular to the beam axis (40m from the focal point). The red line is the 1µSv/h border.

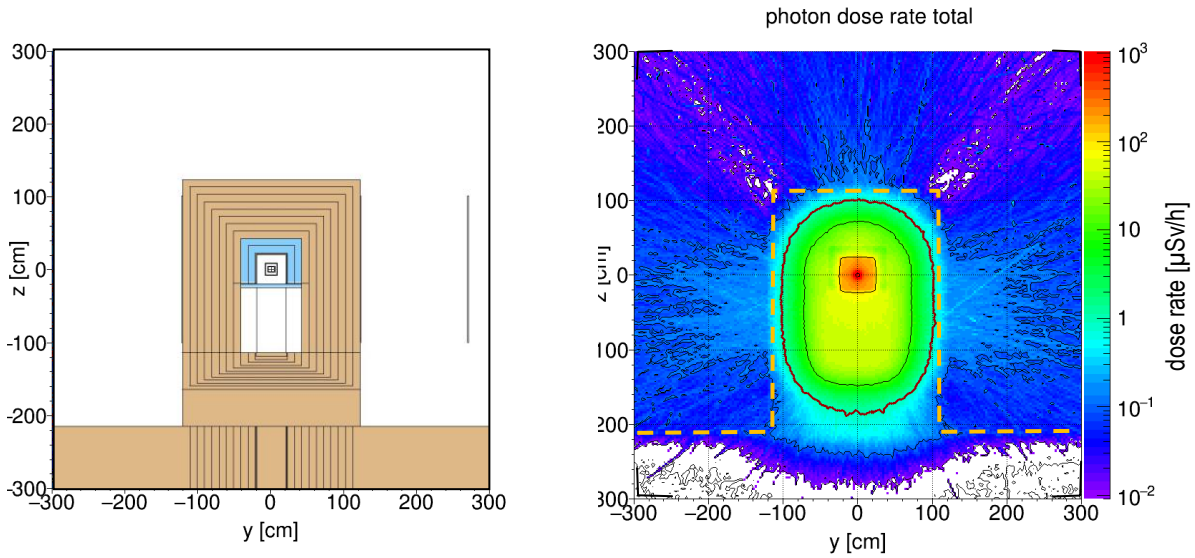

Fig. 247: Vertical generated gamma dose rate distribution through the guide shielding perpendicular to the beam axis (40m from the focal point). The red line is the 1µSv/h border.

7.7.1 Closed chopper FOC5

The gamma dose rate distribution for a chopper pit shielding consisting of 20cm steel and 70cm concrete was already presented in previous chapters. The shielding is sufficient for this case.

7.8 Conclusion

The 5cm steel layer below the neutron guide is also sufficient. The dose rate on the outer surface of the guide shielding between bunker wall and chopper pit is now at the limit of 1.5µSv/h.

7.9 Shielding version 3F with collimators and interface between bunker wall and guide shielding

In this version collimators made from copper are included at the entrance and the exit of the chopper pit and at the entrance of the cave. In addition the interface between the bunker wall and the guide shielding is included. The shielding thickness is smaller here but the heavy concrete as used for the bunker wall is applied. The inner width of the shielding in the interface is 64cm. The distance from the guide axis to the inner upper surface of the shielding is 22cm.

No steel layer is applied below the neutron guide. Hence the results have to be compared with version 3C in order to see the effect of the collimators.

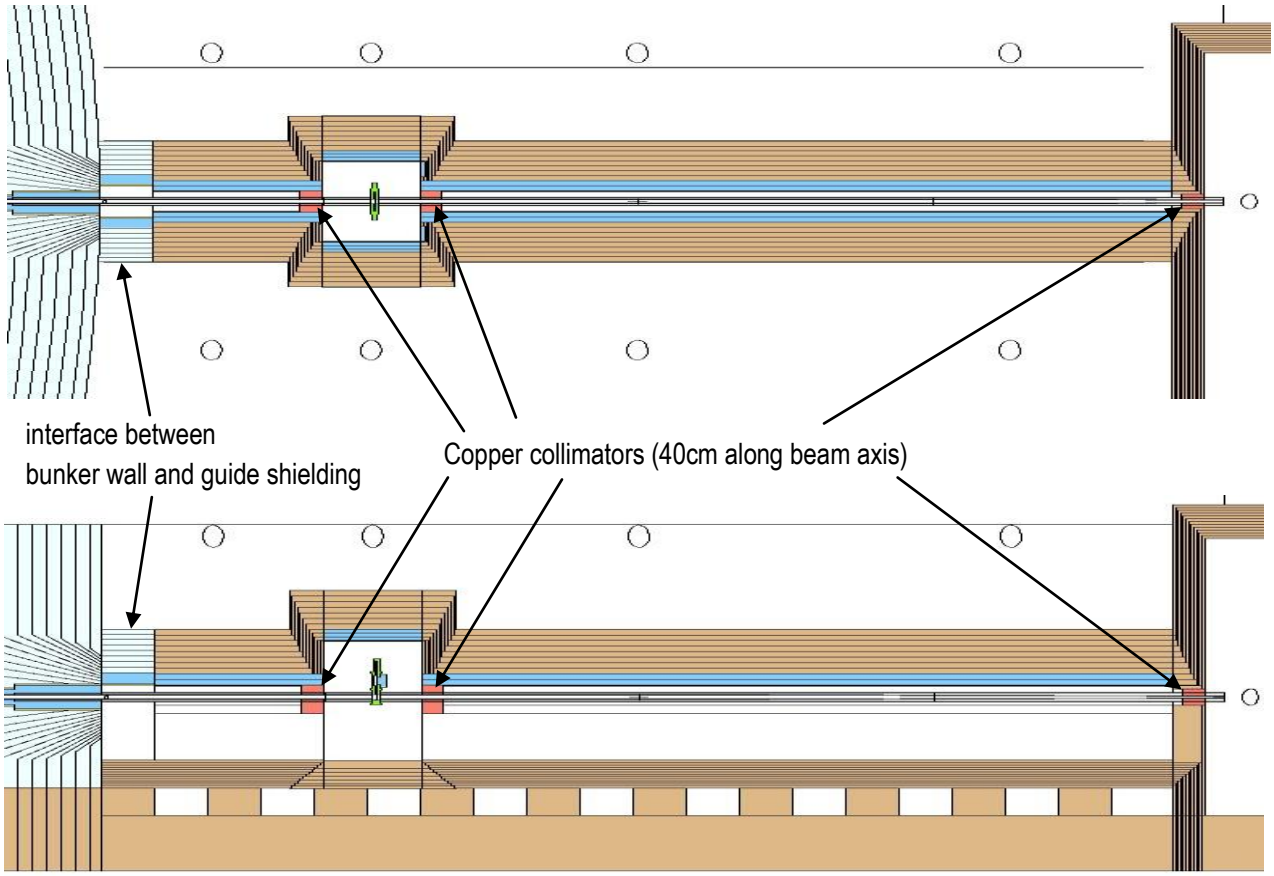

Fig. 248: Horizontal (top) and vertical cut (bottom) through the Monte Carlo model of the guide shielding

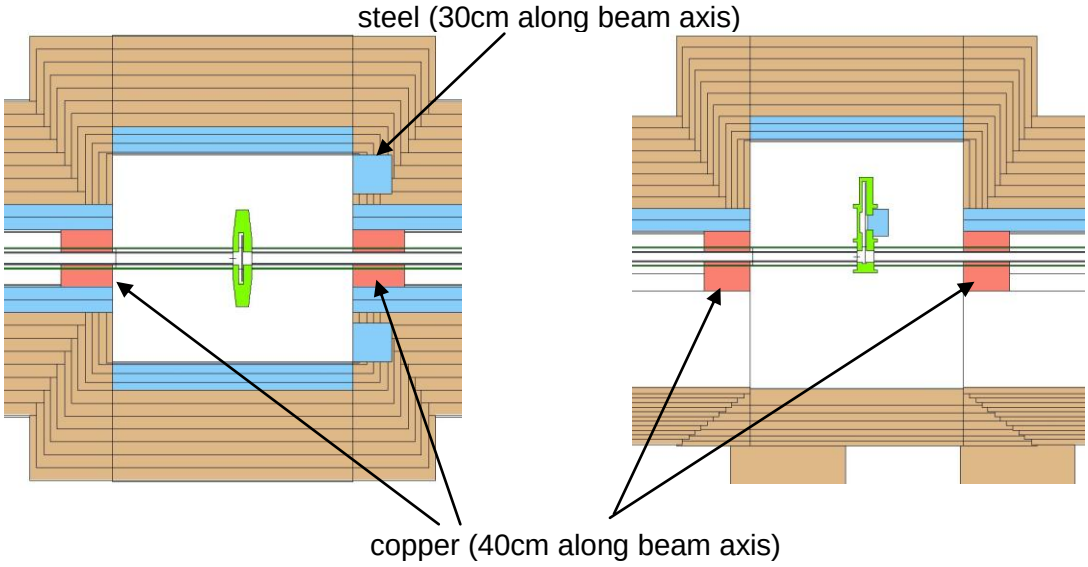

Fig. 249: Horizontal (left hand side) and vertical cut (right hand side) through the Monte Carlo model of the chopper pit

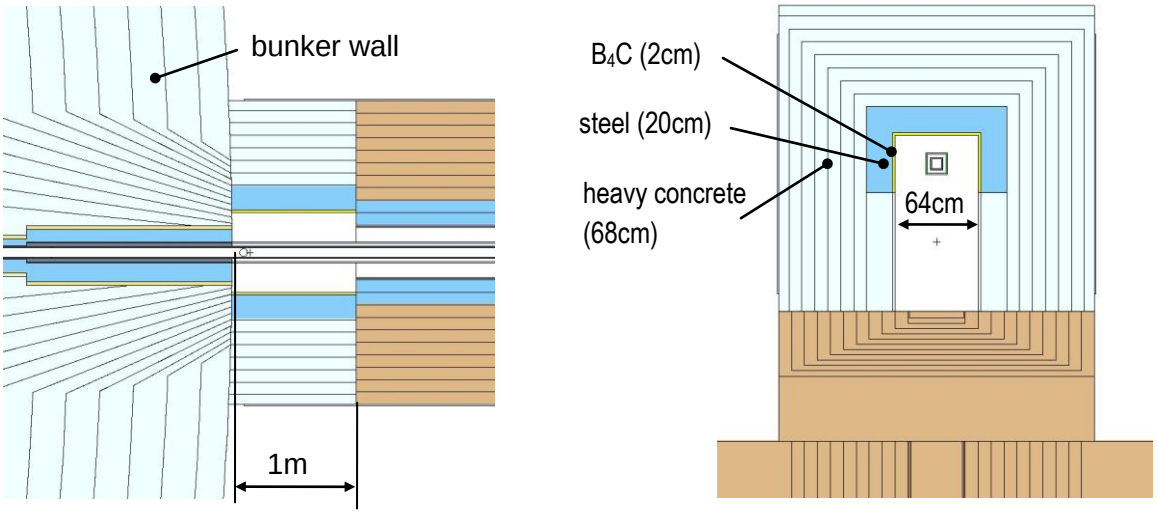

Fig. 250: Horizontal (left hand side) and vertical cut (right hand side) through the Monte Carlo model of the interface between the bunker wall and the guide shielding

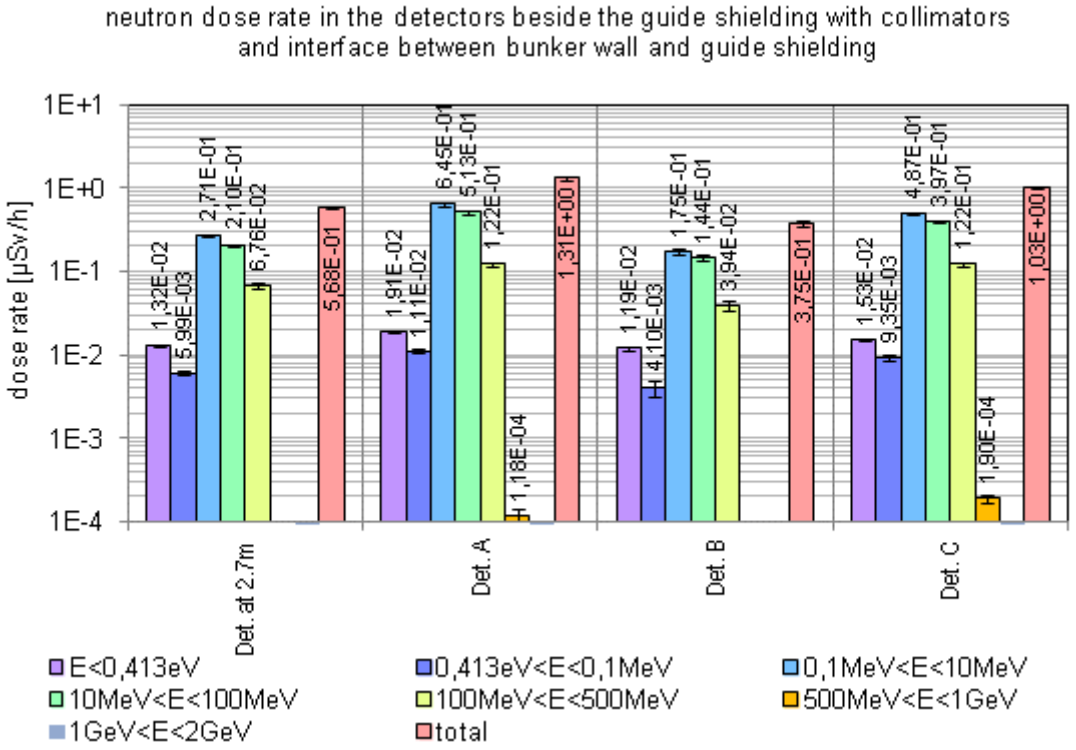

Fig. 251: Neutron dose rate in the detectors beside the guide shielding with collimators and interface between bunker wall and guide shielding

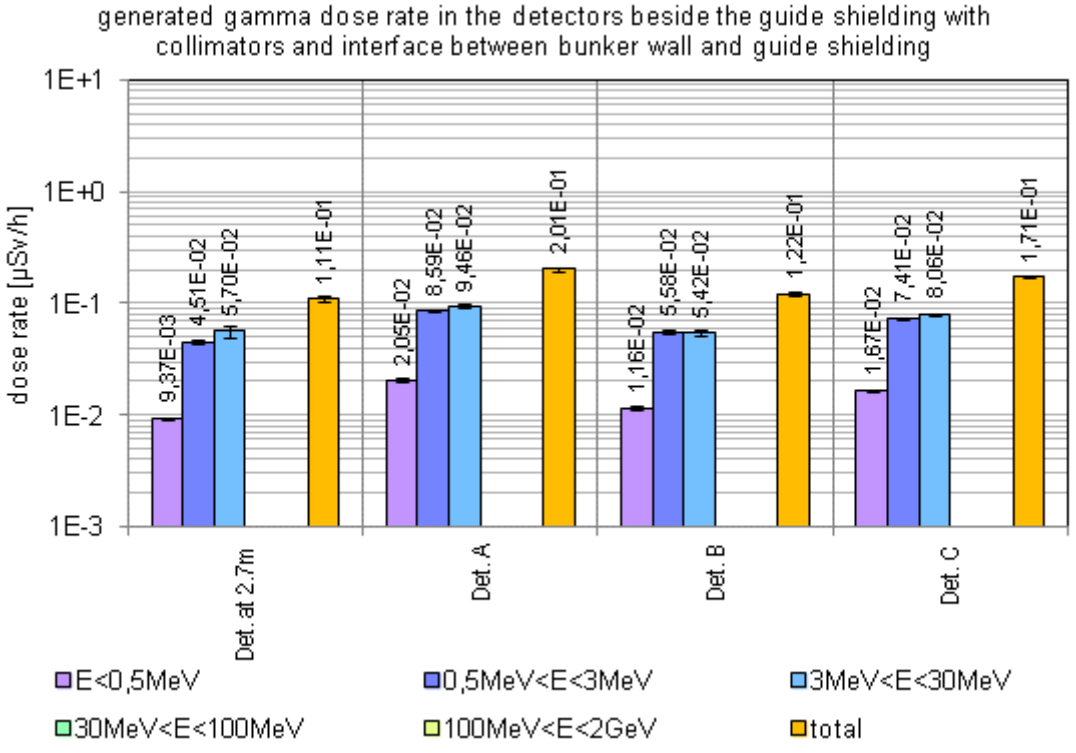

Fig. 252: Generated gamma dose rate in the detectors beside the guide shielding with collimators and interface between bunker wall and guide shielding

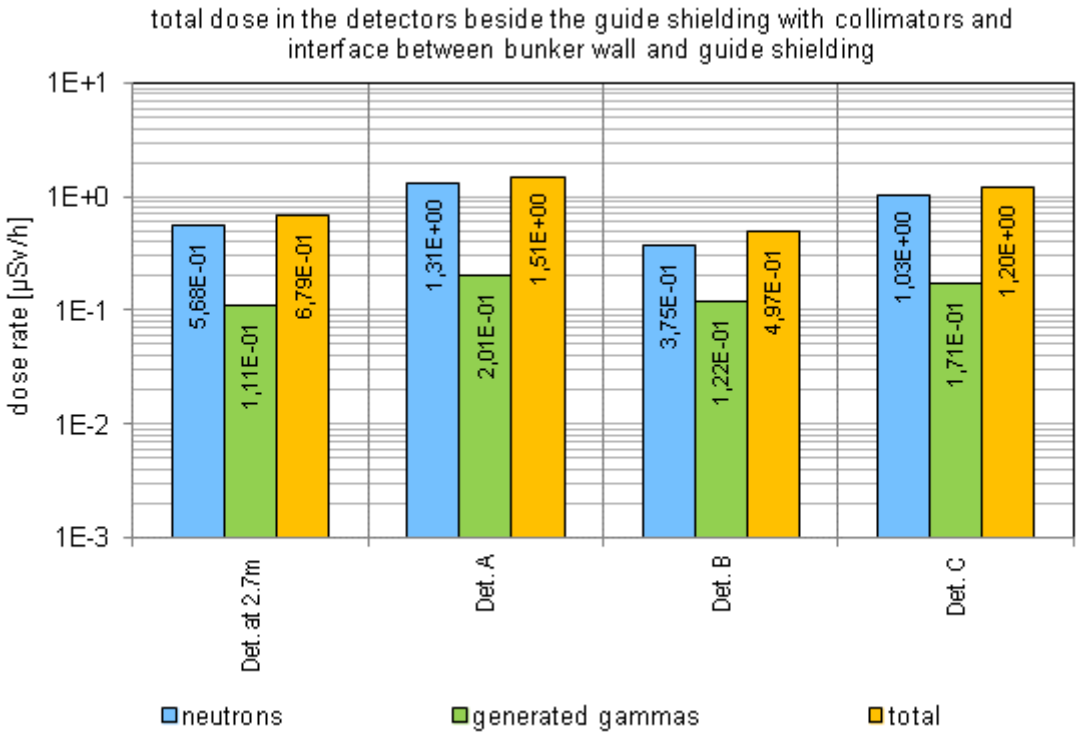

Fig. 253: Total dose rate in the detectors beside the guide shielding with collimators and interface between bunker wall and guide shielding

The dose rate distributions in horizontal and vertical planes through the shielding are shown in the following images.

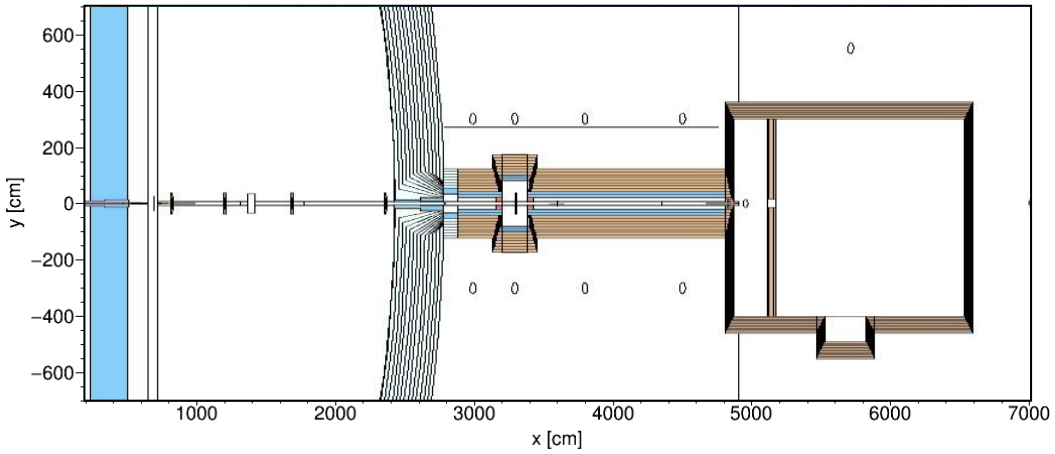

Fig. 254: Horizontal area through the Monte Carlo model of the ODIN instrument for which the radiation distribution is shown in the following image

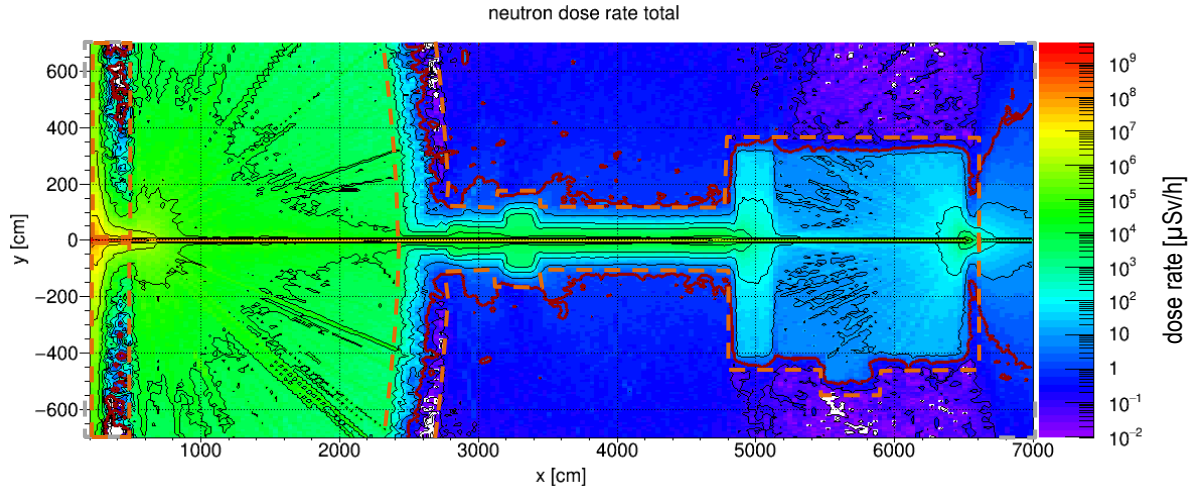

Fig. 255: Total neutron dose rate distribution in the horizontal area. The red line is the 1µSv/h border.

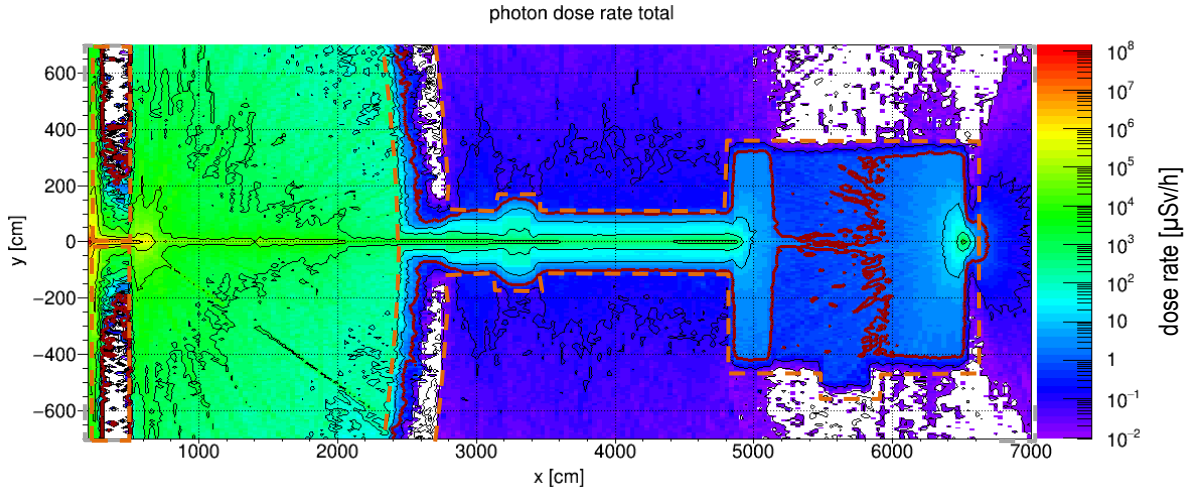

Fig. 256: Total generated gamma dose rate distribution in the horizontal area. The red line is the 1µSv/h border.

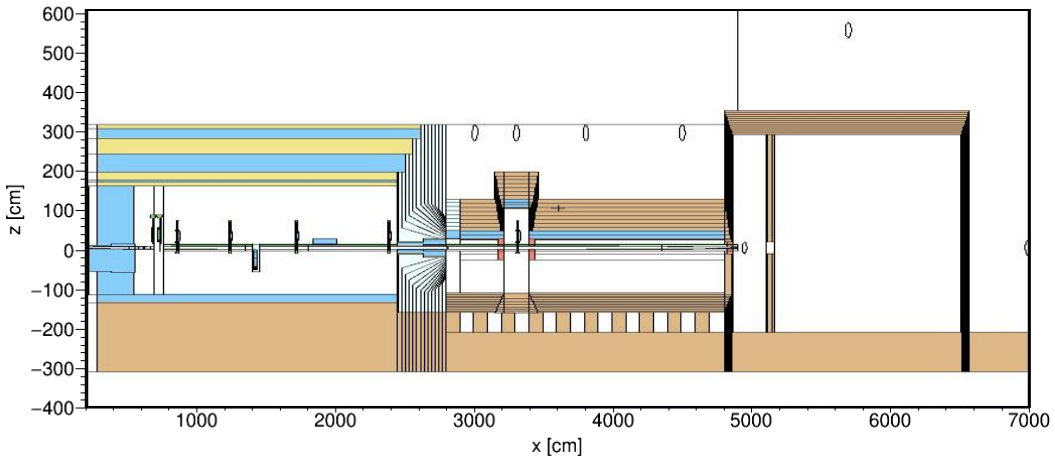

Fig. 257: Vertical area through the Monte Carlo model of the ODIN instrument for which the radiation distribution is shown in the following image

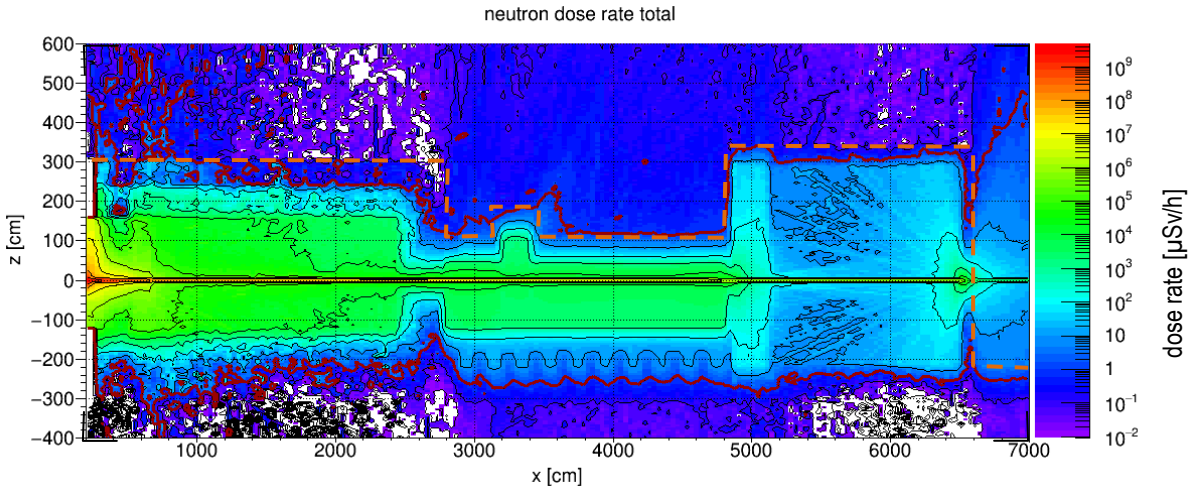

Fig. 258: Total neutron dose rate distribution in the vertical area. The red line is the 1µSv/h border.

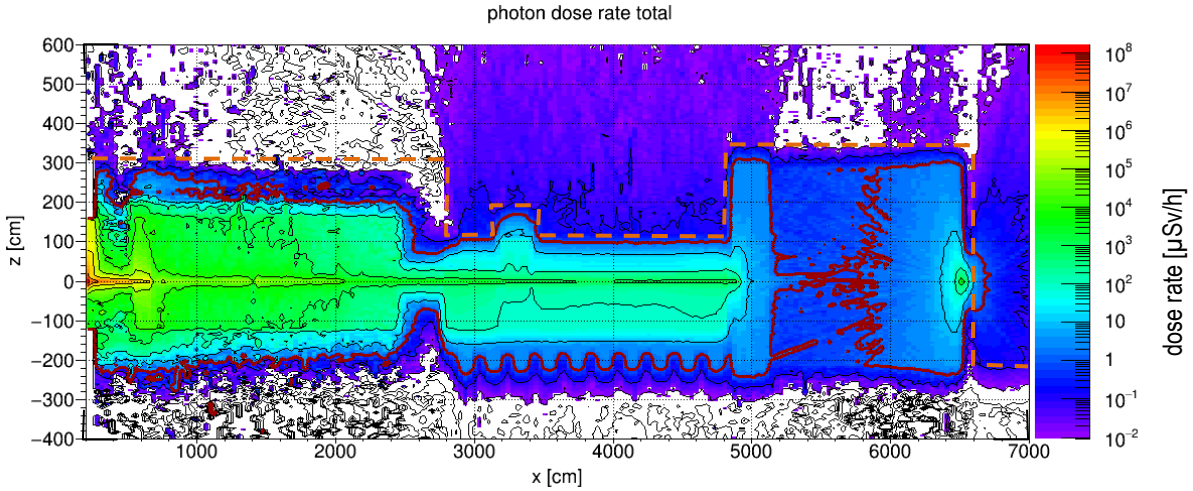

Fig. 259: Total generated gamma dose rate distribution in the vertical area. The red line is the 1µSv/h border.

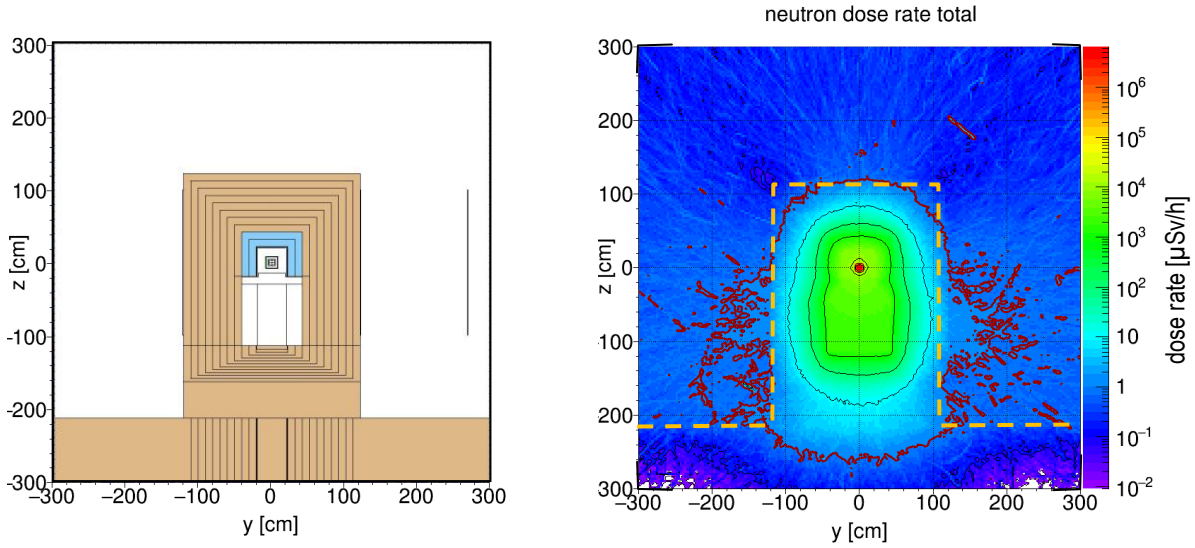

Fig. 260: Vertical neutron dose rate distribution through the guide shielding perpendicular to the beam axis (40m from the focal point). The red line is the 1µSv/h border.

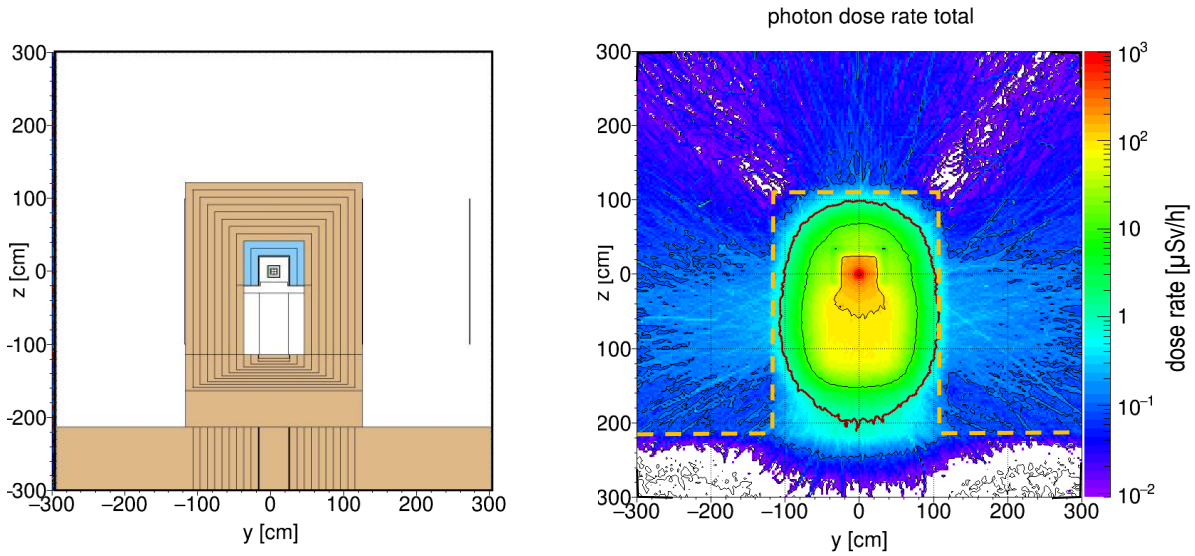

Fig. 261: Vertical generated gamma dose rate distribution through the guide shielding perpendicular to the beam axis (40m from the focal point). The red line is the 1µSv/h border.

7.9.1 Closed chopper FOC5

The gamma dose rate distribution for a chopper pit shielding consisting of 20cm steel and 70cm concrete was already presented in previous chapters. The shielding is sufficient for this case.

7.9.2 Conclusion

The collimators have a beneficial effect on the neutron dose rate outside the guide shielding but the 5cm steel layer below the neutron guide is more effective. The interface structure between the bunker wall and the guide shielding doesn’t increase the dose rate outside the guide shielding.

8 Appendix

8.1 Flux to dose rate conversion factors

All dose rates were calculated from fluxes according to the ESS0019931.3 conversion factors. The conversion factors for neutron and gamma radiation are shown in the diagrams below. For comparison the corresponding ICRP74 values are also plotted. The ICRP74 values for neutrons are higher in the thermal, epithermal and fast energy range up to 1MeV. The ICRP74 values are higher up to a factor of 2. The dose rate $H^*(10)$ is given by:

$$H^*(10) = \int_0^\infty h^*(10)(E) \cdot \phi(E) dE$$

with $h^*(10)(E)$: conversion factor

$\Phi(E)$: flux

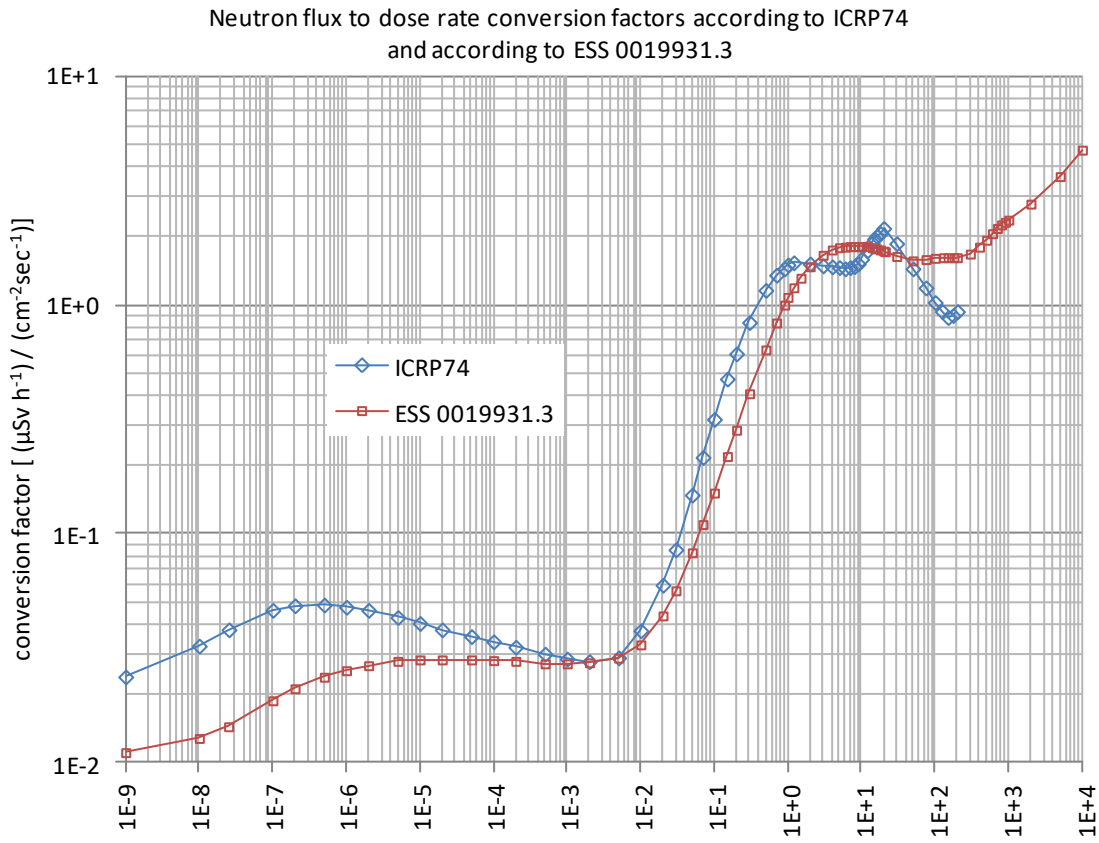

Fig. 262: Neutron flux to dose rate conversion factors according to ICRP74 and according to ESS 0019931.3

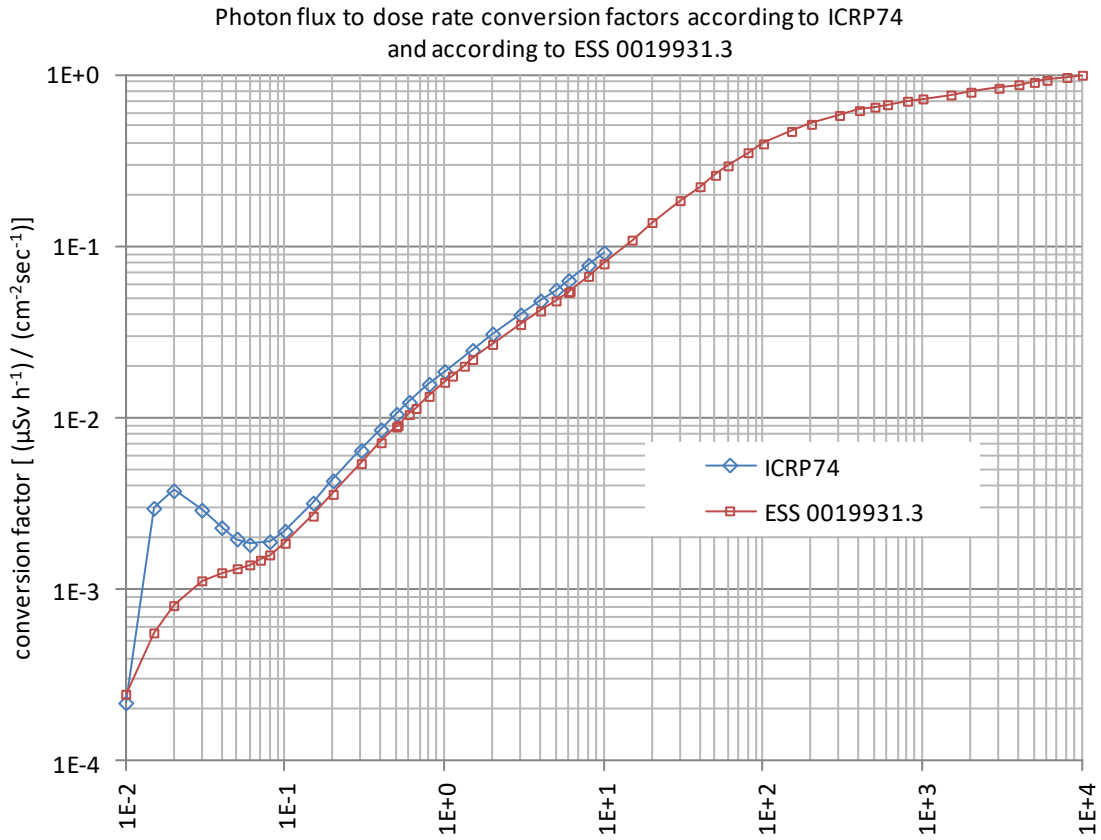

Fig. 263: Photon flux to dose rate conversion factors according to ICRP74 and according to ESS 0019931.3